

RENEWABLE POLYMERS FROM ITACONIC ACID

A Dissertation

Presented to the Faculty of the Graduate School

of Cornell University

In Partial Fulfillment of the Requirements for the Degree of

Doctor of Philosophy

by

Jacob Thomas Trotta

August 2019

RENEWABLE POLYMERS FROM ITACONIC ACID

Jacob Thomas Trotta, Ph. D.

Cornell University 2019

Itaconic acid (IA) is a biorenewable compound that is generated inexpensively and in large amounts by the fermentation of biomass. While a variety of structurally diverse polymers have been accessed from IA, continued exploration of efficient syntheses and polymerizations of novel monomers could lead to the development of sustainable materials that can help reduce society's dependence of petroleum (Chapter 1). We show that from β -monomethyl itaconate, an IA derivative, we can utilize a selective addition strategy that allows access to both α -methylene- γ -butyrolactone (MBL, tulipalin A) and α -methylene- γ,γ -dimethyl- γ -butyrolactone (Me₂MBL), which serve as high value biorenewable analogues to petroleum-derived methyl methacrylate. Subsequent polymerization of both Me₂MBL and MBL through reversible addition-fragmentation chain-transfer (RAFT) polymerization generates well defined poly(Me₂MBL) (PMe₂MBL) and poly(MBL) (PMBL) polymers. Through physiochemical characterization, we show that PMe₂MBL has desirable properties comparable with known PMBL materials (Chapter 2). We then extend our strategy to produce triblock polymers using PMBL end blocks with an IA-derived polyester mid-block. Using catalytic, solvent-free, and high yielding transformations from an itaconate source, we efficiently synthesize a saturated diol, a saturated diester, and an unsaturated diester. Subsequent step-growth polycondensation polymerizations of these monomers leads to polyesters with relatively high molar masses (> 10 kg/mol). Chain-end

functionalization and chain-extension of the saturated polyesters with MBL then provides access to an almost completely IA-derived triblock polymer thermoplastic. Alternatively, we show that thiol-ene cross-linking of unsaturated polyesters allows access to thermosets with tunable mechanical properties based on the cross-linking density. In most cases, high isolated yields, high atom economies, and low process mass intensities for these reactions reflect green and sustainable processes (Chapter 3). We then explore sustainable methods for the oxidation of MBL to its oxide, MBLO. Ring-opening polymerizations of MBLO to PMBLO is performed and gives access to a new, biorenewable, and amorphous polyether that exhibits a high glass transition temperature (106 °C). Comparisons with other common polyethers highlights the potential utility of this new material, and the polymerization of similar renewable epoxide monomers are studied (Chapter 4).

BIOGRAPHICAL SKETCH

Jacob Trotta was born in Boston, Massachusetts in 1992. He grew up in Peabody, Massachusetts and then graduated from Concord-Carlisle Regional High School in Concord, Massachusetts in 2010 before attending college at Villanova University in Pennsylvania. During his time as an undergraduate, Jacob worked as an intern at Alkermes, Inc. during summer and winter breaks, beginning in 2011. He obtained his B.S. from Villanova University in the of Spring 2014 with a major in chemistry and a minor in mathematics. Following this, Jacob began his graduate career at Cornell University in the laboratory of Brett Fors, where he worked on the synthesis and characterization of renewable polymeric materials largely derived from itaconic acid. Starting in the summer of 2019, Jacob will return to Alkermes to work full-time. In his free time, Jacob enjoys running, hiking, playing board games, and watching Game of Thrones.

ACKNOWLEDGMENTS

I never really questioned my decision to pursue chemistry during my undergraduate and then graduate career, and this is probably because I had such a positive experience with the subject as a teenager – it turns out that having good science teachers in high school matters quite a bit. So, because of that, I owe a huge thanks to Mrs. McCaffrey-Clark, a truly phenomenal high school chemistry teacher, who got me interested in chemistry in the first place.

Once I got to college, I met many people who helped me on my path to graduate school. In particular, I would like to thank Professor Deanna Zubris, Professor Eduard Casillas, Professor Nicholas Piro, and Professor Scott Kassel for their support and instruction along the way. I also need to thank my undergraduate roommates for their continued friendships through the years: Francis Polignano (honorary roommate), Connor McGuckin, Matthew Whalen, Steven Stagliano, and Brian Selitto, you all are the best, and I look forward to many more years of friendship.

While I got my undergraduate degree in chemistry from Villanova University, I did most of my undergraduate research at Alkermes, Inc. as an intern. Alkermes fostered an incredibly supportive environment where I first developed an interest in research. I am grateful to everyone at Alkermes that I interacted with, especially Dr. Tarek Zeidan, whose role as a mentor made a hugely positive impact on my development as a scientist. I am very much looking forward to beginning my career at Alkermes this summer.

After graduating from Villanova University, I entered the graduate program in Chemistry and Chemical Biology at Cornell University, in part because I wanted to work with Professor Brett Fors. Joining the lab of a brand-new assistant professor was

a potentially risky move, but looking back, I know I made the right decision. So thank you, Brett, for your instruction, support, and patience over the last five years. I'm glad I spent it making as many things as possible from corn in your lab.

It wasn't just me in the Fors group, and I have many others to thank. Thanks to Dr. Dillon Gentekos: the past five years have had their highs and lows, and several "phases" were gone through, but it was nice to have someone to get through it with. Thanks to Stephen Parker Singleton: though you left the group, your presence was still felt. Righ. Thanks to Vernoika Kottisch, whose editing skills made this thesis possible. Thanks to Michael Supej, who promised to trim my rune armor for free. Thanks to Renee Sifri, who inspired me to pick up the piano again and learn to swing dance. Thanks to Stephanie Rosenbloom and her bird Petrie, who's still learning how to say my name. Thanks to Scott Spring for his love of all things renewable. Thanks to Luis Melecio-Zambrano (here's to another 10 years of friendship). Thanks to Yuting Ma, who always managed to make me laugh.

There were also some postdocs in the Fors group. Thanks to Professor Dongbing Zhao, who supervised my first-year self and always helped when I, panicked, would ask if an experiment was dangerous. Thanks to Professor Quentin Michaudel, who I think about every postdoc appreciation day. Thanks to Dr. Erin Stache, who got me out of my running hiatus.

I am especially grateful to all the undergraduates who have both worked with me and put up with me over the past five years. Mengyuan Jin, Katherine Stawiasz, Allison Wu, Teresa Datta, Zachary Vaughn, and Amanda Innamorato: thank you for your hard work and for the contributions you all made to the research I've worked on

during graduate school. I'm sorry that I made you all clean so many NMR tubes. And although I did not work with them directly, I am grateful to have interacted with both Kathleen Naeher (the most chill undergrad) and Mason Wu.

As a first-year graduate student, I sometimes wasn't 100% sure of what I was doing, and there weren't any older graduate students in the Fors group to turn to for help. So a huge thanks to Dr. Matthew Moschitto, Dr. Tony Tierno, and Dr. Cathy Mulzer for being around late and helping me find chemicals, for answering my many chemistry questions, and for helping me locate products I managed to lose track of during column purification.

I'd also like to thank Professor Geoffrey Coates and Professor David Collum for sitting on my special committee, as well as Professor Phillip Milner for serving as a special committee member proxy for my B exam. Thanks also to Professor Bruce Ganem as well, who always let me walk into his office, unannounced, to talk chemistry. Another thanks goes out to Professor Frank Schroeder, an excellent teacher who always answered my NMR questions (even years after taking his course!) and would discuss immortality and space science with me during visit weekends. I'd also like to thank both Dr. Cynthia Kinsland, whose support and free candy helped get me through my first year, and Dr. Ivan Keresztes, without whom many of my monomers and polymers might have gone uncharacterized. A big thank also goes out to Pat Hine for her support over the years.

I've had the great opportunity to collaborate with a number of people during graduate school. I am particularly thankful to Dr. Annabelle Watts, whose contributions to our work on the generation of thermosets and thermoplastics from itaconic acid

significantly accelerated its progress, and who taught me a lot about the mechanical testing of polymers. I'd also like to thank both Dr. Angelika Neitzel and Dr. Leonel Barreda for the opportunity to contribute to their research on hemicyclic acetal esters. Also a huge thanks to Professor Marc Hillymer, whose group I was very fortunate to collaborate with. And thanks to Professor Christopher Ellison and Aditya Banerji for the use of the Ellison group's DMF SEC.

Of course, graduate school wasn't just about chemistry. Thanks to Dr. Kristina Hugar for running my first half-marathon with me (and for running it at my much slower pace!). Thanks to Dr. Anton Chavez, who was always very quiet during Game of Thrones and never laughed at critical, dramatic moments. Thanks to Dr. Kyle Mack for his many home-cooked meals. Thanks to Dr. Nicole Spiegelman for teaching me about sirtuins. Thanks to Dr. Lilliana Morris for surviving graduate school with me. Thanks to Rachel Synder for introducing me to the movie "Us," which I still haven't totally figured out.

And finally, I owe a huge thanks to my family, who are all awesome. Kristin, Shaina, and Jocelyn: thanks for being great sisters and for listening to me complain so often. Mom and Dad: thank you for encouraging me to go to graduate school in the first place and for your endless love and support. And thanks to my entire family for visiting me so often! I love you all very much.

Research can't happen without funding, and I am very grateful for the funding. This research was supported by the National Science Foundation (NSF) through the Center for Sustainable Polymers (CHE-1413862). This work made use of the Cornell Center for Materials Research Shared Facilities that are supported through the NSF

MRSEC program (DMR- 1120296). This work made use of the NMR Facility at Cornell University that is supported, in part, by the NSF under the award number CHE-1531632.

TABLE OF CONTENTS

Chapter 1 RENEWABLE POLMYERS BASED ON ITACONIC ACID.....	1
ABSTRACT.....	1
INTRODUCTION	1
ITACONIMIDES.....	6
METHYLENE BUTROLACTONES.....	21
PYRROLIDONES	44
MONOMERS FOR METATHESIS POLYMERIZATIONS	64
PHOSPHOROUS CONTAINING POLYMERS BASED ON IA	68
FLUORINE CONTAINING POLYIMIDES BASED ON IA	73
OTHER EXAMPLES OF IA-DERIVED MONOMERS AND POLMYERS.....	75
CONCLUSION.....	83
REFERENCES	83
Chapter 2 SYNTHESIS OF METHYLENE BUTYROLACTONE POLYMERS FROM ITACONIC ACID	102
ABSTRACT.....	102
INTRODUCTION	102
RESULTS AND DISCUSSION	107
CONCLUSIONS	118
EXPERIMENTAL.....	118
APPENDIX.....	124
REFERENCES	134
Chapter 3 THERMOSETS AND THERMOPLASTICS FROM ITACONIC ACID	145
ABSTRACT.....	145
INTRODUCTION	146
RESULTS AND DISCUSSION	149
CONCLUSIONS	170
EXPERIMENTAL.....	171
APPENDIX.....	190
REFERENCES	216
Chapter 4 POLYETHERS FROM ITACONIC ACID.....	234

ABSTRACT.....	234
INTRODUCTION	234
RESULTS AND DISCUSSION	235
CONCLUSIONS	248
EXPERIMENTAL.....	248
APPENDIX.....	260
REFERENCES	276

LIST OF SCHEMES, FIGURES, AND TABLES

Figure 1.1. A wide variety of monomers are accessible from IA for polymerization. IA-derived atoms are marked in red.	5
Figure 1.2. a) Synthesis of II derivatives from IA; b) general scheme for the polymerization of an II derivative; c) R groups of various II derivatives explored in CRP.....	7
Table 1.1. ATRP Systems for the Polymerization of RII.....	9
Figure 1.3. The synthesis of the II-based ATRP initiators explored by Chauhan, Behera, and co-workers. ⁶³	10
Figure 1.4. Structure of the FeBr ₃ (IDipp) catalyst and EBrPA initiator used for the homopolymerization of PhII. ⁶⁴	11
Figure 1.5. Polymerization of PhII using FeBr ₃ (IDipp). A) Kinetic plots of ln([M] ₀ /[M]) vs time; b) Plot of <i>M_n</i> and <i>Đ</i> vs conversion; c) SEC traces using calibration based on linear polystyrene standards; reaction conditions: [PhII]:[EBrPA]:[AIBN]:[FeBr ₃ (IDipp)] = 100:1.0:1.5:0.05, [PhII] = 4.7 M in 50% v/v of anisole at 60 °C for 24 h. Copied with permission from the original manuscript by Okada and Matyjaszewski. ⁶⁴	12
Table 1.2. Physicochemical Properties of RII-based Polymers.	15
Figure 1.6. a) RAFT polymerization of II derivatives; b) RAFT polymerization of PhII from a telechelic poly(diester itaconate) macroinitiator to generate triblock polymer.	16
Figure 1.7. SEC curves for the chain-extension of poly(dialkyl itaconates) with PhII. SEC curves obtained in the block copolymerization from dibutyl itaconate (DBI) or bis(2-ethylhexyl) itaconate (DEHI) to PhII; RAFT agent: monofunctional dithiobenzoate (CTA-3), telechelic bis(dithiobenzoate) (CTA-4); [M] ₀ : [CTA] ₀ : [V-70] ₀ = 100:1.0:0.2 in bulk at 20 °C for the first block; [M] ₀ : [CTA] ₀ : [AIBN] ₀ = 50:1.0:0.2 ([M] ₀ = 1.0 M) in 1,4-dioxane at 50 °C for the second block. Copied with permission from the original manuscript by Kamigaito and co-workers. ⁷⁰	17
Figure 1.8. a) Dynamic tensile storage (E') and loss (E'') moduli and tan(δ) (E''/E') as a function of temperature (heating rate: 10 °C/min; frequency 11 Hz); b) AFM phase images (2 x 2 μm) for morphologies of the PPhII-PDBI-PPhII triblock polymer; <i>M_n</i> = 67.1 kg/mol, <i>Đ</i> = 1.20, DBI:PhII = 73:27 (wt%). Copied with permission from the original manuscript by Kamigaito and co-workers. ⁷⁰	18
Figure 1.9. Synthesis of PhII based triblock PPhII-PL-PPhII.	20
Figure 1.10. Synthesis of MBL and related derivatives from IA. Pathway A: Fisher esterification of IA with MeOH and acid produces dimethyl itaconate (DMI), while refluxing IA with acetyl chloride (AcCl) produces itaconic anhydride (ItAnh). Pathway B: Reduction of DMI with sodium bis(2-methoxyethoxy)aluminium hydride (Red-Al [®]) gives the unsaturated 2-methylene-1,4-butanediol (1.1). Oxidative cyclization of 1.1 with Ag ₂ CO ₃ on celite [®] then produces MBL. Pathway C: allylation of ItAnh allyltrimethylsilane produces DAMBL. Pathway D: The six-step synthesis of β-MeMBL. Pathway E: Reduction of β-MMI with NaBH ₄ to produce MBL or with	

MeMgCl to produce Me ₂ MBL. Pathway F: Polymerization of MBL, Me ₂ MBL, β-MeMBL, or DAMBL generates structurally varied polymers from IA.	24
Figure 1.11. Chain extension of a Br-PBA-Br macroinitiator to PMBL-PBA-PMBL	25
Table 1.3. Tensile Properties of Linear ABA Triblock Polymers Derived from IA or Other Renewable Resources.	27
Figure 1.12. Synthesis of PRMBL-PM-PRMBL triblock polymers by ATRP chain-extension from a Br-PM-Br macroinitiator.	29
Figure 1.13. Synthesis of PMBL-PMBMS-PMBL triblock polymer by chain-extension of a Br-PMBMS-Br IA-derived polyester macroinitiator.	32
Equation 1.1	33
Figure 1.14. Copolymerization of MBL with ε-CL to give poly(ε-CL)- <i>co</i> -PMBL _{ROP} (PCL- <i>co</i> -PMBL _{ROP}).	33
Figure 1.15. Lanthanum and ytterbium catalysts used by Chen and co-workers for the ROP polymerization of MBL. ^{110,112}	35
Figure 1.16. VAP vs ROP polymerization of MBL. Copied with permission from the original manuscript. ¹¹⁰	36
Figure 1.17. a) Initiation of either ROP (I) or VAP (II), b) propagation and c) cross-prpogation via Michael addition (III). Copied with permission from original manuscript. ¹¹⁰	38
Figure 1.18. Lanthanum catalysts used by Ford and co-workers for the ROP polymerization of MBL. ¹¹³	40
Figure 1.19. Cationic ROP of MBL and CL leads to hydroxyl terminated, telecehlic, or star polymers using different initiators.	43
Figure 1.20. a) Synthesis of AB type pyrrolidone monomers from IA; b) Synthesis of AA type bis(pyrrolidone) monomer from IA; c) Synthesis of salt monomers from IA; d) Polycondensation of salt or AB monomers to give polyamides or polyesters; e) Polycondensation of AA diacid with BB amine to give polyamides; f) Substrate scope of diamines studied for these types of polycondensations.	46
Figure 1.21. Intramolecular condensation of polyamides generates polybenzimidazoles.	47
Table 1.4. Table of Physical Properties for Pyrrolidone-Containing Polyamides Derived from IA.	49
Figure 1.22. Degradation of pyrrolidone-based polyamides occurs through ring opening of the pyrrolidone and solubilization. ¹¹⁶	51
Figure 1.23. Tentative mechanism of NaMMT functions to catalyze the ring-opening reaction of pyrrolidone in the main chain to form carboxylic acid that specifically interacts with the MMT surface. Copied with permission from the original manuscript. ¹²¹	54
Figure 1.24. Proposed structure of poly(ester amide)s explored by Zhao and co-workers. ¹¹⁹	58
Figure 1.25. Polymerizations/cross-linking of IA-derived bis(pyrrolidone) with furfural-derived oxazolines. ¹²⁵	61

Figure 1.26. a) 1.6, an oxazoline-containing pyrrolidone, was synthesized by the addition of ethanolamine to acid 1.5, followed by an intramolecular condensation. Alternatively, treatment of the zinc salt of 1.5 with acetylene at elevated temperatures results in the pyrrolidone acrylate, 1.7. b) 1.6 was polymerized cationically with pTsOMe at an elevated temperature. c) 1.7 was polymerized radically with AIBN at an elevated temperature.....	63
Figure 1.27. Synthesis and thermal polymerization of 1.11.....	64
Figure 1.28. Metathesis-derived polymers based on IA. a) ADMET of 1.13 and subsequent post-polymerization modification; b) ROMP of 1.15; c) Synthesis and ROMP of 1.18.	65
Figure 1.29. a) Step-growth polymerization and one-pot functionalization of IA to give phosphorylated IA copolyesters; b) synthesis of phosphorous containing polyamides from IA.	72
Figure 1.30. a) Synthesis of fluorine containing diamine 1.25 based on IA and b) polymerization of 1.25 to give fluorinated polyetherimide 1.26.....	75
Figure 1.31. a) Reduction of IA to MB; b) Saturated IA-based polyester PMBMS generated by the polycondensation of 1.28 and MB; c) Reduction of IA to isoprene; d) Electrochemical coupling of α -MMI to diester 1.29.	77
Figure 1.32. Synthesis of CS, MS, and MB monomers from DMI.	78
Figure 1.33. Synthesis of unsaturated copolymers from all IA-derived monomers used by Fors and co-workers. ¹⁰⁹	79
Figure 1.34. Cross-linking of PMBCS-PMBMS random copolymers. Copied with permission from the original manuscript. ¹⁰⁹	80
Figure 1.35. a) Differential scanning calorimetry (DSC) heat flow vs temperature traces of various prepolymers (solid lines) or thermosets (dashed lines), exo up; b) Dynamic mechanical thermal analysis (DMTA) storage modulus (left axis, solid lines) and tan(delta) (right axis, dashed lines) vs temperature traces of thermosets; c) Stress-strain curves of thermosets, where the end of each curve indicates a break point. Copied with permission from the original manuscript. ¹⁰⁹	81
Figure 1.36. a) Synthesis and polymerization of thiol-ene adducts and their polyesters from IA and b) derivatives explored in the study.	82
Figure 2.1. Our strategy to convert itaconic acid, produced by the fermentation of biomass such as corn or rice, into high value poly(methyl methacrylate) surrogates through the transformation to, and controlled polymerization of, methylene butyrolactones.....	104
Figure 2.2. a-d) Previous work on the synthesis of MBL analogs from IA derivatives and e) this work.	105
Table 2.1. Optimization of the Reduction of β -MMI to Me ₂ MBL.....	108
Table 2.2. Optimization of the Reduction of β -MMI to MBL	110
Figure 2.3. RAFT polymerization of Me ₂ MBL leads to predictable M_n values based on Me ₂ MBL and CTA loading.	112
Table 2.3. Polymerization Conditions for Me ₂ MBL	113

Figure 2.4. Chain extension of PMMA with PMe ₂ MBL to give the block copolymer PMMA- <i>b</i> -PMe ₂ MBL.....	114
Table 2.4. Polymerization Conditions for MBL.....	115
Figure 2.5. Differential scanning calorimetry (DSC) heat flow vs temperature (30 °C/min, second heat) traces of PMe ₂ MBL (synthesized using both uncontrolled and RAFT polymerizations) and PMBL (synthesized using RAFT polymerization), exo up.	116
Figure 2.6. TGA curves of PMe ₂ MBL (synthesized using both uncontrolled and RAFT polymerization) and PMBL (synthesized using RAFT polymerization).	117
Figure S2.1. ¹ H NMR spectrum of the crude reaction mixture for the synthesis of Me ₂ MBL prior to distillation in CDCl ₃	128
Figure S2.2. ¹ H NMR spectrum of Me ₂ MBL in CDCl ₃	128
Figure S2.3. ¹³ C NMR spectrum of Me ₂ MBL in CDCl ₃	129
Figure S2.4. ¹ H NMR spectrum of 2.1 in CDCl ₃	129
Figure S2.5. ¹³ C NMR spectrum of 2.1 in CDCl ₃	130
Figure S2.6. ¹ H NMR spectrum of MBL in CDCl ₃	130
Figure S2.7. ¹ H NMR spectrum of PMe ₂ MBL in CDCl ₃	131
Figure S2.8. ¹³ C NMR spectrum of PMe ₂ MBL in CDCl ₃	131
Figure S2.9. ¹ H NMR spectrum of PMBL in DMSO- <i>d</i> ₆	132
Figure S2.10. ¹ H NMR spectrum of PMMA- <i>b</i> -PMe ₂ MBL in CDCl ₃	132
Figure S2.11. RAFT polymerization of MBL leads to predictable <i>M_n</i> values based on MBL and CTA loading.	133
Figure S2.12. Refractive index vs wavelength obtained from ellipsometry measurements for a thin film of PMMA.	133
Figure S2.13. Refractive index vs wavelength obtained from ellipsometry measurements for a thin film of PMe ₂ MBL.	134
Figure 3.1. (a) Renewable monomers from IA. (b) Renewable thermoplastics and thermosets derived from IA.	148
Figure 3.2. Reduction of dimethyl itaconate (DMI) to dimethyl 2-methylsuccinate (MS).	149
Table 3.1. Reaction Conditions for the Synthesis of 2-Methyl-1,4-butanediol (MB)	151
Table 3.2. Reaction Conditions for the Synthesis of CS	154
Figure 3.3. (a) Synthesis of PMBCS through the step-growth polycondensation of MB and CS. Number-average molar mass (<i>M_n</i>) = 11.7 kg/mol, weight-average molar mass (<i>M_w</i>) = 25.7, dispersity (<i>Đ</i>) = 2.19, glass transition temperature (<i>T_g</i>) = -9 °C, temperature at 5 wt% loss (<i>T_{d,5%}</i>) = 246 °C, and head-to-tail ratio (H:T) = 1:1. (b) Synthesis of PMBMS through the step-growth polycondensation of MB and MS. <i>M_n</i> = 15.7 kg/mol, <i>M_w</i> = 38.9 kg/mol, <i>Đ</i> = 2.48, <i>M_e</i> = 6.3 kg/mol, <i>T_g</i> = -31 °C, <i>T_{d,5%}</i> = 276 °C, and H:T = 1:1.	155
Table 3.3. Statistical Polymerization of MB, MS, and CS to give PMBCS _x -stat-PMBMS _{1-x}	158
Figure 3.4. Thiol-ene click chemistry on PMBCS.	159

Figure 3.5. A potentially renewable retro-synthetic route to pentaerythritol tetrakis(3-mercaptopropionate).....	160
Figure 3.6. Cross-linking of PMBCS _x -stat-PMBMS _{1-x} copolymers.....	162
Table 3.4. Tensile Testing and Thermoset Gel Fraction Data for IA-Based Thermosets	162
Figure 3.7. (a) Differential scanning calorimetry (DSC) heat flow vs temperature traces of various prepolymers (solid lines) or thermosets (dashed lines), exo up. (b) Dynamic mechanical thermal analysis (DMTA) storage modulus (left axis, solid lines) and tan(δ) (right axis, dashed lines) vs temperature traces of thermosets. (c) Stress-strain curves of thermosets, where the end of each curve indicates a break point.	164
Figure 3.8. Chain extension of HO-PMBMS-OH to give PMBL-PMBMS-PMBL. .	166
Figure 3.9. Synthesis and ¹ H NMR spectra of end-group defined polymers.	167
Figure 3.10. SEC traces of the chain extension of Br-PMBMS-Br (black) to PMBL-PMBMS-PMBL (red).	168
Figure 3.11. Stress-strain curves for PMBL-PMBMS-PMBL, where the end of the curve indicates a break point. $E = 185 \pm 26$ MPa, $\sigma_B = 7 \pm 2$ MPa, and $\epsilon_B = 226 \pm 80\%$	168
Table 3.5. Green Metric Evaluation of Various Reactions Presented in this Work...	170
Figure S3.1. ¹ H NMR spectra of 2-(4-methylcyclohex-3-ene)succinate (CS) in CDCl ₃	195
Figure S3.2. ¹ H NMR spectra of dimethyl 2-methylsuccinate (MS) in CDCl ₃	195
Figure S3.3. ¹ H NMR of 2-methyl-1,4-butanediol (MB) in CDCl ₃	196
Figure S3.4. ¹ H NMR of PMBCS in CDCl ₃	196
Figure S3.5. ¹³ C NMR of PMBCS in CDCl ₃	197
Figure S3.6. ¹ H NMR of PMBMS in CDCl ₃	197
Figure S3.7. ¹³ C NMR of PMBMS in CDCl ₃	198
Figure S3.8. ¹ H NMR spectra of dodecanethiol-functionalized PMBCS in CDCl ₃	198
Figure S3.9. ¹ H NMR of PMBCS _x -stat-PMBMS _{1-x} (x = 0.19) in CDCl ₃	199
Figure S3.10. ¹³ C NMR of PMBCS _x -stat-PMBMS _{1-x} (x = 0.19) in CDCl ₃	199
Figure S3.11. Quantitative ¹ H NMR spectrum of PMBCS in CDCl ₃ with assignments.	200
Figure S3.12. Quantitative ¹³ C NMR spectrum of PMBCS in CDCl ₃ with assignments. Insert in top-left depicts the peaks associated with the quaternary carbon (carbon 1).	200
Figure S3.13. COSY spectrum of PMBCS in CDCl ₃ with assignments. Insert in top-left depicts the cross-peaks associated with the methylene protons adjacent to the alcohols (carbons 5 and 8).	201
Figure S3.14. HSQC spectrum of PMBCS in CDCl ₃ with assignments. Insert in top-left depicts the cross-peaks associated with the aliphatic protons not adjacent to the alcohols.	202
Figure S3.15. HMBC spectrum of PMBCS in CDCl ₃ with assignments. Insert in top-left depicts the cross-peaks associated with the methylene protons adjacent to the alcohols (carbons 5 and 8).	202

Figure S3.16. Quantitative ^1H NMR spectrum of PMBMS in CDCl_3 with assignments.	203
Figure S3.17. Quantitative ^{13}C NMR spectrum of PMBMS in CDCl_3 with assignments.....	203
Figure S3.18. COSY spectrum of PMBMS in CDCl_3 with assignments.	204
Figure S3.19. HSQC spectrum of PMBMS in CDCl_3 with assignments.	204
Figure S3.20. HMBC spectrum of PMBCS in CDCl_3 . Insert in top-left depicts the cross-peaks associated with the methylene protons adjacent to the alcohols (carbons 5 and 8).	205
Figure S3.21. SEC results monitoring the polymerization of MB and MS as detected by RI (Table S3.1).	205
Figure S3.22. Plot of M_n vs conversion for the synthesis of PMBMS.	206
Table S3.1. Conversion (p), Degree of Polymerization ($1/(1-p)$), M_n , and \bar{D} as a Function of Time for PMBMS Synthesis	206
Table S3.2. Tabulated Values for the Flory-Rehner Equation Estimation of Molar Mass Between Cross-Links (M_x).....	207
Table S3.3. Gel Fractions and M_x Values Determined for the Thermosets from DMTA and Swell Test Results.....	208
Table S3.4. Degradation (as Percentages of Initial Mass) Data for Thermoset ($F_{\text{MBCS}} = 0.19$) Degradation Experiments.....	208
Figure S3.23. Graphical representation of data in Table S3.4.....	209
Figure S3.24. (a) Thermal gravimetric analysis mass loss (%) vs temperature (10 $^\circ\text{C}/\text{min}$) traces of various prepolymers (solid lines) or cross-linked thermosets (dashed lines).	209
Figure S3.25. ^1H NMR spectra of Br-PMBMS-Br in $\text{DMSO}-d_6$	210
Figure S3.26. ^1H NMR spectra of PMBL-PMBMS-PMBL in $\text{DMSO}-d_6$	210
Figure S3.27. ^{13}C NMR spectra of PMBL-PMBMS-PMBL in $\text{DMSO}-d_6$	211
Figure S3.28. Differential scanning calorimetry heat flow vs temperature (30 $^\circ\text{C}/\text{min}$, second heat) traces of homo- or triblock polymers of PMBMS and PMBL, exo up.	211
Figure S3.29. Thermal gravimetric analysis mass loss (%) vs temperature (10 $^\circ\text{C}/\text{min}$ for PMBMS, 30 $^\circ\text{C}/\text{min}$ for PMBL-PMBMS-PMBL or PMBL) traces of homo- or triblock polymers of PMBMS and PMBL.....	212
Figure S3.30. Superimposed infrared (IR) spectra of the PMBMS, PMBCS, and prepolymers (solid lines) or cross-linked thermosets (dashed lines).....	212
Figure S3.31. Dynamic frequency sweeps of PMBL, measuring the modulus as a function of frequency at 250 and 260 $^\circ\text{C}$. PMBL degraded on the rheometer above 260 $^\circ\text{C}$, and moduli vs frequency data was not acquired at higher temperatures. The plateau modulus, G_N , was roughly estimated to be 358820 Pa at the minimum $\tan(\delta)$ value ($M_e = 10.5$ kg/mol). The strain used in these experiments was 0.05%.	213
Figure S3.32. A master curve of PMBMS generated from applying shift factors (a_T) to dynamic frequency sweep data obtained at various temperatures. The plateau modulus, G_N , was roughly estimated to be 435000 Pa at the minimum $\tan(\delta)$ value ($M_e = 6.3$ kg/mol). The strain used in these experiments was 0.05%.....	214

Figure S3.33. Size exclusion chromatography (SEC) traces for PMBMS, PMBCS, and PMBCS _{x-stat} -PMBMS _{1-x} statistical terpolymers that served as thermoset prepolymers.	215
Figure S3.34. Size exclusion chromatography (SEC) for HO-PMBMS-OH (red) and Br-PMBMS-Br (black), indicating a high molar mass tail in Br-PMBMS-Br after HO-PMBMS-OH functionalization.	216
Figure 4.1. a) MBL and its polymer, PMBL, are well studied. PMBL possesses a high <i>T_g</i> and high solvent resistance. b) MBLO and its polymer, PMBLO, are previously unexplored.	235
Figure 4.2. a-b) Previous methods known for the oxidation of MBL to MBLO; c-d) synthetic strategies for accessing MBLO from MBL, including c) nucleophilic oxidation, d) <i>in situ</i> formation of DMDO for oxidation and e) ring-closing epoxidation of a halohydrin intermediate	237
Figure 4.3. Scaled-up and optimized formation of MBLO from MBL.	239
Figure 4.4. SEC curves for PMBLO samples synthesized by the ROP of MBLO.	240
Table 4.1. Polymerization Conditions for MBLO.	241
Table 4.2. Polymerization Conditions for MeMBLO and Me ₂ MBLO	242
Figure 4.5. Thermal gravimetric analysis (TGA) trace of PMBLO.	243
Figure 4.6. Differential scanning calorimetry (DSC) heat flow vs. temperature (30 °C/min, second heat) traces of PMBLP, exo up.	244
Table 4.3. Physiochemical Properties of Various Polyethers	246
Figure 4.7. Itaconimide based monomers explored in this work.	246
Figure 4.8. Synthesis of itaconimide-based epoxides from ItAnh.	247
Figure 4.9. ROP of itaconimide epoxides leads to oligomers and an allyl alcohol.	247
Figure S4.1. SEC traces (solid line = refractive index trace, dotted line = light scattering trace) for crude (black) and precipitated (red) PMBLO sample (Table 4.1, entry 8).	263
Figure S4.2. ¹ H NMR spectra of α-methylene-γ-butyrolactone oxide (MBLO) in CDCl ₃ .	264
Figure S4.3. ¹ H NMR spectra of γ-methyl-α-methylene-γ-butyrolactone oxide (MeMBLO) in CDCl ₃ .	264
Figure S4.4. ¹ H NMR spectra of γ,γ-dimethyl-α-methylene-γ-butyrolactone oxide (Me ₂ MBLO) in CDCl ₃ .	265
Figure S4.5. ¹³ C NMR spectra of γ,γ-dimethyl-α-methylene-γ-butyrolactone oxide (Me ₂ MBLO) in CDCl ₃ .	265
Figure S4.6. ¹ H NMR spectra of poly(α-methylene-γ-butyrolactone oxide) (PMBLO) in DMSO-d ₆ .	266
Figure S4.7. ¹³ C NMR spectra of poly(α-methylene-γ-butyrolactone oxide) (PMBLO) in DMSO-d ₆ .	266
Figure S4.8. ¹ H NMR spectra of N-phenylitaconamic acid in DMSO-d ₆ .	267
Figure S4.9. ¹³ C NMR spectra of N-phenylitaconamic acid in DMSO-d ₆ .	267
Figure S4.10. ¹ H NMR spectra N-phenylitaconimide (4.1) in CDCl ₃ .	268
Figure S4.11. ¹ H NMR spectra of N-phenylcitraconimide in CDCl ₃ .	268

Figure S4.12. ¹ H NMR spectra of 5-phenyl-1-oxa-5-azaspiro[2.4]heptane-4,6-dione (4.2) in CDCl ₃	269
Figure S4.13. ¹³ C NMR spectra of 5-phenyl-1-oxa-5-azaspiro[2.4]heptane-4,6-dione (4.2) in CDCl ₃	269
Figure S4.14. ¹ H NMR spectra of 3-(hydroxymethyl)-1-phenyl-1H-pyrrole-2,5-dione (4.3) in CDCl ₃	270
Figure S4.15. ¹³ C NMR spectra of 3-(hydroxymethyl)-1-phenyl-1H-pyrrole-2,5-dione (4.3) in CDCl ₃	270
Figure S4.16. ¹ H NMR spectra of N-(<i>p</i> -anisidine)itaconamic acid in DMSO-d ₆	271
Figure S4.17. ¹³ C NMR spectra of N-(<i>p</i> -anisidine)itaconamic acid in DMSO-d ₆	271
Figure S4.18. ¹ H NMR spectra of N-(<i>p</i> -anisidine)itaconimide (4.4) in CDCl ₃	272
Figure S4.19. ¹ H NMR spectra of N-(<i>p</i> -anisidine)itaconimide (4.4) in DMSO-d ₆	272
Figure S4.20. ¹³ C NMR spectra of N-(<i>p</i> -anisidine)itaconimide (4.4) in DMSO-d ₆ ..	273
Figure S4.21. ¹ H NMR spectra of 5-(4-methoxyphenyl)-1-oxa-5-azaspiro[2.4]heptane-4,6-dione (4.5) in CDCl ₃	273
Figure S4.22. ¹³ C NMR spectra of 5-(4-methoxyphenyl)-1-oxa-5-azaspiro[2.4]heptane-4,6-dione (4.5) in CDCl ₃	274
Figure S4.23. ¹ H NMR spectra of 3-(hydroxymethyl)-1-(4-methoxyphenyl)-1H-pyrrole-2,5-dione (4.6), as part of a crude reaction mixture) CDCl ₃	274
Figure S4.24. ¹ H NMR spectra N-furfurylitaconamic acid in DMSO-d ₆	275
Figure S4.25. ¹ H NMR spectra N-furfurylitaconimide (4.7) in CDCl ₃	275
Figure S4.26. ¹ H NMR spectra N-furfurylcitraconimide in CDCl ₃	276

Chapter 1 RENEWABLE POLYMERS BASED ON ITACONIC ACID

ABSTRACT

Itaconic acid (IA), a biorenewable compound generated by the fermentation of biomass, is a relatively cheap feedstock chemical that is produced in large amounts annually (80,000 kton/yr) for only \$2/kg. Due to its cost and availability, IA has significant promise to reduce society's dependence on petroleum feedstocks for the synthesis of monomers and polymers. Many different monomers and polymers have been accessed from IA, and herein we review the synthesis of these materials and their physiochemical properties. A host of structurally diverse monomers derived from IA are known, including itaconimides, methylene butyrolactones, pyrrolidones, myriad Michael addition or Diels-Alder adducts, some of which that contain phosphorous or fluorine, monomers amenable to metathesis polymerization, and step-growth monomers. This wide range of polymers accessible from these small molecules have material applications that include tough thermoplastics, compatibilizers, and flame-resistant additives with comparable or improved properties relative to their commercially utilized analogues. As such, IA-based polymers represent an extremely important class of materials that could revolutionize biobased plastics.

INTRODUCTION

While polymeric materials have been used by humans for milenia,¹ polymer chemistry did not begin to develop until around the time Berzelius coined the term “*polymerische*,” almost 200 years ago.^{2,3} Early examples of polymer chemistry include

the nitration of cellulose to nitrocellulose⁴ and the step-growth polymerization of diols and diacids to produce synthetic polyesters,⁵ among many others.³ During these early years of polymer chemistry, up to the development of the macromolecular hypothesis, the usefulness of polymers did not go unnoticed.^{3,6} Numerous applications for early polymeric materials were explored, including the use of celluloid (a nitrocellulose-based thermoplastic) for movie films,⁷ collodion (a solution of nitrocellulose in an ethereal solvent) for wound dressings,⁸ and Bakelite (a thermoset resin produced from the reaction of formaldehyde and phenol) as a moldable plastic for use in the electrical and automobile industries.⁹ Polymeric materials quickly transformed society, with world plastic production experiencing an explosive growth following World War II.^{10,11} In particular, the development of the polyolefins industry in the 1950s, made possible by the pioneering research of Ziegler and Natta,¹² led to a wide range of polyolefins with countless applications as fibers, blow-molded and injection-molded films, articles, and extrusions.¹³ Continued development of polymeric materials has integrated these materials into almost every aspect of our lives from areas as diverse as energy storage¹⁴ to medical use.¹⁵⁻¹⁷ Today in the United States of America, for example, it is difficult to go a single day without direct interaction with a polymeric material; we very much depend on the use of polymers to sustain our technologies and our lifestyles. But despite the clear need for and the tremendous benefits provided by polymeric materials, their production and use are problematic, mainly in the form of massive plastic waste,¹⁸ greenhouse gas emissions associated with plastic production and incineration,^{19,20} and enormous economic losses associated with single-use plastic products.²¹ These drawbacks pollute our world and contribute to climate change, which has the potential

to drastically affect human life on Earth.²² In fact, plastic pollution is so pervasive that it is being considered as a geological indicator for the Anthropocene, which is considered by many geologists to be the current geological epoch.¹⁰

Plastic use is likely here to stay, but the way we make, use, and dispose of these materials can be changed and made sustainable.²² Following the 1987 definition set forth by the United Nations World Commission on Environment and Development, sustainable products must “meets the needs of the present without compromising the ability of future generations to meet their own needs.”²³ Currently, about 8% of oil production worldwide is used for the generation of plastics, with an estimated 20% to be utilized by 2050.^{11,20} As oil reserves are finite,¹⁹ it is clear that this method of plastic generation is not sustainable and that we need to switch to alternative feedstock chemicals for sustainable polymer production. In particular, fermentation is now being explored for the production of a variety of different monomers from biomass.²⁴ Since production of biomass such as corn or rice can in theory be sustained indefinitely, biomass provides an attractive alternative to petroleum resources.

Though the generation of polymers from biomass is an important component of sustainability, evaluating true sustainability is a complex task requiring life-cycle analysis.^{25,26} In particular, the fate of plastics once they have been created and used is an important factor when considering true sustainability; only about 10% of plastic waste produced between 1950 and 2015 has been recycled, with another 10% being incinerated, and the remaining 80% discarded in either a landfill or the natural environment.¹⁸ Discarding plastics in a landfill or the environment is not a sustainable solution, especially due to the massive economic loss associated with single-use

plastics²³ and the large negative affect this plastic pollution can have on marine wildlife and the entire food chain.²⁷ For this reason, the recycling of plastic waste is a critical issue.²⁸ In particular, the chemical recycling of plastics via depolymerization to their monomers is being explored for compounds like poly(methyl methacrylate)²⁹ or poly(methylene butyrolactone)³⁰ and is a potentially sustainable recycling solution, though the process of depolymerization can be energetically costly²⁹ and low-temperature, catalytic methods should be explored.³¹ An alternative approach to recycling is to continue to design polymers in such a way that they are readily degradable under ambient conditions.³²

The production of renewable polymers has received considerable attention in recent decades, and biorenewable polymers like the compostable poly(lactic acid) (PLA) are beginning to be used as disposable plastic cups or durable textiles in place of their petroleum counterparts such as polystyrene or poly(ethylene terephthalate).^{22,33,34} Another biorenewable polymer that has garnered the interest of polymer scientists is poly(itaconic acid) (PIA), which is produced for ~\$3/kg by the company Itaconix through a robust uncontrolled radical polymerization of itaconic acid (IA).⁵ Importantly, PIA has been shown to be an excellent surrogate for petroleum-based poly(acrylic acid) for applications such as super-absorbents and dispersants,³⁵ and the work done by Itaconix demonstrates that IA can be used as a feedstock chemical for the production of biorenewable alternatives to petroleum-based polymers.

IA, first generated by Baup in 1836 by the decarboxylative distillation of citric acid,³⁶ has considerable potential to lower society's dependence on oil for the production of plastics. Currently, IA is produced through a robust fermentation pathway

from biomass using the fungus *Aspergillus terreus*.^{37,38} Named in 2004 by the U.S. Department of Energy as one of the “top value added chemicals from biomass,” over 80,000 tons of IA is now produced each year for just \$2/kg.^{37–39} Recently, numerous IA-based materials have been explored, including detergents, bleaches, sequestrants, malodour reductants, coatings, and paints, demonstrating that the explosion of interest in IA in recent years is genuine and an indication that “itaconic acid might be a bulk chemical waiting to happen.”⁴⁰

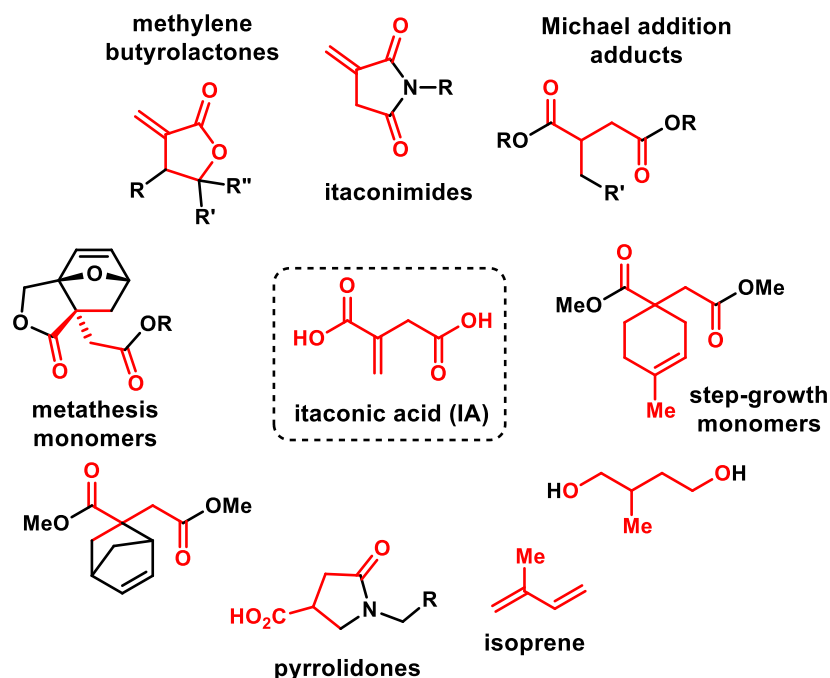


Figure 1.1. A wide variety of monomers are accessible from IA for polymerization. IA-derived atoms are marked in red.

Numerous efforts have been made in the transformation of IA into polymeric materials for a host of applications, and a full analysis of this field is beyond the scope of this review. In particular, the polymerization of itaconic acid, its dialkyl esters, or itaconic anhydride,^{41–57} as well as the generation of IA-based crosslinked resins,^{58,59} will not be the focus of this work. Instead, we will review the synthesis of monomers and

polymers derived from IA, including itaconimides, α -methylene- γ -butyrolactones, pyrrolidones, and other novel monomers based on IA containing phosphorous, fluorine, or used in metathesis or step-growth polymerizations (Figure 1.1).

ITACONIMIDES

Itaconimides (II) are a class of well-known imides derived from IA. They are typically accessed from itaconic anhydride by the addition of an amine to generate an itaconamic acid. Cyclization to the imide is then achieved, typically by refluxing with base and acetic anhydride and often with concomitant isomerization to a citraconimide (CI) byproduct (Figure 1.2a). The synthesis of a wide variety of II derivatives by this general method has been well documented.⁶⁰ Furthermore, the anionic or uncontrolled radical polymerizations of II derivatives have been well studied, and a wealth of information on the kinetics of homo- and copolymerization is available for the various II derivatives (Figure 1.2b).⁶⁰ More recently, the controlled free radical polymerization (CRP) of a number of N-phenyl substituted II derivatives has been investigated using both atom transfer radical polymerization (ATRP) and reversible addition–fragmentation chain-transfer (RAFT) polymerization, which will be subject of this discussion (Figure 1.2c). These polymers exhibit extremely high glass transition temperatures (T_{gs} range from 200 to 300 °C) and the development of controlled polymerizations of II derivatives allows for their incorporation into more complex architectures for applications in high-temperature uses and thermoplastics.⁶⁰

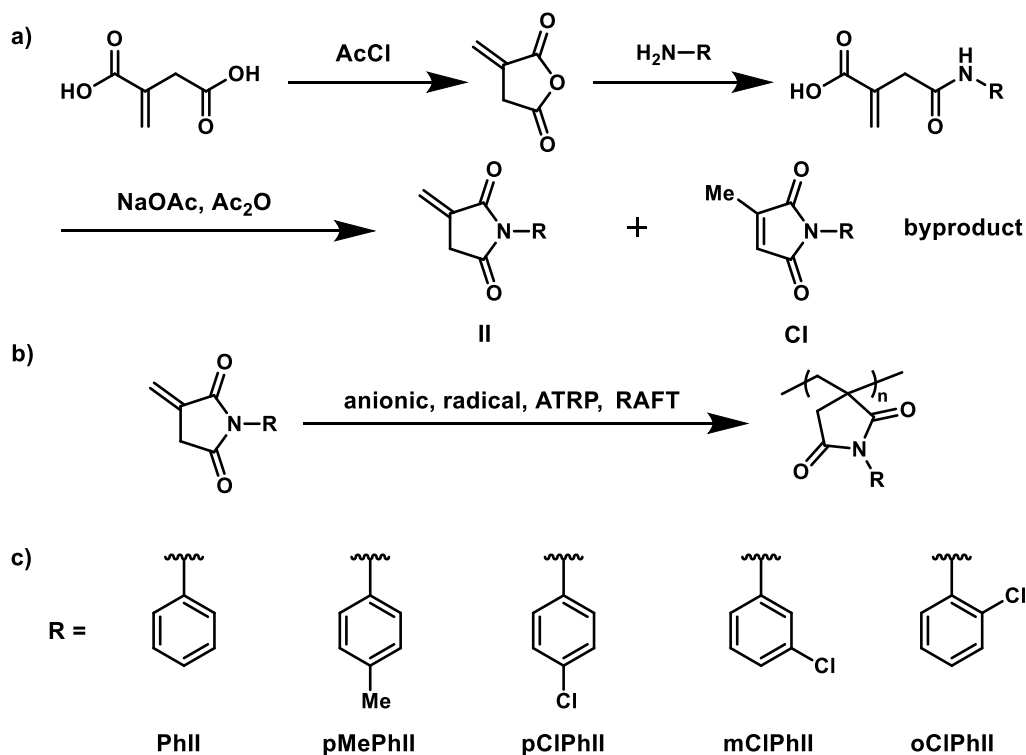


Figure 1.2. a) Synthesis of II derivatives from IA; b) general scheme for the polymerization of an II derivative; c) R groups of various II derivatives explored in CRP.

Early work on the CRP of II derivatives using ATRP was undertaken by Choudhary and co-workers in 2005, who employed three different ATRP systems for the formation of random or block copolymers (Table 1.1, entries 1 – 3).⁶¹ Using a “reverse” ATRP system composed of azobisisobutyronitrile (AIBN), $\text{FeCl}_3 \cdot 6\text{H}_2\text{O}$, and PPh_3 to generate the initiator and catalyst species *in situ*,⁶² the authors polymerized MMA at 85 °C in PhH to > 95% conversion in 4 h. From here, various II derivatives were added directly to the polymerization mixture containing PMMA-Cl and left to react at 85 °C for up to 9 d (Table 1.1, entry 1). Under these conditions, block polymers were obtained in one pot with low molar incorporation of II, ranging from 3 to 6% for PhII and 3 to 4% for pMePhII (determined by ^1H and ^{13}C NMR and elemental analysis).

No polymerization was observed for oClPhII, mClPhII, or pClPhII, even after 7 days of stirring. Alternatively, the PMMA-Cl macroinitiator could be isolated and then mixed with a CuBr/2,2'-bipyridine (bpy) catalyst system in PhMe at 85 °C to polymerize PhII, pMePhII, pClPhII, mClPhII, or oClPhII (Table 1.1, entry 2). While a clear unimodal shift in the size exclusion chromatography (SEC) trace to higher molar mass polymer was observed for the chain extension of PMMA-Cl with pMePhII, the number-average molar masses of the resulting materials indicated the formation of only oligomeric II blocks (1 – 2 kg/mol). The authors postulated that a combination of isomerization of RII to RCI during the polymerization (20 – 30% conversion of RII to RCI was observed for R = Ph, pClPh, mClPh, and pMePh when RII was heated at 85 °C in PhMe for 4 days) and termination via chain-transfer to monomer was the cause of the low molar mass II blocks following chain extension. Finally, copolymerization of MMA with pPhClII using CuBr/bpy catalyzed ATRP with a tosyl chloride (TsCl) initiator was performed in PhMe at 85 °C for 24 h and resulted in a random copolymer with an M_n of 12 kg/mol and a dispersity of 1.43 (Table 1.1, entry 3). For the block polymers, separate T_g s of both the PMMA (114 – 124 °C) and PRII blocks (211 – 227 °C) were observed, indicating microphase separation of the two polymer phases. Conversely, the random copolymer PMMA-*r*-pClPhII showed a single T_g of 143 °C, indicating that a single polymer phase was present. All copolymers showed thermal stabilities up to *ca.* 245 °C, as measured by thermogravimetric analysis (TGA).

The next report of the polymerization of PhII using ATRP came almost a decade later by Chauhan, Behera, and co-workers, who performed copolymerizations of PhII with MMA using a newly synthesized, II-based small molecule initiator.⁶³ The authors

postulated that using an initiator with structural similarity to the monomer could result in similar initiator and monomer reactivity, leading to an increase in control over the polymerization process when coupled with rapid initiation. To obtain their II-derived initiator, the authors subjected PhII or PhCI to bromination with HBr in the absence of any radical source to give the Markovnikov product, PhII-HBr (Figure 1.3). Other alkyl-bromides based on an II were synthesized but were not utilized experimentally as initiators in the copolymerization of PhII and MMA.

Table 1.1. ATRP Systems for the Polymerization of RII.

Entry	Initiator	Catalyst System	Polymer	R
1 ⁶¹	PMMA-Cl	FeCl ₃ ·6H ₂ O/PPh ₃	PMMA- <i>b</i> -PRII	Ph, pMePh
2 ⁶¹	PMMA-Cl	CuBr/bpy	PMMA- <i>b</i> -PRII	Ph, pMePh, pClPh, mClPh, oClPh
3 ⁶¹	TsCl	CuBr/bpy	PMMA- <i>r</i> -PRII	pClPh
4 ⁶³	PhII-HBr	CuBr ₂ /Sn(EH) ₂ /bpy	PMMA- <i>r</i> -PRII	Ph
5 ⁶⁴	EBrPA/AIBN	FeBr ₃ (IDipp)	PRII	Ph
6 ⁶⁴	EBrPA/AIBN	FeBr ₃ (IDipp)	PS-PRII ^a	Ph
7 ⁶⁵	EBiB	CuBr/bpy	PMMA- <i>r</i> -PRII	Ph, pMePh, pClPh, pOMePh
8 ⁶⁵	(PMMA- <i>r</i> -PRII)-Br	CuBr ₂ /Sn(EH) ₂ /bpy	(PMMA- <i>r</i> -PRII)- <i>b</i> -PRII	Ph, pMePh, pClPh, pOMePh
9 ⁶⁶	Br-PL-Br	CuCl/bpy	PRII-PL-PRII	Ph

^aThe architecture of the copolymer varied based on the exact experimental conditions, see text.

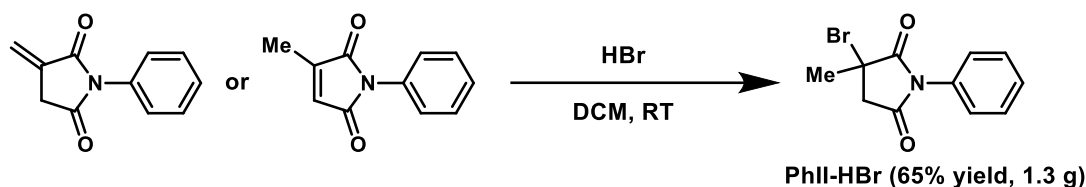


Figure 1.3. The synthesis of the II-based ATRP initiators explored by Chauhan, Behera, and co-workers.⁶³

The authors explored the copolymerization of PhII and MMA with PhII-HBr using activators regenerated by electron transfer (ARGET) ATRP in order to limit oxygen sensitivity known to occur under traditional ATRP methods.⁶² Thus, the copolymerization of PhII with MMA using CuBr₂, bpy, and tin(II) ethylhexanoate (Sn(EH)₂) as the catalyst system with PhII-HBr as an initiator was performed (Table 1.1, entry 4). The authors reported a linear increase in conversion of the comonomer mixture with time, indicating that PhII-HBr can initiate the polymerization of a mixture of PhII and MMA. Under these conditions, PMMA-*r*-PPhII was obtained. When the reaction was monitored over time, PMMA-*r*-PPhII grew in M_n from 3.3 to 13.2 kg/mol with dispersities ranging from 1.30 to 1.56. Computational studies of PhII-HBr and a variety of other structurally similar compounds were also performed, in order to gain insight into their performance as initiators. Notably, the computationally determined K_{ATRP} value of PhII-HBr (1.4×10^{-9}) agreed with the experimentally determined value, highlighting the accuracy of these computational studies.

The first controlled ATRP homopolymerization of PhII was reported by Okada and Matyjaszewski, who explored the homo- and copolymerizations of PhII and styrene (St) (Table 1.1, entries 5 and 6).⁶⁴ Initial attempts made for the homopolymerization of PhII using classical ATRP catalyzed by a CuBr/CuBr₂/amine system resulted in no or uncontrolled polymerization, which was attributed to the base-catalyzed isomerization

of PhII to PhCI (~ 50% conversion for this transformation was observed in 3 h at 60 °C in the presence of N,N,N',N'',N''-pentamethyldiethylenetriamine (PMDETA)). To avoid this side-reaction, the authors utilized initiators for continuous activator regeneration (ICAR) ATRP⁶² with a FeBr₃(IDipp) catalyst system, which would require no amine base (Figure 1.4 and Table 1.1, entry 5). With ethyl α-bromophenyl acetate (EBrPA) and AIBN as initiators and anisole as a solvent, PhII was polymerized at 60 °C. After 24 h, 69% of PhII was converted to polymer, with an $M_{n,exp}$ of 11.9 kg/mol ($M_{n,theo}$ = 13.2 kg/mol) and a dispersity of 1.52. Notably, the system showed first-order kinetics (Figure 1.5a), with the number-average molar mass increasing linearly with conversion (Figure 1.5b) and a unimodal shift to higher molar mass between 5 and 24 h. The slightly broad dispersity and small shoulder in the SEC trace may indicate the presence of some termination events (Figure 1.5c). The PhII homopolymer produced by this method showed a T_g of 219 °C by differential scanning calorimetry (DSC) with no exothermic peaks associated with degradation observed up to 280 °C.



Figure 1.4. Structure of the FeBr₃(IDipp) catalyst and EBrPA initiator used for the homopolymerization of PhII.⁶⁴

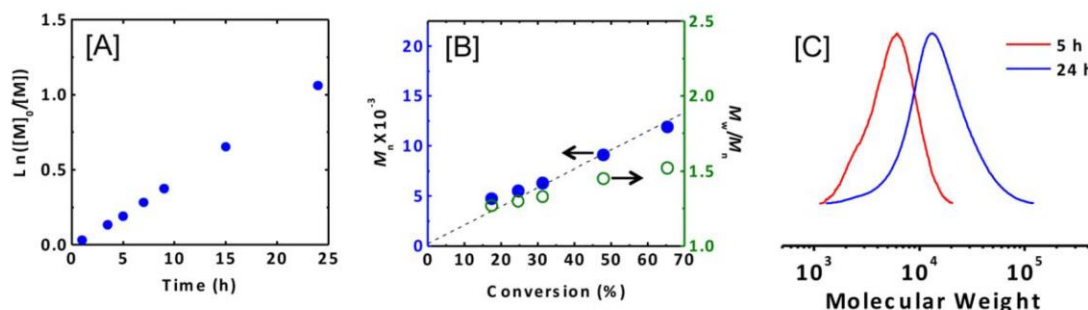


Figure 1.5. Polymerization of PhII using $\text{FeBr}_3(\text{IDipp})$. A) Kinetic plots of $\ln([M]_0/[M])$ vs time; b) Plot of M_n and \bar{D} vs conversion; c) SEC traces using calibration based on linear polystyrene standards; reaction conditions: $[\text{PhII}]:[\text{EBrPA}]:[\text{AIBN}]:[\text{FeBr}_3(\text{IDipp})] = 100:1.0:1.5:0.05$, $[\text{PhII}] = 4.7 \text{ M}$ in 50% v/v of anisole at 60°C for 24 h. Copied with permission from the original manuscript by Okada and Matyjaszewski.⁶⁴

Using the same conditions employed for the homopolymerization of PhII, the copolymerization of PhII with St was performed (Table 1.1, entry 6). The reactivity ratios of PhII and St are known to be less than 1 in uncontrolled free radical polymerization, resulting in an alternating copolymer.^{60,67} Reactivity ratios less than 1 were also determined for the copolymerization of PhII and St in this ATRP system, and so an alternating microstructure was expected for the copolymers. After 24 h of polymerization, conversions between 73 and 99% were obtained, generating polymers with number-average molar masses between 6.4 and 20.2 kg/mol after 72 h. In most cases good agreement with $M_{n,\text{theo}}$ was observed, with moderate to broad dispersities (1.55 to 1.87). Interestingly, when the initial concentration of PhII monomer was greater than St monomer ($[\text{PhII}]_0 > [\text{St}]_0$), the polymerization rate of both comonomers was roughly equal throughout the polymerization, whereas when $[\text{St}]_0 > [\text{PhII}]_0$, the rate of polymerization of styrene greatly increased relative to that of PhII at higher conversion ($> 40 - 60\%$). This behavior would theoretically allow for one-pot synthesis of block polymers based on PhII. Consequently, the authors reported that the synthesis of

copolymers with alternating (PS-*a*-PPhII), alternating-gradient ((PS-*a*-PPhII)-*g*-PPhII), or alternating-block ((PS-*a*-PPhII)-*b*-PPhII) could be achieved by varying $[St]_0/[PhII]_0$. DSC analysis of the copolymers obtained with varying ratios of $[St]_0/[PhII]_0$ showed either a single T_g ranging from 137 to 189 °C, indicative of an alternating or gradient copolymer with a single polymer phase, or two distinct T_g s at 104 and 162 °C, indicative of a polymer ((PS-*a*-PPhII)-*b*-PPhII) with microphase separated blocks of PS-*a*-PPhII and PS. In all cases, no exothermic peaks associated with degradation events were observed below 280 °C in the DSC trace. Notably, the high T_g s of the alternating copolymers with a single phase (between 147 and 189 °C) demonstrates the ability to copolymerize St with PhII in order to access PS-based copolymers with increased T_g s (relative to the T_g of pure PS homopolymer at ~ 107 °C).^{60,68}

More recently, Chauhan and co-workers explored the synthesis of random copolymers of MMA and II, as well as block polymers of the structure (PMMA-*r*-PIt)-*b*-PIt using ARGET ATRP (Table 1.1, entries 7 and 8).⁶⁵ First, random copolymers were obtained by the polymerization of MMA and II using ethyl α -bromoisobutyrate (EBiB) initiator and a CuBr/bpy catalyst system in anisole at 80 °C (entry 7), generating polymers of 4.1 to 5.7 kg/mol (Table 1.2) with dispersities of 1.2 – 1.4 after 45 h. Following isolation, (PMMA-*r*-PIt)-Br was chain-extended using a CuBr₂/bpy/Sn(EH)₂ catalyst system in anisole at 80 °C, leading to block copolymers with a large increase in molar mass and dispersities of *ca.* 1.3 – 1.4 (Table 1.1, entry 8, and Table 1.2). In all cases the observed $M_{n,exp}$ matched up well with $M_{n,theo}$. Interestingly, the authors observed a trend between molar mass and phenyl substituent in the II derivative, where

the highest molar mass polymer was obtained from pOMePhII and the lowest molar mass polymer was obtained from pClPhII. This trend was attributed to the stability of the free radical chain end; more electron rich substituents such as pOMePh were able to better stabilize the chain-end, leading to higher molar masses, whereas electron poor substituents resulted in a less stabilized chain-end and lower molar mass.

Using DSC and TGA, the thermal properties of these polymers were studied. Single T_g s ranging from 160 to 180 °C (Table 1.2) were observed for the random copolymer macroinitiators, with higher T_g s observed for the II derivatives with more electron rich substituents. The authors attributed this trend to the increase in polarity and rigidity of the polymer chains with increasing electron density in the phenyl ring. These high T_g s demonstrate the ability to copolymerize MMA with II derivatives in order to access MMA-based polymers with increased T_g s relative to the T_g of pure PMMA homopolymer (~ 105 °C),⁶⁹ as observed for PS-PPhII copolymers.^{60,64} For the block polymers, two T_g s are observed, indicative of microphase separation. The first glass transition temperature ($T_{g,1}$) matches closely with the T_g of the corresponding macroinitiator, while the second ($T_{g,2}$) corresponds to the II block. These values vary from 242 to 265 °C and increased with increasing electron density of the II derivative. The random copolymer macroinitiators showed thermal stabilities up to 300 °C with a single step-degradation process, while the block polymers showed thermal stabilities up to 330 °C with a two-step degradation process.

Table 1.2. Physiochemical Properties of RII-based Polymers.

(PMMA- <i>r</i> -PRII)-Br			(PMMA- <i>r</i> -PRII)- <i>b</i> -PRII			
R	M_n (kg/mol)	T_g (°C)	$M_{n,exp}$ (kg/mol)	$M_{n,theo}$ (kg/mol)	$T_{g,1}$ (°C)	$T_{g,2}$ (°C)
Ph	4.2	170	93	94	179	250
pMePh	4.9	175	96	97	182	258
pOMePh	5.7	180	100	100	180	265
pClPh	4.1	160	80	81	181	242

Significant progress in the CRP of II was realized in 2014 when Kamigaito, Satoh, and co-workers utilized RAFT for the synthesis of triblock polymers based on dialkyl itaconate mid blocks chain-extended with II hard blocks.⁷⁰ First, the authors developed a RAFT polymerization of RII (R = Ph or pMePh) (Figure 1.6a) with AIBN and various chain transfer agents (CTAs). Under these conditions, II could be effectively polymerized in a controlled fashion using monofunctional CTA-1 and CTA-2 (Figure 1.6c) at 50 or 60 °C in 1,4-dioxane (1,4-DO) using AIBN as an initiator. High conversions (~95%) were obtained after > 150 h of polymerization with M_n s between 8.7 and 17.2 kg/mol, in agreement with theoretical M_n s, with narrow dispersities between 1.29 and 1.50 observed in all cases. Additionally, ¹H NMR revealed successful incorporation of the CTA into the polymer chain, highlighting the chain-end fidelity of this system. T_g s of these homopolymers determined by DSC analysis were between 235 and 245 °C for PPhII and 226 °C for PpMePhII, while TGA showed thermal stabilities for these polymers up to 300 °C. The RAFT polymerization of dialkyl itaconates was

also explored; using a monofunctional (CTA-3) or telechelic (CTA-4) CTA, dibutyl itaconate (BDI) or bis((2-ethyl hexyl) itaconate) (DEHI) were controllably polymerized in bulk at 20 °C using the low temperature V-70 initiator, though the polymerizations were slow (70 – 170 h required for 40 – 60 % conversion using CTA-4) and were run to only low conversion (20 – 60%) to preserve the chain-end fidelity. Importantly, these polymers showed T_{gs} of 12 °C for poly(DBI) (PBDI) and – 28 °C for poly(DEHI) (PDEHI), making them good candidates as mid-blocks for triblock polymer thermoplastics elastomers that could be used in RT applications.

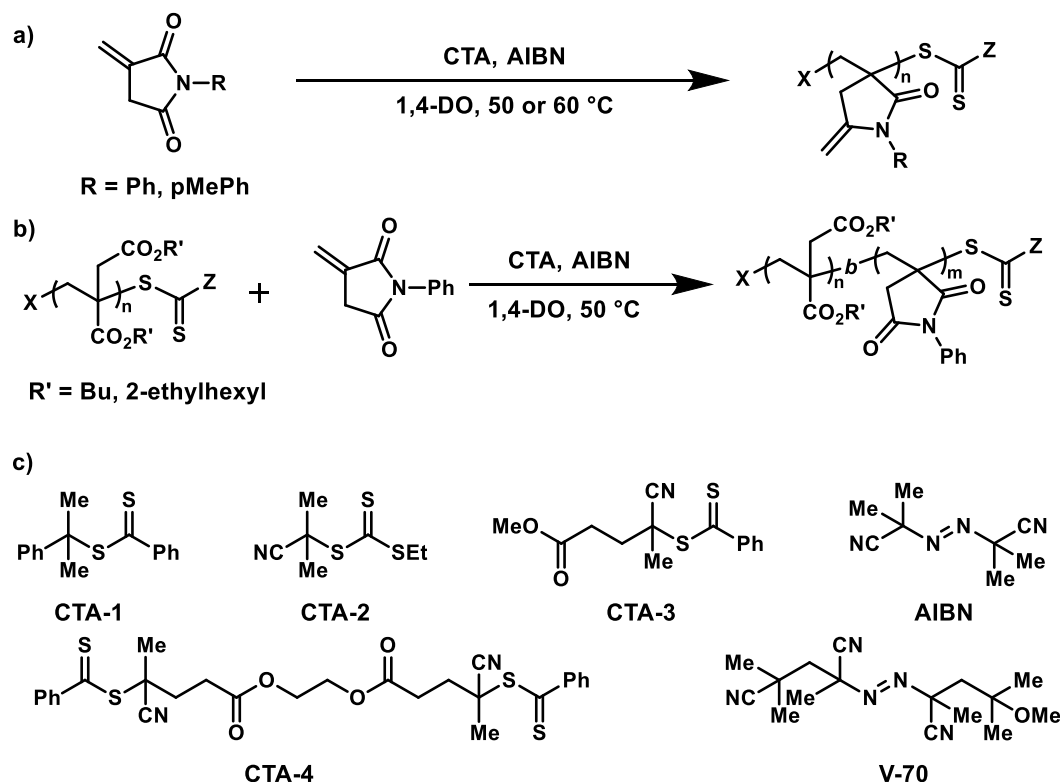


Figure 1.6. a) RAFT polymerization of II derivatives; b) RAFT polymerization of PhII from a telechelic poly(diester itaconate) macroinitiator to generate triblock polymer.

Chain extension of a monofunctional macroinitiator of poly(dibutyl itaconate) synthesized from CTA-3 with PhII (Figure 1.6b) generated a diblock polymer with an

M_n of 10.8 kg/mol and a narrow dispersity of 1.26, demonstrating that the dialkyl itaconate macroinitiators obtained by RAFT were effective macroinitiators. Additionally, this block polymer showed two T_g s at 17 and 219 °C for the dialkyl itaconate and PhII blocks, respectively, showing that microphase separation was obtained. Chain extension of a telechelic macroinitiator (PDBI or PDEHI) at 50 °C with AIBN generated triblock polymers with M_n s ranging from 12.0 to 67.1 kg/mol (hard block incorporation was between 27 and 60 mol%) with narrow dispersities between 1.14 a 1.20 after 19 h. Additionally, clear shifts to higher molar masses were observed in the SEC traces alongside a decrease in dispersity, indicative of the controlled nature of this process (Figure 1.7). Distinct T_g s were obtained for each block, between 204 and 241 °C for PhII and – 8 and 16 °C for the dialkyl itaconate, demonstrating microphase separation.

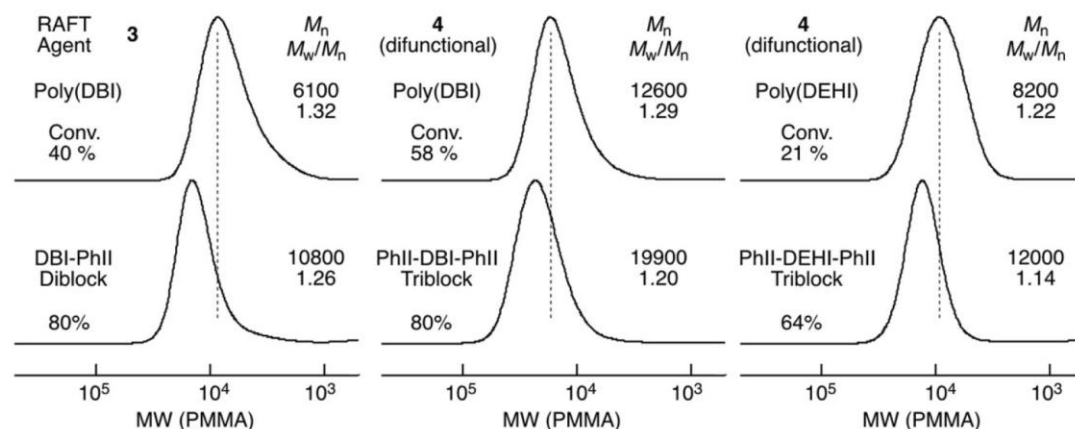


Figure 1.7. SEC curves for the chain-extension of poly(dialkyl itaconates) with PhII. SEC curves obtained in the block copolymerization from dibutyl itaconate (DBI) or bis(2-ethylhexyl) itaconate (DEHI) to PhII; RAFT agent: monofunctional dithiobenzoate (CTA-3), telechelic bis(dithiobenzoate) (CTA-4); $[M]_0:[CTA]_0:[V-70]_0 = 100:1.0:0.2$ in bulk at 20 °C for the first block; $[M]_0:[CTA]_0:[AIBN]_0 = 50:1.0:0.2$ ($[M]_0 = 1.0$ M) in 1,4-dioxane at 50 °C for the second block. Copied with permission from the original manuscript by Kamigaito and co-workers.⁷⁰

To further demonstrate the microphase separation of the soft and hard blocks of the triblocks, the authors performed shear dynamic testing (Figure 1.7a) and atomic force microscopy (AFM) analysis (Figure 1.7b). In the case of shear dynamic testing, two $\tan(\delta)$ peaks were observed for the T_g s of the hard and soft blocks, while AFM demonstrated clear phase separation of the hard and soft domains. Notably, this was the first example of both the CRP of II derivatives using RAFT and the production of a nearly 100% IA-based thermoplastic. While these materials have high hard block contents that likely prohibits elastomeric properties, the targeting of lower hard block incorporation could lead to the synthesis of nearly 100% IA-based thermoplastic elastomers.

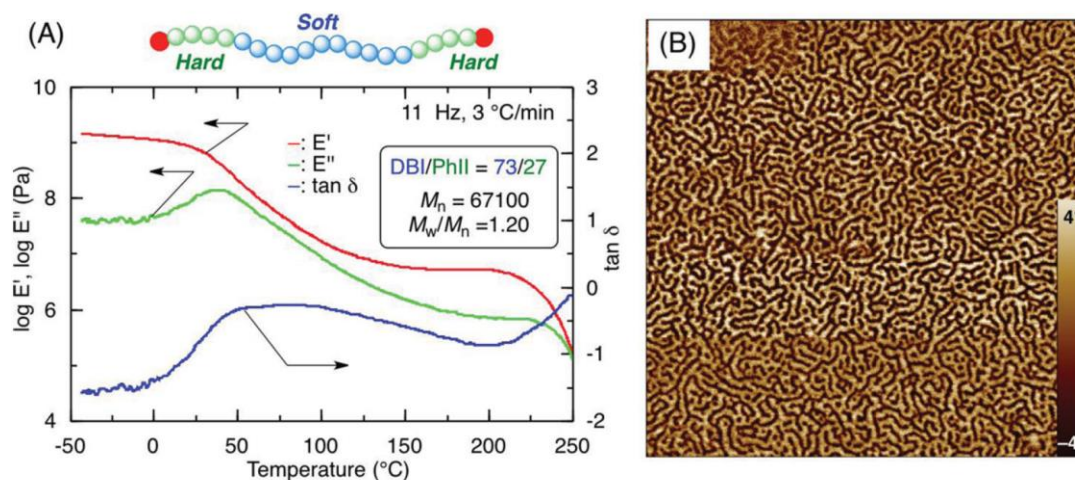


Figure 1.8. a) Dynamic tensile storage (E') and loss (E'') moduli and $\tan(\delta)$ (E''/E') as a function of temperature (heating rate: 10 °C/min; frequency 11 Hz); b) AFM phase images ($2 \times 2 \mu\text{m}$) for morphologies of the PPhII-PDBI-PPhII triblock polymer; $M_n = 67.1 \text{ kg/mol}$, $\bar{D} = 1.20$, DBI:PhII = 73:27 (wt%). Copied with permission from the original manuscript by Kamigaito and co-workers.⁷⁰

The most recent report of the CRP of II comes from Ren, Tao, and co-workers, who chain-extended a telechelic, lysine-derived polyester macroinitiator to give an almost 100% bio-based triblock polymer (Figure 1.9).⁶⁶ In this work, the authors utilized

1,3-dioxolane-2,4-dione derivative based on the biorenewable amino acid lysine as a monomer. From here, controlled ring-opening polymerization with 4-dimethylaminopyridine (DMAP) initiated by diethylene glycol led to a controlled polymerization process that generated a lysine-derived telechelic polyester (PL) with an M_n of 32.0 kg/mol and narrow dispersity of 1.20. M_n grew linearly with conversion (in good agreement with $M_{n,theo}$) and narrow dispersities were observed throughout the polymerization. Importantly, ^1H NMR and matrix-assisted laser desorption/ionization-time of flight (MALDI-TOF) indicated the presence of alcohol chain-ends, and chain-end functionalization using alpha-bromo isobutyryl bromide and triethyl amine installed an ATRP alkyl-bromide initiator on the chain end, whose presence was confirmed by ^{13}C NMR analysis. ATRP using a $\text{CuCl}/\text{CuCl}_2/\text{bpy}$ system was then employed for the chain-extension of Br-PL-Br with PhII at 100 °C in DMF for 160 h (Table 1.1, entry 9). ^1H NMR demonstrated the incorporation of the PhII segments with M_n s of 7.0, 10.0, or 14.0 kg/mol (or 12, 17, and 25 mol% PhII incorporation, respectively). Furthermore, SEC demonstrated clear shifts to higher molar mass for the chain extension. All polymers showed two T_g s at 5 – 7 °C and 200 – 211 °C for the soft (PL) and hard (PPhII) blocks, respectively, demonstrating clear microphase separation with potential for elastomeric properties between these two T_g s. Finally, TGA demonstrated thermal stability up to 240 °C, above which 5 wt% was observed for all three triblocks.

Notably, the tensile properties of these materials were determined (Table 1.3, entries 1, 5, 11), the first example of such a measurement for an II-based triblock. At 12 mol% PhII incorporation, mechanical failure was not observed, whereas the 17 and 25 mol% PhII triblocks showed high strain at break values (500 – 700%) and tensile

strengths at break of 10 – 15 MP. Additionally, higher Young's moduli were observed with increasing molar incorporation of PPhII (6 to 37 MPa). This trend is consistent with stiffer, stronger, and less flexible materials expected at higher molar incorporation of hard block. Notably, these triblock polymers show the highest tensile strength compared with other known triblocks based on IA (Table 1.3). Notably, these properties are also better or comparable to other biomass-sourced triblock polymers such as poly(γ -methyl- α -methylene- γ -butyrolactone)-polymenthide-poly(γ -methyl- α -methylene- γ -butyrolactone) (PMeMBL-PM-PMeMBL),⁷¹ PLA-PM-PLA,^{71–73} or poly(γ -methyl- ε -caprolactone)-P(L)LA- poly(γ -methyl- ε -caprolactone) (P γ MCL-P(L)LA-P γ MCL) (Table 1.3).⁷⁴

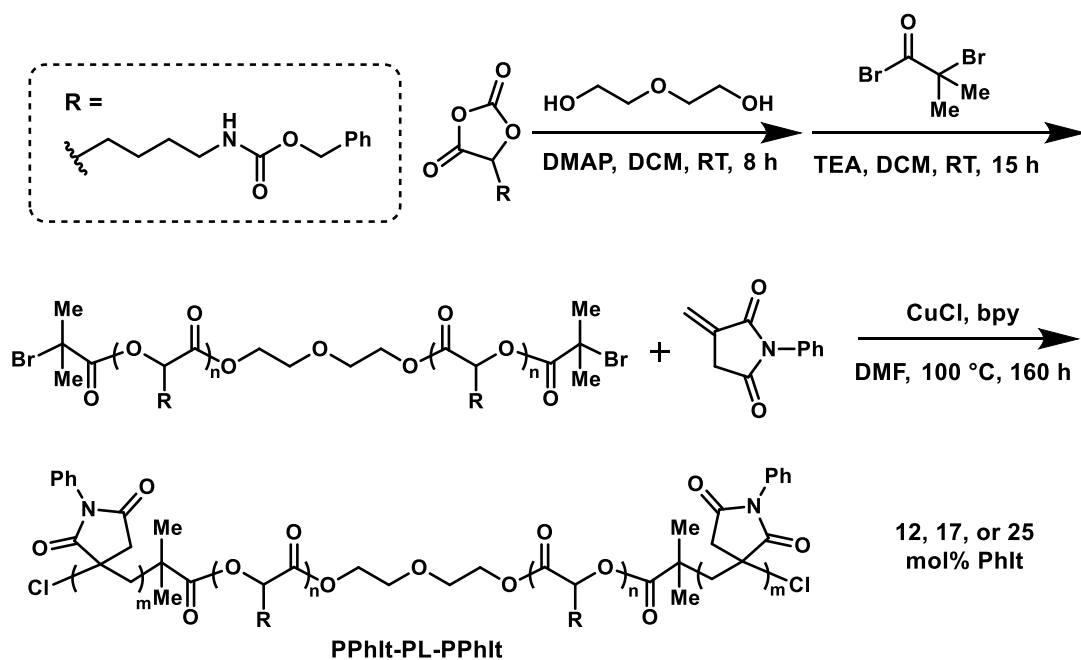


Figure 1.9. Synthesis of PhII based triblock PPhII-PL-PPhII.

Overall, significant progress has been made in the CRP of II derivatives and their incorporation as hard blocks into triblock polymer thermoplastics. Notably, ATRP

and RAFT systems have been established that allow for the controlled homopolymerization of II derivatives, while the copolymerization of II derivatives with MMA and St, as well as the synthesis of architecturally complex materials such as diblock and triblock polymers, has been explored. Future advances in the utilization of II derivatives as biorenewable and high-performance hard block components in triblock polymer thermoplastics or pressure-sensitive adhesives, as well as the CRP of other non-aromatic II derivatives, are expected.

METHYLENE BUTYROLACTONES

α -Methylene- γ -butyrolactone (MBL or Tulipalin A) is a well-known cyclic surrogate of MMA that has been extensively studied for its polymerization to poly(MBL) (PMBL).^{75,76} Like PMMA, PMBL has desirable optical properties including a refractive index of ~ 1.5 ,^{75–78} and the rigid lactone in the PMBL repeat unit imparts an extremely high T_g for PMBL (~ 200 °C) and low solubility in common organic solvents^{75,76} relative to petroleum-derived PMMA, which possess a T_g of ~ 105 °C and good solubility in common organic solvents.⁶⁹ The increased T_g of PMBL relative to PMMA enables the use of PMBL and related polymers for high temperature applications where PMMA would be unsuitable.⁷⁹ The homo- and copolymerization of MBL and related derivatives using both uncontrolled and controlled methods has been extensively studied and will not be the focus of this review.^{75,76,80–93} Instead, highlights of recent developments in the synthesis of MBL derivatives from IA, the recent development of MBL ring-opening polymerizations (ROP), and the synthesis of MBL-based triblock polymer thermoplastics will be reviewed.

Although MBL is found in Tulip biomass, its large scale production from tulips is not practical.⁷⁸ Additionally, while significant work has been performed to generate a wide variety of MBL structures, largely from petroleum-derived starting materials,^{94,95} less attention has been given to the synthesis of MBL derivatives from IA (Figure 1.10). The first example of such a transformation came from Fetizon and co-workers in 1975.⁹⁶ By reducing dimethyl itaconate (DMI), which can be accessed from the Fischer esterification of IA with methanol and acid (Figure 1.10, pathway A),⁹⁷ using Red-Al[®], the unsaturated 2-methylenebutane-1,4-diol, **1.1**, was accessed. Subsequent oxidative cyclization with Ag₂CO₃ on celite[®] then gave MBL in 80% yield (pathway B). Next, Santelli and co-workers demonstrated that allylation of itaconic anhydride (ItAnh), which can be accessed by refluxing IA with catalytic acetyl chloride (AcCl),⁹⁸ using allyltrimethylsilane and stoichiometric TiCl₄, resulted in γ -diallyl- α -methylene- γ -butyrolactone (DAMBL, pathway C).^{99,100} The polymerization of DAMBL was then later studied by Gowda and Chen (pathway F).⁸² Of particular interest in the production of MBLs from IA was the large scale, six step synthesis of β -methyl- α -methylene- γ -butyrolactone (β -MeMBL) from IA reported by Gowda and Chen in 2014 (pathway D), which demonstrated the potential of IA as a chemical feedstock for industrially relevant transformations to green monomers.¹⁰¹ Starting from IA, β -monomethyl itaconate (β -MMI) was synthesized in 80% yield from the selective esterification of IA using AcCl and methanol. From here, olefin-reduction with HCO₂NH₄ gave the saturated β -MMI analogue, **1.2**, in high yield (95%), followed by selective reduction of the carboxylic acid using BH₃SM₂ to give **1.3** in 91% yield. Cyclization then produced the

corresponding lactone (71% yield), **1.4**, upon which a methylene group could be installed using chemistry previously utilized for the synthesis of MBL from γ -butyrolactone (γ -BL).⁹⁵ This produces β -MeMBL in high yield (90%) with an overall yield of 53% from IA. Polymerizations of this monomer have also been reported by Cui, Chen, and co-workers (pathway F).¹⁰² Most recently, Fors and co-workers reported the synthesis of MBL in 42% isolated yield through reduction and cyclization of β -MMI using a method similar to one claimed in a 1992 patent by Yokota and Hirabayashi.^{103,104} Alternatively, when MeMgCl was utilized as a reducing agent, up to 10 g of Me₂MBL, previously unaccessed from IA, could be generated in 39% isolated yield.¹⁰³ Both MBL and Me₂MBL were then shown to be amenable to CRP using RAFT polymerization (pathway F).¹⁰³ Finally, anions of IA analogues have been utilized by Oyler and Carlson to generate carboxylic acid functionalized MBL derivatives, though to our knowledge no reports have been made regarding their polymerization.^{105,106}

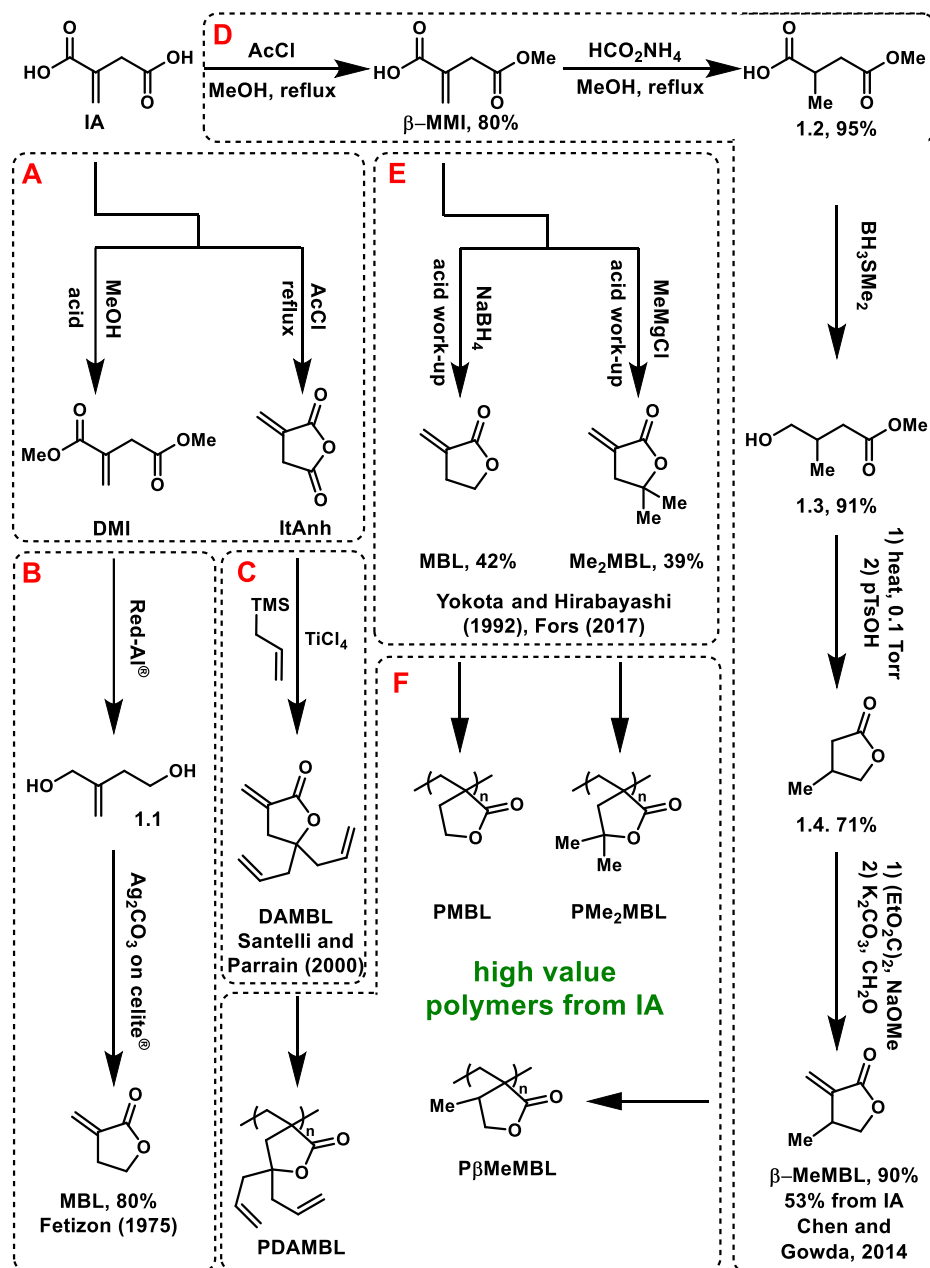


Figure 1.10. Synthesis of MBL and related derivatives from IA. Pathway A: Fisher esterification of IA with MeOH and acid produces dimethyl itaconate (DMI), while refluxing IA with acetyl chloride (AcCl) produces itaconic anhydride (ItAnh). Pathway B: Reduction of DMI with sodium bis(2-methoxyethoxy)aluminium hydride (Red-Al[®]) gives the unsaturated 2-methylene-1,4-butanediol (**1.1**). Oxidative cyclization of **1.1** with Ag₂CO₃ on celite[®] then produces MBL. Pathway C: allylation of ItAnh allyltrimethylsilane produces DAMBL. Pathway D: The six-step synthesis of β-MeMBL. Pathway E: Reduction of β-MMI with NaBH₄ to produce MBL or with MeMgCl to produce Me₂MBL. Pathway F: Polymerization of MBL, Me₂MBL, β-MeMBL, or DAMBL generates structurally varied polymers from IA.

Taking advantage of MBL as a biorenewable, high T_g monomer, researchers have incorporated it as a hard block in triblock polymers. The first synthesis of triblocks based on MBL was reported by Mosnáček and Matyjaszewski in 2008.⁸⁶ Using ATRP, butyl acrylate (BA) was controllably polymerized to give a telechelic Br-poly(BA)-Br (Br-PBA-Br) macroinitiators. Chain-extension of Br-PBA-Br using a CuCl/CuCl₂/bpy system in DMF at 50 °C (4 – 22 h) resulted in PMBL-PBA-PMBL triblock polymers with M_n s between 32 and 62 kg/mol and narrow dispersities (1.09 – 1.12). Uniform shifts of the SEC traces to higher molar mass from the macroinitiator and linear growth of M_n with conversion were also observed, indicative of a controlled polymerization (Figure 1.11). Notably, differences between theoretical and experimental M_n values were attributed to the use of PS standards for M_n determination with a refractive index detector, whereas the $M_{n,NMR}$ matched well with the theoretical value.

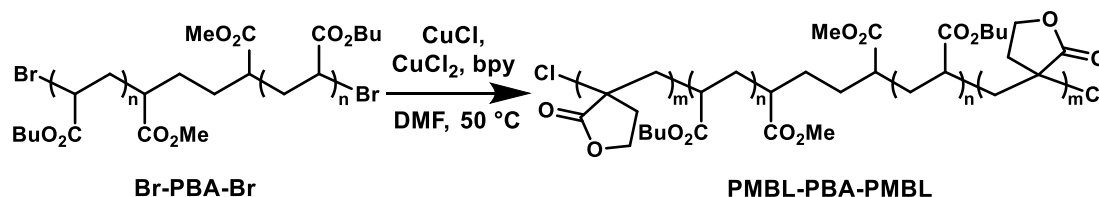



Figure 1.11. Chain extension of a Br-PBA-Br macroinitiator to PMBL-PBA-PMBL

The physiochemical properties of the PMBL-PBA-PMBL triblock were subsequently studied in a follow-up paper.¹⁰⁷ Specifically, the authors prepared a variety of triblocks with M_n s ranging from 30 to 62 kg/mol (8 to 36 mol% MBL incorporation, see Table 1.3 entries 2, 6, 7, and 12). AFM and small-angle X-ray scattering (SAXS) measurements of the triblock polymers demonstrated phase separated morphologies of cylindrical or spherical hard block domains arranged in the soft PBA matrix. The effects of thermal annealing were studied on these samples, and PMBL-PBA-PMBL (M_n s of

30 – 40 kg/mol at 16, 24, or 36 mol% MBL incorporation) showed better ordering after heating at 150 °C for 1 h. Both DSC and dynamic mechanical analysis (DMA) also showed two distinct glass transitions at 50 and 195 °C corresponding to the PBA and PMBL phases, respectively, in support of microphase separation. Thermal stabilities at temperatures up to 300 °C were observed for these polymers. Finally, tensile testing was performed, and samples showed low elongations at break between 40 and 100%, tensile strengths at break between 0.1 and 1.9 MPa, and Young's moduli between 0.2 and 3.3 MPa. Both σ_B and E increased with increasing hard content of the triblock (Table 1.3 entries 2, 6, 7, and 12). Multicomponent block polymers with PMMA-*r*-PMBL hard blocks were also synthesized from a (PMMA-*r*-PMBL)-Br macroinitiator, which showed improved tensile properties relative to their PMBL-PBA-PMBL analogues. In a separate paper, the synthesis of star-like polymers based on PBA-*b*-PMBL were also explored by Matyjaszewski and co-workers. Notably, these materials showed improved tensile properties over their linear counterparts, and demonstrates that polymer architecture can be used to modulate physiochemical properties.¹⁰⁸

Table 1.3. Tensile Properties of Linear ABA Triblock Polymers Derived from IA or Other Renewable Resources.



hardblock (A) (high T_g or T_m)		midblock (B) (low T_g)			hard block (A) (high T_g or T_m)		
Entry	B	A	A (mol%)	E (MPa)	σ_B (MPa)	ϵ_B (%)	M_n^a (kg/mol)
1 ⁶⁶	PL	PPhII	12	6 ^b	4.3	>800	1-36-1
2 ¹⁰⁷	PBA	PMBL	8	0.2 ^c	0.1	80	2-48-2
3 ⁷³	PM	PMBL	10	0.74	3.9	>1800	3-100-3
4 ⁷⁴	P γ MCL	PLLA	13	2.2	7.8	1190	8-135-8
5 ⁶⁶	PL	PPhII	17	20 ^b	9.9	510	2-38-2
6 ¹⁰⁷	PBA	PMBL	16	0.7 ^c	0.1	40	2-28-2
7 ^{107,108}	PBA	PMBL	15	0.75 ^d	0.7	100	3-47-3
8 ⁷³	PM	PMBL	15	1.51	4.1	>1600	5-100-5
9 ⁷¹	PM	PMeMBL	14	0.53	2.2	>1600	5-100-5
10 ⁷¹⁻⁷³	PM	PLA	17	0.32	0.02	1210	6-100-6
11 ⁶⁶	PL	PPhII	25	37 ^b	15.1	470	4-39-4
12 ^{107,108}	PBA	PMBL	25	3.27 ^d	1.9	55	3-27-3
13 ⁷³	PM	PMBL	23	6.0	11	800	9-100-9
14 ⁷¹	PM	PMeMBL	24	0.62	3.5	>1600	10-100-10
15 ⁷⁴	P γ MCL	PLLA	26	4.0	31	1200	16-127-16
16 ⁷⁴	P γ MCL	PLA	26	4.8	24	1029	9-76-9
17 ⁷⁴	P γ MCL	PLLA	26	3.6	30	988	10-76-10

18 ⁷⁰	PDBI	PPhII	27	- ^e	- ^e	- ^e	7-52-7
19 ⁷³	PM	PMBL	30	17.3	13.0	730	13-100-13
20 ⁷¹⁻⁷³	PM	PLA	29	0.45	0.03	630	11-100-11
21 ⁷⁴	P _γ MCL	PLLA	40	13	35	895	12-50-12
22 ⁷⁰	PDBI	PPhII	49	- ^e	- ^e	- ^e	4-11-4
23 ¹⁰⁹	PMBMS	PMBL	50	185	7	226	5-19-5
24 ⁷¹⁻⁷³	PM	PLA	51	1.4	1.7	960	8-29-8
25 ⁷⁴	P _γ MCL	PLLA	53	18	37	786	20-50-20
26 ⁷⁰	PDEHI	PhII	60	- ^e	- ^e	- ^e	3-7-3
27 ⁷⁴	P _γ MCL	PLLA	87	1300	42	314	66-27-66

^a M_{ns} given as the $[(M_n \text{ of A})/2] - (M_n \text{ of B}) - [(M_n \text{ of A})/2]$ for each block of the linear ABA triblock. ^bEstimated from plots in ref.⁶⁶ ^cEstimated from plots in ref.¹⁰⁷ ^dCalculated in ref.⁷³ from plots in ref.^{107,108} ^eTensile properties not reported. Polymer blocks derived from an IA source are **bolded in green**. Non-IA-derived triblocks are shown for comparison.

MBL and its related analogue MeMBL were again utilized as a hard block components in triblock polymers in 2012⁷³ and 2015⁷¹ when a poly((-)-menthide) (PM) macroinitiators (Br-PM-Br) were prepared through controlled ROP and subsequent chain-end functionalization. Br-PM-Br was then chain extended with either MBL to give PMBL-PM-PMBL using a CuCl/CuCl₂/bpy system in DMF at 60 °C for 10 – 12 h, using conditions similar to those reported by Mosnáček and Matyjaszewski.⁸⁶ For all PMBL in PMBL-PM-PMBL incorporations, two glass transitions were observed at – 21 °C and 170 – 190 °C for the PM and PMBL blocks, respectively. The T_g s of the PMBL block at lower incorporation were small in the DSC trace, and the T_g of the

PMBL block was lower than that of pure high molar mass PMBL, likely a result of the low M_n of the PMBL blocks.¹⁰⁹ Similarly, chain extension of Br-PM-Br with MeMBL to give PMeMBL-PM-PMeMBL was accomplished, and the polymer showed two distinct T_g s at -26 and 210 °C, indicative of microphase separation. Additional measurements using AFM and SAXS supported the conclusion of microphase separation, and the authors postulated that both materials show disorganized spherical morphologies, similar to the cylindrical or spherical morphologies reported for PMBL-PBA-PMBL.⁸⁶ PMBL-PM-PMBL showed two-step thermal degradations at $300 - 350$ °C and $380 - 420$ °C, corresponding to the degradation of PM and PMBL, respectively.

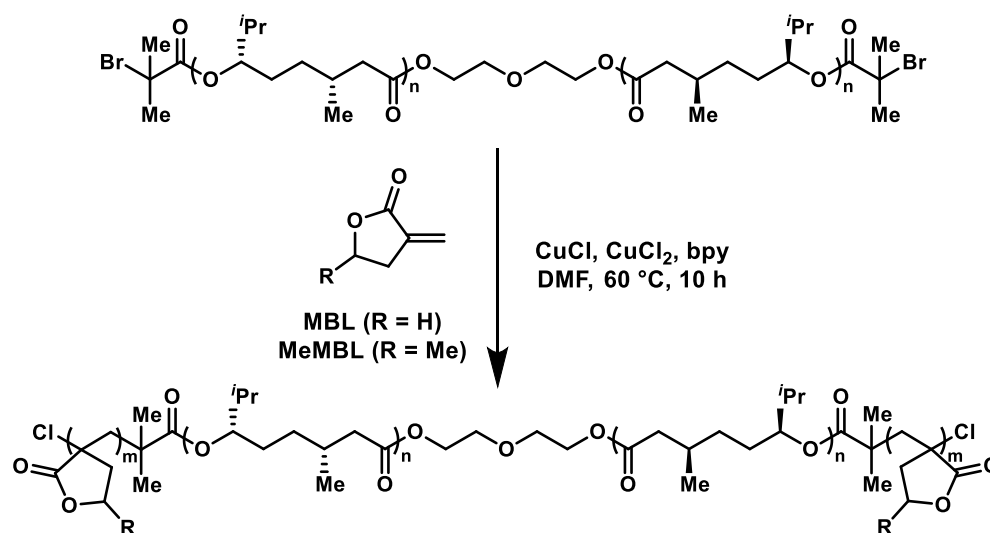


Figure 1.12. Synthesis of PRMBL-PM-PRMBL triblock polymers by ATRP chain-extension from a Br-PM-Br macroinitiator.

Tensile properties of these triblocks were fully characterized (Table 1.3, entries 3, 8, 9, 13, 14, and 19). These materials showed Young's moduli between 0.5 and 17 MPa, tensile strengths at break between 2 and 13 MPa, and strain at breaks between 630 and $> 1800\%$. In general, materials showed increased Young's moduli and tensile strengths at break, and lower elongations at break, with increasing hard block content.

Notably, the MeMBL triblocks showed lower tensile strengths than the analogous PMBL materials, but comparable or better elongations: PMBL-PM-PMBL (9-100-9 kg/mol) had E , σ_B and ϵ_B values of 6 MPa, 11 MPa, and 800%, respectively, while PMeMBL-PM-PMeMBL (10-100-10 kg/mol) had E , σ_B and ϵ_B values 0.6 MPa, 4 MPa, and > 1600 %, respectively. The effect of a single methyl group on the tensile properties of these materials is significant and demonstrates the ability to greatly alter material properties through small structural changes. Additionally, these materials show improved tensile properties over the previously explored PMBL-PBA-PMBL linear triblocks, and are comparable to both commercial thermoplastic elastomers and PLA-PM-PLA triblocks, though the tensile strengths at break in particular are lower than commercial SBS materials (10 – 40 MPa).^{71,73} Recovery of PMBL-PM-PMBL (PM) was also tested for residual strain and exhibited low values (5 – 7 %), demonstrating that excellent recovery occurred at 50% strain and that the triblock polymer was truly elastic. This was thus the first demonstrated example of a truly elastomeric triblock polymer that utilized an IA-derived hard block component. Tensile properties were also explored as a function of temperature, and though they decreased with increasing temperature, the high T_g of PMBL makes it useful for high temperature applications (> 100 °C) where commercial SBS would exhibit flow. PMeMBL-PM-PMeMBL (10-100-10) was also studied as a pressure-sensitive adhesive and in blends with rosin ester tackifiers. The resulting material exhibited a coat weight of 22 g/m², a peel adhesion of 24.8 N/25 mm ($\sigma = 0.51$), and a shear adhesion failure temperature of 150 °C. These values demonstrate the high potential of PMeMBL-PM-PMeMBL as a pressure-sensitive adhesive, especially due to its superior high temperature applications (heat-fail

temperatures for common non-crosslinked commercial PSAs are typically in the range of 90 – 125 °C).⁷¹

More recently, MBL was utilized to chain extend a polyester macroinitiator (Br-PMBMS-Br) derived from the step-growth polymerization of IA-based monomers,¹⁰⁹ representing another example of an almost 100% IA-based thermoplastic (Figure 1.13).⁷⁰ The chain-extension of Br-PMBMS-Br proceeded in a controlled fashion, giving rise to a 5-19-5 kg/mol PMBL-PMBMS-PMBL triblock polymer with a 50 mol% PMBL incorporation (Figure 1.13). Notably, SEC showed a shift to higher molar mass indicative of a controlled chain extension. Additionally, DSC analysis showed two T_g s at – 33 and 178 °C, demonstrating microphase separation of the PMBMS and PMBL phases, respectively, while thermal degradation was not observed until *ca.* 300 °C. Like the PMBL-PM-PMBL triblock prepared by Hillymer,⁷³ the slightly lower T_g of the PMBL blocks relative to homopolymer PMBL was attributed to the lower M_n of the PMBL blocks. This was corroborated by the synthesis of low molar mass PMBL samples: homopolymers of PMBL with M_n s of 2 and 6 kg/mol prepared by RAFT polymerization showed T_g s at 140 and 160 °C, respectively, demonstrating that PMBL homopolymers with small M_n s have lower T_g s.^{103,109} Finally, tensile testing was performed (Table 1.3, entry 23) demonstrating a Young's modulus of ~200 MPa, tensile strength at break of 7 MPa, and elongation at break of 230%. This tough thermoplastic showed improved stiffness and tensile strength compared to a PLA-PM-PLA^{71–73} triblock at similar hard block incorporation, though biomass-derived PLLA-P γ MCL-PLLA materials show superior properties.⁷⁴ While lower hard block incorporation of

MBL content were not explored for this copolymer system, these would potentially show elastomeric properties.

Overall, triblocks using MBL-based hard blocks showed tensile strengths at break approaching those of commercially utilized elastomers, with Young's moduli and elongations at break that vary greatly with hard block incorporation. Future studies on the generation of biomass-derived triblock polymers should explore the use of IA derivatives as both soft and hard blocks and fully characterize the tensile properties of these materials.

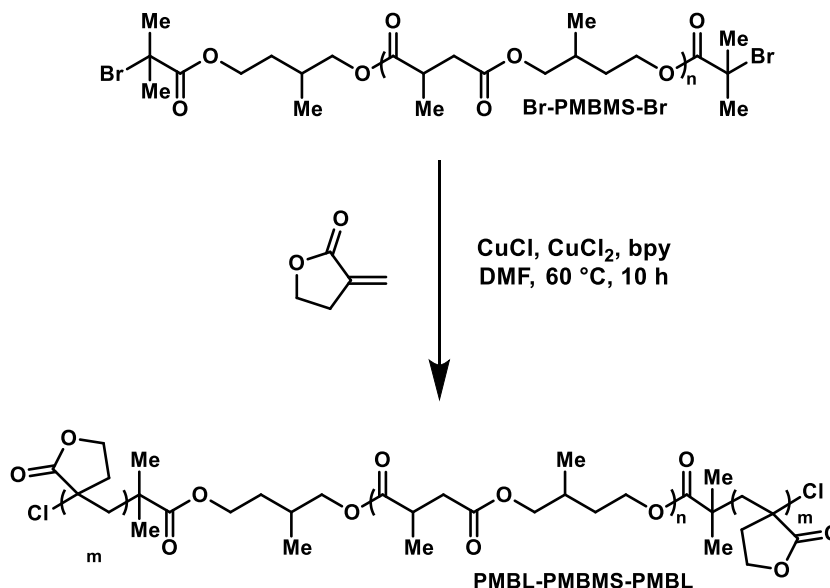


Figure 1.13. Synthesis of PMBL-PMBMS-PMBL triblock polymer by chain-extension of a Br-PMBMS-Br IA-derived polyester macroinitiator.

While the vinyl addition polymerization (VAP) of MBL to PMBL_{VAP} has been extensively explored, the ROP of MBL to give a linear polyester (PMBL_{ROP}) is a more recent accomplishment. The nonpolymerizability of five membered lactones such as MBL or γ -BL is well known to be a result of both low ring strain, or a small and negative enthalpy change (ΔH) for lactone ring-opening, coupled with a large, negative entropy

(ΔS) change for the lactone ring-opening. Combined, this leads to a process with a positive change in free energy (ΔG), making it difficult to accomplish experimentally (Equation 1.1).¹¹⁰

$$\Delta G = \Delta H - T\Delta S$$

Equation 1.1

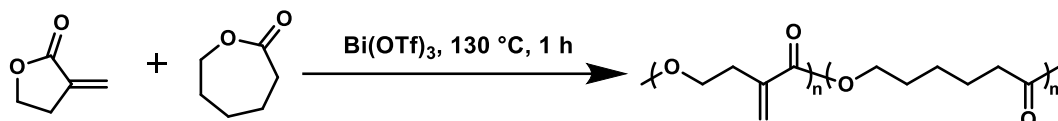


Figure 1.14. Copolymerization of MBL with ϵ -CL to give poly(ϵ -CL)-*co*-PMBL_{ROP} (PCL-*co*-PMBL_{ROP}).

Ritter and co-workers were the first to demonstrate the potential for the ROP of MBL when they copolymerized MBL with ϵ -caprolactone (ϵ -CL) (Figure 1.14) using bismuth(III) trifluoromethanesulfonate ($\text{Bi}(\text{OTf})_3$) that the authors postulated worked through a coordination-insertion mechanism.¹¹¹ Conversion of MBL was observed to be slow relative to ϵ -CL, and M_n s of 4 to 14 kg/mol were obtained with dispersities of 1.5 to 2.3 at ϵ -CL:MBL ratios varying from 1:1 to 50:1. While the authors initially reported that the olefin in MBL remained unreacted as ϵ -CL and MBL converted to poly(ϵ -CL)-*co*-PMBL_{ROP} (PCL-*co*-PMBL_{ROP}), it was later shown by Chen and co-workers that concomitant polymerization through a vinyl addition mechanism occurred and that the apparent stability of the olefin in the BiOTf_3 system was a result of using CDCl_3 and THF for ^1H NMR or SEC analysis, respectively, as PBML_{VAP} is not soluble in these solvents and was therefore not detected.¹¹² Nevertheless, cross-linking reactions of the olefin in PCL-*co*-PMBL_{ROP} were explored by Ritter and co-workers, and the radical polymerization of the pendant olefins with methacrylates resulted in thermoset materials with shape memory effects.

Chen and co-workers studied in detail the copolymerization of ϵ -CL and MBL catalyzed at low temperatures using $\text{Ln}[\text{N}(\text{SiMe}_3)_2]_3$ complexes.¹¹² First, a series of catalysts ($\text{Ln} = \text{La}, \text{Sm}, \text{Nd}, \text{and Y}$) in 0.2 mol% loading were explored for the homopolymerization of MBL to PMBL_{ROP} at 0 or 25 °C in DCM, DMF, or PhMe (500:1 MBL:catalyst). Under these conditions only the formation of PMB_{VAP} was observed. The copolymerization of MBL and ϵ -CL, however, proved more successful; the ROP of a 1:1 feed ratio of these monomers resulted in $\text{PCL-co-PMBL}_{\text{ROP}}$ without any PMB_{VAP} present. The most active and selective catalyst for this transformation was $\text{Ln} = \text{La}$ (La-1, Figure 1.15), which produced $\text{PCL-co-PMBL}_{\text{ROP}}$ with a 5 mol% incorporation of MBL, an M_n of 28.4 kg/mol, and a dispersity of 1.54 from a 1:1 MBL: ϵ -CL feed ratio. Notably, $\text{PCL-co-PMBL}_{\text{ROP}}$ with MBL molar incorporations of up to 14% could be synthesized when the polymerization was run in DCM at 25 °C using La-1 and MBL: ϵ -CL feed ratios that ranged from 2:1 to 10:1, though concomitant formation of PMB_{VAP} was observed at ratios of 3:1 or higher. Under these conditions, using a 10:1 MBL: ϵ -CL ratio, $\text{PCL-co-PMBL}_{\text{ROP}}$ with 14 mol% MBL incorporation was obtained with 51 mol% PMB_{VAP} impurity. Purification by solvent fractionation then gave access to PMB_{VAP} -free $\text{PCL-co-PMBL}_{\text{ROP}}$ with an M_n of 30.7 kg/mol and a dispersity of 2.00. Higher incorporations of up to 27 mol% MBL in $\text{PCL-co-PMBL}_{\text{ROP}}$ could be achieved when PhMe was used in place of DCM at 25 °C from a 10:1 MBL: ϵ -CL ratio, though 35 mol% PMB_{VAP} was observed under the conditions. Lower temperatures (–20 °C) using PhMe as a solvent favored a more selective polymerization, with 10:1 MBL: ϵ -CL ratio leading to up to 40 mol% MBL incorporation in $\text{PCL-co-PMBL}_{\text{ROP}}$ with no PMB_{VAP} detected, an M_n of 23.1 kg/mol, and a dispersity of 1.68. The purity

of these copolyesters were further confirmed by ^{13}C and ^1H - ^{13}C heteronuclear multiple quantum coherence (HMQC) NMR, where crossover peaks between covalently bound PMBL_{ROP} and PCL chains were observed, confirming the presence of copolymers rather than mixtures of homopolymers.

By MALDI-TOF analysis, $\text{N}(\text{SiMe}_3)_2$ chain ends were observed in $\text{PCL-co-PMBL}_{\text{ROP}}$, implying that the polymerization began through monomer coordination to La-1 and initiation by a $\text{N}(\text{SiMe}_3)_2$ ligand, leading to a coordination-insertion polymerization mechanism. Copolymerization of MBL with ϵ -CL offsets the small, positive ΔH for the MBL ring opening, while the low reaction temperature offsets the large, negative ΔS ; the combination of these two factors allows this polymerization to proceed in a controlled fashion. Similar results were obtained with the copolymerization of ϵ -CL and γ -BL, highlighting the applicability to this work to other five-membered lactones. All copolymers showed T_{ms} between 17 and 57 $^\circ\text{C}$ at MBL incorporations between 1 and 40 mol%. High decomposition temperatures of ~ 360 $^\circ\text{C}$ (5% wt loss by TGA) in a single-step were observed for $\text{PCL-co-PMBL}_{\text{ROP}}$.

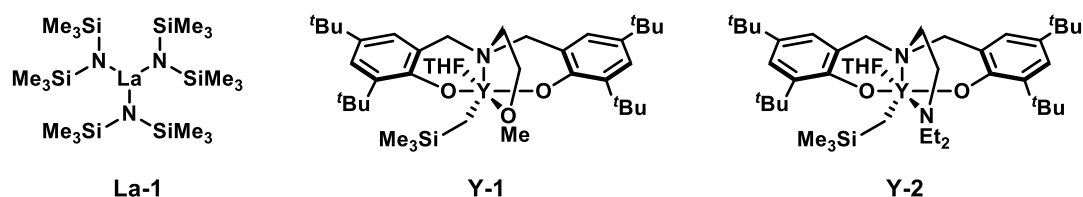


Figure 1.15. Lanthanum and ytterbium catalysts used by Chen and co-workers for the ROP polymerization of MBL.^{110,112}

The next step forward in the ROP of MBL was reported by Chen and co-workers in 2016, who performed the controlled homopolymerization of MBL, selectively, through either ROP (to give PMBL_{ROP}), vinyl addition polymerization (to give

PMBL_{VAP}), or a mixture of two, leading to cross-linked polymer, PMBL_{CLP}) (Figure 1.16).¹¹⁰ This work was based off of their previous report on the ROP of another five-membered lactone, γ -BL.³¹

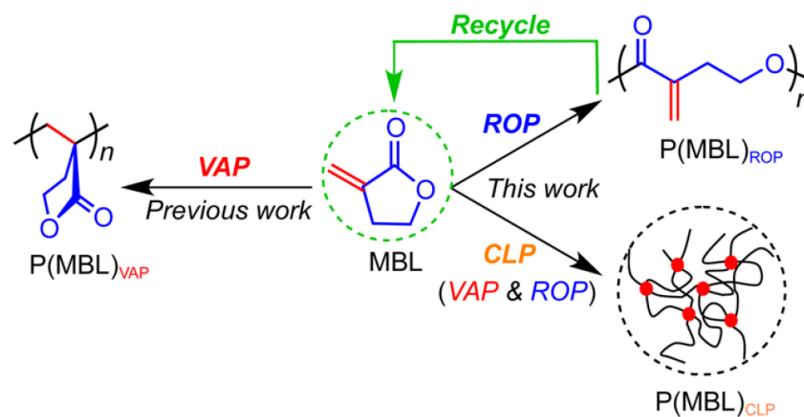


Figure 1.16. VAP vs ROP polymerization of MBL. Copied with permission from the original manuscript.¹¹⁰

La-1, used in their previous study (Figure 1.15), has been shown to be capable of the ROP of γ -BL, and was used for the initial screening of MBL ROP.¹¹² At RT La-1 catalyzed the VAP of MBL to give PMBL_{VAP} rather than PMBL_{ROP}. Even at $-60\text{ }^{\circ}\text{C}$, the formation of PMBL_{VAP} was observed (1 mol% loading catalyst, [MBL] = 5 M in THF). The key to enabling ROP over VAP at this temperature was in the addition of BnOH, which caused the alcoholysis of the La-1 amide bond to produce a highly active metal alkoxide (Figure 1.17a). Using a 1:3 ratio of catalyst to BnOH resulted in the ROP of MBL to give PMBL_{ROP} with an M_n of 5.5 kg/mol and a dispersity of 1.16. Doubling the MBL:catalyst ratio resulted in a doubled M_n of 10.4 kg/mol, showing that the system imparts control over M_n through the MBL:initiator ratio. When a 1:1 ratio of La-1 to BnOH was utilized, PMBL_{CLP} was formed, indicating the presence of both VAP and ROP pathways. These results suggest that the La-NR₂ group exhibits VAP preference, while the La-OBn group produced by alcoholysis of La-1 with BnOH favors ROP. In

support of this claim, the authors synthesized $[\text{La}(\text{OBn})_3]_n$ and showed that it catalyzed the formation of exclusively PMBL_{ROP} .

The authors further explored other factors impacting the polymerization, including catalyst:initiator ratio, concentration, temperature, initiator, and catalyst. Decreasing $[\text{MBL}]$ from 5 to 2 M, even at $-78\text{ }^\circ\text{C}$, resulted in the formation of a small amount of PMBL_{CLP} , whereas increasing the temperature to $-40\text{ }^\circ\text{C}$ resulted in exclusively PMBL_{CLP} , unless $[\text{MBL}]$ was increased to 8 M, at which point ROP could still occur. In addition to BnOH , $\text{Ph}_2\text{CHCH}_2\text{OH}$ and $i\text{PrOH}$ were also effective initiators for the polymerizations, with the bulkier alcohol $\text{Ph}_2\text{CHCH}_2\text{OH}$ producing the highest conversion (52%) and best isolated PMBL_{ROP} yield (43%). Catalyst Y-1, which showed good performance in the ROP of $\gamma\text{-BL}$, also gave the best results for the ROP of MBL, resulting in PMBL_{ROP} with an M_n of 21.0 kg/mol and a dispersity of 1.42 in 55% isolated yield (Figure 1.15). Small changes in catalyst structure from Y-1 to Y-2 resulted in a much lower yield to 5%. Importantly, all these experiments were performed under heterogeneous, nonequilibrium conditions in THF that allowed the formed polymer to precipitate out to exceed the thermodynamic limit of conversion. For better thermodynamic insight into the polymerization, homogenous, equilibrium polymerizations in CD_2Cl_2 were performed to determine ΔH and ΔS for the ROP of MBL, which were found to be -5.9 kJ/mol and ΔS of $-40.1\text{ K/mol}\cdot\text{K}$, respectively. From these results, a ceiling temperature of $-52\text{ }^\circ\text{C}$ was calculated, which demonstrates why low temperatures are needed for the ROP of MBL. Additionally, MALDI-TOF and ^1H NMR analysis showed alkoxide or proton end groups in PMBL_{ROP} , corresponding to initiation by a La-alkoxide for the ROP of MBL with catalyst La-1 or Y-1. The cross-

linking polymerization that occurred at different ratios of La:BnOH (*e.g.* 1:2) at $-60\text{ }^{\circ}\text{C}$ was also probed further: TGA, DSC, and FT-IR analysis demonstrated the networks consisted mainly of PMBL_{VAP} chains with a distinct T_g of $180\text{ }^{\circ}\text{C}$, consistent with some flexible ROP chains incorporated into the network. A putative mechanism involving VAP or ROP initiation by La-OR or La-NR₂ attack, homopropagation, and cross-propagation via Michael addition was proposed (Figure 1.17) and computational studies using density functional theory were performed in support of these mechanisms.

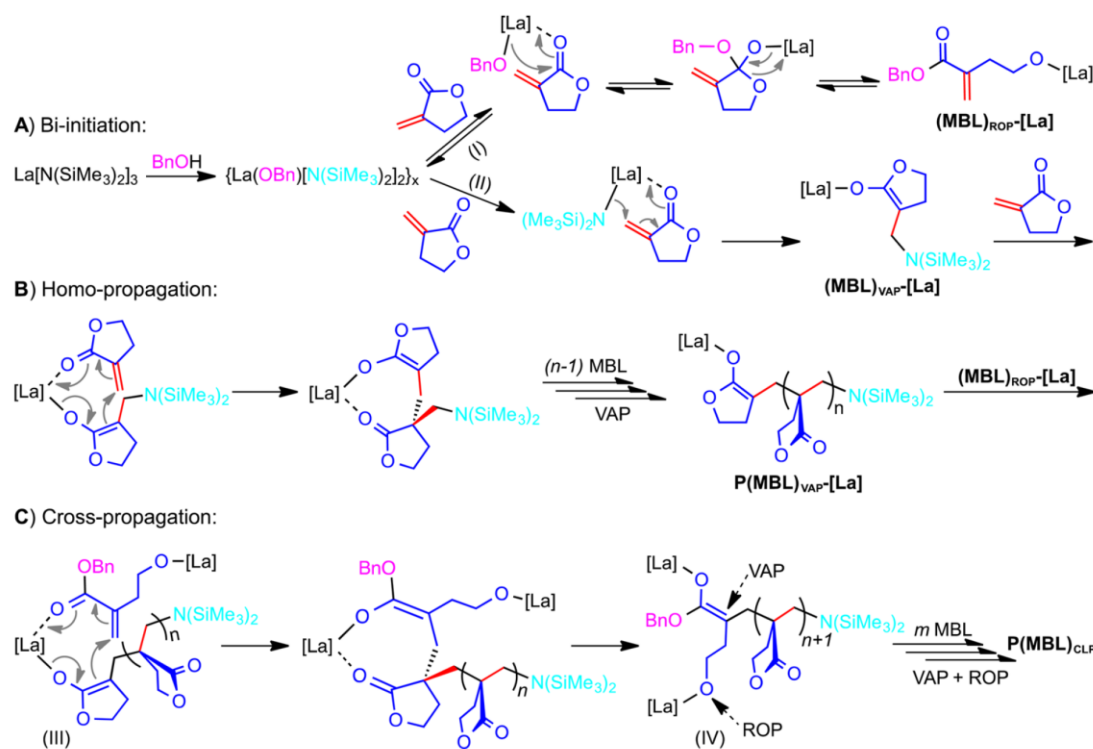


Figure 1.17. a) Initiation of either ROP (I) or VAP (II), b) propagation and c) cross-propagation via Michael addition (III). Copied with permission from original manuscript.¹¹⁰

Thermal and mechanical properties of PMBL_{ROP} were studied. Degradation occurred as a three-step process, corresponding to extrusion of MBL at $\leq 250\text{ }^{\circ}\text{C}$, cross-linking of the pendant olefin, and then decomposition, though at higher M_n (18 kg/mol) only two degradation steps were observed beginning at *ca.* $290\text{ }^{\circ}\text{C}$. By DSC, T_g s were

observed in the range of -40 to -35 °C and increased with M_n . Cross-linking of PMBL_{ROP} occurred at 250 °C during DSC, while thermal decomposition was observed at 340 °C by TGA. DMA showed a storage modulus (E') of 3.6 GPa and a loss modulus (E'') of 119 MPa for PMBL_{ROP} in the glassy state (at -100 °C) and an E' of 160 MPa and E'' of 10.5 MPa in the rubbery state (at 25 °C), with a T_g of -22 °C determined from the $\tan(\delta)$ peak.

Post-functionalization of the PMBL_{ROP} was performed under UV irradiation with 2,2-dimethoxy-2-phenylacetophenone (DMPA) initiator. A cross-linked film was obtained with no apparent T_g and thermal degradation behavior similar to PMBL_{ROP}, supporting the claim that PMBL_{ROP} first undergoes cross-linking prior to degradation. This thermally cross-linked material contained mainly ester groups and were different than chemically cross-linked materials obtained with from the polymerization of MBL 1:3 La:BnOH ratios at -60 °C, which contained mainly VAP groups. Thiol-ene click reaction was also performed on PMBL_{ROP} to give the fully thiolated polyester and demonstrated the ability to tune physiochemical properties through post-functionalization. Finally, quantitative depolymerization of PMBL_{ROP} back to MBL occurred when PMBL_{ROP} was heated between 60 to 130 °C for 1 to 24 h with 1 mol% La-1 (or other metal halides such as LaCl₃) and 3.5 mM water (as a polymerization inhibitor), demonstrating the ability to chemically recycle PMBL_{ROP}. Degradation testing of PMBL_{ROP} under aqueous conditions was also performed over 120 days. PMBL_{ROP} showed complete degradation under basic (1 M NaOH) conditions but was stable under neutral (DI H₂O) and acidic (1 M H₂SO₄) conditions, similar to what has

been reported for other materials based on IA-derived polyesters.¹⁰⁹ Similarly, PMBL_{VAP} also degraded over 120 days under basic conditions.

Another example of the ROP of MBL was presented by Ford and co-workers, who employed several different La catalysts that they synthesized (La-2, La-3, and La-4, Figure 1.18).¹¹³ ROP of MBL was performed in DMSO at 0 °C for 2 h at 500:1 MBL:catalyst ratio. While no reaction occurred using catalyst La-2, significant polymerization occurred with catalysts La-3 and La-4, resulting in extremely high M_{ns} of 580 and 750 kg/mol (*ca.* 25x larger than the expected for the formation of PMBL_{ROP}) and dispersities of 1.34 and 1.32, respectively. They attributed these large M_{ns} to the formation of branched polymers through competing VAP, which is supported by loss of the olefin signal in the ¹H NMR of the polymers. By DMA the T_g s of these polymers were determined to be 88 and 123 °C, respectively, and so these materials are likely highly branched or cross-linked polymer networks intermediate in structure between PMBL_{CLP} and thermally crosslinked PMBL_{ROP} reported by Chen and co-workers.¹¹²

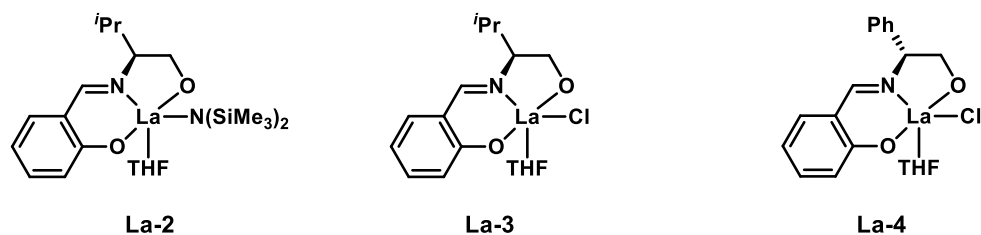


Figure 1.18. Lanthanum catalysts used by Ford and co-workers for the ROP polymerization of MBL.¹¹³

More recently, Mosnáček and co-workers reported the ROP of mixtures of MBL and ϵ -CL using $\text{Al}(\text{O}^i\text{Pr})_3$ as a catalyst operating through a coordination-insertion mechanism.¹¹⁴ Alternatively, the use of acid or diphenyl phosphate (DPP) to facilitate a cationic ring opening copolymerization of MBL and ϵ -CL was explored.¹¹⁴ Like the

first report of ROP of MBL with ϵ -CL, the authors observed that concomitant VAP of MBL occurred when MBL was subjected to ROP conditions at 80 °C using tin octanoate as a catalyst and butyl alcohol as an initiator. Next, the authors utilized $\text{Al}(\text{O}^i\text{Pr})_3$ as a catalyst at 80 °C, and found 40% of MBL polymerized through VAP in THF solvent whereas only 8% polymerized through VAP in PhMe solvent. Subsequent use of lower temperatures (RT or 0 °C) with PhMe solvent resulted in exclusively ROP of MBL and ϵ -CL to give $\text{PCL-co-PMBL}_{\text{ROP}}$ without the formation of PMBL_{VAP} . Furthermore, the polymerization was well-controlled and followed first-order kinetics, though MBL conversion proceeded to only 5%, and k_{MBL} (0.019 M/s) was ~ 50 times lower than $k_{\epsilon\text{-CL}}$ (1.03 M/s). Under these conditions, with a monomer concentration of 2.0 M in PhMe, a copolyester with an M_n of 25 kg/mol and a dispersity of 1.11 was obtained. By lowering the catalyst:monomer ratio, a higher M_n copolymer (61 kg/mol) with a broader dispersity of 1.51 and a similar molar incorporation of MBL of 5% could be prepared. To achieve higher mol% incorporation of MBL in $\text{PCL-co-PMBL}_{\text{ROP}}$, a higher MBL: ϵ -CL ratio of $\sim 10:1$ (in bulk, with no added solvent) was utilized. While 17 mol% incorporation of MBL was achieved under these conditions, concomitant formation of PMBL_{VAP} was observed, consistent with previous observations by Chen and co-workers for copolymerizations at high MBL: ϵ -CL ratios.¹¹² The concomitant formation of PMBL_{VAP} was overcome by diluting the reaction mixture ($[\text{monomer}] = 1.0 \text{ M}$), but this led to lower mol% incorporation of MBL at 14%. The authors then showed that at a lower temperature of 0 °C, increasing the MBL: ϵ -CL feed ratio from 1:1 to 10:1 at various monomer concentrations resulted in copolyesters with 7 to 25 mol% incorporation of PMBL_{ROP} with M_n s of *ca.* 16 to 45 k/mol and dispersities of 1.12 to

1.21. Further decreases in temperature were not explored, as the polymerization rate was slow 0 °C (reactions were run for up to 170 h) and lower temperatures would result in even slower polymerizations. Notably, despite higher molar incorporations at higher feed ratios of MBL, conversion of MBL was very low and in the range of 2 – 4 %. A slightly higher conversion of 7% could be obtained when ϵ -CL comonomer was added dropwise into an MBL polymerization mixture, which maintained a high excess of MBL relative to ϵ -CL.

In the same paper, Mosnáček and co-workers also reported the cationic ROP of MBL with ϵ -CL,¹¹⁴ where they used an alcohol initiator in conjunction with an acid (trifluoromethanesulfonic acid (TfOH) or DPP). Polymerization of MBL and ϵ -CL with *i*PrOH with TfOH catalyst at RT for 4 h, for example, gave PCL-*co*-PMBL_{ROP} an M_n of 18 kg/mol and 4 mol% MBL incorporation. Furthermore, this system was also capable of chain extension: a 3.3 kg/mol sample of PCL-*co*-PMBL_{ROP} with a dispersity of 2.2 was prepared, and then chain-extended with ϵ -CL to obtain a 7.7 kg/mol block (PCL-*co*-PMBL_{ROP})-*b*-PCL with a decreased dispersity of 1.8. Similar results were obtained using DPP, and chain ends from the alcohol initiator and -OH tail group were observed by MALDI-TOF analysis. Furthermore, ethylene glycol could be utilized as an initiator in the cationic polymerization of MBL with ϵ -CL to produce a telechelic copolyester, while di(trimethylolpropane) was used to make a star polymer with 4 – 8 mol% MBL incorporation, each (Figure 1.19). Of the two polymerization systems (coordination-insertion or cationic), the cationic polymerization mechanism showed higher activity, as a *ca.* 1:3 MBL: ϵ -CL feed ratio resulted in 4 mol% incorporation of MBL into PCL-*co*-PMBL_{ROP}, whereas a similar feed ratio using the coordination-insertion process

catalyzed by $\text{Al}(\text{O}^i\text{Pr})_3$ resulted in only a 1 mol% incorporation of MBL into $\text{PCL-co-PMBL}_{\text{ROP}}$.

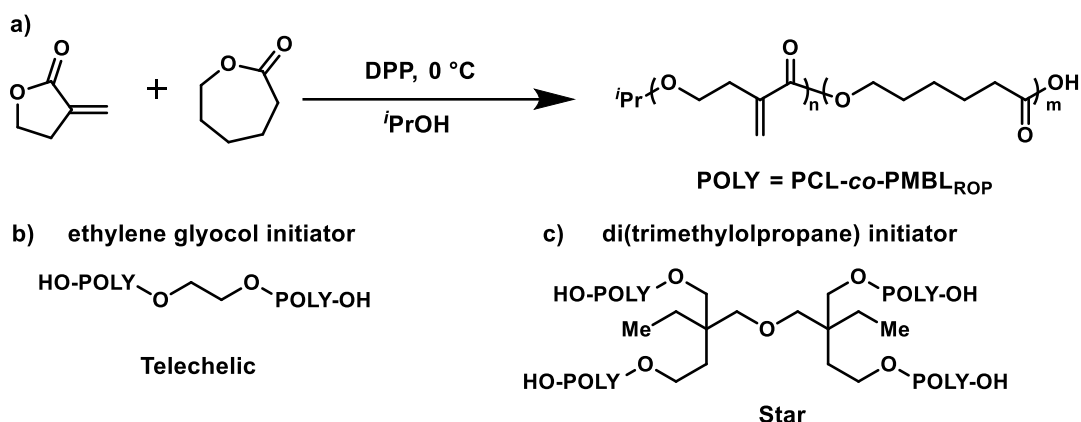


Figure 1.19. Cationic ROP of MBL and CL leads to hydroxyl terminated, telechelic, or star polymers using different initiators.

DSC analysis showed two melting peaks for the various copolymers that were independent of copolymer molar mass and observed for both the linear and star copolyesters. The presence of two melting peaks was attributed to reorganization of the copolyester chains during the thermal scan. Higher MBL incorporation in the copolyester results in lower T_m s (24 °C for 25 mol% MBL incorporation; 55 °C for 1 mol% MBL incorporation; 57 °C for pure PCL). Degradation for all copolymers was observed by TGA to begin around 200 °C, with increasing MBL content broadening the T_d to higher values with multistep profiles. Notably, cationic-derived $\text{PCL-co-PMBL}_{\text{ROP}}$ had a thermal stability $\sim 100\text{ }^\circ\text{C}$ higher than $\text{PCL-co-PMBL}_{\text{ROP}}$ obtained through coordination-insertion, which the authors attributed to trace metal catalyst left in coordination-insertion-derived polymers, which can accelerate degradation. Finally, post-polymerization modification using thiol-ene chemistry was explored and either benzothioxanthene fluorophore or *N*-acetylcysteine were appended to PCL-co-

PMBL_{ROP}. Successful modification was observed by disappearance of the vinyl protons in the ¹H NMR spectrum, demonstrating the ability to modify these polymers after the polymerization.

PYRROLIDONES

Pyrrolidones are five-membered lactam rings that can be accessed from the treatment of IA with amines. Typically, three types of pyrrolidone monomers are accessed from IA. By heating IA with one equivalent of diamine or an alkanolamine, an AB type pyrrolidone is generated (Figure 1.20a). Alternatively, by using an excess of IA (≤ 0.5 equiv diamine), AA diacid bis(pyrrolidone)s can be produced under similar conditions (Figure 1.20b). Finally, by treating IA with one equivalent of diamine in an appropriate solvent at RT, IA/diammonium salts can be produced (Figure 1.20c). All three of these types of monomers have been used in the synthesis of polymers through polycondensation polymerizations. Typically, an AB type pyrrolidone or IA/diammonium salt are heated (up to 240 °C) under vacuum to promote polycondensation, leading to the synthesis of polyamides or polyesters (Figure 1.20d). Often, non-IA-derived comonomers (diacids, diamines, or diols) are added to the mixture to produce structurally varied copolymers. Alternatively, AA type bis(pyrrolidones) can be mixed with non-IA-derived diamines and heated (up to 340 °C) under vacuum to produce polyamides (Figure 1.20e). As with the AB type polymerizations, these polycondensation reactions are often performed with the addition of non-IA-derived comonomers (diacids, diamines, or diols) to produce structurally varied copolymers. Pyrrolidone-containing poly(ester amide)s have also been synthesized by the direct step-growth polycondensation polymerization of IA (without the separate monomer

synthesis or purification steps) with other diacid monomers, diamines, and diols. Numerous alkyl and aromatic diamine components have been explored for these polymerizations (Figure 1.20f).

An early example utilizing IA-derived pyrrolidones for polymer synthesis comes from Zilkha and co-workers, who in 1972 studied a variety of aromatic-based polyamides.¹¹⁵ The authors synthesized a series of bis(pyrrolidone) monomers by condensation of IA with 0.2 equiv of various aromatic diamines (Figure 1.20f, diamine backbones A – I) under vacuum high temperatures (150 – 200 °C, Figure 1.20b). Catalyst-free step-growth polycondensation polymerizations were then performed by heating the desired bis(pyrrolidone) between 250 and 340 °C for up to 1.5 h with a diamine containing a matching or non-matching aromatic functionality (Figure 1.20e), resulting in 24 polyamides containing aromatic functionalities. M_n s (determined from end-group titration) between 2.3 and 100 kg/mol were obtained, and the highest molar masses were observed for polyamides with B or G backbones on the bis(pyrrolidone) monomers (Figure 1.20f). Notably, when a sixth diamine (structure E) was used, intramolecular condensation led to the formation of polybenzimidazoles, though only partial conversion may have been achieved (Figure 1.21). The high temperature required for the polyamide condensation resulted in discolored materials, and so the polymers were also synthesized by refluxing mixtures of bis(pyrrolidone) diacid anhydrides with diamines in the presence of 1 equiv of triethylamine in chloroform. Under these conditions, similar degrees of polymerization were observed, though the high temperature polymerization method afforded higher M_n s for bis(pyrrolidone)s containing B or G backbones.

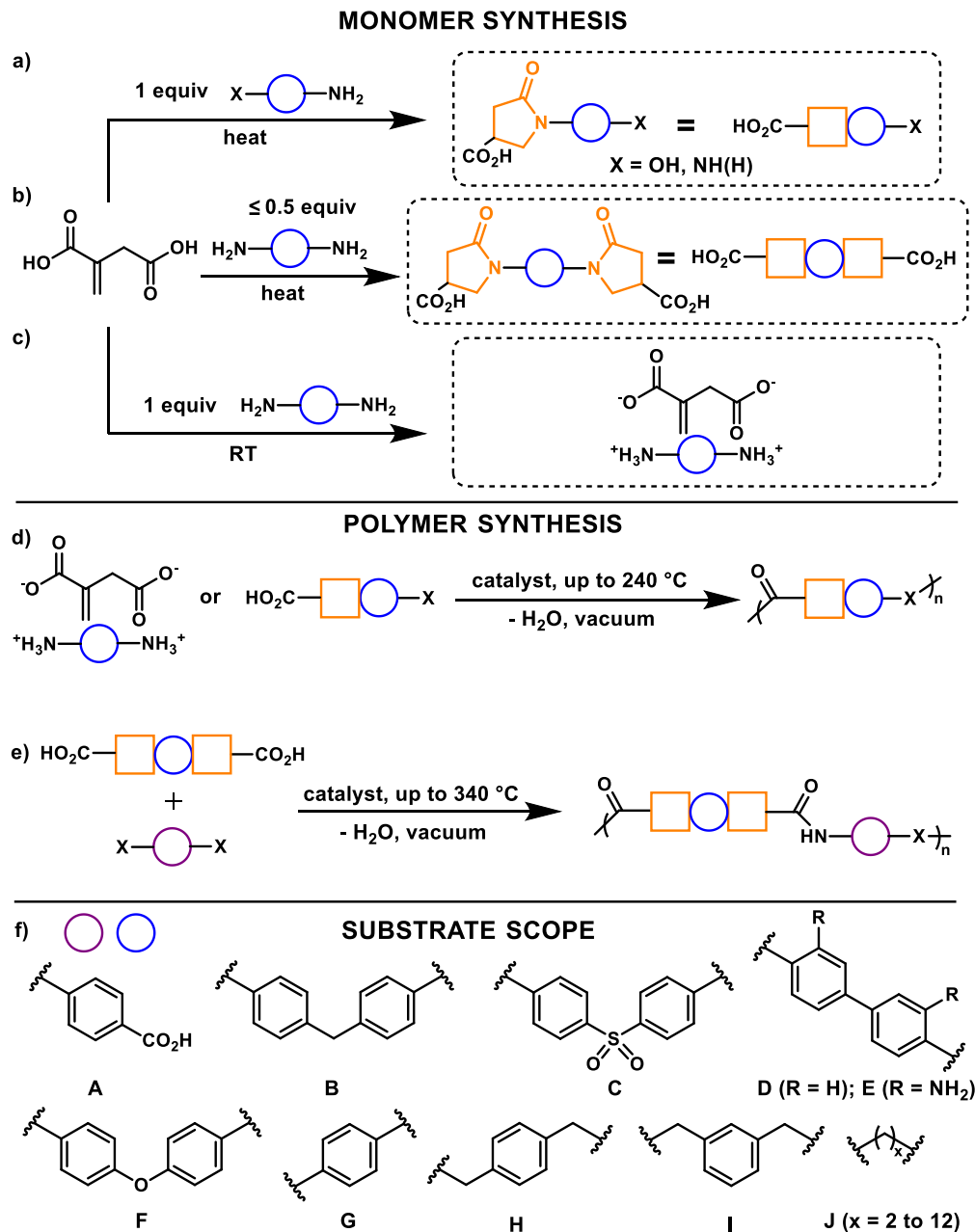


Figure 1.20. a) Synthesis of AB type pyrrolidone monomers from IA; b) Synthesis of AA type bis(pyrrolidone) monomer from IA; c) Synthesis of salt monomers from IA; d) Polycondensation of salt or AB monomers to give polyamides or polyesters; e) Polycondensation of AA diacid with BB amine to give polyamides; f) Substrate scope of diamines studied for these types of polycondensations.

All polyamides studied were amorphous and showed thermal stabilities up to 300 °C by TGA (5 wt% loss). Notably, the polybenzimidazoles showed increased

thermal stability compared to the polyamides (5 wt% loss at 350 °C). All polymers were soluble in concentrated sulfuric acid, and partial solubility was observed in DMF or DMSO for some of the polymers.

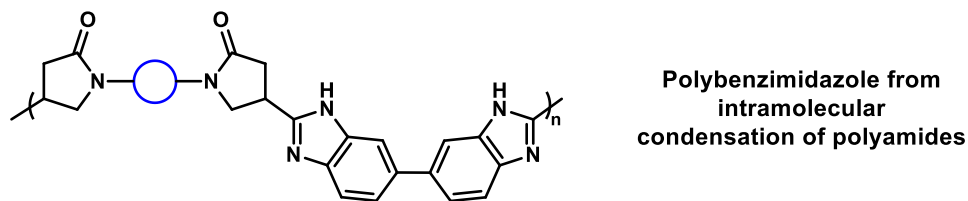


Figure 1.21. Intramolecular condensation of polyamides generates polybenzimidazoles.

In 2013, Kaneko and co-workers looked at the synthesis of pyrrolidone-containing polyamides and their environmental degradation.¹¹⁶ Rather than form pyrrolidone monomers, the authors prepared IA/diammonium salt monomers by mixing IA with aliphatic amines (Figure 1.20f, J2 – J6 backbones) at RT in EtOH. After just 0.5 h, salt monomers precipitated and were isolated in good yields (94 – 98%). Subsequently, these monomers were heated at 230 °C under vacuum while stirring for 6 – 8 h in the presence of NaH₂PO₄ catalyst (0.1 wt%). Under these conditions, the authors showed using a model reaction between IA and benzylamine that aza-Michael addition occurred prior to amidation. Thus, in the polymerization of the IA/diammonium salt monomers, the formation of pyrrolidone monomers should occur *in situ* prior to further polycondensation to give the pyrrolidone-containing polyamides. 2D correlational spectroscopy established the presence of the pyrrolidone ring in the polyamide, demonstrating that the IA/diammonium salt monomers can be used to directly form pyrrolidone-containing polyamides. The M_n s of the resulting polyamides ranged from 31.0 to 67.2 kg/mol with D s ranging from 1.4 to 2.1. Notably, while this reaction could proceed in the absence of a catalyst, higher M_n s were obtained in the

presence of NaH_2PO_4 . Additionally, the melt polymerization of mixtures of IA and diamines in the presence of NaH_2PO_4 catalyst resulted in lower molar masses compared to the melt polymerization of IA/diammonium salts, which the authors attribute to branch formation and subsequent stoichiometric imbalance in the non-salt mixture.

The polyamides showed insolubility in water and common organic solvents such as acetone or tetrahydrofuran but showed solubility in more polar solvents such as *N,N*-dimethylacetamide, *N*-Methyl-2-pyrrolidone, or dimethyl sulfoxide. Glass transition temperatures for these materials increased with decreasing alkyl backbone length ($T_g = 154\text{ }^\circ\text{C}$ for J2, 80 to $100\text{ }^\circ\text{C}$ and J3 to J6), while high decomposition temperatures increased with increasing backbone length (10 wt% loss observed at $365\text{ }^\circ\text{C}$ for J2, $400\text{ }^\circ\text{C}$ for J6). Notably, the glass transition temperatures were higher than those of commercial polyamides Nylon-6,6 or Nylon-6 at 57 and $53\text{ }^\circ\text{C}$, respectively, though decomposition temperatures of the commercial ($390 - 400\text{ }^\circ\text{C}$ at 10 wt% loss) and pyrrolidone-based polyamides ($365 - 400\text{ }^\circ\text{C}$ at 10 wt% loss) were similar. Remarkably, the tensile strength at break of these IA-based polyamides were significantly improved over commercial polyamides Nylon-6,6 and Nylon-6 (Table 1.4, entries 1 – 5, 25, and 26): for higher molar mass polyamides obtained by NaH_2PO_4 catalysis, σ_B was in the range of $90 - 165$ compared to $41 - 68$, for the commercial polyamides. Additionally, E and ε_B were $430 - 2800\text{ MPa}$ and 1.8 to 4.9% , respectively, for the pyrrolidone-containing polyamides, compared to $440 - 1700\text{ MPa}$, and $6 - 18\%$ for commercial polyamides. Polyamides with J2 aliphatic backbones showed the highest E and σ_B , but lowest ε_B .

Table 1.4. Table of Physical Properties for Pyrrolidone-Containing Polyamides Derived from IA.

Entry	M1 (%) ^a	M2 (%) ^a	M3 (%) ^a	M4 (%) ^a	<i>E</i> (MPa)	σ_b (MPa)	ϵ_b (%)	<i>M_n</i> (kg/mol)
1 ¹¹⁶	IA-J2 (50:50)				2800	165	1.8	31.0
2 ¹¹⁶	IA-J3 (50:50)				450	90	2.3	46.0
3 ¹¹⁶	IA-J4 (50:50)				430	90	2.4	62.6
4 ¹¹⁶	IA-J5 (50:50)				550	90	4.9	67.2
5 ¹¹⁶	IA-J6 (50:50)				580	95	2.5	36.5
6 ¹¹⁷	IA-G/J2 (50:0.5:49.5)				1400	47	7	21.3
7 ¹¹⁷	IA-G/J2 (50:1.5:48.5)				1500	61	6	23.7
8 ¹¹⁷	IA-G/J2 (50:2.5:47.5)				2300	72	5	28.3
9 ¹¹⁷	IA-G/J2 (50:5:45)				1200	62	5	22.6
10 ¹¹⁷	IA-G/J2 (50:7.5:42.5)				900	31	6	22.9
11 ¹¹⁷	IA-G/J2 (50:10:40)				500	42	4	16.4
12 ¹¹⁷	IA-G/J2 (50:12.5:37.5)				200	20	4	20.1
13 ¹¹⁸	IA/C8-J4/J10 (7.5:42.5:25:25)				680 ^b	30	40	-
14 ¹¹⁸	IA/C8-J4/J10 (12.5:37.5:25:25)				300 ^b	42	460	20.0 ^c
15 ¹¹⁸	IA/C8-J4/J10 (15:35:25:25)				210 ^b	33	500	23.7 ^c
16 ¹¹⁸	IA/C8-J4/J10 (17.5:32.5:25:25)				340 ^b	43	600	20.5 ^c
17 ¹¹⁸	IA/C8-J4/J10 (20:30:25:25)				140 ^b	24	440	-
18 ¹¹⁸	IA/C8-J4/J10 (25:25:25:25)				380 ^b	39	620	33.3 ^c
19 ¹¹⁸	IA/C8-J4/J10 (40:10:25:25)				680 ^b	43	330	46.3 ^c

20 ¹¹⁸	IA-J4/J10 (50:25:25)				650 ^b	40	6	64.8 ^c
21 ¹¹⁹	IA (7.1)	C8 (40.5)	J10 (5.2)	DO-4 (47.1)	140 ^d	14	38	22.1
22 ¹¹⁹	IA (7.1)	C8 (40.5)	J10 (16.7)	DO-4 (36.7)	90 ^d	22	32	25.2
23 ¹¹⁹	IA (7.1)	C8 (40.5)	J10 (26.2)	DO-4 (26.2)	80 ^d	28	30	29.4
24 ¹¹⁹	IA (7.1)	C8 (40.5)	J10 (36.7)	DO-4 (15.7)	0 – 20 ^d	49	17	28.4
25 ¹¹⁶	Nylon 6,6				590 – 1700	65 – 68	6	
26 ¹¹⁶	Nylon 6				440 – 1400	41 – 60	18	

^aM1, M2, M3, and M4 represent the percentages of each monomer in the monomer feed ratio used for polymerization. Ratios inside a single parenthesis indicate that a single IA/ammonium salt with various components was utilized as a monomer. ^d*E* was estimated from the stress-strain curves in the original manuscript.¹¹⁸ ^cViscosity-average molar mass (*M_v*). ^d*E* was estimated from the stress-strain curves in the original manuscript.¹¹⁹ M1, M2, M3, M4 refer to feed ratios.

In addition to mechanical testing, the authors tested the environmental degradation of the polyamides. Ring-opening of the pyrrolidone unit was observed in alkaline solution, soil, and under UV-irradiation, generating hydrophilic carboxylic side chains (Figure 1.22). The water-insoluble polyamides thus became water-soluble following ring-opening, and corrosion was observed after being immersed in soil for one year, with polyamides possessing J3, J4, and J6 backbones disappearing entirely. Similarly, polyamides with J2 and J5 backbones showed weight loss of 96 and 98 wt%, respectively. Degradation of these polymers were greatly improved relative to commercially available PLA, which only showed 16 wt% after one year under the same conditions. Though degradation occurred, this was due to solubilization, as chain scission along the amide backbone functionality was not observed. These materials

could serve as biorenewable alternatives to commercial Nylon, as they excellent good degradation properties and superior thermal and mechanical behavior.

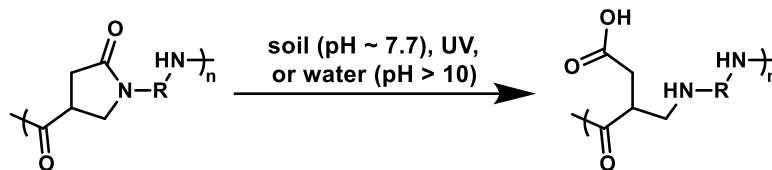


Figure 1.22. Degradation of pyrrolidone-based polyamides occurs through ring opening of the pyrrolidone and solubilization.¹¹⁶

In a follow up to their work generating aliphatic pyrrolidone-containing polyamides accessed from IA, Kaneko and co-workers next explored the synthesis of pyrrolidone-containing polyamides possessing aromatic functionalities (Figure 1.20f, diamines F, G, H, and I) using the same method for IA/diammonium salt formation and subsequent polymerization with NaH_2PO_4 catalysis.¹¹⁷ Following polymerization, polyamides with aromatic functionalities were obtained with M_n s ranging from ~ 28 kg/mol to 61 kg/mol and dispersities from 1.4 to 2.0. The polyamides were soluble in polar solvents such as *N,N*-dimethylformamide, trifluoroacetic acid, or *N*-Methyl-2-pyrrolidone, as well as dimethyl sulfoxide and *N,N*-dimethylacetamide when heated to 50 °C. The polyamides were insoluble in water, acetone, tetrahydrofuran, methanol, ethanol, isopropanol, hexane, and dichloromethane, showing increased solvent resistance over their aliphatic counterparts.¹¹⁶ T_g s varied from 156 (H backbone) to 242 °C (G backbone), while T_d s (10 wt% loss) ranged from 370 to 400 °C, showing improved thermal stability of previously reported IA-based polyamides by Zilkha and co-workers.¹²⁰ Unfortunately, the authors were unable to mechanically test the aromatic polyamides due to their hardness. To overcome this, different IA/diammonium salt monomers formed from 1 equiv of IA with 1 equiv of a diamine mixture (composed of

aliphatic J2 and G backbones) were synthesized and polymerized. Compositions varying from 70% to 99% J2/G were explored and showed M_n s between 21 and 28 kg/mol, with \bar{D} s between 2.1 and 2.7. T_g s of these polyamides decreased with increasing aliphatic content and ranged from 119 to 148 °C, while decomposition temperatures were observed between 350 and 400 °C (at 10 wt% loss). Since these materials were softer and tougher than their aromatic counterparts, mechanical testing could be performed (except on the 70% J2 sample). Mechanical testing (Table 1.4, entries 6 – 12) showed E values between 200 and 2300 MPa and σ_B values between 20 and 72 MPa, with maximums of both at an aliphatic composition (J2) of 95%. Elongations at break also increased from 4 to 7% from 75% to 99% aliphatic content. Notably, these tensile properties show σ_B values comparable with commercial Nylon 6,6 and Nylon 6, though weaker than the fully aliphatic analogues previously studied.¹¹⁶ Additionally, the copolymers also showed water absorptions between 1.5 and 2.0%, which are less than that of Nylon 6,6 or Nylon 6.

Finally, the degradation behavior of the polyamides was explored. Both the aromatic and aromatic/aliphatic polyamides showed UV-induced dissolution in water resulting from ring-opening of the lactam ring in the polymer backbone to a more soluble form. Additionally, soil degradation was studied over one year. Aromatic polyamides based on diamines F, G, H, and I (Figure 1.20f) showed 34, 23, 76, and 100 wt% loss, respectively (relative to 16 wt% loss for PLA).¹¹⁶

Kaneko and co-workers also reported the cryogenic nanohybridization of biopolyamides from IA with montmorillonites (MMT) in 2017.¹²¹ MMTs are layered silicate clays which can form nanocomposites with polyamides to generate materials

with improved properties. The authors found that the addition of MMTs as nanofillers to IA-based polyamides allowed for the tuning of material properties through cryogenic nanohybridization. Using the same synthetic method, they previously employed for monomer synthesis, a diammonium salt composed of IA with diamine J6 was prepared. The salt was then melt-polymerized at 170 °C for 18 h, generating a polyamide with an M_n of 36.5 kg/mol and a dispersity of 2.31. Various MMT fillers were employed for nanohybridization, including NaMMT, ArMMT, or OHMMT in 1 to 7 wt% loadings. The fillers were loaded by melt-mixing the MMT and polymer for 5 h at 170 to 210 °C. These nanohybrid materials were then heated at 170 – 220 °C, treated cryogenically by cooling in liquid nitrogen, and brought to room temperature. This cycle was repeated five times prior to testing. T_g s of these materials were slightly decreased relative to the pure polyamide (61 – 68 °C for the nanohybrids vs 73 °C for the polyamide), while thermal stabilities was slightly improved (10 wt% loss on TGA observed at 423 °C for NaMMT material vs 399 °C for the pure polyamide). The mechanical properties were then established via tensile testing. Tensile strengths (σ_B) and Young's moduli (E) ranged from 65 – 241 MPa and 2200 – 5500 MPa, respectively, and were comparable to conventional glass-fiber-reinforced Nylon-6,6. Nanohybridization with NaMMT improved toughness relative to the pure polyamide, with elongations at break (ϵ_B) of *ca.* 20% obtained for the hybrid relative to 5% for the pure polymer. Notably, these nanohybrid materials showed improved mechanical properties when cryogenically treated compared to nanohybrid materials that were not cryogenically treated. The authors postulated that the presence of NaMMT can catalyze the ring-opening of the pyrrolidone ring in the main chain polyamide to form a pendant carboxylic acid. The

difference in material properties of the nanohybrid materials compared their pure polyamide counterparts was attributed to, in the case of NaMMT, interactions between pendant carboxylic acids in the polyamides and the MMT surface (Figure 1.23). Supporting this claim, a more recent paper by Ali *et al.* shows that these nanohybrids showed molecular orientation of the polymer resins during the fiber formation at the yield point, which was attributed to the strong interaction between the MMT layers and the polyamide matrix.¹²²

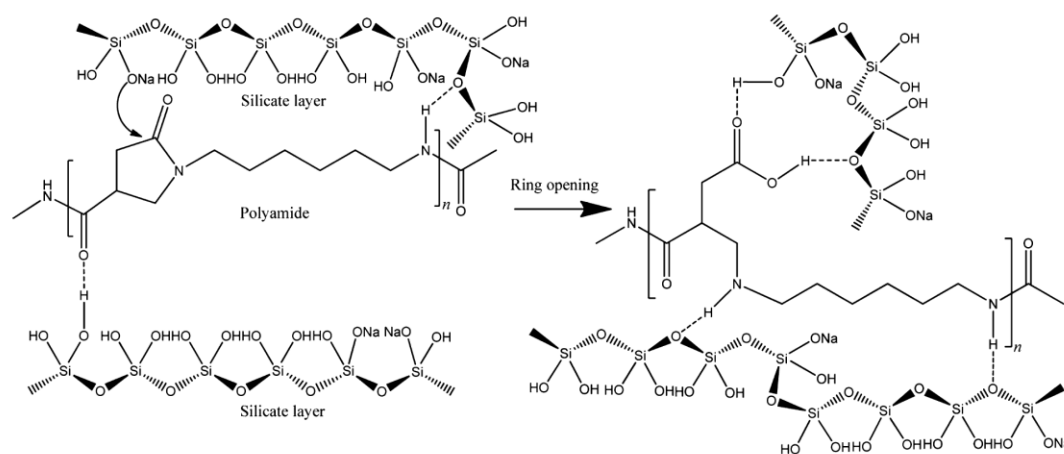


Figure 1.23. Tentative mechanism of NaMMT functions to catalyze the ring-opening reaction of pyrrolidone in the main chain to form carboxylic acid that specifically interacts with the MMT surface. Copied with permission from the original manuscript.¹²¹

Using a strategy similar to that by Zilka and co-workers,¹¹⁵ Dole and co-workers explored the behavior of aliphatic pyrrolidone-containing polyamides accessed from IA as poly(butylene succinate) / starch compatibilizers.¹²⁰ They synthesized a variety of aliphatic bis(pyrrolidone) (Figure 1.20b and f, J2 and J6 backbones) by condensation of IA with the corresponding diamine at reflux for 16 h. The resulting bis(pyrrolidone) diacids were then reacted with diamines (structures J2 and J6) using pTsoH as a catalyst (3 mol%) in two stages. First, the reaction mixture was heated for 1 h at 100 °C and then

the temperature was increased to 170 °C, vacuum was applied, and the reaction was continued for 3 days. Polymerization reactions were not run for longer or at higher temperatures to avoid degradation. Molar mass stopped increasing after 3 days at 170 °C. Under these conditions, polymers with M_n s ranging from 11.3 to 17.2 kg/mol and D s ranging from 1.80 to 2.12 were obtained, with the highest molar masses observed when both the bis(pyrrolidone) and diamine (Figure 1.20f, J) contained two methylene units. The T_g s of these materials decreased with increasing length (124 °C for both diacid and diamine J2, 48 °C for both diacid and diamine J6) and increasing relative humidity (– 15 °C for both diacid and diamine J2), though the longer alkyl chain polymers were less sensitive to humidity ($T_g = 29$ °C at 50% relative humidity for both diacid and diamine J6). In particular, the ability to tune hydrophilicity based on alkyl chain length of the backbone repeat unit is of great interest in the production of compatibilizers. These materials were effective as compatibilizers, as the addition of 1 wt% of the polyamides (either the J2/J6 diacid/diamine backbone or J6/J2 diacid/diamine backbone) improved the mechanical properties of the PBS/starch blends.

Like Kanako and co-workers, Jia, Zhang, and co-workers performed polycondensation polymerizations of diacid/diamine salt monomers derived from IA (Figure 1.20d).¹¹⁸ To obtain these salts, they mixed equimolar amounts of diacids (composed of IA and sebacic acid, or C8, ranging from 15 to 100% IA) with diamines (composed of J10 and J4 backbones in a 1:1 ratio) in EtOH and stirred for 0.5 h at 60 °C. Solvent removal and drying under vacuum afforded the pure diacid/diamine salt monomers. The salt monomers were then polymerized without catalyst in three stages in the presence of hydroquinone (0.05 wt%) and orthophosphoric acid (0.01 wt%)

inhibitors. First, the mixture was heated at 180 °C for 1 h, and then the temperature was increased to 200 °C and the reaction was continued for another 2 h. Finally, the temperature was increased to 210 °C, the pressure was reduced (to *ca.* 2 Torr), and the reaction was continued for another 3 h. By varying the IA:C8 ratio, varying content of pyrrolidone ring in the final polyamide could be achieved. Higher content of IA in the diacid feed (80 and 100%) resulted in polymers only soluble in DMF, DMSO, or EtOH in the case of 100% IA, and structural analysis was performed by ¹H NMR in DMSO-d₆ or sulfuric acid-d₂. Due to the low solubility of many of the polymers, viscosity measurements were performed for molar mass analysis rather than SEC. Based on these measurements, larger viscosity-average molar masses (M_v) were observed with increasing IA content, and ranged from 20.0 to 64.8 kg/mol at 25 to 100% IA. The larger M_v at increased IA content was attributed to the higher reactivity of IA relative to C8. T_m s of the polymers decreased from 185 – 190 °C at 0 – 15% IA to 158 at 30% IA, above which no melting temperatures were observed. Additionally, T_g s increased from 22 to 63 °C from 0 to 100% IA content, while thermal degradation temperatures (at 5 wt% loss) decreased slightly with increasing IA content from 415 °C to 400 °C.

Additionally, the tensile properties of these materials were elucidated (Table 1.4, entries 13 – 20). E and σ_B values varied from 140 to 680 and 24 to 43 MPa, respectively, while elongations ranged widely between 6 and 620%. Notably, elongations > 300% for the 25 to 80% IA compositions demonstrate the ability to add long chain aliphatic groups into the polyamides to increase their flexibility. The water absorption properties of these polyamides were also studied and showed increasing water absorption with increasing IA content, ranging from ~ 3% to 20% for 15 to 80% IA content after 15

days of soaking (compared to typical values of 1 to 3% for commercial polyamides). Notably, the water-swollen polyamide (with IA an composition of 80%) exhibited shape-memory effects and reverted to its original shape following twisting, though both tensile strength and elongation at break decreased significantly with the absorption of water. Finally, these polyamides were shown to be nontoxic towards mouse fibroblasts, which makes them potentially applicable in biomedical applications.

In a follow-up to their original work, Jia, Zhang, and co-workers comprehensively studied the effects of renewable plasticizers (water, glycerol, and soybean oil) on the 80% IA-based polyamide they explored in the previous paper (Table 1.4, entry 19).¹²³ Notably, they observed water as the most efficient plasticizer, followed by glycerol and then soybean oil. Addition of these small molecules to the polyamide resulted in lowered T_g s, tensile strengths, and elongations at break, representing plasticization of the polymer matrix. These plasticizers also increased the toughness of the IA-based polyamide, and the polyamide plasticized by water showed good biocompatibility.

Next, poly(ester amide)s containing pyrrolidone structures derived from IA were studied by Zhao and co-workers in 2016.¹¹⁹ Rather than synthesize an IA/ diammonium salt or pyrrolidone in a separate step, the authors directly reacted IA, C8 diacid, J10 diamine (Figure 1.20f, J10), and 1,4-butanediol (DO-4) to form a pyrrolidone-containing poly(ester amide). In this strategy, the ratio of IA:C8 was fixed (15% IA) while the ratio of diamine to diol was varied (from 10 to 70% diamine) in order to alter the ester/amide content of the copolymer. The polymerization was run in two stages. First, in the absence of catalyst, the reactants were heated for 2 h at 180 °C, and then

Ti(BuO)₄ (0.02 wt%) was added, the temperature was increased to 200 °C, the pressure was lowered to 300 Pa, and the reaction was continued for 2 h. Polymers with M_n s of 22 to 29 kg/mol and dispersities of 1.8 to 2.6 were obtained with varying amounts of ester/amide linkages (Figure 1.24). Though the authors report a structure with a bis(pyrrolidone) functionality in the repeat unit, due to the use of > 0.5 equiv diamine relative to IA in the feed ratios of their polymerizations (Table 1.4, entries 21 – 24), it is likely that the poly(ester amide)s include AB type pyrrolidone repeat units (Figure 1.20a and d) in addition to (or potentially in place of) the AA + BB bis(pyrrolidone) / diamine repeat units depicted (Figure 1.20b and e).

The poly(ester amide)s showed T_g s from – 44 to 18 °C, which increased with increasing polyamide content. T_m s of 51 and 59 °C were observed at 10 and 30% amide content and likely corresponding to crystalline domains of polyesters, whereas T_m s of 100, 135, and 161 °C were observed at 30, 50, and 70% amide content and likely correspond to crystalline domains of polyamides. All polymers showed degradation temperatures above 340 °C as determined by TGA.

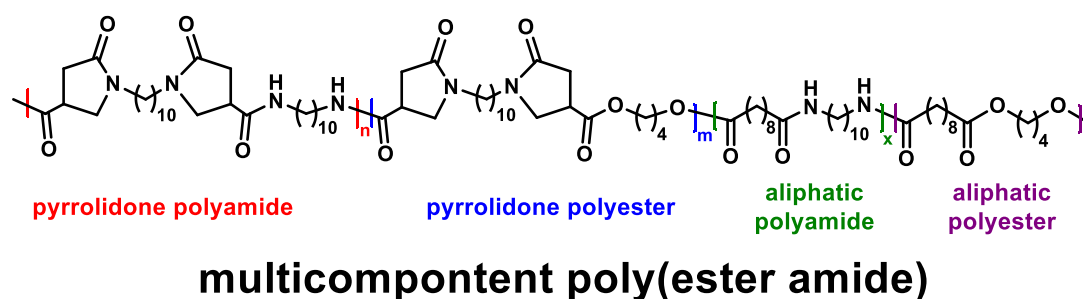


Figure 1.24. Proposed structure of poly(ester amide)s explored by Zhao and co-workers.¹¹⁹

Mechanical testing was also performed (Table 1.4, entries 21 – 24). Poly(ester amide)s showed tensile strengths between 14 and 49 MPa that increased with increasing

amide content, and elongations at break between 17 and 39% that decreased with decreasing amide content. Young's moduli varied from *ca.* 20 to 140 MPa. Notably, the elongations at break exhibited by these poly(ester amide)s are significantly higher than other IA-based polyamides (typically between 1 and 7%), demonstrating the ability to tune mechanical properties by incorporation of ester linkages in the polymer backbone. Finally, degradation testing in phosphate buffer at a pH of 7.4 at 37 °C was performed on the 10 and 30% ester poly(ester amide)s, which showed between 10 and 40 wt% loss after 50 days, with faster degradation attributed to increasing ester content attributed to faster degradation.

While IA-based pyrrolidone monomers have typically been used to generate polyamides (or poly(ester amide)s), a recent report by Miller and co-workers in 2016 showed that pure pyrrolidone-containing polyesters could also be generated.¹²⁴ To do this, both mono-pyrrolidone and bis(pyrrolidone) monomers were synthesized: IA was reacted with either 0.55 equiv of ethanolamine or 0.55 equiv diamine (J2, J3, J4, J5, or J6 backbones) at reflux to give the mono-pyrrolidone AB acid/alcohol monomer (Figure 1.20, X = OH) or the AA bis(pyrrolidone) diacid monomer, respectively. A two-step process was then used to perform polymerizations. First, Sb₂O₃ (2 mol%) was added to either the AB monomer or a mixture of an AA bis(pyrrolidone) with the desired diol, and the monomers were heated at 180 °C for 4 h. Next, the temperature was then increased to 240 °C over 8 h while vacuum was introduced into the system. The AB polymerization resulted in a polymer with an M_n of 20.8 kg/mol with a dispersity of 2.1, while the AA + BB polymerization resulted in polymers with M_n s from 10.0 to 23.4 kg/mol with dispersities of 2.1 to 4.1. T_g s of these pyrrolidone-containing polyesters

ranged from 24 to 60 °C and generally decreased with increasing backbone length. All polymers showed good thermal degradation temperatures, with 50 wt% loss observed by at 370 to 390 °C. The properties of these polymers were comparable to commercial PLA and PET, which showed T_g s of 52 and 83, and T_d s of 343 and 414 °C, respectively.

The authors also performed degradation studies on these materials and tracked the loss of molar mass over time, along with the degradation products. Degradation studies were done in both air and water over one year. After ~30 days in water, the polyesters were fully dissolved and showed steady loss in M_n to ~ 0.5 kg/mol. Samples exposed to air also underwent degradation, though only partial loss in M_n was observed (*e.g.* from 20 kg/mol to 18 kg/mol for bis(pyrrolidone) J2 sample). ^1H NMR, MALDI-TOF, and electron spray ionization-time of flight (ESI-TOF) were utilized to study the degradation pathway and showed regeneration of the original alcohol and bis(pyrrolidone) monomers, as well as oligomers, after 1 year. This degradation pathway, likely proceeding through hydrolysis of the ester chains in the backbone, contrasts with the polyamides, where degradation via pyrrolidone ring-opening and solubilization occurred, but where no chain scission along the polymer backbone was observed.¹¹⁶

Wilsens and co-workers next reported the formation of polyamides using IA-derived bis(pyrrolidone)s with furfural-based oxazolines to make completely bio-based, polyamides with branched/cross-linked structures (Figure 1.25).¹²⁵

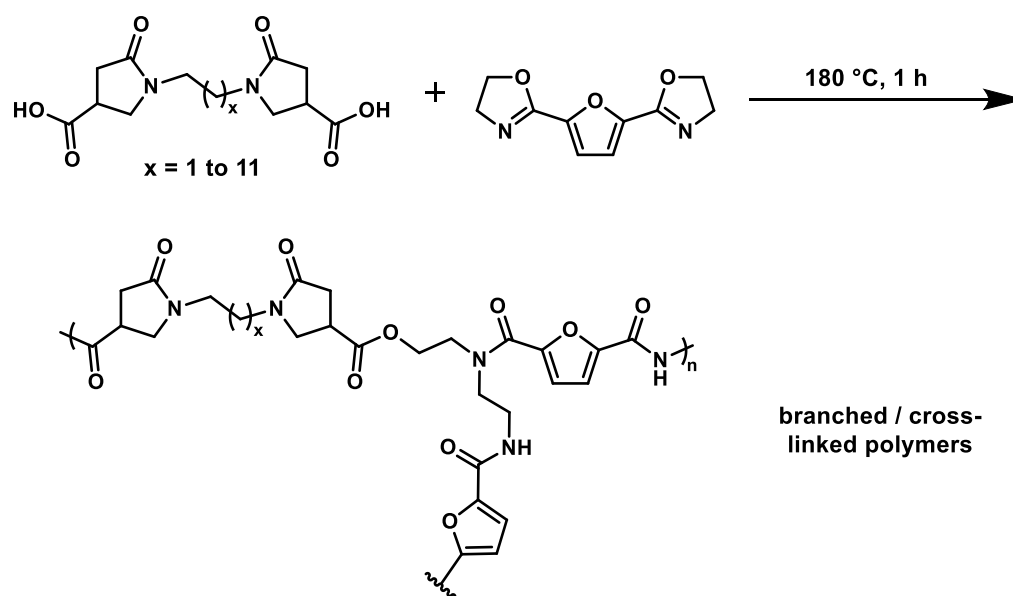


Figure 1.25. Polymerizations/cross-linking of IA-derived bis(pyrrolidone) with furfural-derived oxazolines.¹²⁵

Bis(pyrrolidone)s (Figure 1.20, J2 to J12 aliphatic backbone) and furfural-derived oxazolines were melt-polymerized without solvent or catalyst. As the produced amide bond can react with the oxazolone, non-linear branched / crosslinked structures were obtained. Polymerizations were run by mixing the bis(pyrrolidone) and oxazoline in the desired ratio with triphenyl phosphite (TPP, 1 wt%) added as a catalyst. These mixtures were then heated at 180 °C for 1 h. Under these conditions, polymerizations reached *ca.* 80% conversion within 5 minutes. While molar masses were not directly determined for this system, due to the lack of solubility of the cross-linked materials prohibiting SEC analysis, reaction of a bis(pyrrolidone) with a non-furfural derived oxazoline less reactive to cross-linking resulted in M_w values of 10 to 20 kg/mol after just 1 minute of heating. T_g s of the furfural/IA based materials ranged from *ca.* 60 to 120 °C and decreased with increasing backbone length from J2 to J12. Notably, these materials were particularly susceptible to plasticization by water, which resulted in

lower T_{gs} (*ca.* 20 to 70 °C). Degradation testing was also performed and studied by UV-Vis, which demonstrated that these materials are susceptible to enzymatic depolymerization.

While the majority of papers reporting the synthesis of polymers from IA-derived pyrrolidones utilize step-growth polymerizations, an early report by Sorrestino and co-workers appended the pyrrolidone unit to an acrylate or oxazoline functional group for subsequent free radical polymerization.¹²⁰ Notably, these polymers serve as *N*-vinylpyrrolidone surrogates (Figure 1.26). First, *N*-methyl-2-pyrrolidone-3-carboxylic acid or its zinc salt was prepared from IA with methyl amine (Figure 1.20a, **1.5**). From the acid of **1.5**, amidation with ethanol amine followed by ring-closing gave the oxazoline pyrrolidone **1.6**, while treatment of the zinc salt of **1.5** with acetylene at high temperature gives the acrylate pyrrolidone, **1.7** (Figure 1.26a). Subsequently, cationic polymerization of **1.6** initiated by TsOMe (Figure 1.26b)¹²⁶ or radical polymerization of **1.7** initiated by AIBN (Figure 1.26c) results in pyrrolidone-based polymers from IA.

The oxazoline polymers (**1.8**) had M_{n} s of 4.3 to 12.1 kg/mol and T_{gs} of 133 to 151 °C, whereas the acrylate polymers (**1.9**) had M_{n} s of 8.3 to 13.5 kg/mol and T_{gs} of 77 to 83 °C. Like poly(vinylpyrrolidone) (PVP), **1.9** showed good solubility in organic solvents, whereas **1.8** showed lower solubility (*e.g.* **1.8** was insoluble in DCM, chloroform). Both **1.8** and **1.9** were water-soluble. Interestingly, both polymers had high iodine complexation affinity, with the complexation of the **1.9** higher than that of PVP, which the authors attributed to distancing of the lactam moiety away from the polymer backbone.

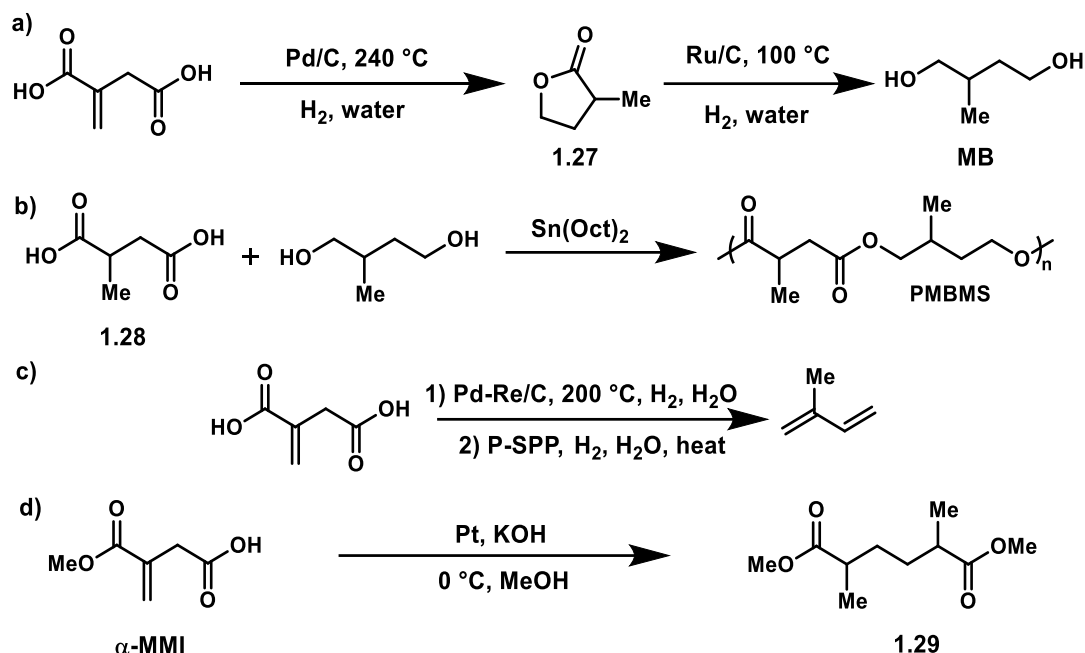


Figure 1.26. a) **1.6**, an oxazoline-containing pyrrolidone, was synthesized by the addition of ethanolamine to acid **1.5**, followed by an intramolecular condensation. Alternatively, treatment of the zinc salt of **1.5** with acetylene at elevated temperatures results in the pyrrolidone acrylate, **1.7**. b) **1.6** was polymerized cationically with pTsOMe at an elevated temperature. c) **1.7** was polymerized radically with AIBN at an elevated temperature.

A final example of pyrrolidone-containing polymers comes from a report by Schmitt and co-workers in 1969 (Figure 1.27).¹²⁰ From a methyl or ethyl IA diester, a cyanide group was added to DMI through a Michael addition under acidic conditions to give the cyano adduct, **1.10**, in ~75% yield. Reduction using hydrogen and Raney nickel then produces the six membered lactam, **1.11**, in 90% yield. Interestingly, the authors did not observe the formation of the five-membered pyrrolidone in the transformation of **1.10** to **1.11**. Subsequent heating of **1.11** at 175 °C without catalyst and with or without inert solvent in the presence of a few drops of water resulted in polymerization to a polyamide containing a pyrrolidone in the unit directly along the backbone (**1.12**). The authors postulated that during the polymerization process, **1.11** isomerized to an

anhydride intermediate, which then underwent polycondensation to yield polymer **1.12**. Polymer characterization was performed with ^1H NMR and IR spectroscopy, and no NH or CO_2H groups were detected. **1.12** was insoluble in common organic solvents and only dissolved in solvents such as formic acid, *m*-cresol, trifluoroethanol, or sulfuric acid. A T_g of 135 °C was observed by DSC, and a decomposition temperature (1% wt% loss) of 300 °C was observed by TGA, demonstrating the thermal stability of this **1.12**. Additionally, tensile testing determined that the polymer exhibited very high tensile strength at relatively low elongation.

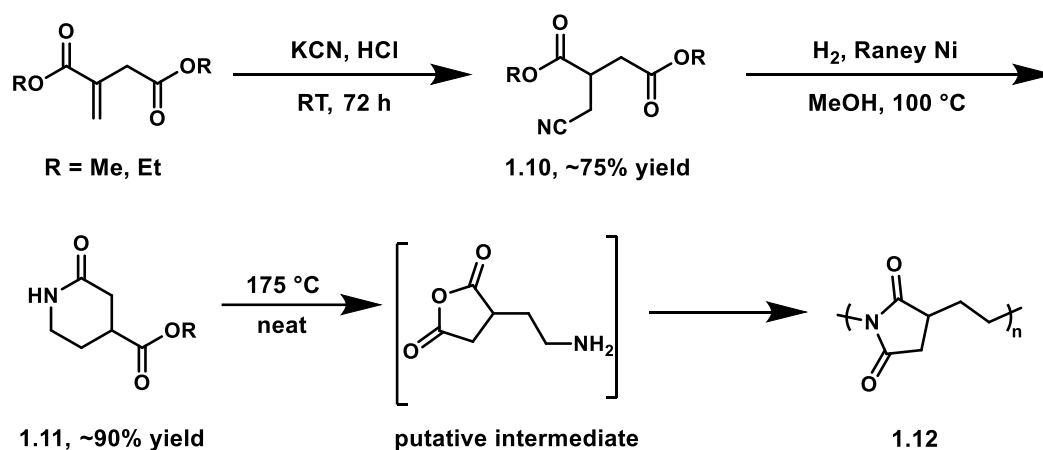


Figure 1.27. Synthesis and thermal polymerization of **1.11**.

MONOMERS FOR METATHESIS POLYMERIZATIONS

Metathesis polymerizations have been utilized in the past few decades as a power method for the generation of polymers with varying molar masses, architectures, and applications.^{127,128} Recently, IA-derived monomers amenable to metathesis polymerization have been explored for the generation of biorenewable materials.

Metathesis polymerization from IA derivatives was first explored in 2014 by Li and co-workers,¹²⁹ who used an acyclic diene metathesis (ADMET) strategy to

polymerize **1.13** to **1.14**, which could be functionalized following their synthesis (Figure 1.28a).

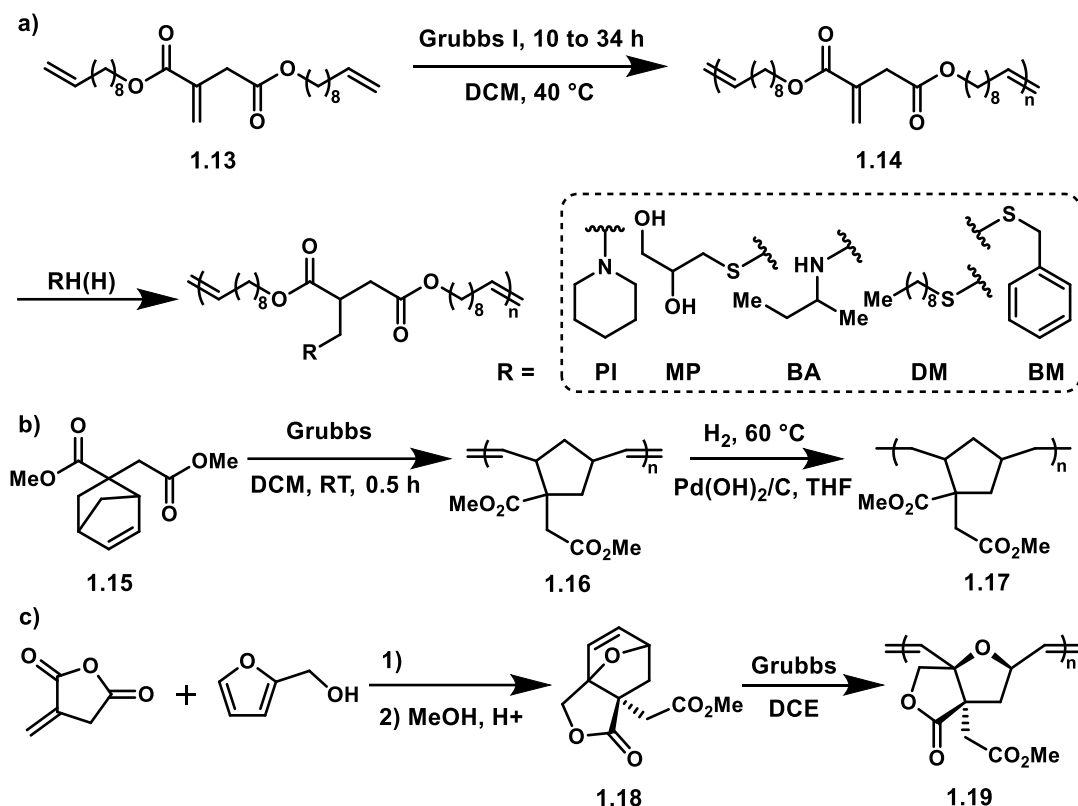


Figure 1.28. Metathesis-derived polymers based on IA. a) ADMET of **1.13** and subsequent post-polymerization modification; b) ROMP of **1.15**; c) Synthesis and ROMP of **1.18**.

An unsaturated polyester (**1.14**) with an M_n of *ca.* 23.4 kg/mol and a dispersity of 1.75 was obtained following the polymerization of **1.13** at 40 °C using generation I Grubb's catalyst. The M_n of **1.14** could be increased to 44 kg/mol with a lower dispersity of 1.46 after reaction for a total of 34 h under slightly more dilute conditions, while cross-linking occurred when the reaction was run in bulk over 3 d. Spontaneous cross-linking of **1.14** also occurred upon storage at RT, though this could be avoided by storing the material at 0 °C. Following polymerization under the ideal, diluted conditions in DCM, ¹H NMR established that the olefin in **1.13** was retained in **1.14**,

demonstrating that no side reactions occurred. The post-polymerization modification of **1.14** was also explored using thiol-ene or Michael-ene click chemistry with a variety of substrates, including hexahydropyridine (PI), 3-mercapto-1,2-propanediol (MP), *sec*-butyl amine (BA), dodecyl mercaptan (DM), or benzyl mercaptan (BM). These substrates were added to **1.14** and left to react at 0 or 25 °C for 12 – 20 h, using triethyl amine as a base for the thiol-ene reactions. At substrate:olefin ratios of 15:1, with a 1:1 substrate:triethyl amine ratio for thiol substrates, near quantitative conversion to the functionalized polyesters were observed for DM, MP, BM, or PI. Alternatively, lower conversions were obtained at lower (3:1) substrate:olefin ratios, and under these conditions sequential modifications of the unsaturated polyester could be achieved. Thus, *ca.* 30% conversion of the unsaturated polyester with MP (3 equiv), followed by the addition of PI (12 equiv) to convert the remaining olefin, gave a multi-functional polyester.

While the thermal properties of **1.14** were difficult to probe due to cross-linking at higher temperatures, DSC analysis revealed variable T_g s for the DM-, MP-, BM-, or PI-functionalized polyesters were – 15 °C, – 31 °C, – 47 °C, and – 51 °C, respectively. Additionally, decomposition temperatures (at 5 wt% loss) varied between 210 and 370 °C. These materials also exhibited crystallinity, with T_m s between – 11 °C and 31 °C. Functionalization with a secondary amine (BA) led to chain scission due to internal cyclization to a pyrrolidone, resulting in the loss of molar mass. Because of this, the addition of a secondary amine can potentially be utilized as a controlled degradation method.

Next, Meier and co-workers employed a ring-opening metathesis polymerization (ROMP) strategy using an IA-derived norbornene (Figure 1.28b, **1.15**).¹³⁰ The polycondensation of IA with various alcohols and the post-functionalization of the resulting polyesters were also explored, though that topic is beyond the scope of this review.

A neat, catalyst-free Diels-Alder reaction between cyclopentadiene and DMI provided the **1.15** in 80% yield as a mixture of diastereomers. ROMP of **1.15** using Umicore M3₁ or Grubbs 3rd generation catalysts was then explored, and the polymer **1.16** with M_n s varying from 16 to 88 kg/mol and dispersities of 1.07 to 1.42 was synthesized. The M_n of **1.16** grew linearly with an increasing [M]/[I] ratio, showcasing the control over this process, with cis/trans ratio of 43/57 for **1.16** observed in all cases. While $M_{n,exp}$ values were higher than their theoretical counterparts, this was likely due to the use of PMMA standards for molar mass determination by SEC. The Hoveyda-Grubbs catalyst also led to polymerization, though broader dispersities of 1.5 – 1.9 were obtained. The T_g s of **1.16** generally increased with increasing M_n from 57 to 82 °C. After polymerization, hydrogenation of **1.16** resulted in fully saturated polymer **1.17** with lower glass transition temperatures compared to the unsaturated analogues (T_g s of 25 or 60 °C following hydrogenation), which the authors attributed to the increase in polymer backbone flexibility.

Another Diels-Alder adduct monomer (**1.18**) based on IA was synthesized for ROMP polymerization by Farmer and co-workers (Figure 1.28c).¹³¹ Concurrently, a detailed mechanistic study of the Diels-Alder reaction for the formation of **1.18** was studied in detail by Hoya and co-workers.¹³²

While homopolymerization of **1.18** occurred homogeneously at RT in DCE with either Grubbs 2nd generation or Hoveyda-Grubbs catalysts, after quenching with ethyl vinyl ether the obtained polymer (**1.19**) was insoluble in all solvents tested. Thus, copolymerizations with dimethyl *endo-cis*-5-norbornene-2,3-dicarboxylate were investigated. Mixtures of **3**, *endo-cis*-5-norbornene-2,3-dicarboxylate, and catalyst (Grubbs 2nd generation or Hoveyda-Grubbs) ranging from 25:25:1 to 200:200:1 in 1,2-dichloroethane (DCE) at RT or 40 °C resulted in soluble copolymers with M_n s ranging from 9.5 to 63.2 kg/mol that increased with increasing monomer:catalyst ratio and that were in good agreement with $M_{n,theo}$. Dispersities for these copolymers were low and ranged from 1.15 to 1.27, and the materials showed high T_g s of 158 – 163 °C. While copolymerizations proceeded in a controlled manner in DCE, polymerizations run in different solvents (such as THF or EtOAc) resulted low molar mass samples with M_n values that did not agree with $M_{n,theo}$.

The synthesis and polymerization of other alkyl esters of **1.18** was explored in a follow-up publication by Farmer and coworkers.¹³³ While polymerization of the shorter chain-length esters of **1.18** using Grubbs 2nd generation catalyst in DCE at RT (typically for 72 h) resulted in insoluble polymers, the ROMP of esters from alcohols with five or more carbons gave polymers with improved solubilities. In these cases, the polymerizations proceed in a controlled fashion with living characteristics. Most polymers had high thermal stabilities above 300 °C, with T_g s around 70 to 100 °C.

PHOSPHOROUS CONTAINING POLYMERS BASED ON IA

Phosphorous-containing materials are often sought after for their flame-retardant properties.¹³⁴ For this reason, the incorporation of phosphorous into polymer

backbones, especially those that are derived from biorenewable resources, represents an important class of materials that could see use in flame resistance applications. An early report exploring phosphorous-containing IA-derivatives that could be used in polymer synthesis came in 1991 from Borisov and Doseva.¹³⁵ The authors performed Michael additions of alkyl phosphites to IA to generate phosphorylated IA derivatives, though only oligomers ($M_n < 1$ kg/mol) of these compounds were generated. Alternatively, unsaturated oligomers ($M_n < 1$ kg/mol) made by condensing IA esters with diols were functionalized with dimethyl phosphite as a way to add phosphorous to the oligomer backbone. The authors demonstrated that these phosphorylated IA-based oligomers could then be incorporated industrial polyurethane compositions to modify the flame inhibition properties; in modifications with 8, 14, and 27 wt% of the phosphorylated materials showed oxygen index percentages of 22, 23, and 24%, relative to 21% for the unmodified composition. Oxygen indices demonstrate the relative flammability of a material and are measured by burning a material sample in a controlled oxygen/nitrogen atmosphere. The oxygen level is decreased over time until combustion of the sample is no longer supported, at which point the oxygen index has been achieved.¹³⁴ Thus, the addition of phosphorylated IA-based oligomers to industrial polyurethane compositions increased the required oxygen content needed for combustion by up to 3%, decreasing the material's relative flammability.

A significant step towards the production of flame-resistant polymers based on IA came in 1999, when Chang and Chang reported the direct polymerization and functionalization of IA to generate IA-based phosphorylated copolyesters that could serve as flame-resistant PET modifications. (Figure 1.29a).¹³⁶ To synthesize these

polyesters, they mixed IA, terephthalic acid, ethylene glycol, and 9,10-dihydro-9-*oxa*-10-phosphanephenanthrene-10-oxide (DOP), a well-known phosphorous-containing flame retardant.¹³⁷ A multi-stage step-growth procedure was then performed. Notably, rather than making a DOP-functionalize IA derivative separately, the procedure was optimized to allow for Michael addition of DOP to IA *in situ*. In the first step of the polymerization, H₂PtCl₆ was added as a microaddition catalyst to facilitate the Michael addition of DOP to IA; this proceeded at 110 °C for 4 h. In the second step, after the microaddition reaction was complete, the temperature was raised to 230 °C to promote esterification. Once high conversion (> 95%) of esterification was achieved, Ti(OBu)₄ was added as a transesterification catalyst and the temperature was increased to 275 °C at low pressure (< 1 mm Hg) to promote polycondensation to a high molar mass polymer. Under these conditions, polymers with high intrinsic viscosities (0.62 – 0.64 dL/g) and low acid values (20 – 23 mEq/kg) were obtained with phosphorous contents of 0.7 to 3.0 wt% (or 4.5 to 22.6 mol% DOP incorporation). This method proved more efficient than the same reaction run in the absence of H₂PtCl₆ microaddition catalyst, which produced polymers with lower intrinsic viscosities (0.49 or 0.50 dL/g) and higher acid values (34 or 37 mEq/kg). Alternatively, the DOP-IA derivative could be first synthesized in a separate step by heating DOP with IA at 160 °C for 1.5 h. When DOP-IA was mixed with terephthalic acid and ethylene glycol and subjected to the second and third stages of their polycondensation procedure (230 °C for esterification, followed by Ti(OBu)₄ addition and heating at ~270 °C for polycondensation at < 1 mm Hg), a polymer with a high intrinsic viscosity (0.640 dL/g) and a low acid value (21 mEq/kg) was obtained.

The physiochemical properties of the copolyesters obtained from the three-step polymerization of IA with H_2PtCl_6 and $\text{Ti}(\text{OBu})_4$ were evaluated. Glass transition temperatures for all polymers were observed at *ca.* 77 °C regardless of phosphorous content (0.7 – 3.0 wt%) and were close to that of PET (82 °C for a sample of intrinsic viscosity 0.64 dL/g, with an acid value of 19.5 mEq/kg). Additionally, the presence of the bulky phosphorous side group inhibited crystallinity in the polymer: T_{m} s of 236, 228, and 188 °C were observed for 0.7, 1.2, and 2.0 wt% phosphorous containing polymers, respectively, whereas the 3 wt% composition was amorphous. This contrasts with the T_{m} of PET, which was observed at 257 °C. The polymers showed thermal decomposition temperatures under nitrogen ranging from 431 to 413 °C (relative to 442 °C for PET) that decreased with increasing phosphorous content, while thermal decomposition temperatures under oxygen that ranged from 386 to 397 °C and increased with increasing phosphorus content (relative to 382 °C for PET). Notably, the oxygen index increased from 33.3% to 35.2% with increasing phosphorous content and showed a large improvement relative to PET (23.7%). Finally, mechanical testing demonstrated that the polyesters exhibited similar rheological behavior compared to PET and that, while tensile strength decreased with increasing phosphorous content (41 – 30 MPa relative to 60 MPa for PET), impact strength increased (24 to 28 J/M relative to 21 J/M for PET). These IA/PET-based copolyesters demonstrated significant increases in oxygen indices relative to PET while maintaining similar rheological behavior, and serve as potential high-performance, flame resistant, and renewable PET analogues.

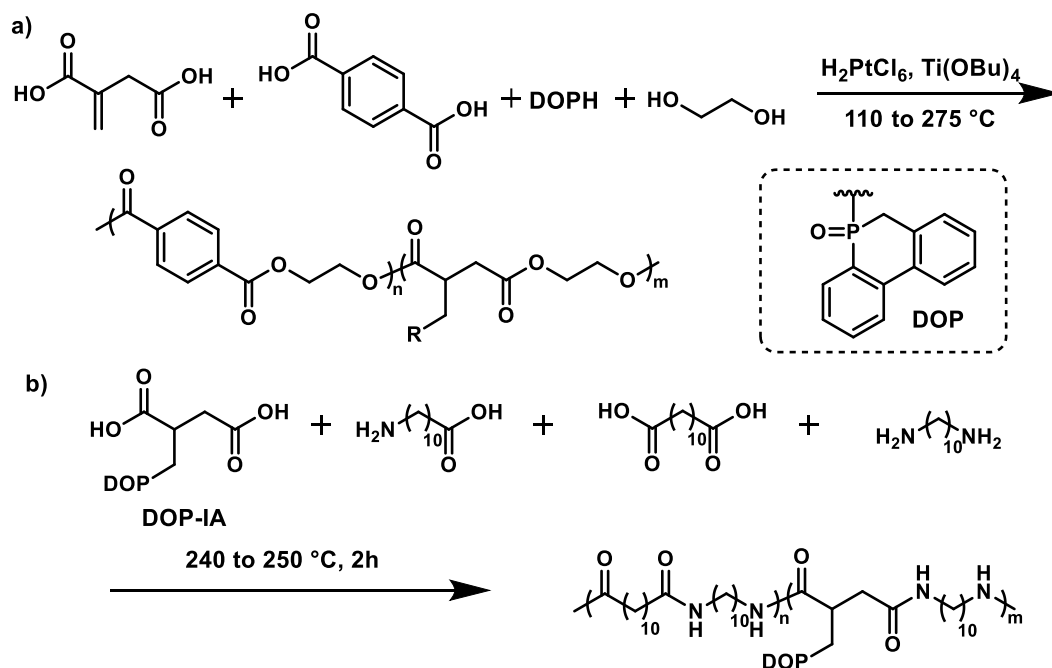


Figure 1.29. a) Step-growth polymerization and one-pot functionalization of IA to give phosphorylated IA copolyesters; b) synthesis of phosphorous containing polyamides from IA.

The most recent report of phosphorous-containing IA-based polymers came from Negrell *et al.* in 2016, who synthesized flame-resistant polyamides based on DOP-IA (Figure 1.29b).¹³⁸ Polycondensation polymerization of DOP-IA with 11-aminoundecanoic acid, 1,10-diaminodecane, and 1,10-decanoic diacid in varying ratios were performed, typically by stirring at 220 °C for 45 min with 600 ppm of acid catalyst. Under these conditions, polyamides ranging from 0.3 to 1.0 wt% phosphorous (or 3.3 to 11.1 wt% DOP-IA) content were synthesized. The polymers had intrinsic viscosities ranging from 0.46 to 1.07 dL/g that decreased with increasing phosphorous content, T_g s between 40 and 42 °C, and T_m s between 155 and 158 °C. Notably, the T_g s and T_m s of these polymers were lower than the commercially available biobased polyamide 11 (T_g = 52 °C, T_m = 194 °C). Thermal degradation was also studied, and polymers with 0.5 or

1.0 wt% phosphorous content showed 5% mass losses by TGA at 393 and 387 °C, respectively. Finally, oxygen indices were roughly assessed to be 28 and 40 – 45% for the 0.5 and 1.0 wt% phosphorous-containing polymers, respectively, while commercial polyamide 11 had an oxygen index of 22%. Other flame inhibition testing, such as the UL94 or cone calorimeter tests, were performed and confirmed that incorporation of DOP-IA into the polyamide backbone imparted flame inhibition on the resulting copolymers.

FLUORINE CONTAINING POLYIMIDES BASED ON IA

Fluorinated polyimides are an important class of polymers that see use in membrane-based applications.¹³⁹ In 2002, Mas and co-workers utilized IA to generate a fluorinated diamine for the synthesis of a fluorinated polyetherimide (Figure 1.30a).¹⁴⁰ First, they reacted DMI with perfluorohexyliodide in the presence of zinc and AcOH to give the Michael addition adduct, **1.20**, in 90% yield. From here, reduction of the ester groups of **1.20** with LiAlH₄ produced the fluorinated diol, **1.21**, in 91% yield. Subsequent tosylation of the diol to **1.22**, followed by substitution with sodium iodide (NaI), gave the diiodo species, **1.23**, in 82% yield. Finally, substitution of the iodo groups with NaN₃ gave the diazide species, **1.24**, in 96% yield, with reduction of the azides using hydrogen gas and Pd/C, producing the desired fluorinated diamine, **1.25**, in 89% yield. An alternative route involving bromination of the alcohols, substitution with phthalimide, and then reduction to the amine was also explored.

The synthesis of the fluorinated polyetherimide proceeded through step-growth polymerization (Figure 1.30b). When **1.25** mixed with an aromatic anhydride and heated at 120 °C for 2 d in NMP, polymerization occurred to give a poly(ether amic

acid) that was isolated by precipitation. Subsequently, ring-closing was performed with additional heating at 120 °C under vacuum for 12 h to afford the fluorinated, IA-based poly(ether imide) (**1.26**) with an M_n of 6.0 kg/mol and a dispersity of 2.03. The authors attributed the long reaction time required for the polymerization to the strong electron-withdrawing nature of diamine **1.25**. The T_g of the polymer sample was 113 °C, and it degraded (10 wt% loss) at 440 °C in air or 485 °C in argon. Thin films of **1.25** were prepared and contact angles were measured in water and diiodomethane, showing values of 90 and 77°, respectively.

In a follow-up paper published in 2005, Mas and co-workers reported the synthesis of copolymers of the fluorinated polyetherimide with non-fluorinated polyetherimides with phenylene diamines in place of **1.25**.¹⁴¹ Copolymers with 25, 50, or 75% fluorinated polyetherimide backbone were synthesized by the previously employed method, generating copolymers with M_n s ranging from 7.0 to 15.6 kg/mol and dispersities of 2.55 to 3.43. Relative to fully fluorinated **1.26**, incorporation of the non-fluorinated material into the copolymer backbone increased the T_g from 121 °C (at 75% **1.26**) to 217 °C (non-fluorinated poly(ether imide)). Conversely, decomposition temperatures (at 5 wt% loss) of the copolymers were lower (400 and 370 °C for all copolymers in argon and air, respectively) than either **1.26** or the non-fluorinated material (520 °C in both argon and air). Interestingly, contact angles of copolymer thin films varied from 84.4 to 90.4° in water and 32.0 to 61.0° in diiodomethane, demonstrating that hydrophobicity is increased as incorporation of **1.25** increases in the copolymer. Notably, these polymers showed solubility in THF and chloroform under ambient conditions, demonstrating their organophilic properties.

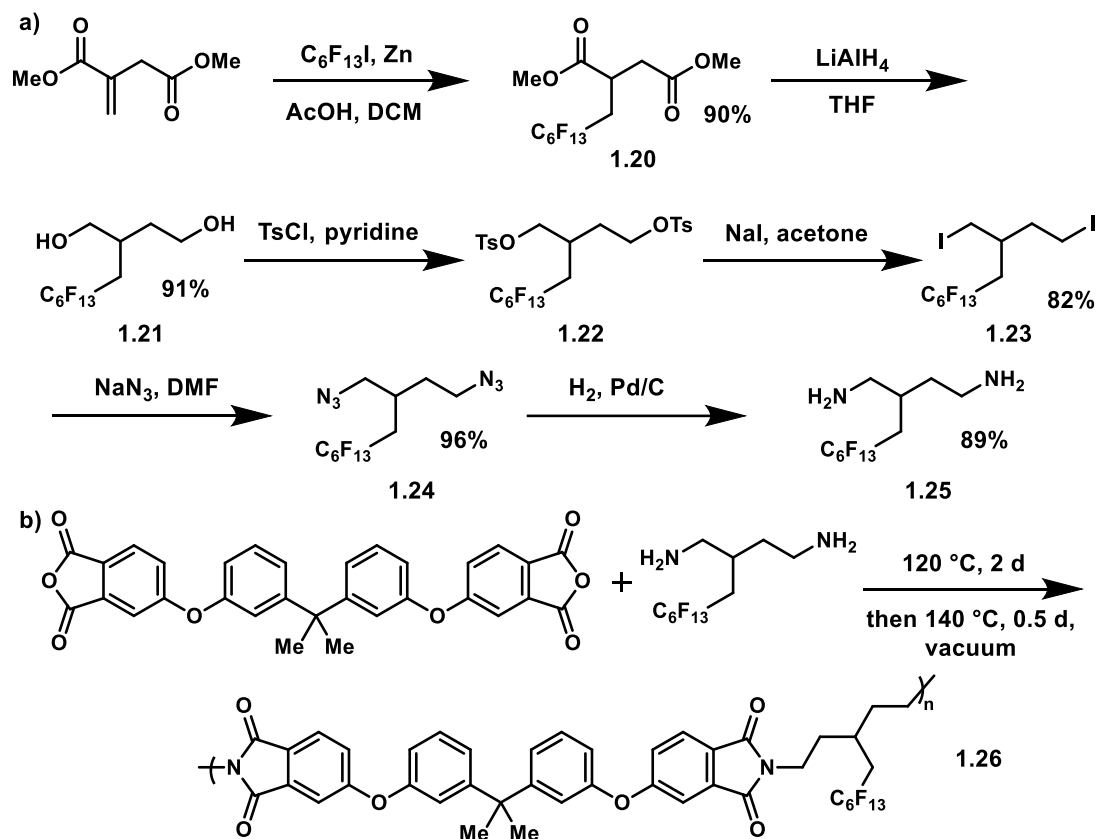


Figure 1.30. a) Synthesis of fluorine containing diamine **1.25** based on IA and b) polymerization of **1.25** to give fluorinated polyetherimide **1.26**.

OTHER EXAMPLES OF IA-DERIVED MONOMERS AND POLYMERS

In 2016, Dauenhauer and co-workers explored the reduction of various biorenewable diacids, including IA, to a number of diols that could be used in step-growth polymerizations to generate polyesters (Figure 1.31a and b).¹⁴² They found that under aqueous conditions, reduction of IA using high temperatures (240 °C) and high pressures of hydrogen produced α -methyl- γ -butyrolactone (**1.27**), which could be subsequently reduced with Ru/C (100 °C, H₂) to form 2-methyl-1,4-butanediol (MB) in 80% yield (Figure 1.31a). Subsequent polymerization of MB with the potentially IA-derived 2-methylsuccinic acid (**1.28**) was then performed using a two-step procedure: first, the monomers were mixed with Sn(Oct)₂ (11 mol%) and heated at 120 °C for 24

h under vacuum (10 torr) and then the temperature was increased to 150 °C under vacuum (0.1 torr) and the reaction was allowed to proceed for 12 h. Under these conditions, the polyester PMBMS was obtained with an M_n of 10.8 kg/mol and a dispersity of 1.20 (Figure 1.31b). PMBMS showed a T_g of – 36 °C and a T_d (in nitrogen) of 311 °C (at 5 wt%). Additionally, in contrast to the unsubstituted poly(butylene succinate), PMBMS was amorphous and did not exhibit a T_m . The transformation of IA to **1.28** was also explored in 2017 by Palkovits and co-workers, who performed chemical and electrochemical reductions of IA to **1.28** in acidic media or crude fermentation broth.¹⁴³ Importantly, using a separated single electrolysis cell operating at – 1.41 V vs. standard hydrogen electrode (SHE) in aqueous, acidic medium, a Pb electrode showed high activity and up to 98% yield was obtained for the transformation of IA to **1.28** at RT. More recently, IA was shown to be a starting point for the synthesis of isoprene, when Dauenhauer and co-workers performed reductions of IA to isoprene in a two-step process.¹⁴⁴ First, IA was reduced to 3-methyltetrahydrofuran under high temperature (200 °C), aqueous conditions with hydrogen and a Pd-Re/C catalyst, and then 3-methyltetrahydrofuran was further reacted in the presence of a self-pillared pentasil (SPP) phosphorous containing zeolite to give isoprene (Figure 1.31c). Likewise, other reports have been made regarding the transformation of an itaconate to valued polymers: Chang and co-workers in 2017, for example, reported the electrochemical coupling of α -monomethyl itaconate (α -MMI) to diester **1.29**, which could be used in step-growth polymerization to generate polyesters (Figure 1.31d).¹⁴⁵

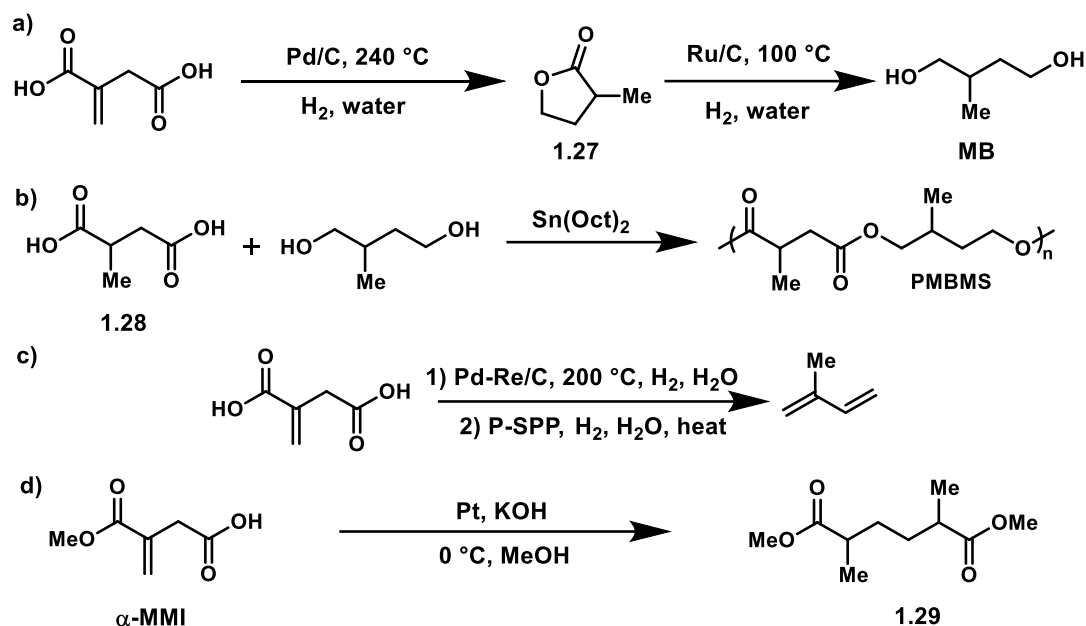


Figure 1.31. a) Reduction of IA to MB; b) Saturated IA-based polyester PMBMS generated by the polycondensation of **1.28** and MB; c) Reduction of IA to isoprene; d) Electrochemical coupling of α -MMI to diester **1.29**.

The synthesis of PMBMS was also explored by Fors and co-workers, who performed large-scale syntheses of dimethyl 2-methylsuccinate (MS) and MB (Figure 1.32).¹⁰⁹ From DMI, these saturated monomers were produced in large amounts (100 and 33 g), high isolated yields (96 and 82%), with good atom economies (100 and 65%) and low process mass intensities (PMIs of 1.1 and 2.6), representing green and sustainable synthetic processes. The step-growth polymerization of MB and MS was then performed by a two-step process: first, MB and MS were mixed with 4-methoxyphenol inhibitor (0.4 wt%) and $\text{Ti}(\text{O}^i\text{Pr})_4$ (1 mol%) and heated to 180 °C for 3 h. Then the pressure was reduced (0.05 Torr), the heat increased to 200 °C, and the reaction was run for an additional 2 h. The resulting polymer, PMBMS, was obtained with an M_n of 15.7 kg/mol, a dispersity of 2.48, a T_g of – 31 °C, and a T_d of 276 °C (5 wt% loss), in agreement with values determined by Dauenhauer and co-workers.¹⁴²

Importantly, rheological measurements determined the molar mass between entanglements to be 6.3 kg/mol, while 2D NMR experiments showed that PMBMS had a regiorandom microstructure, with a 1:1 head:tail ratio along the polymer backbone. While exclusively alcohol end groups were not obtained elusively at lower diol:diester ratios (a 1.2:1.0 ratio, for example, produced PMBMS with only ~80% alcohol chain ends), α,ω -hydroxy PMBMS (HO-PMBMS-OH) could be obtained using a 2:1 MB:MS ratio in the polymerization process. Subsequent chain-end functionalization of HO-PMBMS-OH, followed by chain-extension with MBL, gave access to an almost 100% IA-derived triblock polymer (Figure 1.13) whose tensile properties were established (Table 1.3, entry 23) and discussed earlier in this review.

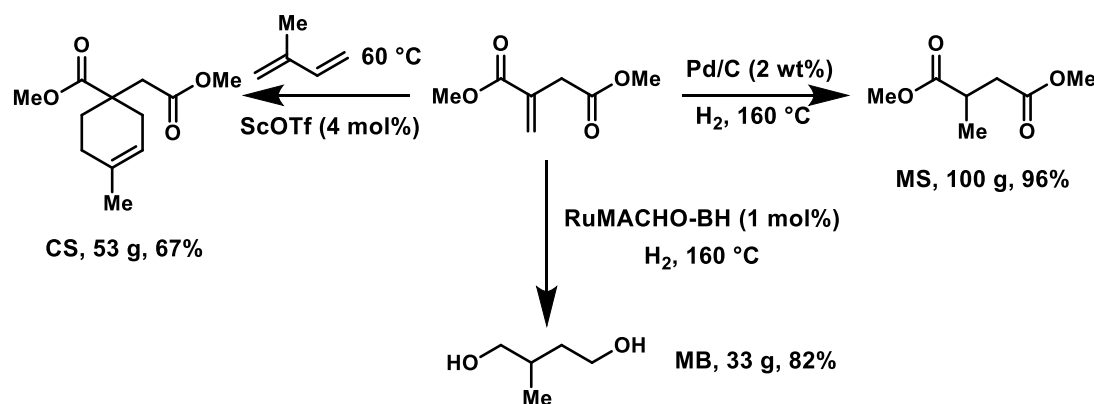


Figure 1.32. Synthesis of CS, MS, and MB monomers from DMI.

With an almost 100% IA-derived triblock polymer synthesized, Fors and co-workers then turned their attention to the generation of IA-based thermosets.¹⁰⁹ Previous work has been done generating thermosets based on IA, though uncontrolled cross-linking of the pendant olefin present in IA can occur during the relatively harsh conditions of the step-growth process.^{58,59,146} To avoid this, the conjugation of α,β -unsaturated system of DMI was broken through a catalytic Diels-Alder reaction with

the potentially IA-derived isoprene to generate CS (53 g in 67% isolated yield) with an excellent atom economy (100%) and PMI of 12. Notably, $\text{Sc}(\text{OTf})_3$ was employed as a potentially recyclable catalyst for the Diels-Alder reaction between CS and isoprene, which represents an improvement over the previous method for this reaction that utilized stoichiometric AlCl_3 .¹⁴⁷ Additionally, as isoprene has been shown to be accessible from IA, CS represents a potentially 100% IA-derived monomer.¹⁴⁴ Step-growth polycondensation polymerizations using similar conditions utilized for the synthesis of PMBMS generated PMBCS with an M_n of 11.7 kg/mol, a dispersity of 2.19, a T_g of -9 °C, and a T_d (at 5 wt% loss) of 246 °C. Like PMBMS, PMBCS synthesized with this method also exhibited a regiorandom microstructure with a head:tail ratio of 1:1. Additionally, terpolymerizations of MS, CS, and MB generated statistical copolymers ($\text{PMBCS}_x\text{-stat-PMBMS}_{1-x}$) with varying olefin content (20, 30 or 40%), M_n s of 8.3 to 21.5 kg/mol, and dispersities of 2.36 to 4.8 (Figure 1.33). T_g s of the copolyesters decreased with increasing olefin content from -21 to -27 °C, while T_d s (5 wt% loss) remained relatively constant at 244 to 251 °C.

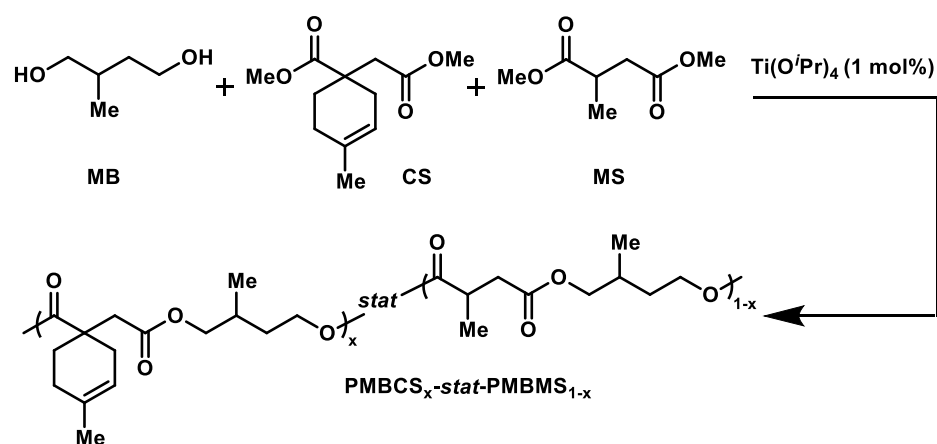


Figure 1.33. Synthesis of unsaturated copolymers from all IA-derived monomers used by Fors and co-workers.¹⁰⁹

PMBCS_x-stat-PMBMS_{1-x} was then cross-linked via thiol-ene click chemistry under 250 nm light irradiation with DMPA using a potentially renewable tetrathiol crosslinker (Figure 1.34).¹⁰⁹ The resulting thermosets showed T_g s of -13 to -22 °C that increased with increasing cross-linking density (*i.e.* increasing olefin content in the polymer prior to cross-linking) (Figure 1.35c), with T_d s (5 wt%) from 248 to 276 °C. Dynamic mechanical testing was used to probe the physical network of the material (Figure 1.35b), and established that the molar masses between crosslinks increased with decreasing cross-linking density, from 1.4 to 6.3 kg/mol. E and σ_B values determined by tensile testing increased from 1.4 – 6.2 MPa and 0.5 – 0.9 MPa, respectively, as cross-linking density increased. Conversely, ϵ_B decreased with increasing cross-linking density, from 46 to 17% (Figure 1.35c). Overall, the synthesis of both almost exclusively IA-derived triblocks (PMBL-PMBMS-PMBL) and thermosets demonstrates the utility of IA for the synthesis of a wide range of materials for different applications.

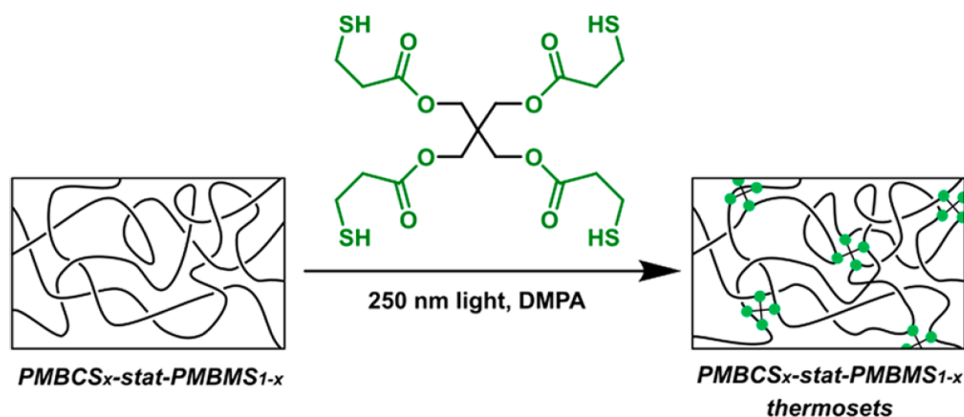


Figure 1.34. Cross-linking of PMBCS-PMBMS random copolymers. Copied with permission from the original manuscript.¹⁰⁹

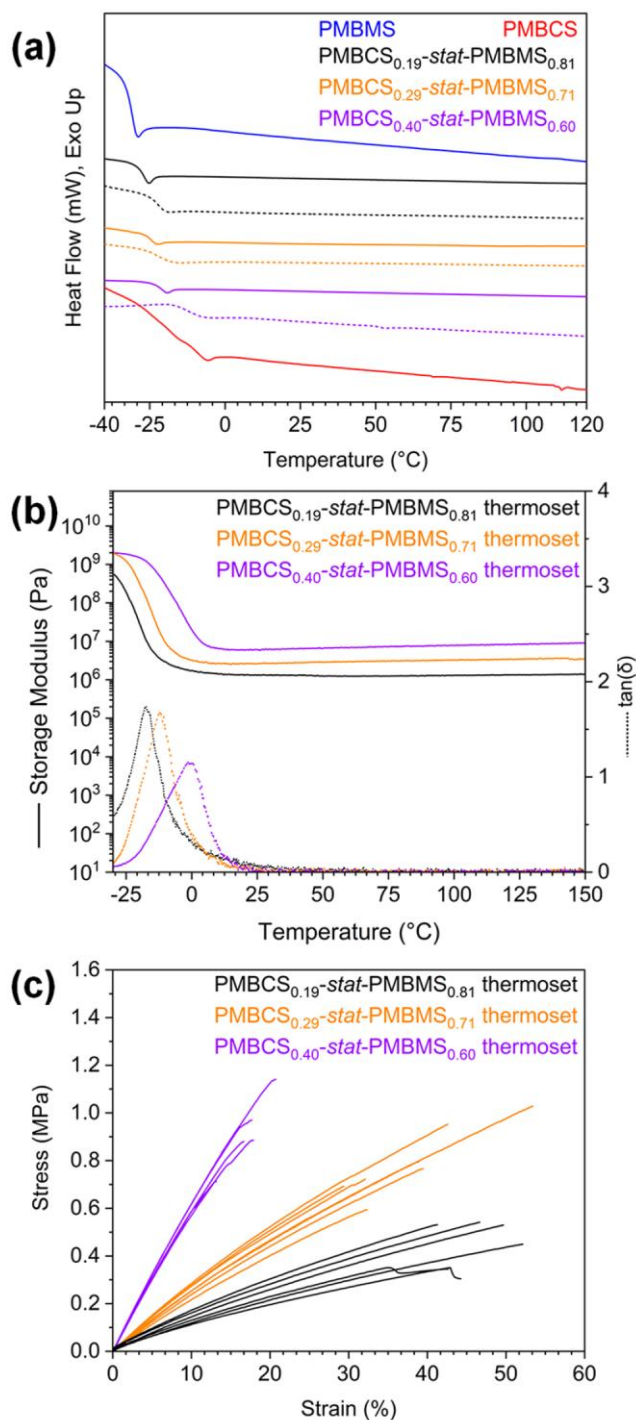


Figure 1.35. a) Differential scanning calorimetry (DSC) heat flow vs temperature traces of various prepolymers (solid lines) or thermosets (dashed lines), exo up; b) Dynamic mechanical thermal analysis (DMTA) storage modulus (left axis, solid lines) and tan(δ) (right axis, dashed lines) vs temperature traces of thermosets; c) Stress-strain curves of thermosets, where the end of each curve indicates a break point. Copied with permission from the original manuscript.¹⁰⁹

The most recent example of the use IA-derived monomers for polymerization comes from a report in 2019 by Gioia and co-workers, who utilized thiol-ene click chemistry to functionalize DMI.¹⁴⁸ **1.30** was obtained in 99% yield after reacting DMI with 1-octanethiol in acetone at RT with 30 wt% K₂CO₃ (Figure 1.36a). **1.30** was then mixed with butanediol and polymerized in a two-step process: first, the mixture was heated at 200 °C with Ti(OBu)₄ (175 ppm) for 2 h with a 2:1 **1.30**:butanediol ratio. Then, the temperature was increased to 210 – 230 °C while the pressure was reduced to 0.08 torr, and the reaction was continued for 3 h. Under these conditions, **1.31** (R = butyl, Figure 1.36b) with an *M_n* of 88.8 kg/mol, a dispersity of 2.5, and a *T_g* of – 63 °C was obtained with an onset degradation temperature of 364 °C. Polyesters with other diols (Figure 1.36b) were also synthesized using the similar polymerization conditions, and *M_n*s of 6.7 to 16.0 kg/mol with dispersities of 2.0 to 2.6 were obtained. Under these conditions, *T_g*s between – 40 to – 8 °C were obtained, with higher *T_g*s corresponding to less flexible diols.

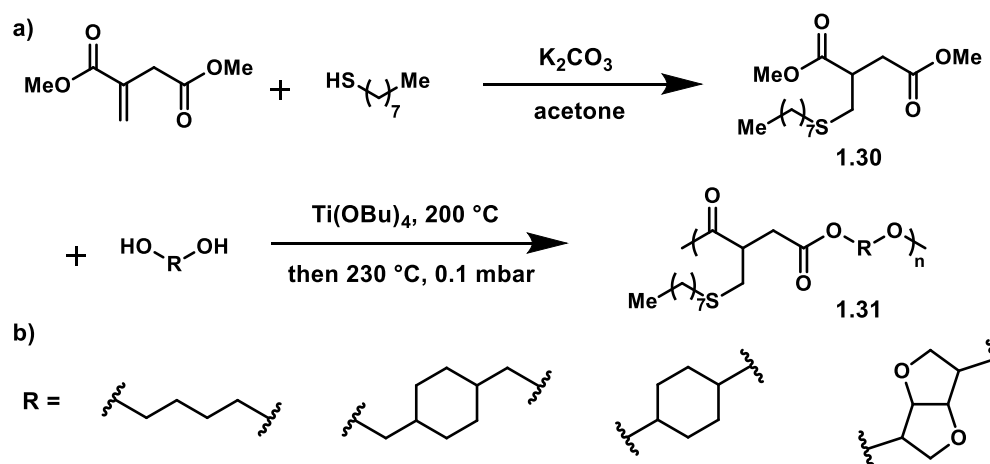


Figure 1.36. a) Synthesis and polymerization of thiol-ene adducts and their polyesters from IA and b) derivatives explored in the study.

CONCLUSION

IA is a high value feedstock chemical generated from biomass fermentation that can be transformed into structurally diverse monomers including itaconimides, methylene butyrolactones, pyrrolidones, and numerous Michael addition or Diels-Alder adducts. Subsequent polymerization through a host of methods (including ATRP, RAFT polymerization, step-growth polymerization, ROP, metathesis polymerization, or crosslinking) gives rise to polymeric materials with tunable properties for use in a number of different applications. IA-based polymers represent a major class of biorenewable materials with desirable properties, often comparable or improved relative to their petroleum counterparts, that have the potential to be economically competitive with fossil fuel-derived polymers. Altogether, research in this area will further our ability to generate plastics in a sustainable manner, and new monomers and polymers derived from IA with better properties are of no doubt on the horizon.

REFERENCES

- (1) Hosler, D.; Burkett, S. L.; Tarkanian, M. J. Prehistoric Polymers: Rubber Processing in Ancient Mesoamerica. *Science* **1999**, 284, 1988–1991.
- (2) Berzelius, J. J. Jahres-Bericht Über Die Fortschritte Der Physischen Wissenschaften. *Jahres-Bericht* **1833**, 12.
- (3) Stahl, G. A. A Short History of Polymer Science. *ACS Symp. Ser.* **1981**, 175, 25–44.
- (4) Braconnot, M. H. De La Transformation de Plusieurs Substances Végétales En Un Principe Nouveau. *Ann. Chim. Phys.* **1833**, 52, 290–294.
- (5) Lourenço, M. A.-V. Recherches Sur Les Composés Polyatomiques. *Ann. Chim.*

- Phys.* **1863**, 67, 257–339.
- (6) Feldman, D. Polymer History. *Des. Monomers Polym.* **2008**, 11, 1–15.
 - (7) Painter, P. C.; Coleman, M. M. *Essentials of Polymer Science and Engineering*; DEStech Publications, Inc.: Lancaster, PA, 2009.
 - (8) Maynard, J. P. Discovery and Application of the New Liquid Adhesive Plaster. *Bost. Med. Surg. J.* **1848**, 38, 178–183.
 - (9) Seymour, R. B. Polymers Are Everywhere. *J. Chem. Educ.* **1988**, 65, 327.
 - (10) Zalasiewicz, J.; Waters, C. N.; Ivar do Sul, J. A.; Corcoran, P. L.; Barnosky, A. D.; Cearreta, A.; Edgeworth, M.; Gahuska, A.; Jeandel, C.; Leinfelder, R.; et al. The Geological Cycle of Plastics and Their Use as a Stratigraphic Indicator of the Anthropocene. *Anthropocene* **2016**, 13, 4–17.
 - (11) Thompson, R. C.; Swan, S. H.; Moore, C. J.; vom Saal, F. S. Our Plastic Age. *Philos. Trans. R. Soc. B Biol. Sci.* **2009**, 364, 1973–1976.
 - (12) Sinn, H.; Kaminsky, W. Ziegler-Natta Catalysis. *Adv. Organomet. Chem.* **1980**, 18, 99–149.
 - (13) Stürzel, M.; Mihan, S.; Mülhaupt, R. From Multisite Polymerization Catalysis to Sustainable Materials and All-Polyolefin Composites. *Chem. Rev.* **2016**, 116, 1398–1433.
 - (14) Xue, Z.; He, D.; Xie, X. Poly(Ethylene Oxide)-Based Electrolytes for Lithium-Ion Batteries. *J. Mater. Chem. A* **2015**, 3, 19218–19253.
 - (15) Gebelein, C. G. Medical Applications of Polymers. *ACS Symp. Ser.* **1985**, 285, 535–556.
 - (16) Maitz, M. F. Applications of Synthetic Polymers in Clinical Medicine.

Biosurface and Biotribology **2015**, *1*, 161–176.

- (17) Sakurada, Y.; Takakura, K. *Macromolecular Concept and Strategy for Humanity in Science, Technology and Industry, Ch. 8: Impact of Medical Technology Utilizing Macromolecules on Society*; Okamura, S., Rånby, B., Ito, Y., Eds.; Springer, Berlin, Heidelberg, 1992.
- (18) Geyer, R.; Jambeck, J. R.; Law, K. L. Production, Use, and Fate of All Plastics Ever Made. *Sci. Adv.* **2017**, *3*, 1–5.
- (19) Oil consumption http://www.bpf.co.uk/Press/Oil_Consumption.aspx (accessed Feb 15, 2019).
- (20) Hopewell, J.; Dvorak, R.; Kosior, E. Plastics Recycling: Challenges and Opportunities. *Philos. Trans. R. Soc. B Biol. Sci.* **2009**, *364*, 2115–2126.
- (21) The New Plastics Economy: Rethinking the Future of Plastics & Catalysing Action <https://www.ellenmacarthurfoundation.org/publications/the-new-plastics-economy-rethinking-the-future-of-plastics-catalysing-action> (accessed Feb 15, 2019).
- (22) Schneiderman, D. K.; Hillmyer, M. A. 50th Anniversary Perspective: There Is a Great Future in Sustainable Polymers. *Macromolecules* **2017**, *50*, 3733–3749.
- (23) Our Common Future, Chapter 2 : Towards Sustainable Development <http://un-documents.net/ocf-02.htm> (accessed Feb 15, 2019).
- (24) Lee, J. W.; Na, D.; Park, J. M.; Lee, J.; Choi, S.; Lee, S. Y. Systems Metabolic Engineering of Microorganisms for Natural and Non-Natural Chemicals. *Nat. Chem. Biol.* **2012**, *8*, 536–546.
- (25) Ayres, R. U.; Ayres, L. W.; Martínas, K. Energy, Waste Accounting, and Life-

- Cycle Analysis. *Energy* **1998**, 23, 355–363.
- (26) Curran, M. A. Life Cycle Assessment: A Review of the Methodology and Its Application to Sustainability. *Curr. Opin. Chem. Eng.* **2013**, 2, 273–277.
 - (27) Allsopp, M.; Walters, A.; Santillo, D.; Johnston, P. Plastic Debris in the World's Oceans https://www.greenpeace.org/archive-international/en/publications/reports/plastic_ocean_report/ (accessed Feb 15, 2019).
 - (28) Al-Salem, S. M.; Lettieri, P.; Baeyens, J. Recycling and Recovery Routes of Plastic Solid Waste (PSW): A Review. *Waste Manag.* **2009**, 29, 2625–2643.
 - (29) Godiya, C. B.; Gabrielli, S.; Materazzi, S.; Pianesi, M. S.; Stefanini, N.; Marcantoni, E. Depolymerization of Waste Poly(Methyl Methacrylate) Scraps and Purification of Depolymerized Products. *J. Environ. Manage.* **2019**, 231, 1012–1020.
 - (30) Akkapeddi, M. K. . Poly(α -Methylene- γ -Butyrolactone) Synthesis, Configurational Structure, and Properties. *Macromolecules* **1979**, 12, 546.
 - (31) Hong, M.; Chen, E. Y.-X. Completely Recyclable Biopolymers with Linear and Cyclic Topologies via Ring-Opening Polymerization of γ -Butyrolactone. *Nat. Chem.* **2016**, 8, 42–49.
 - (32) Luckachan, G. E.; Pillai, C. K. S. Biodegradable Polymers- A Review on Recent Trends and Emerging Perspectives. *J. Polym. Environ.* **2011**, 19, 637–676.
 - (33) Hillmyer, M. A. The Promise of Plastics from Plants. *Science* **2017**, 358, 868–870.

- (34) Zhu, Y.; Romain, C.; Williams, C. K. Sustainable Polymers from Renewable Resources. *Nature* **2016**, *540*, 354–362.
- (35) ITACONIX, L. *Development of Integrated Production of Polyitaconic Acid from Northeast Hardwood Biomass*; 2009.
- (36) Baup, S. Ueber Eine Neue Pyrogen-Citronensäure, Und Über Benennung Der Pyrogen-Säuren Überhaupt. *Ann. Pharm.* **1836**, *19*, 29–38.
- (37) Klement, T.; Büchs, J. Itaconic Acid - A Biotechnological Process in Change. *Bioresource Technol.* **2013**, *135*, 422–431.
- (38) Okabe, M.; Lies, D.; Kanamasa, S.; Park, E. Y. Biotechnological Production of Itaconic Acid and Its Biosynthesis in *Aspergillus Terreus*. *Appl. Microbiol. Biotechnol.* **2009**, *84*, 597–606.
- (39) Werpy, T.; Petersen, G.; Aden, A.; Bozell, J.; Holladay, J.; White, J.; Manheim, A. *Top Value Added Chemicals from Biomass Volume I — Results of Screening for Potential Candidates from Sugars and Synthesis Gas*; 2004.
- (40) de Carvalho, J. D.; Magalhães Jr., A. I.; Soccol, C. R. Biobased Itaconic Acid Market and Research Trends - Is It Really a Promising Chemical? *Chim. Oggi* **2018**, *36*, 56–58.
- (41) Fernández-García, M.; Fernández-Sanz, M.; De La Fuente, J. L.; Madruga, E. L. Atom-Transfer Radical Polymerization of Dimethyl Itaconate. *Macromol. Chem. Phys.* **2001**, *202*, 1213–1218.
- (42) Hirano, T.; Takeyoshi, R.; Seno, M.; Sato, T. Chain-Transfer Reaction in the Radical Polymerization of Di-n-Butyl Itaconate at High Temperatures. *J. Polym. Sci., Part A: Polym. Chem.* **2002**, *40*, 2415–2426.

- (43) Yokota, K.; Hirabayashi, T.; Takashima, T. The Preparation of Poly(Itaconic Acid). *Die Makromol. Chem.* **1975**, 176, 1197–1205.
- (44) Grespos, E.; Hill, D. J. T.; Donnelly, J. H. O.; Sullivan, P. W. O.; Young, T. L.; East, G. C.; Zvin, K. J. Polymerization of Itaconic Acid in Aqueous Solution: Structure of the Polymer and Polymerization Kinetics at 25 °C, Studied by ¹³C NMR. *Makromol. Chem., Rapid Commun.* **1984**, 5, 489–494.
- (45) Veličković, J.; Filipović, J.; Djakov, D. P. The Synthesis and Characterization of Poly(Itaconic) Acid. *Polym. Bull.* **1994**, 32, 169–172.
- (46) Mao, Z.; Yang, C. Q. Polymeric Multifunctional Carboxylic Acids as Crosslinking Agents for Cotton Cellulose: Poly(Itaconic Acid) and In Situ Polymerization of Itaconic Acid. *J. Appl. Polym. Sci.* **2001**, 79, 319–326.
- (47) Lárez, C.; Canelón, F.; Millán, E.; Perdomo, G.; Katime, I. New Results on the Polymerisation of the Itaconic Acid in Aqueous Medium. *Polym. Bull.* **2002**, 49, 119–126.
- (48) Stawski, D.; Połowiński, S. Polymerization of Itaconic Acid. *Polimery* **2005**, 50, 118–122.
- (49) Bednarz, S.; Błaszczuk, A.; Błazejewska, D.; Bogdał, D. Free-Radical Polymerization of Itaconic Acid in the Presence of Choline Salts: Mechanism of Persulfate Decomposition. *Catal. Today* **2015**, 257, 297–304.
- (50) Szablan, Z.; Toy, A. A.; Davis, T. P.; Hao, X.; Stenzel, M. H.; Barner-Kowollik, C. Reversible Addition Fragmentation Chain Transfer Polymerization of Sterically Hindered Monomers: Toward Well-Defined Rod/Coil Architectures. *J. Polym. Sci., Part A: Polym. Chem.* **2004**, 42, 2432–

2443.

- (51) Szablan, Z.; Toy, A. A.; Terrenoire, A.; Davis, T. P.; Stenzel, M. H.; Müller, A. H. E.; Barner-Kowollik, C. Living Free-Radical Polymerization of Sterically Hindered Monomers: Improving the Understanding of 1,1-Disubstituted Monomer Systems. *J. Polym. Sci., Part A: Polym. Chem.* **2006**, *44*, 3692–3710.
- (52) Kassi, E.; Loizou, E.; Porcar, L.; Patrickios, C. S. Di(n-Butyl) Itaconate End-Functionalized Polymers: Synthesis by Group Transfer Polymerization and Solution Characterization. *Eur. Polym. J.* **2011**, *47*, 816–822.
- (53) Marvel, C. S.; Shepherd, T. H. Polymerization Reactions of Itaconic Acid and Some of Its Derivatives. *J. Org. Chem.* **1959**, *24*, 599–605.
- (54) Nagai, S.; Yoshida, K. Studies on Polymerization and Polymers of Itaconic Acid Derivatives. IV. Polymerization of Itaconic Acid in Aqueous Solution. *Kobunshi Kagaku* **1960**, *17*, 748–752.
- (55) Braun, V. D.; El Sayed, I. A. A. Über Die Struktur Der Polymeren Aus Itaconsäure. *Die Makromol. Chem.* **1966**, *96*, 100–121.
- (56) Tate, B. E. Polymerization of Itaconic Acid and Derivatives. *Adv. Polym. Sci.* **1967**, *5*, 214–232.
- (57) Askarov, M. A.; Semenova, L. N.; Babadzhanova, E. N. Properties of Some Synthetic Water-Soluble Polymers Based on Itaconic Acid. *Uzb. Khim. Zh.* **1968**, *12*, 38–40.
- (58) Robert, T.; Friebe, S. Itaconic Acid – a Versatile Building Block for Renewable Polyesters with Enhanced Functionality. *Green Chem.* **2016**, *18*, 2922–2934.

- (59) Kumar, S.; Krishnan, S.; Samal, S. K.; Mohanty, S.; Nayak, S. K. Itaconic Acid Used as a Versatile Building Block for the Synthesis of Renewable Resource-Based Resins and Polyesters for Future Prospective: A Review. *Polym. Int.* **2017**, *66*, 1349–1363.
- (60) Solanki, A.; Anand, V.; Choudhary, V.; Varma, I. K. Effect of Structure on Thermal Behavior of Homopolymer and Copolymers of Itaconimides. *J. Macromol. Sci. - Polym. Rev.* **2001**, *41*, 253–284.
- (61) Anand, V.; Agarwal, S.; Greiner, A.; Choudhary, V. Synthesis of Methyl Methacrylate and N-Aryl Itaconimide Block Copolymers via Atom-Transfer Radical Polymerization. *Polym. Int.* **2005**, *54*, 823–828.
- (62) Matyjaszewski, K. Atom Transfer Radical Polymerization (ATRP): Current Status and Future Perspectives. *Macromolecules* **2012**, *45*, 4015–4039.
- (63) Deoghare, C.; Baby, C.; Nadkarni, V. S.; Behera, R. N.; Chauhan, R. Synthesis, Characterization, and Computational Study of Potential Itaconimide-Based Initiators for Atom Transfer Radical Polymerization. *RSC Adv.* **2014**, *4*, 48163–48176.
- (64) Okada, S.; Matyjaszewski, K. Synthesis of Bio-Based Poly(N-Phenylitaconimide) by Atom Transfer Radical Polymerization. *J. Polym. Sci., Part A: Polym. Chem.* **2015**, *53*, 822–827.
- (65) Deoghare, C.; Nadkarni, V. S.; Behera, R. N.; Chauhan, R. Synthesis and Characterization of Copolymers of Methyl Methacrylate with N-Arylitaconimides via AGET-ATRP. *J. Polym. Mater.* **2017**, *34*, 455–466.
- (66) Liu, S.; Zhang, X.; Li, M.; Ren, X.; Tao, Y. Precision Synthesis of Sustainable

- Thermoplastic Elastomers from Lysine-Derived Monomers. *J. Polym. Sci., Part A: Polym. Chem.* **2017**, *55*, 349–355.
- (67) Odian, G. *Principles of Polymerization*; Wiley: New York, 2004.
- (68) Rieger, J. The Glass Transition Temperature of Polystyrene. *J. Therm. Anal.* **1996**, *46*, 965–972.
- (69) Teng, H.; Koike, K.; Zhou, D.; Satoh, Z.; Koike, Y.; Okamoto, Y. High Glass Transition Temperature of Poly(Methyl Methacrylate) Prepared by Free Radical Initiators. *J. Polym. Sci., Part A: Polym. Chem.* **2009**, *47*, 315–317.
- (70) Satoh, K.; Lee, D. H.; Nagai, K.; Kamigaito, M. Precision Synthesis of Bio-Based Acrylic Thermoplastic Elastomer by RAFT Polymerization of Itaconic Acid Derivatives. *Macromol. Rapid Commun.* **2014**, *35*, 161–167.
- (71) Ding, K.; John, A.; Shin, J.; Lee, Y.; Quinn, T.; Tolman, W. B.; Hillmyer, M. A. High-Performance Pressure-Sensitive Adhesives from Renewable Triblock Copolymers. *Biomacromolecules* **2015**, *16*, 2537–2539.
- (72) Martello, M. T.; Shrestha, M.; Hillmyer, M. A.; Tolman, W. B.; Wissinger, J. E.; Shin, J. Pressure-Sensitive Adhesives from Renewable Triblock Copolymers. *Macromolecules* **2010**, *44*, 87–94.
- (73) Shin, J.; Lee, Y.; Tolman, W. B.; Hillmyer, M. A. Thermoplastic Elastomers Derived from Menthide and Tulipalin A. *Biomacromolecules* **2012**, *13*, 3833–3840.
- (74) Watts, A.; Kurokawa, N.; Hillmyer, M. A. Strong, Resilient, and Sustainable Aliphatic Polyester Thermoplastic Elastomers. *Biomacromolecules* **2017**, *18*, 1845–1854.

- (75) Gowda, R. R.; Chen, E. Y.-X. Sustainable Polymers from Biomass-Derived α -Methylene- γ -Butyrolactone. *Encycl. Polym. Sci. Technol.* **2013**.
- (76) Agarwal, S.; Jin, Q.; Maji, S. Biobased Polymers from Plant-Derived Tulipalin A. *ACS Symp. Ser.* **2012**, *1105*, 197–212.
- (77) Brandenburg, C. J. Graft Copolymers of Methylene Lactones and Process for Emulsion Polymerization of Methylene Lactones. U.S. Patent 6,841,627 B2, 2011.
- (78) van Rossum, M. W. P. C.; Alberda, M.; van der Plas, L. H. W. Tulipaline and Tuliposide in Cultured Explants of Tulip Bulb Scales. *Phytochemistry* **1998**, *49*, 723–729.
- (79) Sakashita, K.; Iwasaka, K.; Tsukamoto, Y.; Aoyagi, A. Polymer Composition, Plastic Optical Fiber, Plastic Optical Fiber Cable and Method for Producing Plastic Optical Fiber. EP 1,834,968 A1, 2007.
- (80) Hu, Y.; Wang, X.; Chen, Y.; Caporaso, L.; Cavallo, L.; Chen, E. Y.-X. Rare-Earth Half-Sandwich Dialkyl and Homoleptic Trialkyl Complexes for Rapid and Stereoselective Polymerization of a Conjugated Polar Olefin. *Organometallics* **2013**, *32*, 1459–1465.
- (81) Tang, J.; Chen, E. Y.-X. Organopolymerization of Naturally Occurring Tulipalin B: A Hydroxyl-Functionalized Methylene Butyrolactone. *Org. Chem. Front.* **2015**, *2*, 1625–1631.
- (82) Gowda, R. R.; Chen, E. Y.-X. Organocatalytic and Chemoselective Polymerization of Multivinyl-Functionalized γ -Butyrolactones. *ACS Macro Lett.* **2016**, *5*, 772–776.

- (83) Suenaga, J.; Sutherlin, D. M.; Stille, J. K. Polymerization of (RS)- and (R)- α -Methylene- γ -Methyl- γ -Butyrolactone. *Macromolecules* **1984**, *17*, 2913–2916.
- (84) Sogah, D. Y.; Hertler, W. R.; Webster, O. W.; Cohen, G. M. Group Transfer Polymerization. Polymerization of Acrylic Monomers. *Macromolecules* **1987**, *20*, 1473–1488.
- (85) Qi, G.; Nolan, M.; Schork, J. F.; Jones, C. W. Emulsion and Controlled Miniemulsion Polymerization of the Renewable Monomer γ -Methyl- α -Methylene- γ -Butyrolactone. *J. Polym. Sci. Part A Polym. Chem.* **2008**, *46*, 5929–5944.
- (86) Mosnáček, J.; Matyjaszewski, K. Atom Transfer Radical Polymerization of Tulipalin A: A Naturally Renewable Monomer. *Macromolecules* **2008**, *41*, 40–42.
- (87) Miyake, G. M.; Newton, S. E.; Mariott, W. R.; Chen, E. Y.-X. Coordination Polymerization of Renewable Butyrolactone-Based Vinyl Monomers by Lanthanide and Early Metal Catalysts. *Dalton Trans.* **2010**, *39*, 6710–6718.
- (88) Zhang, Y.; Miyake, G. M.; Chen, E. Y.-X. Alane-Based Classical and Frustrated Lewis Pairs in Polymer Synthesis: Rapid Polymerization of MMA and Naturally Renewable Methylene Butyrolactones into High-Molecular-Weight Polymers. *Angew. Chem. Int. Ed.* **2010**, *49*, 10158–10162.
- (89) Hu, Y.; Xu, X.; Zhang, Y.; Chen, Y.; Chen, E. Y.-X. Polymerization of Naturally Renewable Methylene Butyrolactones by Half-Sandwich Indeyl Rare Earth Metal Dialkyls with Exceptional Activity. *Macromolecules* **2010**, *43*, 9328–9336.

- (90) Miyake, G. M.; Zhang, Y.; Chen, E. Y.-X. Living Polymerization of Naturally Renewable Butyrolactone-Based Vinylidene Monomers by Ambiphilic Silicon Propagators. *Macromolecules* **2010**, *43*, 4902–4908.
- (91) Hu, Y.; Gustafson, L. O.; Zhu, H.; Chen, E. Y.-X. Anionic Polymerization of MMA and Renewable Methylene Butyrolactones by Resorbable Potassium Salts. *J. Polym. Sci., Part A: Polym. Chem.* **2011**, *49*, 2008–2017.
- (92) Zhang, Y.; Gustafson, L. O.; Chen, E. Y.-X. Dinuclear Silylium-Enolate Bifunctional Active Species: Remarkable Activity and Stereoselectivity toward Polymerization of Methacrylate and Renewable Methylene Butyrolactone Monomers. *J. Am. Chem. Soc.* **2011**, *133*, 13674–13684.
- (93) Higaki, Y.; Okazaki, R.; Takahara, A. Semirigid Biobased Polymer Brush: Poly(α -Methylene- γ -Butyrolactone) Brushes. *ACS Macro Lett.* **2012**, *1*, 1124–1127.
- (94) Kitson, R. R. A.; Millemaggi, A.; Taylor, R. J. K. The Renaissance of α -Methylene- γ -Butyrolactones: New Synthetic Approaches. *Angew. Chem. Int. Ed.* **2009**, *48*, 9426–9451.
- (95) Grieco, P. A. Methods for the Synthesis of α -Methylene Lactones. *Synthesis* **1975**, 67–82.
- (96) Fetizon, M.; Golfier, M.; Louis, J.-M. Oxydations Par Le Carbonate d'argent Sur Celite-XIII. Preparation de Lactones. *Tetrahedron* **1975**, *31*, 171–176.
- (97) Malferrari, D.; Armenise, N.; Decesari, S.; Galletti, P.; Tagliavini, E. Surfactants from Itaconic Acid: Physicochemical Properties and Assessment of the Synthetic Strategies. *ACS Sustainable Chem. Eng.* **2015**, *3*, 1579–1588.

- (98) Galanti, M. C.; Galanti, A. V. Kinetic Study of the Isomerization of Itaconic Anhydride to Citraconic Anhydride. *J. Org. Chem.* **1982**, *47*, 1572–1574.
- (99) Michaut, M.; Santelli, M.; Parrain, J.-L. Efficient Synthesis of Spirolactones from Cyclic Anhydrides via an Allylation/Alkylation-RCM Sequence. *J. Organomet. Chem.* **2000**, *606*, 93–96.
- (100) Pellissier, H.; Wilmouth, S.; Santelli, M. Preparation of Tertiary Alcohols and γ -Lactones from Allylsilanes and Anhydrides. *Bull. Chem. Soc. Fr.* **1995**, *132*, 637–641.
- (101) Gowda, R. R.; Chen, E. Y.-X. Synthesis of β -Methyl- α -Methylene- γ -Butyrolactone from Biorenewable Itaconic Acid. *Org. Chem. Front.* **2014**, *1*, 230–234.
- (102) Hu, Y.; Miyake, G. M.; Wang, B.; Cui, D.; Chen, E. Y.-X. Ansa-Rare-Earth-Metal Catalysts for Rapid and Stereoselective Polymerization of Renewable Methylene Methylbutyrolactones. *Chem. - A Eur. J.* **2012**, *18*, 3345–3354.
- (103) Trotta, J. T.; Jin, M.; Stawiasz, K. J.; Michaudel, Q.; Chen, W.-L.; Fors, B. P. Synthesis of Methylene Butyrolactone Polymers from Itaconic Acid. *J. Polym. Sci., Part A: Polym. Chem.* **2017**, *55*, 2730–2737.
- (104) Yokota, K.; Hirabayashi, T. Manufacture of α -Methylene- γ -Butyrolactone. JP Patent 04,049,288, 1992.
- (105) Carlson, R. M.; Oyler, A. R. A Direct α -Methylene Lactone Synthesis via an Itaconic Acid Ester. *Tetrahedron Lett.* **1975**, No. 47, 4099–4102.
- (106) Carlson, R. M.; Oyler, A. R. Direct Methods for α -Methylene Lactone Synthesis Using Itaconic Acid Derivatives. *J. Org. Chem.* **1976**, *41*, 4065–

4069.

- (107) Mosnáček, J.; Yoon, J. A.; Juhari, A.; Koynov, K.; Matyjaszewski, K. Synthesis, Morphology and Mechanical Properties of Linear Triblock Copolymers Based on Poly(α -Methylene- γ -Butyrolactone). *Polymer* **2009**, *50*, 2087–2094.
- (108) Juhari, A.; Mosnáček, J.; Yoon, J. A.; Nese, A.; Koynov, K.; Kowalewski, T.; Matyjaszewski, K. Star-like Poly (n-Butyl Acrylate)-b-Poly (α -Methylene- γ -Butyrolactone) Block Copolymers for High Temperature Thermoplastic Elastomers Applications. *Polymer* **2010**, *51*, 4806–4813.
- (109) Trotta, J.; Watts, A.; Wong, A.; LaPointe, A. M.; Hillmyer, M. A.; Fors, B. P. Renewable Thermosets and Thermoplastics from Itaconic Acid. *ACS Sustainable Chem. Eng.* **2019**, *7*, 2691–2701.
- (110) Tang, X.; Hong, M.; Falivene, L.; Caporaso, L.; Cavallo, L.; Chen, E. Y.-X. The Quest for Converting Biorenewable Bifunctional α -Methylene- γ -Butyrolactone into Degradable and Recyclable Polyester: Controlling Vinyl-Addition/Ring-Opening/Cross-Linking Pathways. *J. Am. Chem. Soc.* **2016**, *138*, 14326–14337.
- (111) Zhou, J.; Schmidt, A. M.; Ritter, H. Bicomponent Transparent Polyester Networks with Shape Memory Effect. *Macromolecules* **2010**, *43*, 939–942.
- (112) Hong, M.; Chen, E. Y.-X. Coordination Ring-Opening Copolymerization of Naturally Renewable α -Methylene- γ -Butyrolactone into Unsaturated Polyesters. *Macromolecules* **2014**, *47*, 3614–3624.
- (113) Binda, P.; Barnes, Z.; Guthrie, D.; Ford, R. Highly Branched Poly(α -

- Methylene- γ -Butyrolactone) from Ring-Opening Homopolymerization. *Open J. Polym. Chem.* **2017**, *7*, 76–91.
- (114) Danko, M.; Basko, M.; Ďurkáčová, S.; Duda, A.; Mosnáček, J. Functional Polyesters with Pendant Double Bonds Prepared by Coordination-Insertion and Cationic Ring-Opening Copolymerizations of ϵ -Caprolactone with Renewable Tulipalin A. *Macromolecules* **2018**, *51*, 3582–3596.
- (115) Avny, Y.; Saghian, N.; Zilkha, A. Thermally Stable Polymers Derived from Itaconic Acid. *Isr. J. Chem.* **1972**, *10*, 949.
- (116) Ali, M. A.; Tateyama, S.; Oka, Y.; Kaneko, D.; Okajima, M. K.; Kaneko, T. Syntheses of High-Performance Biopolyamides Derived from Itaconic Acid and Their Environmental Corrosion. *Macromolecules* **2013**, *46*, 3719–3725.
- (117) Ali, M. A.; Tateyama, S.; Kaneko, T. Syntheses of Rigid-Rod but Degradable Biopolyamides from Itaconic Acid with Aromatic Diamines. *Polym. Degrad. Stab.* **2014**, *109*, 367–372.
- (118) Wang, Z.; Wei, T.; Xue, X.; He, M.; Xue, J.; Song, M.; Wu, S.; Kang, H.; Zhang, L.; Jia, Q. Synthesis of Fully Bio-Based Polyamides with Tunable Properties by Employing Itaconic Acid. *Polymer* **2014**, *55*, 4846–4856.
- (119) Wang, R.; Ren, T.; Bai, Y.; Wang, Y.; Chen, J.; Zhang, L.; Zhao, X. One-Pot Synthesis of Biodegradable and Linear Poly(Ester Amide)s Based on Renewable Resources. *J. Appl. Polym. Sci.* **2016**, *133*, 43446.
- (120) Reimschuessel, H. K.; Klein, K. P.; Schmitt, G. J. Polyimides. Synthesis and Polymerization of 4-Carboxy-2-Piperidone. *Macromolecules* **1969**, *2*, 567–569.
- (121) Ali, M. A.; Tandon, N.; Kaneko, T. Simultaneous Hardening/Ductilizing

- Effects of Cryogenic Nanohybridization of Biopolyamides with Montmorillonites. *ACS Omega* **2017**, 2, 9103–9108.
- (122) Ali, M. A.; Tandon, N.; Nag, A.; Takada, K. Molecular Orientation of Bio-Polyamides After Cryogenic Nanohybridization with Montmorillonites. *Arab. J. Sci. Eng.* **2019**, 44, 153–158.
- (123) He, M.; Wang, Z.; Wang, R.; Zhang, L.; Jia, Q. Preparation of Bio-Based Polyamide Elastomer by Using Green PLasticizers. *Polymers (Basel)*. **2016**, 8, 257.
- (124) Qi, P.; Chen, H. L.; Nguyen, H. T. H.; Lin, C. C.; Miller, S. A. Synthesis of Biorenewable and Water-Degradable Polylactam Esters from Itaconic Acid. *Green Chem.* **2016**, 18, 4170–4175.
- (125) Roy, M.; Noordzij, G. J.; Van Den Boomen, Y.; Rastogi, S.; Wilsens, C. H. R. M. Renewable (Bis)Pyrrolidone Based Monomers as Components for Thermally Curable and Enzymatically Depolymerizable 2-Oxazoline Thermoset Resins. *ACS Sustainable Chem. Eng.* **2018**, 6, 5053–5066.
- (126) Aoi, K.; Okada, M. Polymerization of Oxazolines. *Prog. Polym. Sci.* **1996**, 21, 151–208.
- (127) Mutlu, H.; de Espinosa, L. M.; Meier, M. A. R. Acyclic Diene Metathesis: A Versatile Tool for the Construction of Defined Polymer Architectures. *Chem. Soc. Rev.* **2011**, 40, 1404–1445.
- (128) Bielawski, C. W.; Grubbs, R. H. Living Ring-Opening Metathesis Polymerization. *Prog. Polym. Sci.* **2007**, 32, 1–29.
- (129) Lv, A.; Li, Z. L.; Du, F. S.; Li, Z. C. Synthesis, Functionalization, and

- Controlled Degradation of High Molecular Weight Polyester from Itaconic Acid via ADMET Polymerization. *Macromolecules* **2014**, *47*, 7707–7716.
- (130) Winkler, M.; Lacerda, T. M.; Mack, F.; Meier, M. A. R. Renewable Polymers from Itaconic Acid by Polycondensation and Ring-Opening-Metathesis Polymerization. *Macromolecules* **2015**, *48*, 1398–1403.
- (131) Bai, Y.; Naguib, M.; De bruyn, M.; North, M.; Honoré, M.; Clark, J. H.; Farmer, T. J.; Dodson, J. R.; Ingram, I. D. V.; Whitwood, A. C. Ring Opening Metathesis Polymerisation of a New Bio-Derived Monomer from Itaconic Anhydride and Furfuryl Alcohol. *Green Chem.* **2016**, *18*, 3945–3948.
- (132) Pehere, A. D.; Xu, S.; Thompson, S. K.; Hillmyer, M. A.; Hoye, T. R. Diels–Alder Reactions of Furans with Itaconic Anhydride: Overcoming Unfavorable Thermodynamics. *Org. Lett.* **2016**, *18*, 2584–2587.
- (133) Bai, Y.; Clark, J. H.; Farmer, T. J.; Ingram, I. D. V.; North, M. Wholly Biomass Derivable Sustainable Polymers by Ring-Opening Metathesis Polymerisation of Monomers Obtained from Furfuryl Alcohol and Itaconic Anhydride. *Polym. Chem.* **2017**, *8*, 3074–3081.
- (134) Granzow, A. Flame Retardation by Phosphorus Compounds. *Acc. Chem. Res.* **1978**, *11*, 177–183.
- (135) Doseva, V. N.; Borisov, G. Phosphorous Containing Monomers, Oligomers, and Polymers from Itaconic Acid Esters and Dialkyl Phosphites. *Acta Polym.* **1991**, *42*, 66–74.
- (136) Chang, S.-J.; Chang, F.-C. Synthesis and Characterization of Copolyesters Containing the Phosphorous Linking Pendent Groups. *J. Appl. Polym. Sci.*

1999, 72, 109–122.

- (137) Qian, X.; Song, L.; Jiang, S.; Tang, G.; Xing, W.; Wang, B.; Hu, Y.; Yuen, R. K. K. Novel Flame Retardants Containing 9,10-Dihydro-9-Oxa-10-Phosphaphenanthrene-10-Oxide and Unsaturated Bonds: Synthesis, Characterization, and Application in the Flame Retardancy of Epoxy Acrylates. *Ind. Eng. Chem. Res.* **2013**, 52, 7307–7315.
- (138) Negrell, C.; Frénéhard, O.; Sonnier, R.; Dumazert, L.; Briffaud, T.; Flat, J.-J. Self-Extinguishing Bio-Based Polyamides. *Polym. Degrad. Stab.* **2016**, 134, 10–18.
- (139) Ghosh, A.; Mistri, E. A.; Banerjee, S. *Chapter 3 - Fluorinated Polyimides: Synthesis, Properties, and Applications*; William Andrew, 2015.
- (140) Romero, R. E.; Mas, A.; Laurent, P.; Schué, F.; Blancou, H. Synthesis of Aliphatic Diamine and Polyetherimide with Long Perfluoroalkyl Side Chain. *J. Fluor. Chem.* **2002**, 117, 27–33.
- (141) Kaba, M.; Romero, R. E.; Essamri, A.; Mas, A. Synthesis and Characterization of Fluorinated Copolyetherimides with -CH₂-C₆F₁₃ Side Chains Based on the ULTEMTM Structure. *J. Fluor. Chem.* **2005**, 126, 1476–1486.
- (142) Spanjers, C. S.; Schneiderman, D. K.; Wang, J. Z.; Wang, J.; Hillmyer, M. A.; Zhang, K.; Dauenhauer, P. J. Branched Diol Monomers from the Sequential Hydrogenation of Renewable Carboxylic Acids. *ChemCatChem* **2016**, 8, 3031–3035.
- (143) Holzhäuser, F. J.; Artz, J.; Palkovits, S.; Kreyenschulte, D.; Büchs, J.; Palkovits, R. Electrocatalytic Upgrading of Itaconic Acid to Methylsuccinic

- Acid Using Fermentation Broth as a Substrate Solution. *Green Chem.* **2017**, *19* (10), 2390–2397.
- (144) Abdelrahman, O. A.; Park, D. S.; Vinter, K. P.; Spanjers, C. S.; Ren, L.; Cho, H. J.; Zhang, K.; Fan, W.; Tsapatsis, M.; Dauenhauer, P. J. Renewable Isoprene by Sequential Hydrogenation of Itaconic Acid and Dehydra-Decyclization of 3-Methyl-Tetrahydrofuran. *ACS Catal.* **2017**, *7*, 1428–1431.
- (145) Wong Chang, M.-A.; Arnaud, S. P.; Farmer, T. J.; Mascal, M.; Wu, L. Electrochemical Coupling of Biomass-Derived Acids: New C 8 Platforms for Renewable Polymers and Fuels. *ChemSusChem* **2016**, *10*, 166–170.
- (146) Retuert, J.; Yazdani-Pedram, M.; Martinez, F.; Jeria, M. Soluble Itaconic Acid-Ethylene Glycol Polyesters. *Bull. Chem. Soc. Jpn.* **1993**, *66*, 1707–1708.
- (147) Kato, J.; Seo, A.; Kiso, K.; Kudo, K.; Shiraishi, S. Synthesis of 2,8-Dioxaspiro[4.5]Decane-1,3,7,9-Tetrone and the Reactions with Amines. *Bull. Chem. Soc. Jpn.* **1999**, *72*, 1075–1081.
- (148) Giacobazzi, G.; Gioia, C.; Colonna, M.; Celli, A. Thia-Michael Reaction for a Thermostable Itaconic-Based Monomer and the Synthesis of Functionalized Biopolyesters. *ACS Sustainable Chem. Eng.* **2019**, *7*, 5553–5559.

Chapter 2 SYNTHESIS OF METHYLENE BUTYROLACTONE POLYMERS FROM ITACONIC ACID

ABSTRACT

Herein we report the transformation of β -monomethyl itaconate (β -MMI), an inexpensive and biorenewable alternative to petroleum feedstocks, to the high value monomer α -methylene- γ,γ -dimethyl- γ -butyrolactone (Me_2MBL) through a selective addition strategy. This strategy is also applied to the synthesis of α -methylene- γ -butyrolactone (MBL, tulipalin A), a monomer that can be polymerized to give materials with desirable properties (high T_d , T_g , and refractive index). Subsequent polymerization of both Me_2MBL and MBL through reversible addition-fragmentation chain-transfer (RAFT) polymerization generates well defined poly(Me_2MBL) (PMe_2MBL) and poly(MBL) (PMBL). Characterization of PMe_2MBL shows good physical properties comparable with known PMBL materials. This thesis chapter was adapted from published work.¹

INTRODUCTION

In recent years, the development of biorenewable resources in the chemical industries has become a major research area.² As the discovery of sustainable solutions for material production using non-petroleum chemical feedstocks is a critical need, the advancement of high value polymers from “green” monomers is a challenge that must be met. This need to “go green” is coupled with the necessity of developing sustainable polymers in a way that makes them economically competitive with their petroleum-based equivalents. To accomplish this, the production of high value monomers from inexpensive, biosourced small molecule feedstocks is necessary.

Itaconic acid (IA, Figure 2.1) is a biorenewable feedstock that holds considerable promise in reducing society's dependence on petroleum-based chemicals. Named in 2004 by the U.S. Department of Energy as one of the "top value added chemicals from biomass," IA is currently produced globally on an 80 kiloton/yr scale for ~\$2/kg from the fermentation of biomass such as corn or rice.³⁻⁵ Recognizing the potential of this feedstock chemical for industrial use, the company Itaconix has developed a robust uncontrolled radical polymerization process that provides poly(itaconic acid) (PIA) for ~\$3/kg.⁶ PIA has been shown to be an excellent surrogate for petroleum-based poly(acrylic acid) for applications such as super-absorbents and dispersants.⁶

While the industrial development of PIA clearly establishes it as an important polymer, its synthesis is currently limited to uncontrolled radical polymerization.⁷⁻¹⁸ Importantly, the polymerization of IA and its derivatives (such as the various mono- and diesters) in controlled radical polymerization (CRP) processes would allow these monomers to be incorporated into polymers with precisely controlled architectures, which would greatly increase the number of applications these materials could be used in. Unfortunately, common CRP methods used on itaconates do not typically result in a well controlled process.¹⁹⁻²³ On this basis, we sought a simple and efficient transformation that would convert IA into a monomer that could be used effectively in CRP.

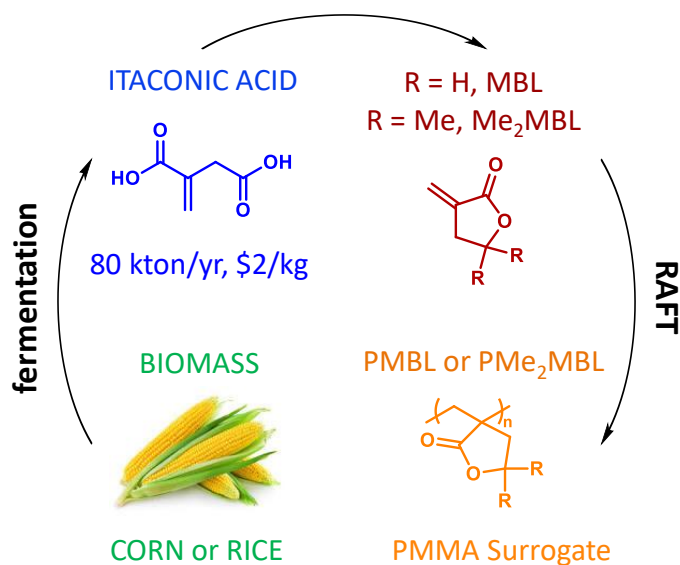


Figure 2.1. Our strategy to convert itaconic acid, produced by the fermentation of biomass such as corn or rice, into high value poly(methyl methacrylate) surrogates through the transformation to, and controlled polymerization of, methylene butyrolactones.

In our search for chemical transformations of IA that would afford monomers compatible with CRP methods, we noticed its structural similarity to α -methylene- γ -butyrolactone (MBL, Figure 2.1). MBL has been shown to be compatible with a wide variety of controlled polymerization strategies such as atom transfer radical polymerization (ATRP).^{24–43} Additionally, PMBL has been established as a suitable surrogate for petroleum-derived poly(methyl methacrylate) (PMMA), due to its similar structure and optical properties.^{44–46} Interestingly, the thermal properties of PMMA and PMBL differ greatly, with PMBL possessing a glass transition temperature (T_g) approximately 100 °C higher than that of PMMA (~200 °C for PMBL and ~100 °C for PMMA).^{44,45} This increased T_g enables the use of PMBL and related polymers for high temperature applications for which PMMA would be unsuitable.⁴⁷ Therefore, the efficient production of MBL and related derivatives from IA lends itself towards numerous applications.

MBL is a naturally occurring compound found in tulips; however, its large scale production is not practical.⁴⁸ This limited availability of MBL hampers the potential use of PMBL as a PMMA surrogate. Additionally, while the synthesis of MBL and related derivatives from inexpensive starting materials has been extensively studied since the 1960s, these syntheses generally require several steps and often rely on petroleum-based acrylates as starting materials.^{49–51} Thus, the use of IA as a feedstock chemical to produce MBL and related compounds represents a grand challenge in green monomer synthesis.

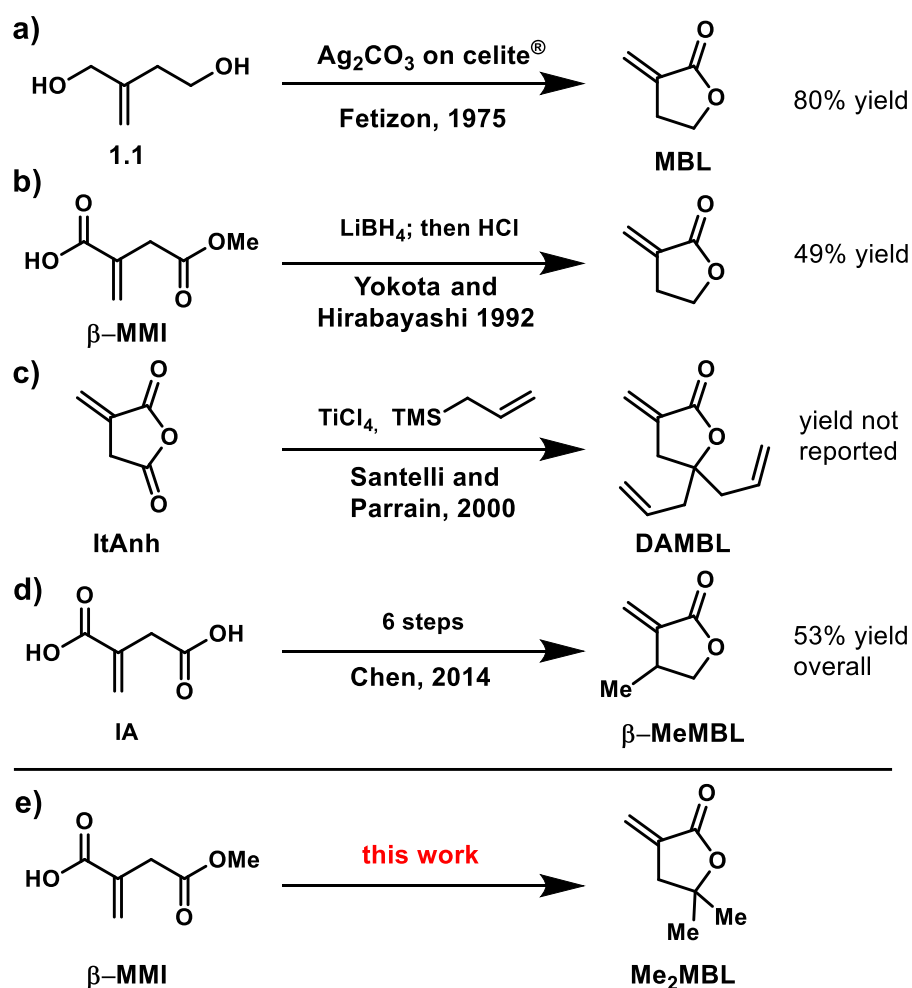


Figure 2.2. a-d) Previous work on the synthesis of MBL analogs from IA derivatives and e) this work.

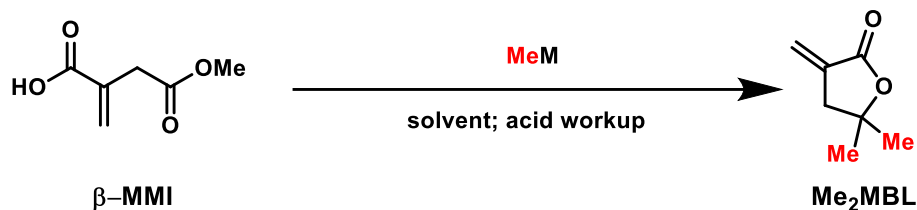
A few methods to produce MBLs from IA derivatives have been demonstrated in the past. Notably, Fetizon showed in 1975 that dimethyl itaconate (DMI) can be reduced to diol **1.1** with Red-Al[®], followed by oxidative cyclization with Ag₂CO₃ on celite[®] to yield MBL in 80% yield from **1** (Figure 2.2a).⁵² Anions of IA derivatives have also been added to aldehydes and ketones, followed by lactonization, to generate carboxylic acid functionalized MBLs.⁵³ Additionally, a patent by Yokota and Hirabayashi in 1992 claims that selective reduction of β -monomethyl itaconate (β -MMI), followed by acid-catalyzed cyclization, could produce MBL in 49% yield (Figure 2.2b).⁵⁴ Allylation of commercially available itaconic anhydride (ItAnh) with allyltrimethylsilane and stoichiometric TiCl₄ was reported in 2000 by Santelli and Parrain to generate γ -diallyl- α -methylene- γ -butyrolactone (DAMBL) (Figure 2.2c).⁵⁵ More recently, β -methyl- α -methylene- γ -butyrolactone (β -MeMBL), a well-studied MBL derivative, was synthesized on large scale in six steps from IA by Chen in 2014 (Figure 2.2d), demonstrating the potential of this chemical feedstock for industrially relevant transformations to green monomers.⁵⁶ While these methods set the foundation for the construction of MBL derivatives from IA, we wished to improve upon their efficacy by reducing the number of steps required and by adding new functionality into the lactone backbone not previously accessed from IA.

Herein we report a new strategy for the synthesis of α -methylene- γ,γ -dimethyl- γ -butyrolactone (Me₂MBL, Figure 2.2e) in a single step from commercially available β -MMI through selective Grignard addition. Additionally, a similar reduction strategy was employed to produce MBL from β -MMI in a single step in 42% overall yield.

Subsequent RAFT polymerizations of both MBL and Me₂MBL were performed and the physical properties of these materials were studied.

RESULTS AND DISCUSSION

Synthesis of α -methylene- γ,γ -dimethyl- γ -butyrolactone (Me₂MBL). We postulated that selective addition of a methyl anion to β -monomethyl itaconate (β -MMI), followed by acid catalyzed cyclization, would yield Me₂MBL. To test this, we added methyl lithium (MeLi) to β -MMI in THF at 0 °C. After an acid workup, Me₂MBL was formed in 8% yield (Table 2.1, entry 1). Interestingly, the replacement of MeLi with MeMgCl resulted in an increase in yield to 49% (entry 2). Switching the solvent from THF to DCM resulted in a similar yield of 51% with 3.1 equiv of MeMgCl and 55% with 4.1 equiv of MeMgCl (entries 3 and 4). Slow addition of the MeMgCl to a solution of β -MMI, or of a solution of β -MMI to MeMgCl, led to reduced yields of 43% and 31% yield, respectively (entries 5 and 6).

Table 2.1. Optimization of the Reduction of β -MMI to Me₂MBL

Entry ^a	Solvent	Methyl Source (equiv)	% Yield ^b
1	THF	MeLi (5.1)	8
2	THF	MeMgCl (3.1)	49
3	DCM	MeMgCl (3.1), 1M in DCM	51
4	DCM	MeMgCl (4.1), 1M in DCM	55
5	THF	MeMgCl ^c (3.1)	43
6	THF	MeMgCl ^d (3.1)	31
7	THF	CeCl ₃ /MeLi (4.1)	15
8	THF	CeCl ₃ /MeMgCl (4.1)	23
9 ^e	THF	MeMgCl (3.1)	39 ^f

^aReactions conditions: 1.0 mmol scale at 1 M in THF unless otherwise specified;

^bYields were determined by ¹H NMR spectroscopy using 1,3,5-trimethoxybenzene or toluene as an internal standard; ^cSlow addition of Grignard reagent; ^dSlow addition of β -MMI; ^eReaction was performed on a 0.21 mol scale (30 g of β -MMI) at 1.5 M;

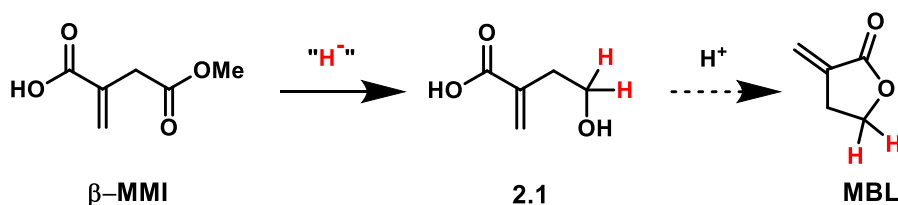
^fIsolated yield.

Based on the NMR spectrum of the reaction mixtures, we hypothesized that some of the mass balance consisted of a complex mixture of aliphatic products (Figure S2.1). To increase selectivity towards 1,2-addition and to avoid any potential enolate based reaction pathways, we sought to change our methyl anion source. Using chemistry developed by Imamoto in the 1980s, we employed organocerium reagents, which have shown excellent selectivity for 1,2-addition.^{57–59} Unfortunately, transmetallation of

CeCl₃ to either MeLi or MeMgCl, followed by addition to β -MMI, did not lead to improved yields (Table 2.1, entries 7 and 8).

Using the conditions in entry 2 (Table 2.1), the reaction was scaled up and performed on 30 g of β -MMI, generating 10 g of Me₂MBL in 39% isolated yield after distillation (entry 9). This result clearly demonstrates that this is a practical method for the synthesis of Me₂MBL.

Reduction of β -MMI to MBL. Encouraged by our results on the synthesis of Me₂MBL, we wanted to investigate the reduction of β -MMI to give the parent MBL. Yokota and Hirabayashi patented a procedure that allowed this transformation using LiBH₄ followed by acidic workup; however, we only observed unreacted starting material when we attempted the reported conditions.⁵⁴ Therefore, we probed other reducing agents and conditions for this reaction. Adding NaBH₄ to β -MMI in THF/MeOH resulted in unreacted starting material with no desired product detected (Table 2.2, entry 1). Switching to a stronger reducing agent, DIBAL-H, produced mainly undesired diol **1.1**, with a trace of desired product **2.1**, observed by NMR (Table 2.2, entry 2).⁵² Comparable results were observed using LiAlH₄, Red-Al[®], and LiEt₃BH (Table 2.2, entries 3–5). Additional reactions with NaBH₄ at elevated temperatures were also attempted, resulting in complex mixtures of degradation products with only trace quantities of **2.1** (Table 2.2, entry 6). Similarly, the use of Na(OAc)₃BH did not produce any **2.1**, resulting instead in only unreacted starting material (Table 2.2, entry 7).

Table 2.2. Optimization of the Reduction of β -MMI to MBL

Entry	Solvent ^a	T (°C)	t (h)	Red. ^b	% Yield ^c
1	MeOH:THF (3:2)	RT	144	NaBH ₄ (6)	0
2	THF	-78	7	DIBAL-H (3)	Trace
3	THF	-78	2	LiAlH ₄ (3)	0
4	THF	-78	0.5	Red-Al [®] (4)	0
5	THF	-78	2	LiEt ₃ BH (4)	Trace
6	MeOH:THF (3:2)	60	2	NaBH ₄ (6)	Trace
7	MeOH:THF (3:2)	60	96	Na(OAc) ₃ H (10)	0
8	H ₂ O:THF (1:4)	60	24	NaCNBH ₃ (3)	0
9	H ₂ O:THF (1:19)	40	1	NaBH ₄ (6)	25
10	H ₂ O:THF (2:3)	40	4	NaBH ₄ (6)	41
11	H ₂ O:THF (1:4)	30	6.5	NaBH ₄ (6)	56
12	H ₂ O:THF (1:4)	60	5	LiBH ₄ (6)	11
13	H ₂ O:THF (1:4)	30	6.5	NaBH ₄ (6)	45 ^d (42 ^e)

^aSolvent (v/v); ^bReducing agent (equiv); ^cYield of **2.1** determined by ¹H NMR spectroscopy using 1,3,5-trimethoxybenzene or toluene as an internal standard prior to acid workup; ^dNMR yield of MBL determined by ¹H NMR spectroscopy using 1,3,5-trimethoxybenzene or toluene as an internal standard following acidic workup; ^eIsolated yield of MBL.

Based on the above results we tested NaCNBH₃, a milder reducing agent compared to NaBH₄. Using this reagent at 60 °C (Table 2.2, entry 8) in a mixture of

THF and water, no reaction occurred, and only unreacted starting material was observed. Despite this outcome, we decided to apply the aqueous conditions used with NaCNBH₃ to NaBH₄. Interestingly, 25% yield of the desired alcohol product was detected after 1 h at 40 °C (entry 9). Optimization of the THF to water ratio and the reaction temperature led to the selective reduction of β-MMI to give alcohol **2.1** in 56% yield (entries 10 and 11). Substitution of NaBH₄ with LiBH₄ using these aqueous conditions (entry 12) resulted in a lowered yield of 11%. Using the optimized conditions reported in entry 11, treatment of **2.1** with acid upon workup enabled the one-pot formation of MBL in 42% isolated yield (entry 13). The positive effect of the aqueous media on yield, as well as the relative ratio of water to THF, deserves discussion. For NaBH₄, aqueous conditions can lead to the formation of NaB(OH)H₃, a known intermediate in the stepwise hydrolysis of NaBH₄.^{60–63} This hydroxyborohydride has been reported to reduce esters.^{64–66} The varying ratios of water likely affect the rate of formation and stability of NaB(OH)H₃. Additionally, IA forms as a side-product under these reaction conditions, so the ratio of water to THF was modified to maximize the formation of alcohol **2.1**.

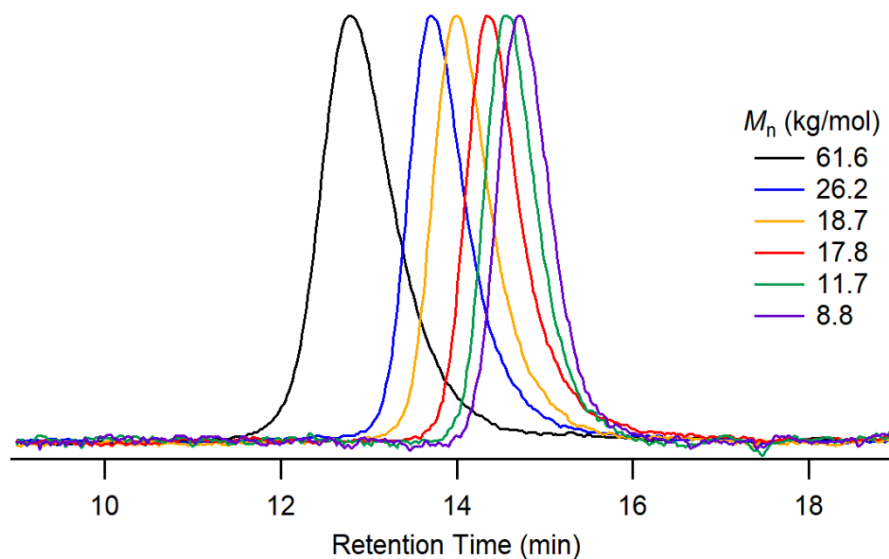
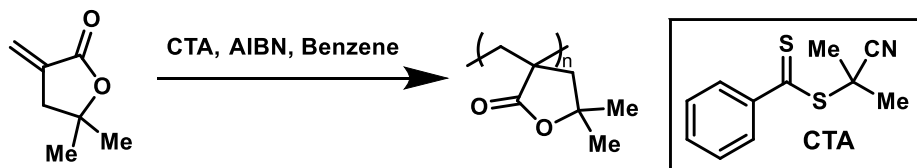


Figure 2.3. RAFT polymerization of Me₂MBL leads to predictable M_n values based on Me₂MBL and CTA loading.

Controlled Radical Polymerization of Me₂MBL and MBL. To demonstrate Me₂MBL was a monomer capable of CRP, we investigated its use as a monomer in RAFT polymerization.⁶⁷ To begin, we utilized known RAFT conditions used for the polymerization of MMA with a commercially available chain transfer agent (CTA), 2-cyano-2-propyl benzodithioate (Table 2.3). Under these conditions at 60 °C, Me₂MBL polymerized slowly to give PMe₂MBL with a number-average molar mass (M_n) of 22.5 kg/mol and a dispersity (\bar{D}) of 1.21 after 60 h (Table 2.3, entry 1). Increasing the temperature to 80 °C resulted in high conversion within 15 h (entry 2) and gave a polymer with an M_n of 17.8 kg/mol and a narrower \bar{D} of 1.07. Modulating the ratio of monomer to CTA enabled the synthesis of polymers with controlled M_n values ranging from 8.8 – 61.1 kg/mol (entries 2 – 7 and Figure 2.3). Under these conditions, polymerizations generally gelled after 50% conversion, after which the reaction was stopped. These results clearly illustrate that this monomer, which is synthesized directly from an IA derivative, can be efficiently used in CRP processes. Additionally,

PMe₂MBL was synthesized using AIBN without CTA, producing PMe₂MBL with an M_n of 55.7 kg/mol and a broad \bar{D} of 2.25 (entry 8) and demonstrating that a CTA is needed to control the polymerization.

Table 2.3. Polymerization Conditions for Me₂MBL



Entry ^a	M:CTA:I ^b	M_n^c (kg/mol)	\bar{D}^c	$M_{n,theo}^d$ (kg/mol)
1 ^e	1100:5:1	22.5	1.21	19.2
2	1100:5:1	17.8	1.07	15.8
3	1100:8:1	8.8	1.25	8.4
4	1100:6:1	11.7	1.15	11.8
5	1100:3:1	18.7	1.26	21.7
6	1100:2:1	26.2	1.25	36.8
7	1100:1:1	61.1	1.41	95.8
8	1100:0:1	55.7	2.25	54.1

^aReactions were run at 80 °C in a 2:1 monomer:solvent (v/v) ratio on a 1.6 mmol scale for 10 – 20 h; ^bMonomer:CTA:AIBN ratios; ^c M_n and \bar{D} determined by a light scattering detector; ^dDetermined using the M:CTA ratio and % conversion from ¹H NMR; ^eThe reaction was run at 60 °C for 60 h.

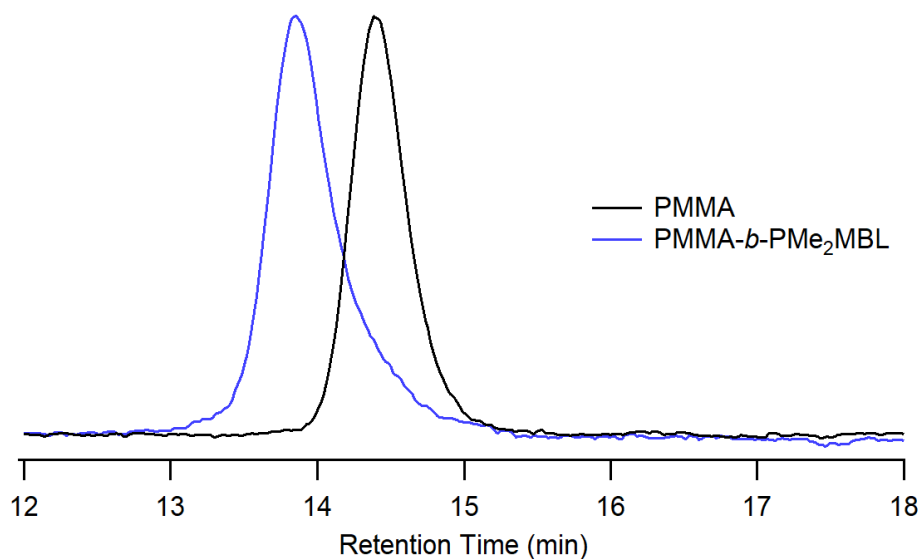
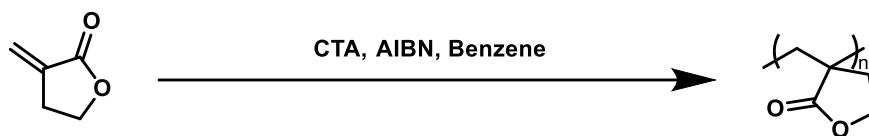


Figure 2.4. Chain extension of PMMA with PMe₂MBL to give the block copolymer PMMA-*b*-PMe₂MBL.

To take advantage of the living characteristics of the RAFT polymerization, we utilized our optimized conditions to grow diblock copolymers. To this end, we synthesized PMMA ($M_n = 9.7$ kg/mol) and used it as a macroinitiator for the polymerization of Me₂MBL, which gave a PMMA-*b*-PMe₂MBL diblock copolymer with an M_n of 22.2 kg/mol and a narrow \mathcal{D} of 1.11. A clear shift to higher molar mass was observed without any major termination (Figure 2.4), clearly showing that Me₂MBL can be utilized in the synthesis of copolymers.

Table 2.4. Polymerization Conditions for MBL

Entry ^a	M:CTA:I ^b	M_n ^{c,d} (kg/mol)	\bar{D} ^c	$M_{n,theo}$ ^d (kg/mol)
1	1100:5:1	14.8	1.22	13.9
2	1100:3:1	22.0	1.21	31.4
3	1100:7:1	12.1	1.23	10.9

^aReactions were run at 80 °C in a 2:1 monomer:solvent (v/v) ratio on a 1.6 mmol scale for 0.5 h; ^bMonomer:CTA:AIBN ratios; ^c M_n and \bar{D} determined by SEC against PS standards; ^dDetermined using the M:CTA ratio and % conversion from ¹H NMR.

We next set out to extend the RAFT polymerization procedure used in the polymerization of Me₂MBL to the polymerization of MBL. Under these conditions, the polymerization of MBL gelled after 0.5 h at 80 °C to give PMBL with an M_n of 14.8 kg/mol and a \bar{D} of 1.22 (Table 2.4, entry 1). Subsequent variation of the MBL:CTA ratio gave control over M_n while maintaining narrow \bar{D} s (entries 2 and 3, Figure S2.11).

Physical Properties. PMBL and its derivatives are known for having high T_g values relative to their acyclic PMMA analogue.^{44,45} Differential scanning calorimetry (DSC) performed on PMe₂MBL (M_n = 19.7 kg/mol) generated by RAFT polymerization showed a T_g value of 209 °C (Figure 2.5). The T_g of RAFT-derived PMe₂MBL is comparable both to PMe₂MBL generated by uncontrolled radical polymerization (M_n = 55.7 kg/mol, T_g = 204 °C) and PMBL generated by RAFT (M_n = 12.1 kg/mol, T_g = 187 °C). Additionally, thermal gravimetric analysis (TGA) showed a high decomposition temperature (T_d) for PMe₂MBL generated by both RAFT (T_d = 337 °C) and uncontrolled

radical polymerization ($T_d = 310\text{ }^{\circ}\text{C}$) (Figure 2.6). These results demonstrate that the dithioester chain end does not lower the stability of the polymers synthesized using RAFT. Additionally, PMBL exhibits a similar decomposition temperature ($T_d = 337\text{ }^{\circ}\text{C}$) as PMe_2MBL .

A difference in solubility between the two polymers was also apparent: PMe_2MBL readily dissolved in THF and other common organic solvents, while PMBL only readily dissolved in polar aprotic solvents such as dimethyl sulfoxide or *N,N*-dimethylformamide.

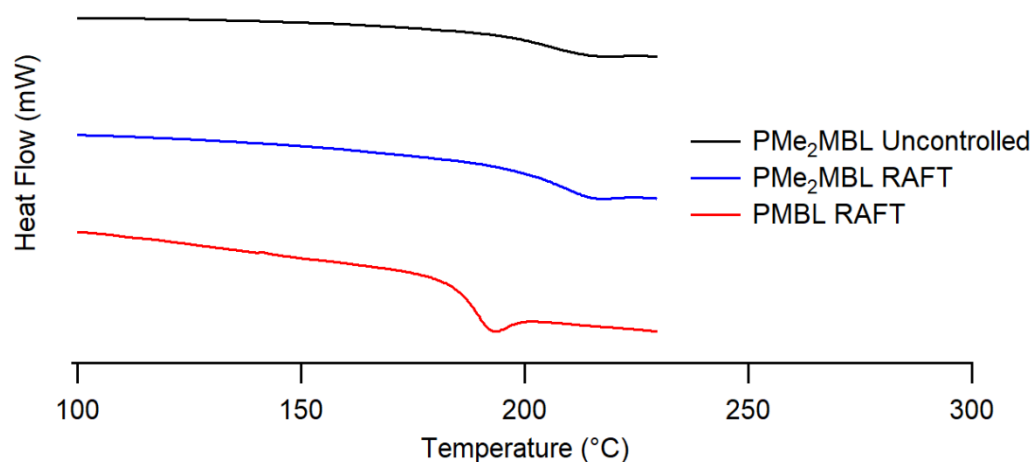


Figure 2.5. Differential scanning calorimetry (DSC) heat flow vs temperature (30 $^{\circ}\text{C}/\text{min}$, second heat) traces of PMe_2MBL (synthesized using both uncontrolled and RAFT polymerizations) and PMBL (synthesized using RAFT polymerization), exo up.

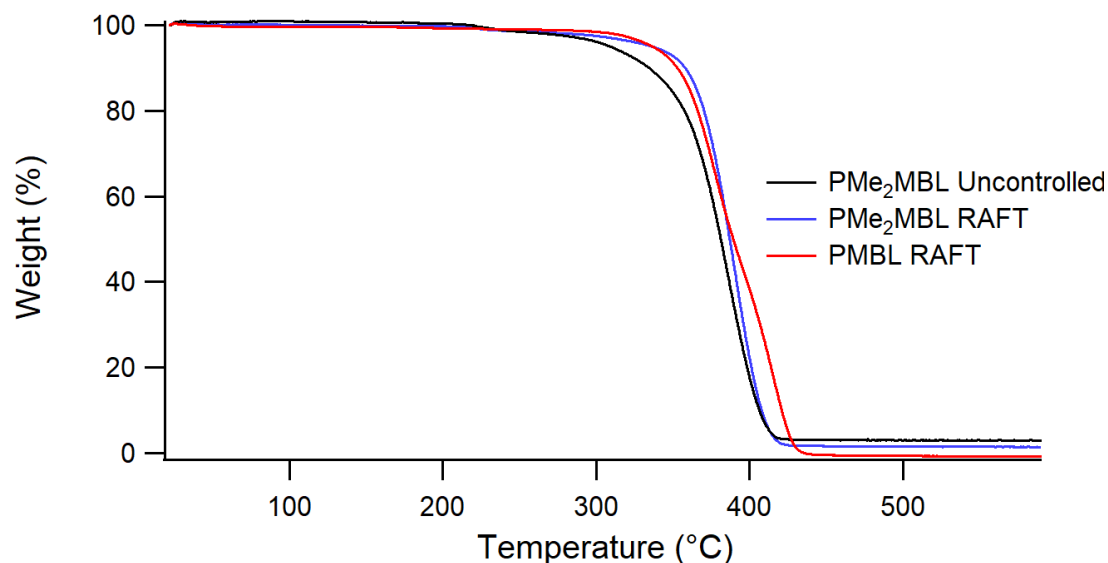


Figure 2.6. TGA curves of PMe₂MBL (synthesized using both uncontrolled and RAFT polymerization) and PMBL (synthesized using RAFT polymerization).

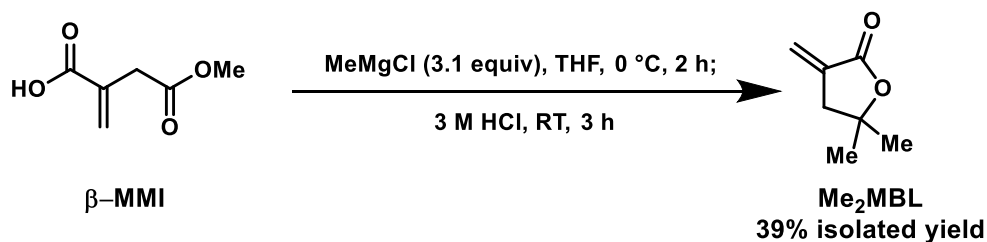
One of the attractive features of PMBL is its similar optical properties to PMMA.⁴⁴ On this basis we wanted to measure the refractive index and extinction coefficient of PMe₂MBL in order to assess its potential use for optical-based applications. As the determination of optical constants such as refractive index and extinction coefficient are sensitive to the exact modeling conditions used following the measurement of raw data, we also measured the optical properties of PMMA synthesized by RAFT polymerization. A thin film of PMMA gave a refractive index of 1.57 at 250 nm with an Abbe number of 53 (Figure S2.12), which is in agreement with the known values and demonstrates that our method for refractive index determination is accurate.⁶⁸ Measurement of the refractive index of PMe₂MBL by ellipsometry gave a refractive index of 1.52 at 250 nm with an Abbe number of 34 (Figure S2.13), which is comparable to that of PMMA and suggests this polymer could be suitable for applications such as plastic optical fibers.⁴⁷

CONCLUSIONS

In this work we have shown the first synthesis of Me₂MBL from β -MMI in a single step through a selective reduction strategy. This synthetic method is facile, scalable, and generates monomer that can be purified by simple distillation. Subsequent controlled polymerization of both MBL and Me₂MBL through RAFT polymerization generates well-defined polymers with predictable M_n s and narrow D s. Additionally, PMe₂MBL shows improved solubility over PMBL in common organic solvents, making it a potentially more processable polymer. Furthermore, PMe₂MBL shows a higher T_g compared with PMBL and both polymers show high T_d s. This new method provides a high value monomer synthesized from a commercially available itaconate in a single step that can be polymerized in a controlled fashion.

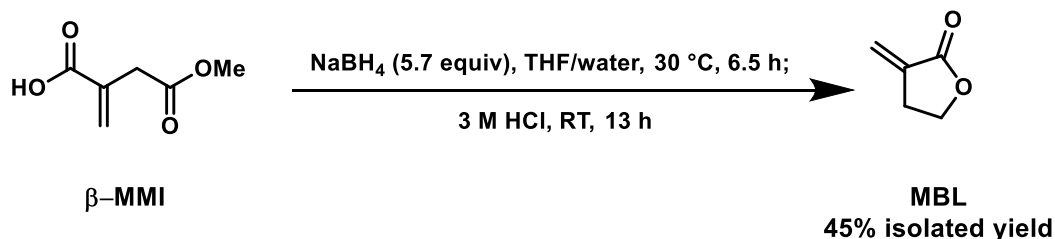
EXPERIMENTAL

Preparation of Polymer Thin Films for Optical Property Measurements. Thin films of PMBL and PMe₂MBL were prepared by spin coating a 60 mg/mL polymer solution of PMBL in dimethyl sulfoxide or PMe₂MBL in chloroform onto a silicon wafer. Prior to spin coating, the silicon wafers were cut, cleaned with a piranha solution, rinsed with water, dried, and cleaned with plasma.



Synthesis of α -methylene- γ,γ -dimethyl- γ -butyrolactone (Me₂MBL). β -MMI (30. g, 0.21 mol, 1.0 equiv) was weighed out and transferred to a dry 1 L round bottom flask

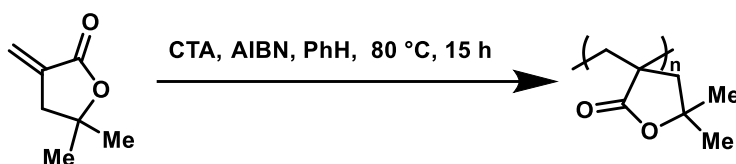
equipped with a stir bar and capped with a rubber septum. The flask was then evacuated and backfilled with nitrogen three times. THF (0.14 L, 1.5 M of β -MMI in THF) was added by syringe and the solution was cooled to 0 °C. Methyl magnesium chloride (0.22 L, 3.0 M, 0.65 mol, 3.1 equiv) was then added slowly over 15 minutes by syringe. The reaction was stirred at 0 °C for 2 h and then quenched by slow addition of HCl (0.33 L, 3 M, 0.99 mol, 4.7 equiv) to give a biphasic mixture with a pH of 0 in the aqueous phase. The biphasic mixture was then warmed to room temperature and stirred vigorously for 3 h. The reaction mixture was extracted three times with EtOAc and the organic layers were combined, dried with anhydrous magnesium sulfate, filtered, and concentrated under reduced pressure to give a dark brown oil. Fractional distillation of the crude oil at 85 °C under reduced pressure (50 mTorr) gave a 35 °C vapor that condensed to give Me₂MBL as a clear, colorless liquid with a measured density of 1.0 g/mL isolated in 39% yield (10.3 g, 0.082 mol). ¹H NMR (Figure S2.2, 500 MHz, CDCl₃, δ , ppm): 6.19 (t, J = 2.5 Hz, 1H), 5.59 (t, J = 2.4 Hz, 1H), 2.73 (s, 2H), 1.41 (s, 6H); ¹³C NMR (Figure S2.3, 125 MHz, CDCl₃, δ , ppm): 169.9, 136.2, 122.2, 81.7, 41.3, 28.5; IR (ATR, cm⁻¹): ν = 2972, 1749, 1663, 1373, 1262, 1186, 1094, 1080, 935, 929, 813, 749, 619; HRMS (DART-MS, m/z): [MH]⁺ calcd for C₇H₁₁O₂, 127.076; [MH]⁺ found, 127.076.



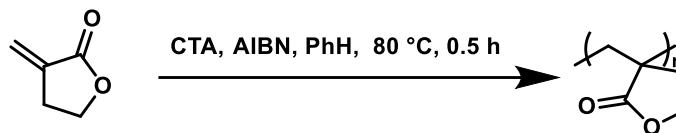
Synthesis of α -methylene- γ -butyrolactone (MBL). A 2-dram glass vial equipped with a stir bar was charged with β -MMI (29 mg, 0.21 mmol, 1.0 equiv) and NaBH₄ (46 mg, 1.2 mmol, 5.7 equiv). The vial was capped with a septum and evacuated and backfilled

with nitrogen three times. THF (1.6 mL, 0.13 M of β -MMI in THF) was then added via syringe at 0 °C and the mixture was stirred for 5 min. Water (0.4 mL, 22.2 mmol, 106 equiv) was then added dropwise at 0 °C, and after another 5 min the reaction mixture was placed in an oil bath pre-heated to 30 °C and was stirred for 6.5 h. The reaction was cooled to room temperature and quenched with HCl (3 M) and diluted with EtOAc. The mixture was then extracted three times with EtOAc and the organic layers were combined, dried with anhydrous MgSO_4 , filtered, and concentrated under reduced pressure in a rotary evaporator. Purification by chromatography (SiO_2 , 50% ethyl acetate, 49% hexanes, 1% acetic acid) gave the pure alcohol, **2.1**, γ -hydroxy- α -methylenebutiric acid in 56% yield. Characterization was consistent with that previously reported in the literature.⁶⁹ ^1H NMR (Figure S2.4, 500 MHz, CDCl_3 , δ , ppm): 6.70 (br s, 1H), 6.37 (s, 1H), 5.77 (s, 1H), 3.79 (t, 2H, $J = 6.1$ Hz), 2.58 (t, 2H, $J = 6.2$ Hz); ^{13}C NMR (Figure 2.5, 125 MHz, CDCl_3 , δ): 172.0, 137.0, 129.7, 61.7, 35.2; IR (ATR, cm^{-1}): $\nu = 3590 - 2350$, 1690, 1620, 1410, 1280, 1200, 1150, 1030, 946, 864, 823, 773, 679; HRMS (DART-MS, m/z): $[\text{MH}]^+$ calcd for $\text{C}_5\text{H}_9\text{O}_3$, 117.055; found, 117.055. Cyclization of **2.1** was performed in a separate step or as part of an acid workup after reduction of β -MMI. *As a separate step:* after concentration of the organic layers following extraction, 1.0 mL of THF and 1.0 mL of 3 M HCl were added to the crude oil. The mixture was then stirred for 9 h and extracted three times with EtOAc. The combined organic layers were dried with MgSO_4 , filtered, and concentrated on the rotary evaporator to give MBL in 93% yield from the alcohol (52% yield from β -MMI). *As part of the acid workup:* After 6.5 h at 30 °C, 2.0 mL of 3 M HCl was added to the reaction mixture and stirred for 13 h. The mixture was then extracted with EtOAc five

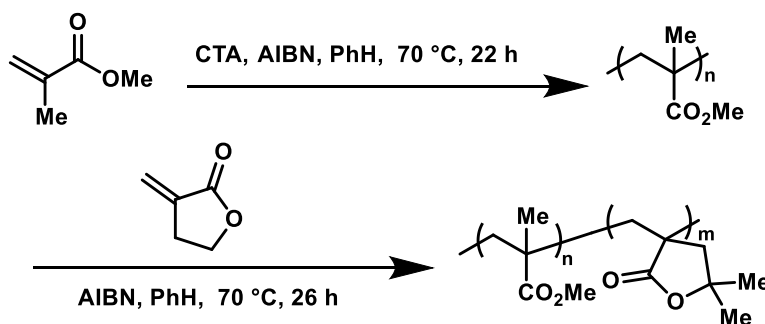
times, dried with Na₂SO₄, filtered, and concentrated on the rotary evaporator to give the crude lactone product, MBL. Purification by chromatography (SiO₂, 30% ethyl acetate, 69% hexanes, 1% acetic acid) gave pure MBL in 42% isolated yield from β -MMI. Characterization data matched those reported in the literature.⁷⁰ ¹H NMR (Figure S2.6, 500 MHz, CDCl₃, δ , ppm): 6.26 (t, 1H, J = 2.9 Hz), 5.67 (t, 1H, J = 2.6 Hz), 4.38 (t, 2H, J = 7.4 Hz), 2.99 (tt, 2H, J = 2.8 Hz, J = 7.4 Hz).



RAFT polymerization of Me₂MBL. Me₂MBL (0.20 mL, 0.20 g, 1.6 mmol, 1100 equiv) was added by syringe to a 2-dram vial equipped with a stir bar and a cap with a Teflon septum. Following this, AIBN (0.05 mL, 4.6 mg/mL in benzene, 0.23 mg, 0.0014 mmol, 1.0 equiv) and 2-cyano-2-propyl benzodithioate (0.05 mL, 31 mg/mL in benzene, 1.6 mg, 0.0070 mmol, 5.0 equiv) were added to the vial by syringe. The combined reagents were mixed to homogeneity and then degassed by three freeze-pump-thaw cycles. The degassed solution was kept under vacuum and submerged in an oil bath preheated to 80 °C. The reaction was stirred for 15 h. After the reaction mixture had gelled, it was removed from the heat and dissolved in THF. Aliquots were then taken for ¹H NMR analysis in CDCl₃ to obtain conversion and SEC analysis in THF to obtain M_n , M_w , and \bar{D} . The viscous solution was then precipitated in cold (−30 °C) hexanes and the solid polymer was isolated by filtration. The light pink powder was then dried overnight at 100 °C in a vacuum oven prior to thermal analysis. ¹H NMR (Figure S2.7, 500 MHz, CDCl₃, δ , ppm): 2.20 (br s, 4H), 1.54 (br s, 3H), 1.47 (br s, 3H); ¹³C NMR (Figure S2.8, 125 MHz, CDCl₃, δ , ppm): 179.3, 82.2, 48.7, 48.1, 45.0, 30.2.



RAFT Polymerization of MBL. MBL (0.14 mL, 0.16 g, 1.6 mmol, 1100 equiv) was added by syringe to a 2-dram vial equipped with a stir bar and a cap with a Teflon septum. Following this, AIBN (0.05 mL, 4.6 mg/mL in benzene, 0.23 mg, 0.0014 mmol, 1.0 equiv) and 2-cyano-2-propyl benzodithioate (0.05 mL, 31 mg/mL in benzene, 1.6 mg, 0.0070 mmol, 5.0 equiv) were added to the vial by syringe. The combined reagents were mixed to homogeneity and then degassed by three freeze-pump-thaw cycles. The degassed solution was kept under vacuum and submerged in an oil bath pre-heated to 80 °C. The reactions were stirred for 0.5 h. After the reaction mixture had gelled, it was removed from the heat and dissolved in DMF. Aliquots were then taken for ^1H NMR analysis in DMSO- d_6 to obtain conversion and SEC analysis in DMF to obtain M_n , M_w , and \bar{D} . The viscous solution was then precipitated in cold (−30 °C) MeOH and the solid polymer was isolated by filtration. The light pink powder was then dried overnight at 100 °C in a vacuum oven prior to thermal analysis. Characterization data matched those reported in the literature.³⁷ ^1H NMR (Figure S2.1, 600 MHz, DMSO- d_6 , δ , ppm): 4.34 (m, 2H), 2.05 (m, 4H). SEC curves for different MBL:CTA ratios were taken (Figure S2.11).



Synthesis of PMMA-*b*-PMe₂MBL by RAFT Polymerization.

Synthesis of the PMMA macroinitiator: AIBN (2.5 mg, 0.015 mmol, 1.0 equiv), 2-cyano-2-propyl benzodithioate (15.5 mg, 0.070 mmol, 4.7 equiv), and methyl methacrylate (MMA, 0.85 mL, 0.80 g, 8.0 mmol, 530 equiv) were added to a 2-dram vial equipped with a stir bar and a cap with a Teflon septum. The combined reagents were diluted with benzene (0.60 mL, 1.4:1.0 v/v MMA:PhH ratio), mixed to homogeneity, and then degassed by three freeze-pump-thaw cycles. The degassed solution was kept under vacuum, submerged in an oil bath pre-heated to 70 °C, and stirred for 22 h. After the reaction mixture had gelled, it was removed from the heat and dissolved in THF. An aliquot was then taken for ¹H NMR analysis in CDCl₃ to obtain conversion (83%). The polymer was then crashed out of cold (− 30 °C) MeOH, filtered, and dried to obtain a pink powder (0.44 g) in 55% isolated yield. This process was repeated twice. SEC analysis in THF gave M_n , M_w , and \bar{D} as 9.7 kg/mol, 10.2 kg/mol, and 1.06, respectively for the PMMA macroinitiator. $M_{n,theo}$ = 9.5 kg/mol (based on MMA:CTA loading and % conversion). Characterization data matched those reported in the literature.⁷¹

*Synthesis of PMMA-*b*-PMe₂MBL from the PMMA macroinitiator:* The PMMA macroinitiator (degree of polymerization = 97, 71.7 mg, 0.0074 mmol, 5.8 equiv) was added to a 2-dram vial equipped with a stir bar and a cap with a Teflon septum. Following this, Me₂MBL (0.18 mL, 0.18 g, 1.43 mmol, 1100 equiv) and AIBN (0.20 mL, 1.05 mg/mL in benzene, 0.21 mg, 0.0013 mmol, 1.0 equiv, 0.9:1.0 v/v Me₂MBL:PhH ratio) were added to the vial by syringe. The combined reagents were mixed to homogeneity and then degassed by three freeze-pump-thaw cycles. The

degassed solution was kept under vacuum and submerged in an oil bath pre-heated to 70 °C for 26 h. An aliquot was then taken for ^1H NMR analysis in CDCl_3 to obtain conversion (33%). The polymer was then dissolved in a 1:1 mixture of THF and CDCl_3 and was then crashed out of cold ($-30\text{ }^\circ\text{C}$) hexanes, filtered, and dried on high vacuum overnight. SEC analysis in THF gave M_n , M_w , and \bar{D} as 22.2 kg/mol, 24.5 kg/mol, and 1.11, respectively, for the diblock copolymer. The $M_{n,\text{theo}}$ was 8.0 kg/mol (based on the $\text{Me}_2\text{MBL}:\text{CTA}$ loading and % conversion) for the PMe_2MBL block and 17.5 kg/mol for the entire diblock. ^1H NMR (Figure S2.10, 500 MHz, CDCl_3 , δ , ppm): 3.60 (s, 3H, PMMA block), 2.27 (br s, 4H, PMe_2MBL block), 1.90 (br s, 3H, PMe_2MBL block), 1.81 (s, 2H, PMMA block), 1.56 (br s, 3H, PMe_2MBL block), 1.25 (s, $-\text{CH}_3$, PMMA block), 1.02 (s, $-\text{CH}_3$, PMMA block), 0.85 (s, $-\text{CH}_3$, PMMA block).

APPENDIX

General Reagent Information. β -monomethyl itaconate (β -MMI, 98%, TCI), Celite[®] 545 (Sigma-Aldrich), ethyl acetate (EtOAc, 99.5%, Fisher), hexanes (98.5%, Fisher), methanol (MeOH, 99.8%, Fisher), benzene (99.0%, EMD Millipore), chloroform (99.8%, J.T. Baker), dimethyl sulfoxide (99.9%, Fisher), acetic acid (glacial, EMD Millipore), chloroform-D (99.8%, Cambridge Isotope Laboratories, Inc.), dimethyl sulfoxide-D6 (DMSO-d_6 , 99.9%, Cambridge Isotope Laboratories, Inc.), anhydrous magnesium sulfate (98.0%, EMD Millipore), anhydrous sodium sulfate (99.0%, BDH), methyl magnesium chloride (MeMgCl , 3.0 M in THF, Sigma-Aldrich), methyl methacrylate (MMA, 99%, Aldrich), sodium borohydride (NaBH_4 , 98%, Acros), lithium borohydride (LiBH_4 , 95%, Strem), sodium cyanoborohydride (NaCNBH_3 , 95%, Sigma-Aldrich), lithium aluminum hydride (LiAlH_4 , 1.0 M in THF, Aldrich), lithium

triethylborohydride (Super-Hydride[®], LiEt₃BH, 1.0M in THF, Aldrich) diisobutylaluminum hydride (DIBAL-H, 1.0M in hexanes, Aldrich), sodium bis(2-methoxyethoxy)aluminumhydride (Red-Al[®], 60 wt% in toluene, Aldrich), sodium triacetoxymborohydride (Na(OAc)₃BH, 95%, Aldrich) and 2-cyano-2-propyl benzodithioate (97%, Sigma-Aldrich) were used as received. Water was obtained by reverse osmosis. Tetrahydrofuran (THF, 99%, Macron) was purified by passing through two neutral alumina columns on the JC Meyer solvent system. HCl (Macron) was used as received and diluted with water to make a 3 M solution. Azobisisobutyronitrile (AIBN, Sigma, 98.0%) was recrystallized from MeOH prior to use. Piranha solution was prepared by mixing sulfuric acid (95–98%, BDH) and hydrogen peroxide (30%, Fisher) in a 3:1 (v/v) ratio. Anhydrous cerium (III) chloride (CeCl₃) was prepared from cerium(III) chloride heptahydrate (99.9%, Sigma-Aldrich) by drying.⁵⁷ Silicon wafers for spin coating were purchased from Purewafer, a WRS material company (item no. 4N0SSP-004). Silica used for column chromatography was purchased from SiliCycle (SiliaFlash[®] Irregular Silica Gels, P60, 40-63μm, 60Å).

General Analytical Information. All PMe₂MBL samples were analyzed using a Tosoh EcoSec HLC 8320GPC system with two SuperHM-M columns in series at a flow rate of 0.350 mL/min at 40 °C. THF was used as the eluent and all number-average molar masses (M_n), weight-average molar masses (M_w), and dispersities (\bar{D}) for PMe₂MBL were determined by light scattering using a Wyatt miniDawn Treos multi-angle light scattering detector. The dn/dc values of PMe₂MBL was estimated to be 0.0853 mL/g² using size exclusion chromatography with samples of known concentrations in THF. This indirect ("in-line") method uses the total area of the RI signal and the assumption

that 100% of the sample mass is recovered to calculate the polymer dn/dc values. All PMBL polymer samples were analyzed using a GPC system composing of a Waters 515 pump and three PSS GRAM columns (100-1000-3000) in series at a flow rate of 1.0 mL/min at 25 °C. DMF was used as the eluent and all M_n s, M_w s, and \bar{D} s for PMBL were determined from refractive index chromatograms against Fluka polystyrene standards using an Agilent 1200 refractive index detector. Nuclear magnetic resonance spectra were recorded on a Mercury 300 MHz, a Varian 400 MHz, a Bruker 500 MHz, or a Varian 600 MHz instrument. Mass spectra were performed on an Exactive Plus Orbitrap Mass Spectrometer with a DART SVP ion source from Ion Sense. IR spectra were recorded on a Thermo Scientific Smart Orbit Nicolet Avatar 370 DTGS FTIR equipped with a diamond ATR attachment (30,000 – 200 cm^{-1}). Differential scanning calorimetry (DSC) measurements of polymer samples were performed on a Mettler-Toledo Polymer DSC instrument equipped with a chiller and an autosampler. Samples were prepared in aluminum pans and were analyzed using the following heating program: $-70\text{ }^{\circ}\text{C}$ to $240\text{ }^{\circ}\text{C}$ at $10\text{ }^{\circ}\text{C}/\text{min}$, $240\text{ }^{\circ}\text{C}$ to $-70\text{ }^{\circ}\text{C}$ at $10\text{ }^{\circ}\text{C}/\text{min}$, and then $-70\text{ }^{\circ}\text{C}$ to $240\text{ }^{\circ}\text{C}$ at $10\text{ }^{\circ}\text{C}/\text{min}$. Data were processed using StarE software. All reported T_g s were observed on the second heating cycle. Thermogravimetric analysis (TGA) was performed on a TA Instruments Q500 Thermogravimetric Analyzer. Samples were heated under nitrogen atmosphere at a rate of $20\text{ }^{\circ}\text{C}/\text{min}$ from $25\text{ }^{\circ}\text{C}$ to $600\text{ }^{\circ}\text{C}$. Data were processed using Universal Analysis software.

General Ellipsometry Information. Refractive indices and Abbe numbers were determined by ellipsometry. Spectroscopic ellipsometry measurements were performed on a variable angle spectroscopic ellipsometer (VASE, J.A. Woollam Co.) controlled

by WVASE32 software (J.A. Woollam Co.). Film thickness data were collected at incidence angles of 65, 70, and 75° over wavelengths ranging from 250 to 1000 nm in 10 nm increments. Data were fit to a model comprising a Si substrate, SiO₂ layer (with a 2 nm thickness), and a Cauchy layer. The material files for the Si and SiO₂ layers were supplied with the WVASE32 software. The Cauchy layer was fit using thickness, and the Cauchy parameters A_n, B_n, and C_n. After fitting thickness and Cauchy parameters were determined, the optical parameters n and k were then calculated by fitting at individual wavelengths based on the experimental data and the model. For the PMe₂MBL film, the thickness-nonuniformity model was applied in the Cauchy layer due to the inhomogeneity of the spin-coated film. The non-uniformity was simulated by calculating data for the structure using a series of slightly different thicknesses for the Cauchy layer. The number of different structures was 5 while the weighting profile for convolution was square. The maximum change in thickness from the model thickness, which defines the maximum and minimum deviation from the model thickness at the edges of the convolution profile, was set as the fitting parameter. The resulting mean square error was improved and the resulting film non-uniformity ($689.021 \pm 10.034\%$) fits well within the range of AFM measurements (739 ± 85 nm; point 1 = 792 nm, point 2 = 641 nm, point 3 = 785 nm). Traces of refractive index and extinction coefficient for both PMMA and PMe₂MBL are depicted in Figure S2.12 and Figure S2.13, respectively.

Supplementary Figures

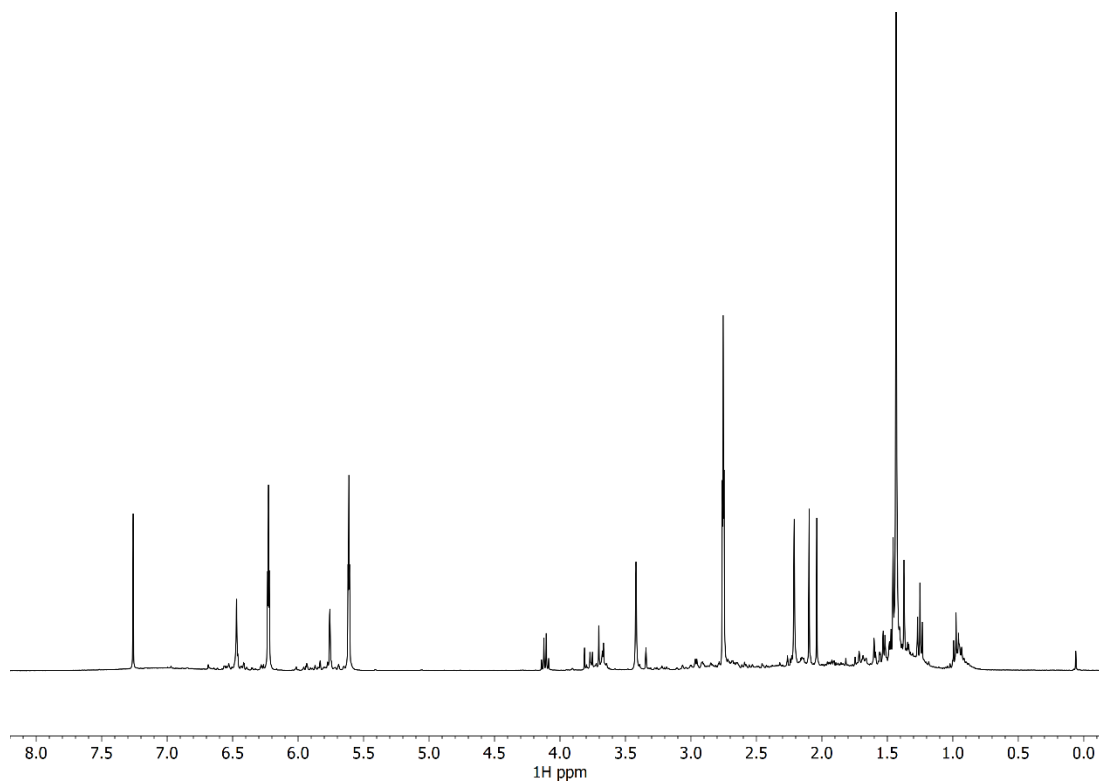


Figure S2.1. ^1H NMR spectrum of the crude reaction mixture for the synthesis of Me_2MBL prior to distillation in CDCl_3 .

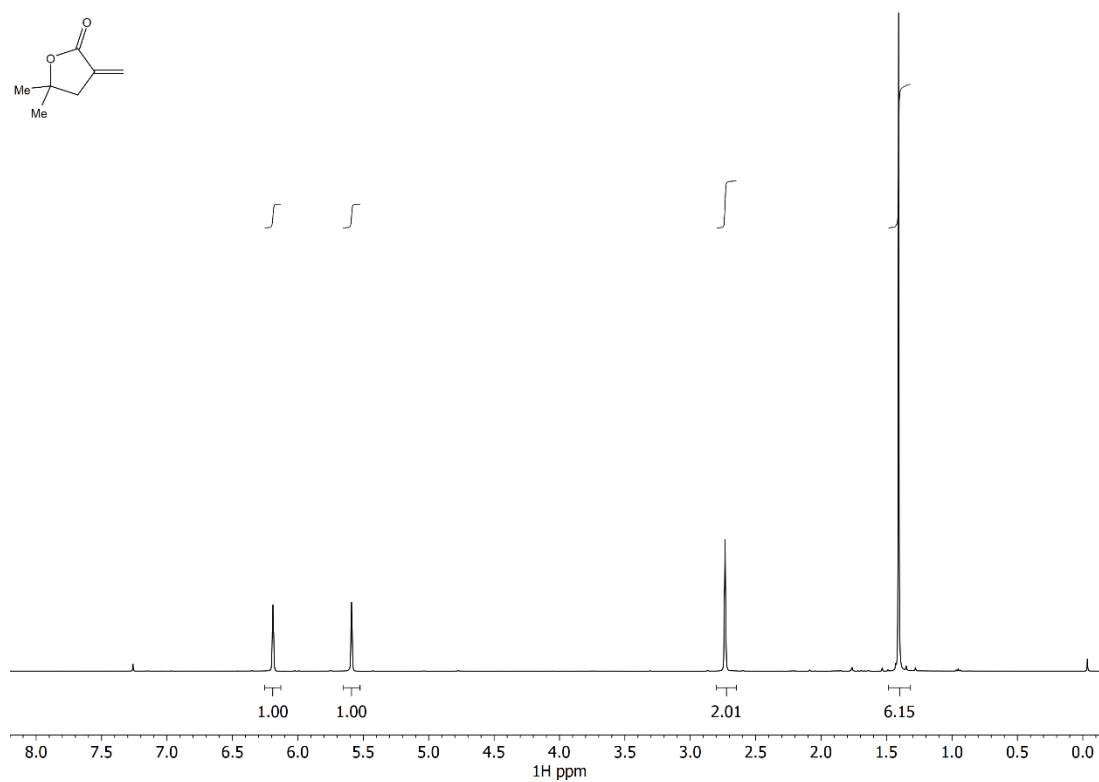


Figure S2.2. ^1H NMR spectrum of Me_2MBL in CDCl_3 .

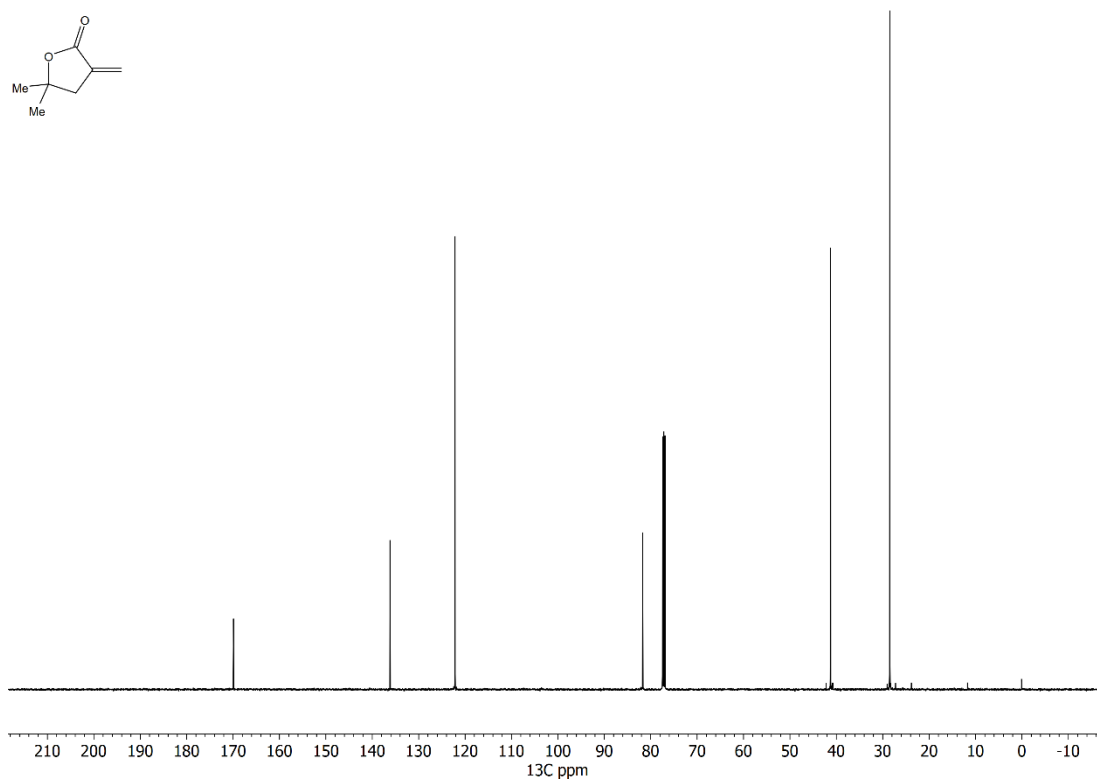


Figure S2.3. ¹³C NMR spectrum of Me₂MBL in CDCl₃.

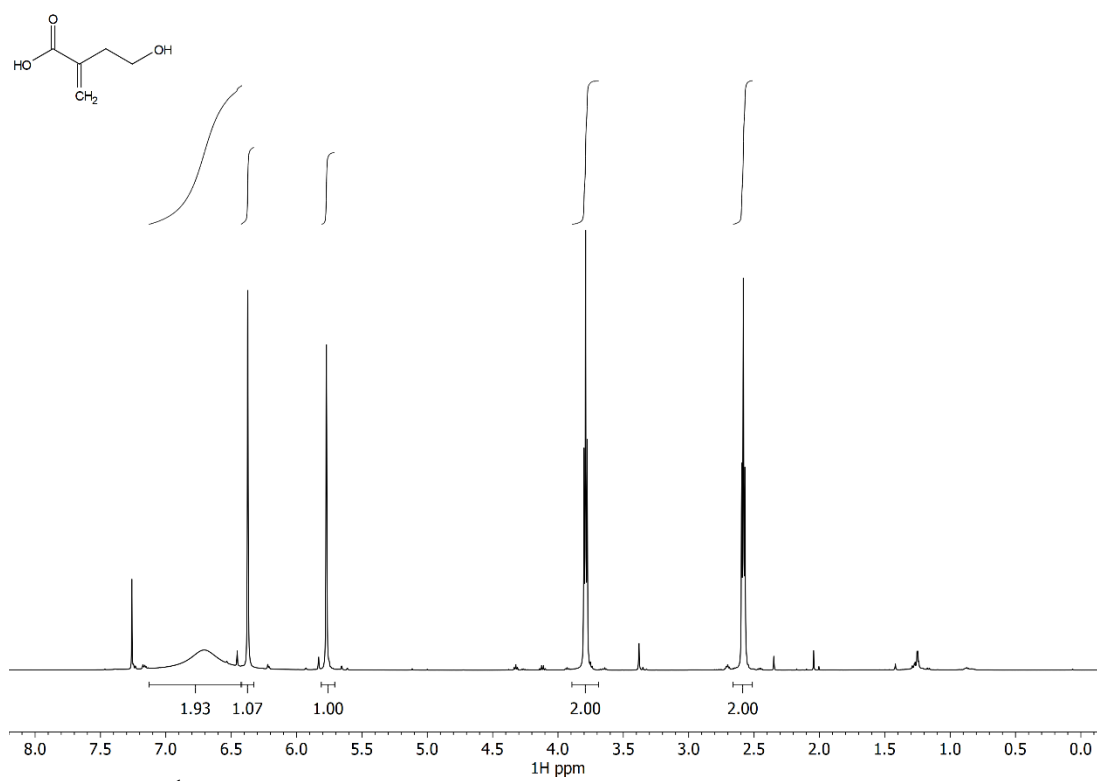


Figure S2.4. ¹H NMR spectrum of **2.1** in CDCl₃.

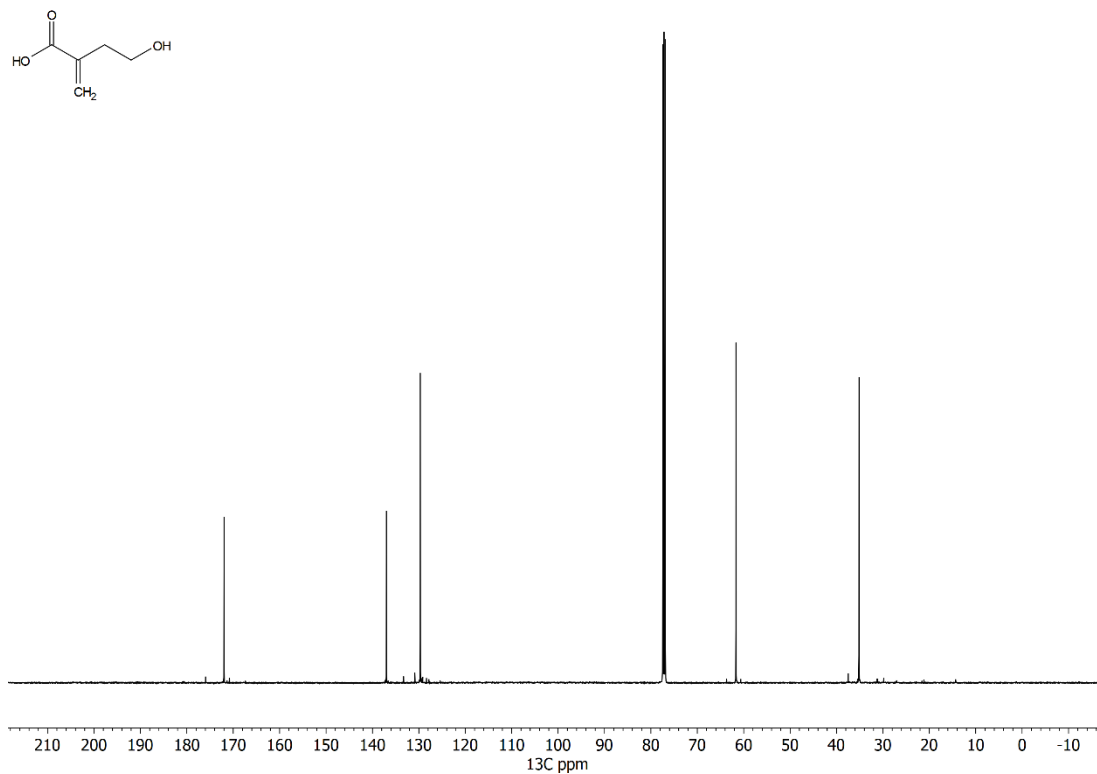


Figure S2.5. ¹³C NMR spectrum of **2.1** in CDCl₃.

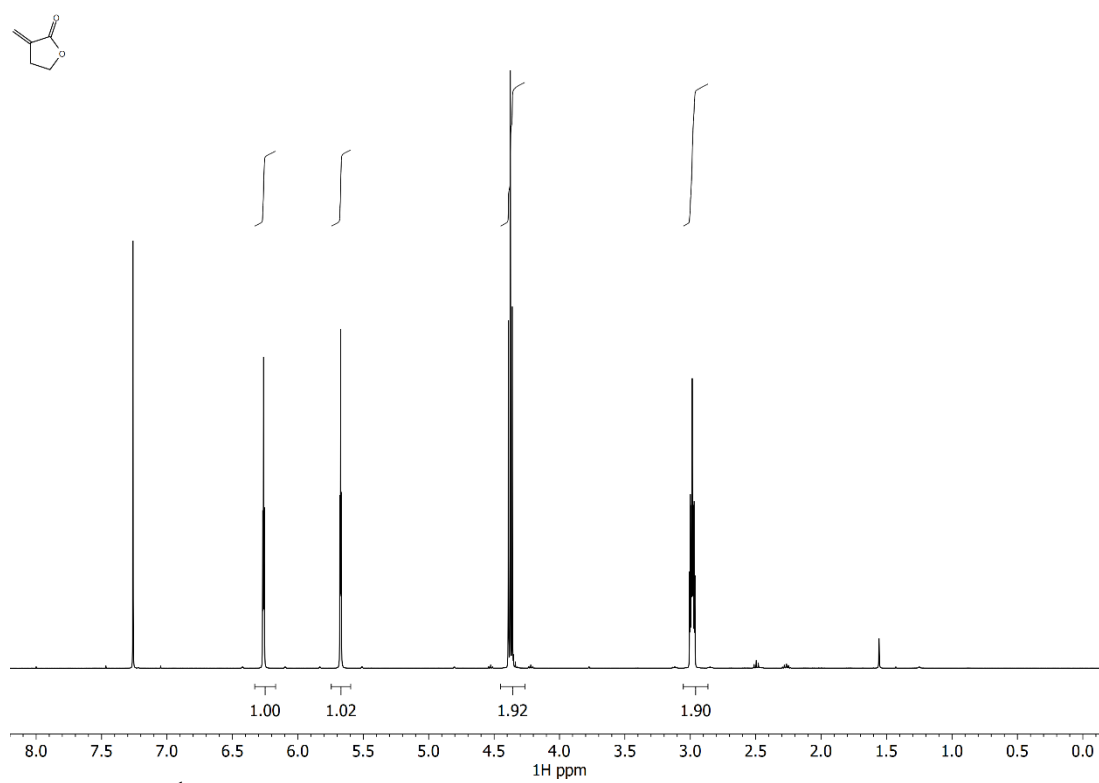


Figure S2.6. ¹H NMR spectrum of **MBL** in CDCl₃.

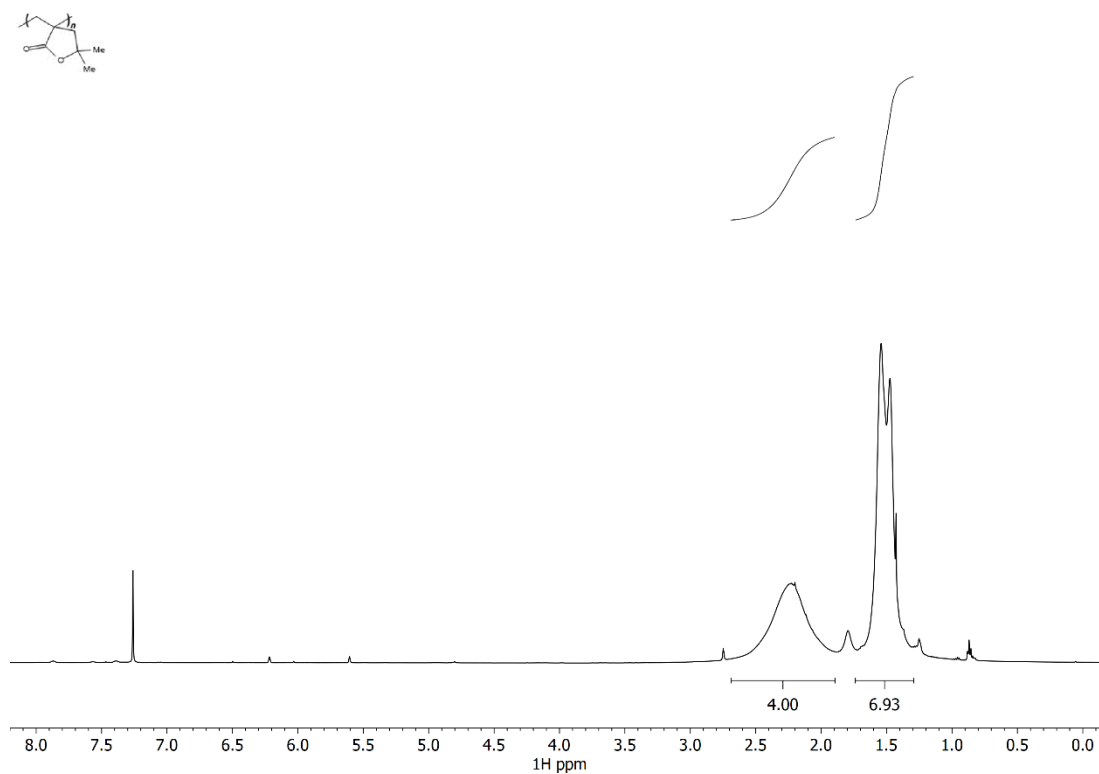


Figure S2.7. ¹H NMR spectrum of PMe₂MBL in CDCl₃.

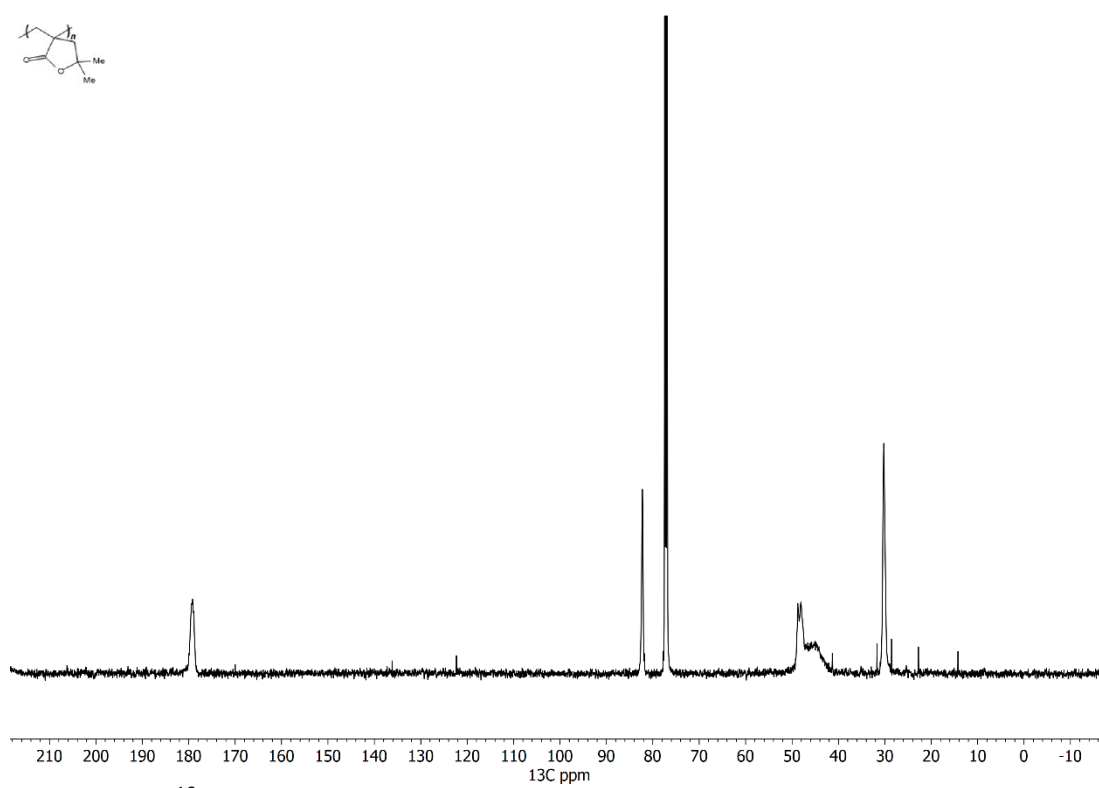


Figure S2.8. ¹³C NMR spectrum of PMe₂MBL in CDCl₃.

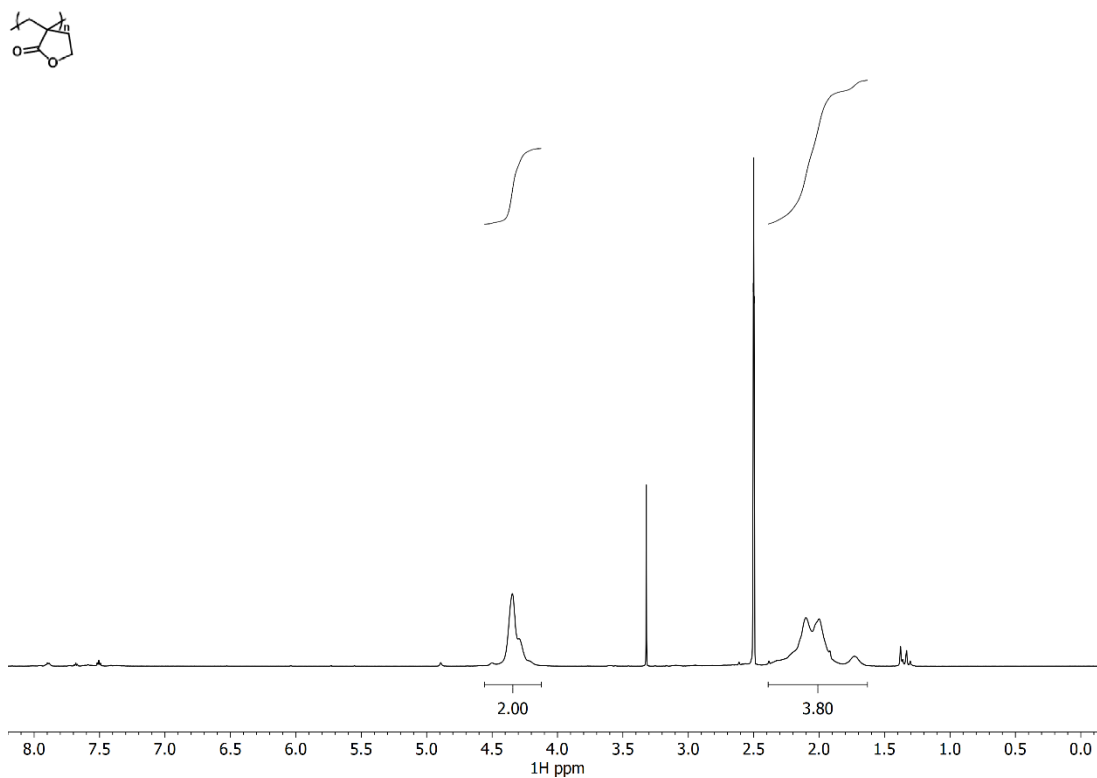


Figure S2.9. ^1H NMR spectrum of PMBL in DMSO-d_6 .

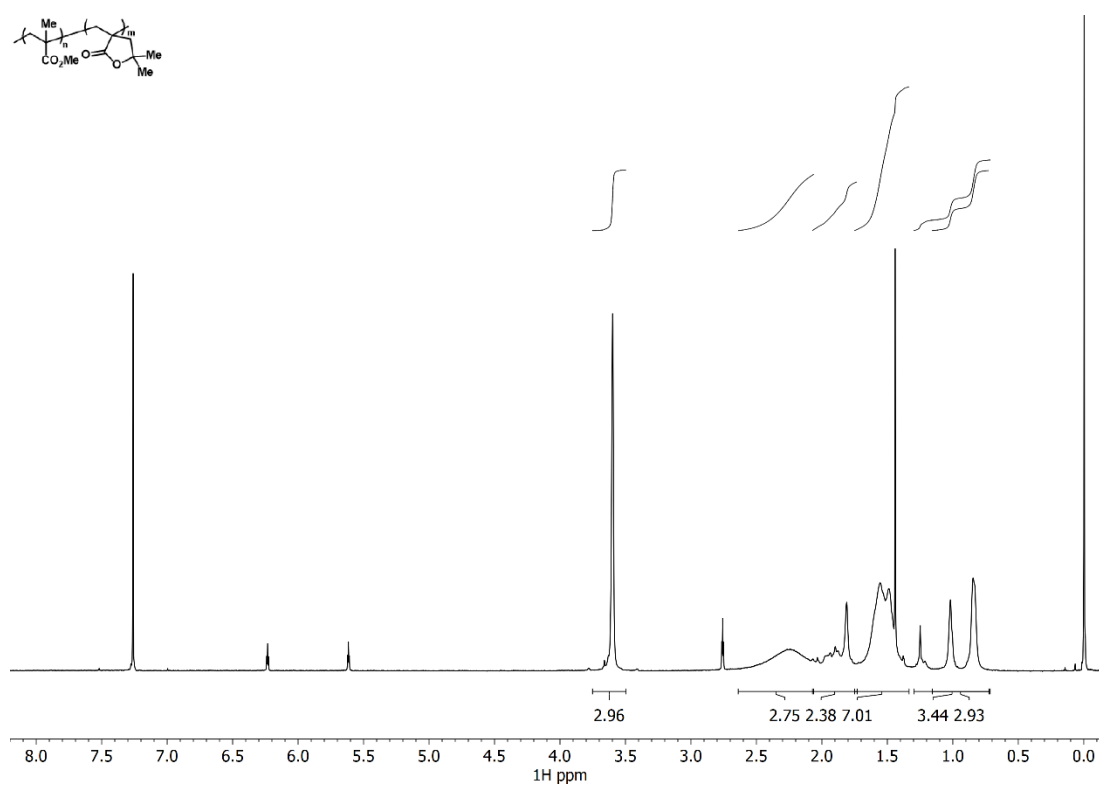


Figure S2.10. ^1H NMR spectrum of $\text{PMMA-}b\text{-PMe}_2\text{MBL}$ in CDCl_3 .

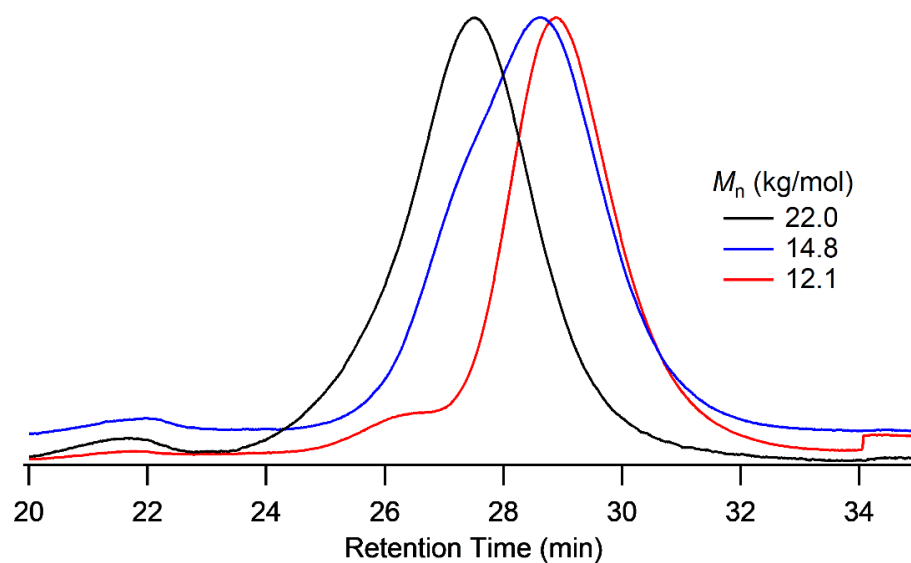


Figure S2.11. RAFT polymerization of MBL leads to predictable M_n values based on MBL and CTA loading.

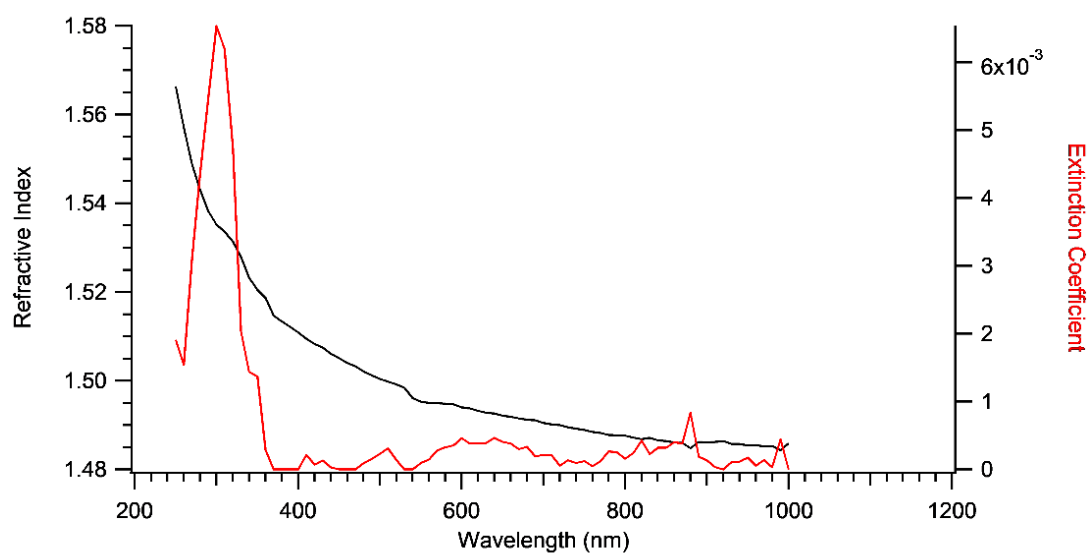


Figure S2.12. Refractive index vs wavelength obtained from ellipsometry measurements for a thin film of PMMA.

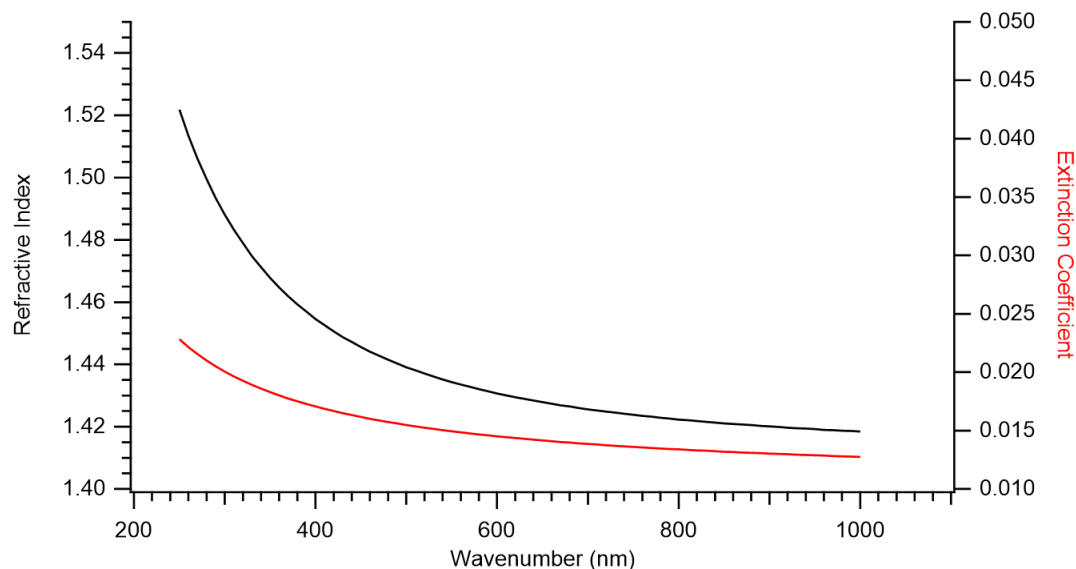


Figure S2.13. Refractive index vs wavelength obtained from ellipsometry measurements for a thin film of PMe₂MBL.

REFERENCES

- (1) Trotta, J. T.; Jin, M.; Stawiasz, K. J.; Michaudel, Q.; Chen, W.-L.; Fors, B. P. Synthesis of Methylene Butyrolactone Polymers from Itaconic Acid. *J. Polym. Sci., Part A: Polym. Chem.* **2017**, *55*, 2730–2737.
- (2) Nikolau, B. J.; Perera, M. A. D. N.; Brachova, L.; Shanks, B. Platform Biochemicals for a Biorenewable Chemical Industry. *Plant J.* **2008**, *54*, 536–545.
- (3) Werpy, T.; Petersen, G.; Aden, A.; Bozell, J.; Holladay, J.; White, J.; Manheim, A. *Top Value Added Chemicals from Biomass Volume I — Results of Screening for Potential Candidates from Sugars and Synthesis Gas*; 2004.
- (4) Okabe, M.; Lies, D.; Kanamasa, S.; Park, E. Y. Biotechnological Production of Itaconic Acid and Its Biosynthesis in *Aspergillus Terreus*. *Appl. Microbiol. Biotechnol.* **2009**, *84*, 597–606.

- (5) Klement, T.; Büchs, J. Itaconic Acid - A Biotechnological Process in Change. *Bioresource Technol.* **2013**, *135*, 422–431.
- (6) ITACONIX, L. *Development of Integrated Production of Polyitaconic Acid from Northeast Hardwood Biomass*; 2009.
- (7) Marvel, C. S.; Shepherd, T. H. Polymerization Reactions of Itaconic Acid and Some of Its Derivatives. *J. Org. Chem.* **1959**, *24*, 599–605.
- (8) Nagai, S.; Yoshida, K. Studies on Polymerization and Polymers of Itaconic Acid Derivatives. IV. Polymerization of Itaconic Acid in Aqueous Solution. *Kobunshi Kagaku* **1960**, *17*, 748–752.
- (9) Stawski, D.; Połowiński, S. Polymerization of Itaconic Acid. *Polimery* **2005**, *50*, 118–122.
- (10) Bednarz, S.; Błaszczuk, A.; Błazejewska, D.; Bogdał, D. Free-Radical Polymerization of Itaconic Acid in the Presence of Choline Salts: Mechanism of Persulfate Decomposition. *Catal. Today* **2015**, *257*, 297–304.
- (11) Braun, V. D.; El Sayed, I. A. A. Über Die Struktur Der Polymeren Aus Itaconsäure. *Die Makromol. Chem.* **1966**, *96*, 100–121.
- (12) Tate, B. E. Polymerization of Itaconic Acid and Derivatives. *Adv. Polym. Sci.* **1967**, *5*, 214–232.
- (13) Askarov, M. A.; Semenova, L. N.; Babadzhanova, E. N. Properties of Some Synthetic Water-Soluble Polymers Based on Itaconic Acid. *Uzb. Khim. Zh.* **1968**, *12*, 38–40.

- (14) Yokota, K.; Hirabayashi, T.; Takashima, T. The Preparation of Poly(Itaconic Acid). *Die Makromol. Chem.* **1975**, 176, 1197–1205.
- (15) Grespos, E.; Hill, D. J. T.; Donnel, J. H. O.; Sullivan, P. W. O.; Young, T. L.; East, G. C.; Zvin, K. J. Polymerization of Itaconic Acid in Aqueous Solution: Structure of the Polymer and Polymerization Kinetics at 25 °C, Studied by ¹³C NMR. *Makromol. Chem., Rapid Commun.* **1984**, 5, 489–494.
- (16) Veličković, J.; Filipović, J.; Djakov, D. P. The Synthesis and Characterization of Poly(Itaconic) Acid. *Polym. Bull.* **1994**, 32, 169–172.
- (17) Mao, Z.; Yang, C. Q. Polymeric Multifunctional Carboxylic Acids as Crosslinking Agents for Cotton Cellulose: Poly(Itaconic Acid) and In Situ Polymerization of Itaconic Acid. *J. Appl. Polym. Sci.* **2001**, 79, 319–326.
- (18) Lárez, C.; Canelón, F.; Millán, E.; Perdomo, G.; Katime, I. New Results on the Polymerisation of the Itaconic Acid in Aqueous Medium. *Polym. Bull.* **2002**, 49, 119–126.
- (19) Fernández-García, M.; Fernández-Sanz, M.; De La Fuente, J. L.; Madruga, E. L. Atom-Transfer Radical Polymerization of Dimethyl Itaconate. *Macromol. Chem. Phys.* **2001**, 202, 1213–1218.
- (20) Hirano, T.; Takeyoshi, R.; Seno, M.; Sato, T. Chain-Transfer Reaction in the Radical Polymerization of Di-n-Butyl Itaconate at High Temperatures. *J. Polym. Sci., Part A: Polym. Chem.* **2002**, 40, 2415–2426.
- (21) Szablan, Z.; Toy, A. A.; Davis, T. P.; Hao, X.; Stenzel, M. H.; Barner-

- Kowollik, C. Reversible Addition Fragmentation Chain Transfer Polymerization of Sterically Hindered Monomers: Toward Well-Defined Rod/Coil Architectures. *J. Polym. Sci., Part A: Polym. Chem.* **2004**, *42*, 2432–2443.
- (22) Szablan, Z.; Toy, A. A.; Terrenoire, A.; Davis, T. P.; Stenzel, M. H.; Müller, A. H. E.; Barner-Kowollik, C. Living Free-Radical Polymerization of Sterically Hindered Monomers: Improving the Understanding of 1,1-Disubstituted Monomer Systems. *J. Polym. Sci., Part A: Polym. Chem.* **2006**, *44*, 3692–3710.
- (23) Kassi, E.; Loizou, E.; Porcar, L.; Patrickios, C. S. Di(n-Butyl) Itaconate End-Functionalized Polymers: Synthesis by Group Transfer Polymerization and Solution Characterization. *Eur. Polym. J.* **2011**, *47*, 816–822.
- (24) Suenaga, J.; Sutherlin, D. M.; Stille, J. K. Polymerization of (RS)- and (R)- α -Methylene- γ -Methyl- γ -Butyrolactone. *Macromolecules* **1984**, *17*, 2913–2916.
- (25) Sogah, D. Y.; Hertler, W. R.; Webster, O. W.; Cohen, G. M. Group Transfer Polymerization. Polymerization of Acrylic Monomers. *Macromolecules* **1987**, *20*, 1473–1488.
- (26) Hu, Y.; Gustafson, L. O.; Zhu, H.; Chen, E. Y.-X. Anionic Polymerization of MMA and Renewable Methylene Butyrolactones by Resorbable Potassium Salts. *J. Polym. Sci., Part A: Polym. Chem.* **2011**, *49*, 2008–2017.
- (27) Zhang, Y.; Gustafson, L. O.; Chen, E. Y.-X. Dinuclear Silylium-Enolate Bifunctional Active Species: Remarkable Activity and Stereoselectivity toward Polymerization of Methacrylate and Renewable Methylene Butyrolactone

- Monomers. *J. Am. Chem. Soc.* **2011**, *133*, 13674–13684.
- (28) Shin, J.; Lee, Y.; Tolman, W. B.; Hillmyer, M. A. Thermoplastic Elastomers Derived from Menthide and Tulipalin A. *Biomacromolecules* **2012**, *13*, 3833–3840.
- (29) Higaki, Y.; Okazaki, R.; Takahara, A. Semirigid Biobased Polymer Brush: Poly(α -Methylene- γ -Butyrolactone) Brushes. *ACS Macro Lett.* **2012**, *1*, 1124–1127.
- (30) Hu, Y.; Wang, X.; Chen, Y.; Caporaso, L.; Cavallo, L.; Chen, E. Y.-X. Rare-Earth Half-Sandwich Dialkyl and Homoleptic Trialkyl Complexes for Rapid and Stereoselective Polymerization of a Conjugated Polar Olefin. *Organometallics* **2013**, *32*, 1459–1465.
- (31) Hong, M.; Chen, E. Y.-X. Coordination Ring-Opening Copolymerization of Naturally Renewable α -Methylene- γ -Butyrolactone into Unsaturated Polyesters. *Macromolecules* **2014**, *47*, 3614–3624.
- (32) Ding, K.; John, A.; Shin, J.; Lee, Y.; Quinn, T.; Tolman, W. B.; Hillmyer, M. A. High-Performance Pressure-Sensitive Adhesives from Renewable Triblock Copolymers. *Biomacromolecules* **2015**, *16*, 2537–2539.
- (33) Tang, J.; Chen, E. Y.-X. Organopolymerization of Naturally Occurring Tulipalin B: A Hydroxyl-Functionalized Methylene Butyrolactone. *Org. Chem. Front.* **2015**, *2*, 1625–1631.
- (34) Gowda, R. R.; Chen, E. Y.-X. Organocatalytic and Chemoselective

- Polymerization of Multivinyl-Functionalized γ -Butyrolactones. *ACS Macro Lett.* **2016**, *5*, 772–776.
- (35) Tang, X.; Hong, M.; Falivene, L.; Caporaso, L.; Cavallo, L.; Chen, E. Y.-X. The Quest for Converting Biorenewable Bifunctional α -Methylene- γ -Butyrolactone into Degradable and Recyclable Polyester: Controlling Vinyl-Addition/Ring-Opening/Cross-Linking Pathways. *J. Am. Chem. Soc.* **2016**, *138*, 14326–14337.
- (36) Qi, G.; Nolan, M.; Schork, J. F.; Jones, C. W. Emulsion and Controlled Miniemulsion Polymerization of the Renewable Monomer γ -Methyl- α -Methylene- γ -Butyrolactone. *J. Polym. Sci. Part A Polym. Chem.* **2008**, *46*, 5929–5944.
- (37) Mosnáček, J.; Matyjaszewski, K. Atom Transfer Radical Polymerization of Tulipalin A: A Naturally Renewable Monomer. *Macromolecules* **2008**, *41*, 5509–5511.
- (38) Mosnáček, J.; Yoon, J. A.; Juhari, A.; Koynov, K.; Matyjaszewski, K. Synthesis, Morphology and Mechanical Properties of Linear Triblock Copolymers Based on Poly(α -Methylene- γ -Butyrolactone). *Polymer* **2009**, *50*, 2087–2094.
- (39) Miyake, G. M.; Newton, S. E.; Mariott, W. R.; Chen, E. Y.-X. Coordination Polymerization of Renewable Butyrolactone-Based Vinyl Monomers by Lanthanide and Early Metal Catalysts. *Dalton Trans.* **2010**, *39*, 6710–6718.
- (40) Juhari, A.; Mosnacek, J.; Yoon, J. A.; Nese, A.; Koynov, K.; Kowalewski, T.;

- Matyjaszewski, K. Star-like Poly(n-Butyl Acrylate)-b-Poly(α -Methylene- γ -Butyrolactone) Block Copolymers for High Temperature Thermoplastic Elastomers Applications. *Polymer* **2010**, *51*, 4806–4813.
- (41) Zhang, Y.; Miyake, G. M.; Chen, E. Y.-X. Alane-Based Classical and Frustrated Lewis Pairs in Polymer Synthesis: Rapid Polymerization of MMA and Naturally Renewable Methylene Butyrolactones into High-Molecular-Weight Polymers. *Angew. Chem. Int. Ed.* **2010**, *49*, 10158–10162.
- (42) Hu, Y.; Xu, X.; Zhang, Y.; Chen, Y.; Chen, E. Y.-X. Polymerization of Naturally Renewable Methylene Butyrolactones by Half-Sandwich Indeyl Rare Earth Metal Dialkyls with Exceptional Activity. *Macromolecules* **2010**, *43*, 9328–9336.
- (43) Miyake, G. M.; Zhang, Y.; Chen, E. Y.-X. Living Polymerization of Naturally Renewable Butyrolactone-Based Vinylidene Monomers by Ambiphilic Silicon Propagators. *Macromolecules* **2010**, *43*, 4902–4908.
- (44) Agarwal, S.; Jin, Q.; Maji, S. Biobased Polymers from Plant-Derived Tulipalin A. *ACS Symp. Ser.* **2012**, *1105*, 197–212.
- (45) Gowda, R. R.; Chen, E. Y.-X. Sustainable Polymers from Biomass-Derived α -Methylene- γ -Butyrolactone. *Encycl. Polym. Sci. Technol.* **2013**.
- (46) Brandenburg, C. J. Graft Copolymers of Methylene Lactones and Process for Emulsion Polymerization of Methylene Lactones. U.S. Patent 6,841,627 B2, 2011.

- (47) Sakashita, K.; Iwasaka, K.; Tsukamoto, Y.; Aoyagi, A. Polymer Composition, Plastic Optical Fiber, Plastic Optical Fiber Cable and Method for Producing Plastic Optical Fiber. EP 1,834,968 A1, 2007.
- (48) van Rossum, M. W. P. C.; Alberda, M.; van der Plas, L. H. W. Tulipaline and Tuliposide in Cultured Explants of Tulip Bulb Scales. *Phytochemistry* **1998**, *49*, 723–729.
- (49) Jones, E. R. H.; Shen, T. Y.; Whiting, M. C. Researches on Acetylenic Compounds. Part XXII. The Reaction Between Nickel Carbonyl and Monosubstituted Acetylenic Compounds. *J. Chem. Soc.* **1950**, 230–236.
- (50) Grieco, P. A. Methods for the Synthesis of α -Methylene Lactones. *Synthesis* **1975**, 67–82.
- (51) Kitson, R. R. A.; Millemaggi, A.; Taylor, R. J. K. The Renaissance of α -Methylene- γ -Butyrolactones: New Synthetic Approaches. *Angew. Chem. Int. Ed.* **2009**, *48*, 9426–9451.
- (52) Fetizon, M.; Golfier, M.; Louis, J.-M. Oxydations Par Le Carbonate d'argent Sur Celite-XIII. Preparation de Lactones. *Tetrahedron* **1975**, *31*, 171–176.
- (53) Carlson, R. M.; Oyler, A. R. Direct Methods for α -Methylene Lactone Synthesis Using Itaconic Acid Derivatives. *J. Org. Chem.* **1976**, *41*, 4065–4069.
- (54) Yokota, K.; Hirabayashi, T. Manufacture of α -Methylene- γ -Butyrolactone. JP Patent 04,049,288, 1992.

- (55) Michaut, M.; Santelli, M.; Parrain, J.-L. Efficient Synthesis of Spirolactones from Cyclic Anhydrides via an Allylation/Alkylation-RCM Sequence. *J. Organomet. Chem.* **2000**, *606*, 93–96.
- (56) Gowda, R. R.; Chen, E. Y.-X. Synthesis of β -Methyl- α -Methylene- γ -Butyrolactone from Biorenewable Itaconic Acid. *Org. Chem. Front.* **2014**, *1*, 230–234.
- (57) Dimitrov, V.; Kostova, K.; Genov, M. Anhydrous Cerium(III) Chloride - Effect of the Drying Process on Activity and Efficiency. *Tetrahedron Lett.* **1996**, *37*, 6787–6790.
- (58) Imamoto, T.; Kusumoto, T.; Yokoyama, M. Generation and Reactivities of Organocerium Reagents. *J. Chem. Soc., Chem. Commun.* **1982**, 1042–1044.
- (59) Liu, H.-J.; Shia, K.-S.; Shang, X.; Zhu, B.-Y. Organocerium Compounds in Synthesis. *Tetrahedron* **1999**, *55*, 3803–3830.
- (60) Goubeau, V. J.; Kallfass, H. Die Reaktion Natriumborhydrid Und Wasser. *Zeitschrift für Anorg. und Allg. Chemie* **1959**, *299*, 160–169.
- (61) Gardiner, J. A.; Collat, J. W. The Hydrolysis of Sodium Tetrahydroborate. Identification of an Intermediate. *J. Am. Chem. Soc.* **1964**, *86*, 3165–3166.
- (62) Gardiner, J. A.; Collat, J. W. Kinetics of the Stepwise Hydrolysis of Tetrahydroborate Ion. *J. Am. Chem. Soc.* **1965**, *87*, 1692–1700.
- (63) Wang, F. T.; Jolly, W. L. A Kinetic Study of the Intermediates in the Hydrolysis of the Hydroborate Ion. *Inorg. Chem.* **1972**, *11*, 1933–1941.

- (64) Ruman, T.; Kuśnierza, A.; Jurkiewicz, A.; Leś, A.; Rode, W. The Synthesis, Reactivity and ¹H NMR Investigation of the Hydroxyborohydride Anion. *Inorg. Chem. Commun.* **2007**, *10*, 1074.
- (65) Reed, J. W.; Jolly, W. L. Reduction of Organic Compounds with the Hydroxyborohydride Ion. *J. Org. Chem.* **1977**, *24*, 3963–3965.
- (66) Bounds, P. L.; Pollack, R. M. Affinity Alkylation of 3-Oxo- Δ^5 -Steroid Isomerase by Steroidal 3 β -Oxiranes: Identification of the Modified Amino Acid by Reduction with Hydroxyborohydride. *Biochemistry* **1987**, *26*, 2263–2269.
- (67) Moad, G.; Rizzardo, E.; Thang, S. H. Living Radical Polymerization by the RAFT Process — A Second Update. *Aust. J. Chem.* **2009**, *62*, 1402–1472.
- (68) Sultanova, N.; Kasarova, S.; Nikolov, I. Characteristics of Optical Polymers in the Design of Polymer and Hybrid Optical Systems. *Bulg. J. Phys.* **2013**, *40*, 258–264.
- (69) Mendgen, T.; Scholz, T.; Klein, C. D. Structure-Activity Relationships of Tulipalines, Tuliposides, and Related Compounds as Inhibitors of MurA. *Bioorg. Med. Chem. Lett.* **2010**, *20*, 5757–5762.
- (70) Hutchinson, C. R. A Synthesis of Tulipalin A and B and the Scylglucoside, Tuliposide A, Fungitoxic Agents from *Tulipa Gesneriana*. Carbon-13 Nuclear Magnetic Resonance Analysis of Anomeric Configuration in Acylglucosides. *J. Org. Chem.* **1974**, *39*, 1854–1858.
- (71) Brar, A. S.; Singh, G.; Shankar, R. Structural Investigations of Poly(Methyl

Methacrylate) by Two-Dimensional NMR. *J. Mol. Struct.* **2004**, 703, 69–81.

Chapter 3 THERMOSETS AND THERMOPLASTICS FROM ITACONIC ACID

ABSTRACT

Renewable materials are a research necessity, with the creation of a sustainable chemical industry representing a grand challenge for the field of chemistry and materials science. On this basis, biorenewable resources are being transformed into degradable or recyclable high value polymers with a diverse array of applications. Itaconic acid (IA) is a notable biorenewable resource due to its low cost and large annual production. We report the synthesis of renewable thermosets and thermoplastics that are almost completely derived from IA. Using catalytic, solvent-free, and high yielding transformations from an itaconate source, we efficiently synthesized a saturated diol, a saturated diester, and an unsaturated diester. Subsequent binary step-growth polycondensation polymerizations between the diol and either diester generated polyesters with relatively high molar masses (> 10 kg/mol). Ternary polymerizations of all three monomers in varying feed ratios produced polyesters with tunable amounts of unsaturated units along the backbone. Atom economies and low process mass intensities for these reactions reflect green processes. Thermoset materials were generated from these unsaturated terpolymers through thiol-ene click reactions with a potentially renewable cross-linker. We then established the tensile properties and molar mass between cross-links of these thermosets through mechanical testing and demonstrated hydrolytic stability under acidic and neutral conditions, but hydrolytic degradation under basic conditions. An α,ω -hydroxy terminated saturated polyester was prepared, functionalized with an atom transfer radical polymerization initiator, and then chain-

extended with α -methylene- γ -butyrolactone, which can be derived from IA, to give triblock polymers. This thesis chapter was adapted from published work.¹

INTRODUCTION

In recent decades, the scientific community has recognized the importance of creating a sustainable chemical industry. As a result of this increased awareness, the current outlook toward a renewable future is optimistic,^{2–4} with the synthesis of sustainable thermosets,^{5–8} thermoplastics,^{9–11} and vitrimers^{12–15} generated from biorenewable molecules being active areas of research. Itaconic acid (IA, Figure 3.1a) is an economically viable biorenewable building block, produced by the fermentation of biomass such as corn, rice, or lignocellulosic feedstocks.¹⁶ IA was first synthesized by Baup in 1836 through the decarboxylative distillation of citric acid¹⁷ and gained significant attention over 150 years later when it was named by the U.S. Department of Energy in 2004 as one of the top value-added chemicals from biomass.¹⁸ Importantly, IA is generated in large quantities, currently for \$2/kg, and has potential to become economically competitive with petroleum-based feedstocks.^{19,20} Itaconix, LLC has recently developed a method to polymerize IA to give poly(itaconic acid), a poly(acrylic acid) surrogate, for a suite of applications that include superabsorbents.²¹ On this basis, the design and synthesis of new polymers from IA represents an excellent opportunity to access novel renewable materials.

The polymerization of IA and its derivatives has been extensively studied. Specifically, the radical polymerization of IA and its various alkyl esters has been an active area of research.^{22,23,32–39,24–31} As an example, Kamigaito and co-workers reported the synthesis of an almost completely IA derived triblock copolymer thermoplastic

using reversible addition-fragmentation chain transfer (RAFT) polymerization.⁴⁰ Dialkyl itaconates were polymerized by RAFT polymerization and then chain extended with *N*-phenyl itaconimide to give hard-soft-hard triblocks with glass transition temperatures (T_g) ranging from -8 to 17 °C for the soft block (poly(dialkyl itaconate)) and 204 to 241 °C for the hard block poly(*N*-phenyl itaconimide)). While this remains an excellent proof of concept for a completely IA-derived triblock polymer, the tensile properties of these materials were not reported and the relatively high T_g of the midblock limits the temperature use range.

Like radical polymerizations, the step-growth polymerizations of itaconate derivatives have led to the synthesis of a number of polyesters.^{41,42} Additionally, through the incorporation of non-IA based monomers, followed by chemical cross-linking, researchers have synthesized a number of IA-based polyester thermosets. The tensile properties of these materials, especially Young's Modulus (E), tensile strength at break (σ_B), and elongation at break (ϵ_B) have been well documented, with materials ranging from brittle thermosets to soft elastomers.⁴³⁻⁵¹ Beyond itaconates themselves, monomers derived from IA have also been polymerized to generate a number of interesting materials through processes such as acyclic diene metathesis (ADMET) polymerization⁵² and ring-opening metathesis polymerization (ROMP).⁵³⁻⁵⁷ Nonetheless, taking these studies into consideration, there is a significant amount of chemical space that remains unexplored for the synthesis of high value materials from IA.

Herein, we report the synthesis and characterization of thermosets and thermoplastics that are almost completely derived from IA. We demonstrate the scalable

syntheses of dimethyl 2-(4-methylcyclohex-3-ene)succinate (CS), dimethyl 2-methylsuccinate (MS), and 2-methyl-1,4-butanediol (MB) monomers from commercially available dimethyl itaconate (DMI), an IA derivative (Figure 3.1a). We utilize both binary and ternary step-growth polycondensation polymerizations to make various amorphous polymers of relatively high molar mass (> 10 kg/mol) with low glass transition temperatures (Figure 3.1b). In the step-growth polymerizations we control the amount of unsaturation in the backbone by tuning the feed ratio of CS, giving access to polyesters that are efficiently cross-linked using thiol-ene click chemistry to give thermosets. Additionally, we demonstrate the formation of α,ω -hydroxy telechelic polyesters that are then functionalized and chain-extended with α -methylene- γ -butyrolactone (MBL), which can be derived from IA, to give well-defined triblock polymer thermoplastics. Finally, we explore various green metrics for these systems.

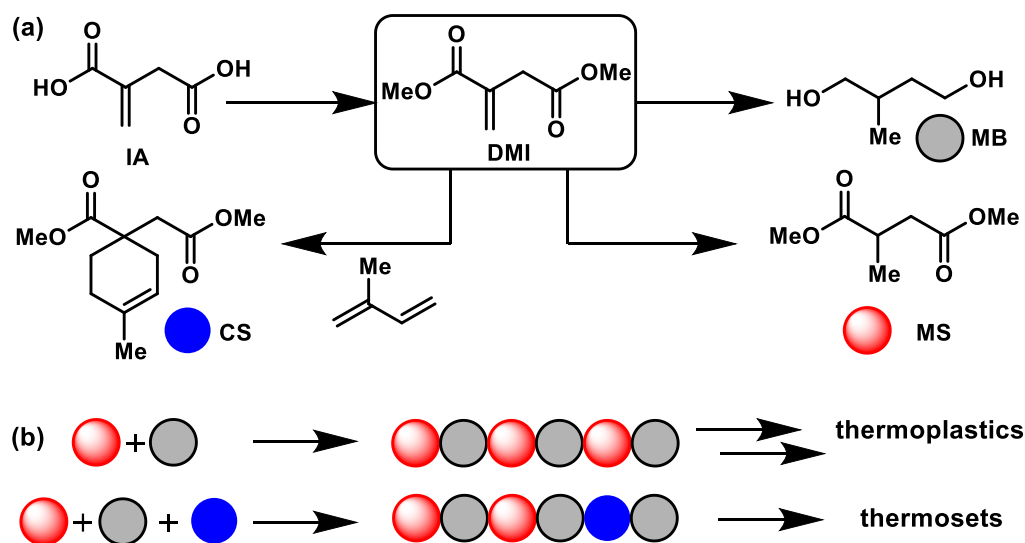


Figure 3.1. (a) Renewable monomers from IA. (b) Renewable thermoplastics and thermosets derived from IA.

RESULTS AND DISCUSSION

Synthesis of Step-Growth Monomers from IA. We first developed efficient and green syntheses of our three proposed monomers (MS, MB, and CS; Figure 3.1a) from DMI to access functional polyesters that can be utilized for making thermosets and thermoplastics. Many reductions of itaconates for use in the synthesis of novel polyesters have been reported.^{58–60} We began by looking at the synthesis of MS from DMI. Frost and co-workers have previously reported a system that gave a 69% yield for this transformation that utilized a Rh-based catalyst and $\text{HSi}(\text{OEt})_3$ as the reducing agent.⁵⁸ To increase the scale and the efficiency of the reaction, we sought a system that used a more readily available catalyst and H_2 as the terminal reductant. With this in mind, we found that DMI could be converted to MS under neat conditions using H_2 and catalytic amounts of Pd/C. Using a 2 wt% loading of Pd/C at 160 °C under 50 bar of H_2 , 103 g of DMI was effectively transformed to 100 g of MS in 96% isolated yield following distillation (Figure 3.2). This new method provides a simple and efficient way to synthesize the saturated diester, MS, on a large scale in high isolated yield.

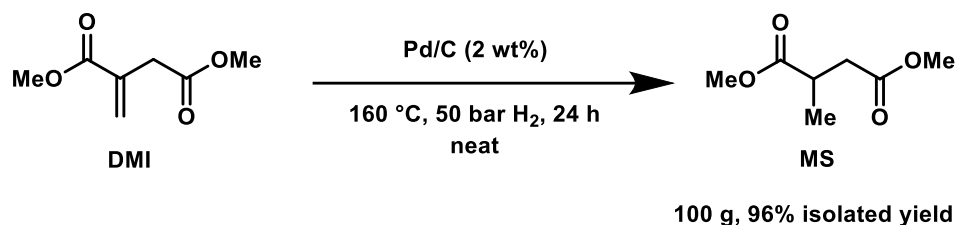
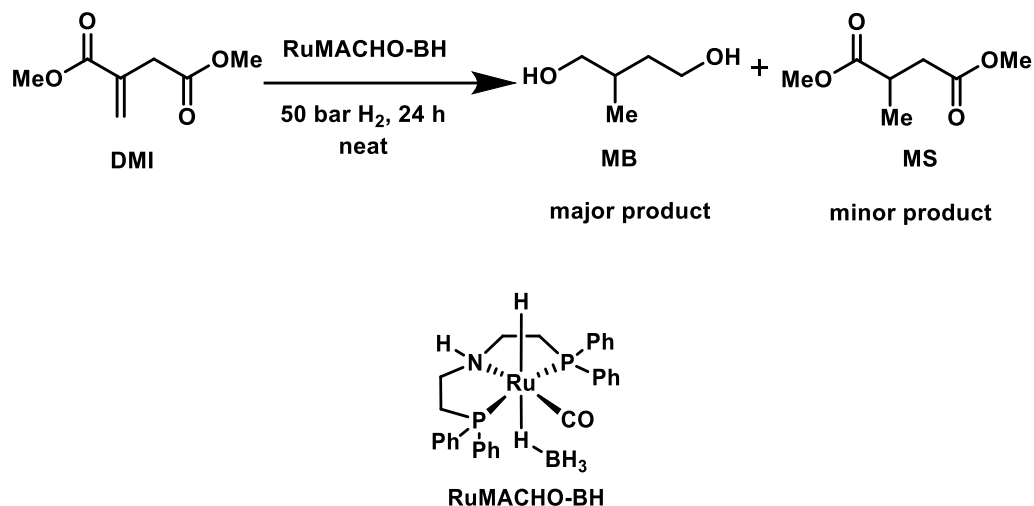


Figure 3.2. Reduction of dimethyl itaconate (DMI) to dimethyl 2-methylsuccinate (MS).

We next focused on the synthesis of the diol MB. The catalytic hydrogenation of DMI to give the fully reduced diol has been previously reported in the literature,^{61–63}

however, all of these examples were performed on small scales (< 1 g) without purification or isolation of MB. We needed a system that could accomplish this transformation on larger scales in high isolated yields. We identified RuMACHO-BH as a potential catalyst,⁶⁴ as it has been previously utilized under neat, base-free conditions on large scales for the homogeneous reduction of fatty acid esters.⁶⁵ Using conditions for the homogeneous hydrogenation of esters in THF at 50 bar of H₂, we found that a 0.2 mol% loading of RuMACHO-BH at 80 °C effectively generated MB in 94% yield after 24 h with a high ratio of the desired diol to the undesired saturated diester (MB:MS 22:1, Table 3.1, entry 1). By increasing the catalyst loading to 1.0 mol%, the product was produced in 98% yield with no detectable MS present (MB:MS > 99:1, entry 2). The reaction could also be run under neat conditions to give the desired diol in 93% yield with a high MB:MS ratio (entry 3). Neat conditions were then performed on a larger scale to avoid the use of solvent. In a 300 mL Parr reactor, the hydrogenation of 62 g of DMI at 80 °C proceeded slowly, with no detectable drop in hydrogen pressure after a few hours. However, raising the temperature to 160 °C enabled the transformation to proceed and generated 33 g of MB in 82% isolated yield following distillation (entry 4).

Table 3.1. Reaction Conditions for the Synthesis of 2-Methyl-1,4-butanediol (MB)

Entry	Catalyst (mol%)	Solvent	T (°C)	DMI (g)	MB:MS ^a	MB Yield (%) ^b
1	0.2	THF	80	1	21:1	94
2	1.0	THF	80	1	>99:1	98
3	1.0	Neat	80	1	26:1	93
4 ^c	1.0	Neat	160	62	>99:1	86 (82 ^d)

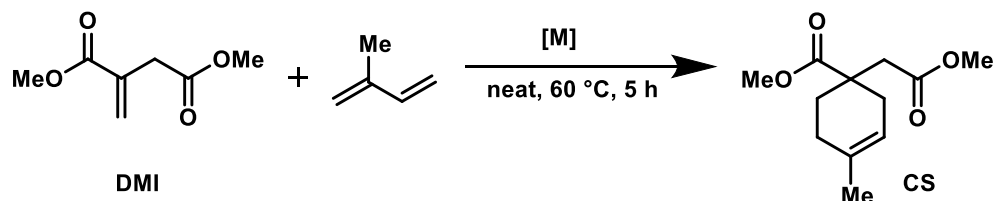
^aMolar MB:MS ratio determined by ¹H NMR spectroscopy. ^bYields were determined by quantitative ¹H NMR spectroscopy using 1,3,5-trimethoxybenzene or toluene as an internal standard. ^cAt this scale, the reaction had to be repressurized during the process (see experimental section). ^dIsolated yield.

To facilitate further functionalization and cross-linking, we envisioned synthesizing a diester containing a functional group handle such as an olefin. DMI itself contains an α,β -unsaturated ester; however, previous attempts to utilize DMI in a step-growth polymerization with a diol led to polymers of low molar mass, as low conversions under mild conditions were required to avoid uncontrolled cross-linking of the pendant olefin.⁶⁶ Since high conversions are required to achieve high molar mass in a step-growth mechanism (Figure S3.22), we anticipated that we would have to alter the nature of the olefin present in DMI. To synthesize a stable, IA-based monomer that

contained a functional alkene, we envisioned that reacting DMI with a diene in a Diels-Alder reaction would yield a monomer with a nonconjugated alkene, increasing its stability.^{53,67,68} In this work, we chose isoprene as the diene in light of the recent report by Dauenhauer and co-workers, who demonstrated its efficient synthesis through a series of heterogeneous catalyzed transformations.⁶⁹ Therefore, this strategy would lead to a monomer (CS) made almost completely from IA. The Diels-Alder reaction between DMI and isoprene has been previously reported by Shirashi and co-workers,⁷⁰ but required stoichiometric amounts of aluminum(III) chloride (AlCl_3) in benzene. We targeted a system that enabled this reaction to be performed with substoichiometric amounts of a Lewis acid on large scale.

To achieve this goal, we investigated multiple conditions for the Diels-Alder reaction between DMI and isoprene. The uncatalyzed reaction at 60 °C resulted in only unreacted starting material, with no desired CS observed (Table 3.2, entry 1). Adding catalytic amounts of AlCl_3 with 3 equiv of isoprene produced CS in low yield (16%); however, the major product was unreacted DMI (entry 2). In contrast to the catalytic conditions, stoichiometric AlCl_3 under conditions adapted from Shirashi's original report⁷⁰ generated the product in 56% isolated yield from 30 g of DMI (entry 3). This demonstrated the need for stoichiometric amounts of AlCl_3 to achieve reasonable yields, indicating that a different catalyst was required. Toste and co-workers have utilized transition metal triflates as efficient catalysts for Diels-Alder reactions,^{71,72} prompting us to investigate these complexes. Three of the metal triflate catalysts, $\text{Y}(\text{OTf})_3$, $\text{Lu}(\text{OTf})_3$, and $\text{La}(\text{OTf})_3$ (entries 4 – 6), were not active and resulted in only unreacted starting material. $\text{Sc}(\text{OTf})_3$, however, proved to be an effective catalyst for this

transformation, and generated CS in 96% yield (entry 7). Next, we sought to optimize the reaction; by cutting the catalyst loading in half (from 8 to 4 mol%), we observed a similar 92% yield (entry 8). Furthermore, by reducing the amount of isoprene utilized to 2 equiv, we observed only a modest drop in yield to 70% (entry 9). Despite this lowered yield, a 33% molar decrease in the IA-derived starting material made this method advantageous. Scaling up the reaction, 53 g of pure CS was synthesized in 67% isolated yield, following distillation, from 55 g of DMI (entry 10). Furthermore, extraction of the crude reaction mixture with water prior to distillation nearly quantitatively recovered the $\text{Sc}(\text{OTf})_3$ (see experimental section), implicating its ability to be recycled as a catalyst.⁷³

Table 3.2. Reaction Conditions for the Synthesis of CS

Entry	Catalyst (mol%)	Isoprene (equiv)	Yield (%) ^a
1	None	10	0
2	AlCl ₃ (8)	3	16
3 ^{b,c}	AlCl ₃ (100)	3	56 ^d
4 ^b	Y(OTf) ₃ (8)	3	0
5 ^b	Lu(OTf) ₃ (8)	3	0
6 ^b	La(OTf) ₃ (8)	3	0
7	Sc(OTf) ₃ (8)	3	96
8	Sc(OTf) ₃ (4)	3	92
9	Sc(OTf) ₃ (4)	2	70
10 ^e	Sc(OTf) ₃ (4)	2	67 ^d

Reactions were run on 1 mmol of DMI unless otherwise specified with [M] indicating the metal catalyst. ^aYields were determined by quantitative ¹H NMR spectroscopy using a known amount of 1,3,5-trimethoxybenzene or toluene as an internal standard. ^bReactions were run for 3 h. ^cReaction was run at room temperature (RT) in toluene with 190 mmol of DMI following an adaptation of the literature prep.⁷⁰ ^dIsolated yields. ^eReaction was run overnight (12 – 18 h) with 350 mmol of DMI.

Step-Growth Polycondensation Polymerizations. With significant quantities of our three monomers in hand, we set out to investigate their use in step-growth polymerizations to give polyesters. The binary step-growth polymerization of MB and MS has been previously reported to generate poly[(2-methyl-1,4-butanediol)-*alt*-(2-methylsuccinate)] (PMBMS) with M_n s up to 10.8 kg/mol.⁶³ In this work, the synthesis of high molar mass polymers from MS, CS, and MB monomers was achieved using titanium(IV) isopropoxide (Ti(O^{*i*}Pr)₄)⁷⁴ in conjunction with high temperature and

vacuum conditions adapted from a known two-step procedure.⁷⁵ In the first step, oligomers are generated under ambient pressure, and in the second step high vacuum (0.05 Torr) is applied to achieve conversions necessary for high molar mass polymers. Using these reaction conditions, poly{[2-methyl-1,4-butanediol]-*alt*-[2-(4-methylcyclohex-3-ene)succinate]} (PMBCS) was obtained from the polymerization of MB and CS with an M_n of 11.7 kg/mol (Figure 3.3a), while PMBMS was obtained from the polymerization of MB and MS with an M_n of 15.7 kg/mol (Figure 3.3b). For both polymers, dispersity values around 2 were observed, typical for a step-growth polymerization. The viscosity at high conversions for these polymerizations inhibits magnetic stirring and likely limits formation of higher molar mass polymers.⁷⁶

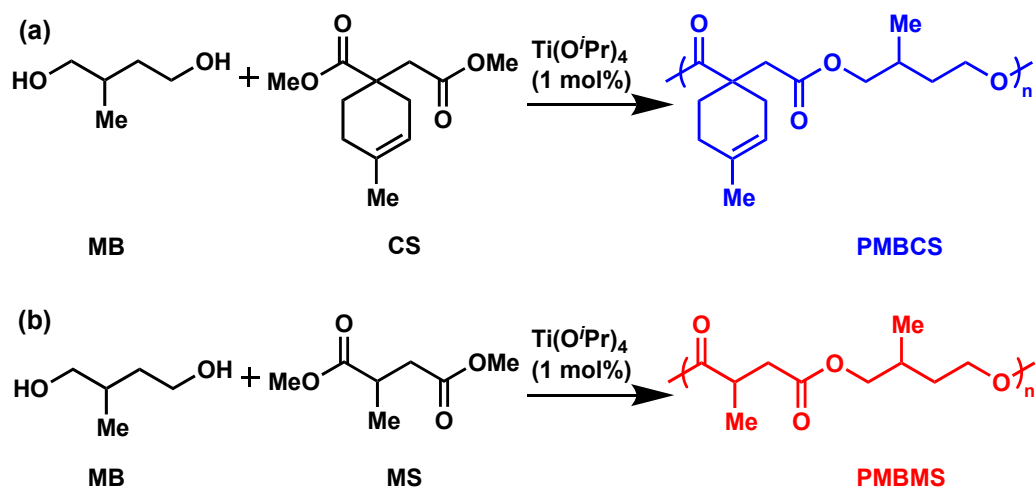


Figure 3.3. (a) Synthesis of PMBCS through the step-growth polycondensation of MB and CS. Number-average molar mass (M_n) = 11.7 kg/mol, weight-average molar mass (M_w) = 25.7, dispersity (\mathcal{D}) = 2.19, glass transition temperature (T_g) = -9 °C, temperature at 5 wt% loss ($T_{d,5\%}$) = 246 °C, and head-to-tail ratio (H:T) = 1:1. (b) Synthesis of PMBMS through the step-growth polycondensation of MB and MS. M_n = 15.7 kg/mol, M_w = 38.9 kg/mol, \mathcal{D} = 2.48, M_e = 6.3 kg/mol, T_g = -31 °C, $T_{d,5\%}$ = 276 °C, and H:T = 1:1.

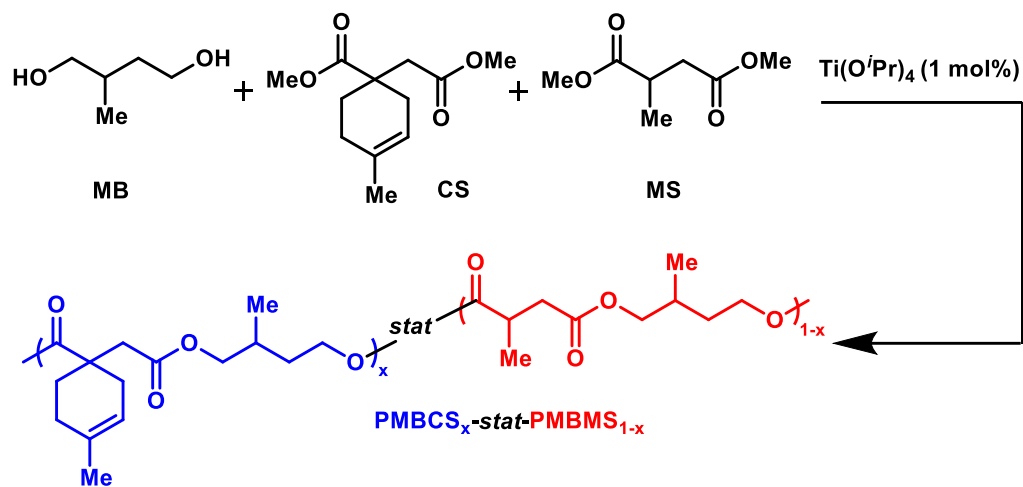
By following the polymerization of MS and MB over time, an M_n vs conversion curve was constructed for the synthesis of PMBMS (Figure S3.22 and Table S3.1), which demonstrates the need for high conversion to obtain high molar mass.⁷⁷ For both PMBCS and PMBMS, 2D NMR experiments establish head to tail (H:T) ratios of 1:1 along the polymer backbone, indicating no regiochemical preferences during the step-growth process (Figure S3.11 to Figure S3.20). For both polymers, we observed low T_g s ($-9\text{ }^{\circ}\text{C}$ and $-31\text{ }^{\circ}\text{C}$, respectively for PMBCS (Figure 3.3a) and PMBMS (Figure 3.3b)), typical for long-chained polyesters containing flexible backbones. The higher T_g of PMBCS relative to PMBMS (a difference of $22\text{ }^{\circ}\text{C}$) indicates a less flexible backbone due to the larger cyclohexene ring pendant to the main chain.⁷⁸ Neither PMBMS nor PMBCS exhibit melting temperatures (T_m)⁷⁸ and both polymers demonstrate a decomposition temperature (T_d , defined by the point where 5% of the mass is lost based on thermogravimetric analysis) above $200\text{ }^{\circ}\text{C}$. In the case of PMBCS, no evidence for a retro Diels-Alder reaction occurring along the polymer backbone was observed prior to the decomposition temperature (Figure S3.24). Integration of the olefin resonance in the ^1H NMR spectrum of PMBCS (Figure S3.4) also indicates full retention of the double bond after it was subjected to step-growth conditions at $240\text{ }^{\circ}\text{C}$. Additionally, we roughly estimated the molar mass between entanglements (M_e) for PMBMS to be 6.3 kg/mol using dynamic mechanical analysis experiments (Figure S3.32), although a well-defined rubbery plateau was not evident in the low molar mass sample used for this analysis.

We also explored the polymerization with all three monomers to generate statistical mixtures of PMBMS and PMBCS (denoted $\text{PMBCS}_x\text{-stat-PMBMS}_{1-x}$, where

x is the molar incorporation of the MBCS repeat unit into the polymer, or F_{MBCS}). This would generate ternary polymers where the desired amount of unsaturated functionality could be controlled for subsequent manipulations, such as cross-linking, to generate thermosets. The binary polymer PMBCS could also be used in this endeavor, but the synthesis of PMBCS is slower, generates lower molar mass materials, and results in higher T_g values relative to PMBMS. We hypothesized that by adding in only the desired amount of CS, we could maximize the molar mass of the final polymer, decrease the required polymerization time, and minimize the T_g of the resulting thermoset. Moreover, fully cross-linking the unsaturated functionality eliminates the possibility of undesired reactions of the olefin after cross-linking.

Ternary statistical polymerizations of these three monomers proceeded identically to the polymerization of PMBMS. In all cases, the feed ratio (f_{CS}) of CS matched closely with the observed ratio of the PMBCS repeat unit (F_{MBCS}) in the crude material after polymerization (Table 3.3). Using our standard conditions, polymers with molar from 8 – 22 kg/mol, M_w s up to 100 kg/mol, and relatively large dispersity values were obtained. Additionally, the ternary polymers exhibited T_g s intermediate between PMBMS and PMBCS, with lower F_{MBCS} leading to lower T_g values. In all cases, T_d values of the polymers are above 200 °C.

Table 3.3. Statistical Polymerization of MB, MS, and CS to give PMBCS_x-stat-PMBMS_{1-x}



Entry	f_{CS}^a	F_{MBCS}^b	T_g (°C) ^c	$T_{d,5\%}$ (°C) ^d	M_n (kg/mol) ^e	M_w (kg/mol) ^e	D^e
1	0.40	0.40	-21	250	15.2	35.9	2.36
2	0.30	0.29	-24	244	8.3	20.1	2.43
3	0.21	0.19	-27	251	21.5	103	4.81

^aDetermined from the molar ratio of CS:MS weighed out prior to polymerization; ^bFraction of MBCS repeat unit in the polymer (F_{MBCS}), determined from the molar ratio of the MBCS repeat unit to the MBMS repeat unit observed by ^1H NMR spectroscopy; ^cDetermined by differential scanning calorimetry (DSC); ^dDetermined by thermal gravimetric analysis (TGA); ^eDetermined by SEC in THF using a light scattering detector with an estimated dn/dc .

IA-Derived Thermosets. To prepare thermosets, we needed conditions that enabled the efficient functionalization and cross-linking of the trisubstituted olefin along the PMBCS backbone. We envisioned that thiol-ene “click” chemistry would be ideal.^{79,80} To test this, a solvent cast polymer mixture of PMBCS, 1-dodecanethiol, and 2,2-dimethoxy-2-phenylacetophenone (DMPA) was irradiated with 250 nm light (Figure 3.4). After 3 h, the reaction reached 75% conversion and further irradiation for 18 h resulted in 84% conversion. This result clearly demonstrated that this chemistry

provided efficient functionalization of the polymer backbone using only 1 equiv of the thiol. Previous thiol-ene methods reported for the functionalizations of polymers of itaconic acid and derivatives have used a superstoichiometric excess of thiol relative to the olefin. However, at high enough excess a multi-functional thiol would not lead to cross-linking even at 100% conversion of the olefin based on the statistics of $A_x + B_y$ polymerizations.^{52,77,81} Thus we targeted a 1:1 thiol:olefin stoichiometry to facilitate successful cross-linking.

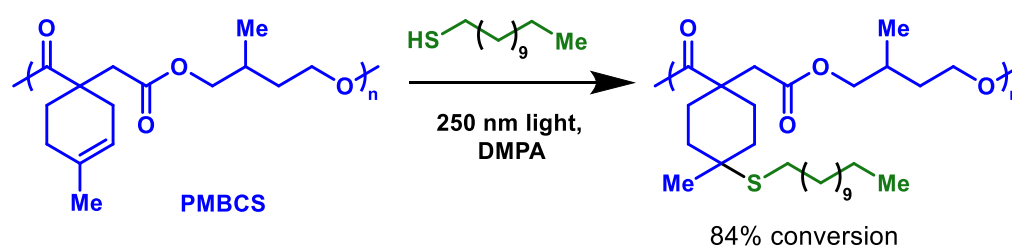


Figure 3.4. Thiol-ene click chemistry on PMBCS.

To cross-link $\text{PMBCS}_x\text{-stat-PMBMS}_{1-x}$, we utilized a potentially renewable tetrathiol cross-linker, pentaerythritol tetrakis (3-mercaptopropionate).⁸² Pentaerythritol is available renewably through the Voxtar platform,⁸³ while 3-mercaptopropionic acid can be generated from renewable acrylonitrile and sodium hydrosulfide (Figure 3.5).^{84–}

⁹¹ Cross-linking of the crude statistical ternary prepolymer, $\text{PMBCS}_x\text{-stat-PMBMS}_{1-x}$ ($x = 0.19 - 0.40$) was performed using the tetrathiol cross-linker and DMPA under 250 nm light irradiation for at least 12 h (Figure 3.6). On the basis of our model reaction using dodecanethiol, we estimate conversions of $>80\%$. Swell tests of these materials give gel fractions above 0.8, demonstrating that the cross-linking reaction efficiently generated a network solid (Table 4).⁹² Prepolymers with less than 20 mol% MBCS repeat units

were also synthesized, but cross-linking produced materials with gel fractions less than 0.6, indicating low cross-linking efficiency.

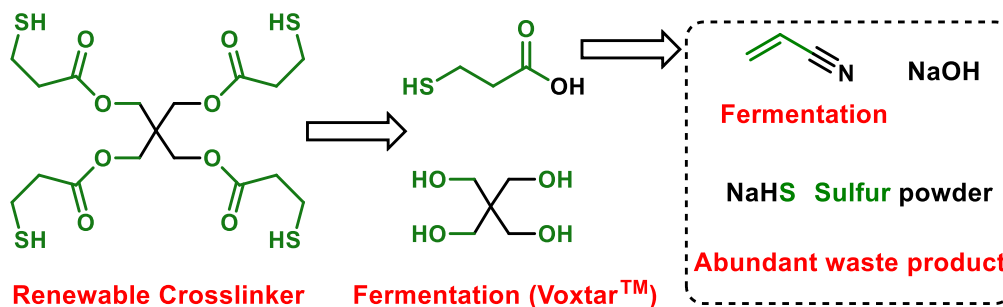


Figure 3.5. A potentially renewable retro-synthetic route to pentaerythritol tetrakis(3-mercaptopropionate).

Like their prepolymers, thermosets showed decomposition temperatures above 200 °C (Table 3.4 and Figure S3.24). Additionally, the glass transition temperatures of the thermosets increase with increasing F_{MBCS} , and in all cases, thermosets show T_g that are 5 – 10 °C higher than their respective prepolymers, indicating that cross-linking leads to a less flexible polymer backbone (Table 3.4 and Figure 3.7a). Additionally, T_g values obtained from dynamic mechanical thermal analysis (DMTA) are in good agreement with values obtained by DSC methods (Table 3.4 and Figure 3.7b). DMTA also indicates a flat, rubbery plateau region for each thermoset that varies with F_{MBCS} . Using the storage modulus (E') at 20 °C, the molar mass between cross-links, M_x , was determined for each thermoset using Equation 3.1, where R is the gas constant and ρ is the thermoset density (1.16 g/mL).

$$M_x = \frac{3\rho RT}{E'(T)} \quad \text{Equation 3.1}$$

M_x for the thermosets decreases with increasing F_{MBCS} (Table 3.4). We also estimated M_x using swell tests and the Flory-Rehner equation. Although this analysis

did not produce results that were in quantitative agreement with DMTA, they followed the same trend (Table S3.3). Disparities in M_x values determined from swelling and DMTA experiments are likely due to the limitations of the Flory-Rehner equation for this system resulting from the lower limit for M_x of just a few hundred grams per mole.^{93–95} On the basis of tensile testing, the Young's modulus (E) was the largest for materials with the highest cross-linking densities (Table 3.4, entry 1, and Figure 3.7c). As F_{MBCS} decreases from 0.40 to 0.19 (entries 1 – 3), E decreases as well, as does tensile strength at break (σ_B).

Due to the presence of ester bonds throughout the thermoset structures, these materials should be susceptible to hydrolysis. When suspended in three different types of aqueous media (3 M HCl, pH = 0; neutral water, pH = 7.5; 3 M NaOH, pH = 14) at room temperature (RT), the mass of the 19% PMBCS thermoset was measured approximately once a week for 4 weeks. After this length of time, the thermoset showed 97%, 99%, and 82% retention of mass in acidic, neutral, and basic media, respectively (Table S3.4). This demonstrates that the PMBCS_{0.19-stat}-PMBMS_{0.81} thermoset is stable in both acidic and neutral media at RT. In contrast to this, PMBCS_{0.19-stat}-PMBMS_{0.81} is not stable in basic media at RT and demonstrates susceptibility to hydrolysis under basic conditions.

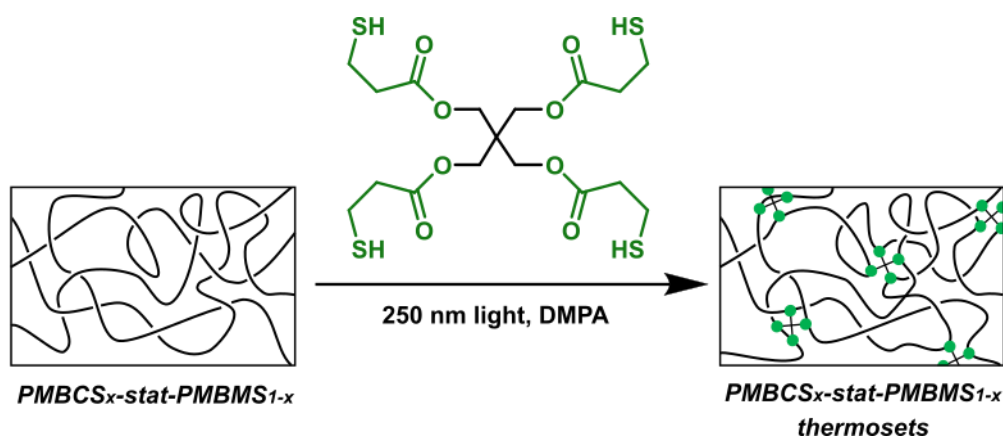


Figure 3.6. Cross-linking of $\text{PMBCS}_x\text{-stat-PMBMS}_{1-x}$ copolymers.

Table 3.4. Tensile Testing and Thermoset Gel Fraction Data for IA-Based Thermosets

Entry	F_{MBCS}^a	Gel Fraction ^b	T_g (°C) ^c	T_g (°C) ^d	$T_{d,5\%}$ (°C) ^e	M_x (kg/mol) ^d	E (MPa) ^f	σ_B (MPa) ^f	ϵ_B (%) ^f
1	0.40	0.95 ± 0.07	-13	-1	248	1.4	6.2 ± 0.2	0.9 ± 0.1	17 ± 2
2	0.29	0.921 ± 0.008	-20	-12	259	3.2	2.6 ± 0.4	0.8 ± 0.1	38 ± 8
3	0.19	0.89 ± 0.01	-22	-17	276	6.3	1.4 ± 0.2	0.5 ± 0.1	46 ± 4

^aFraction MBCS repeat unit in the polymer (F_{MBCS}), determined from the molar ratio of the MBCS repeat unit to the MBMS repeat unit observed by ^1H NMR spectroscopy; ^bDetermined by swell tests described in the experimental section; ^cDetermined by differential scanning calorimetry (DSC); ^dDetermined by dynamic mechanical thermal analysis (DMTA); ^eDetermined by thermal gravimetric analysis (TGA); ^fDetermined by tensile testing.

IA-Derived Thermoplastics. In addition to the generation of thermosets explored in the previous section, we also set out to utilize polyesters in the synthesis of well-defined triblock polymers almost completely derived from IA. The controlled chain extension of step-growth polymers has been previously reported and requires control over the chain ends.^{96,97,106–108,98–105} In the case of PMBMS, variation in the MB:MS feed ratio enabled control over polymer chain-ends, with a 2.0:1.0 molar ratio giving

rise to the saturated polyester with almost 100% alcohol chain-ends (Figure 3.8).¹⁰⁹ Under similar conditions employing a 1.2:1.0 diol:diester ratio, we observed only ~80% alcohol chain-ends with ~20% methyl ester chain-ends, which indicated the need for higher diol:diester ratios.⁹⁶ Following a previously utilized method,¹¹⁰ we chain-end functionalized α,ω -hydroxy terminated PMBMS (HO-PMBMS-OH) with α -bromoisobutyryl bromide to give α,ω -bromo terminated PMBMS (Br-PMBMS-Br) to be used as an ATRP macroinitiator (Figure 3.8). The presence of the type of polymer chain-ends was verified by ¹H NMR spectroscopy (Figure 3.9).

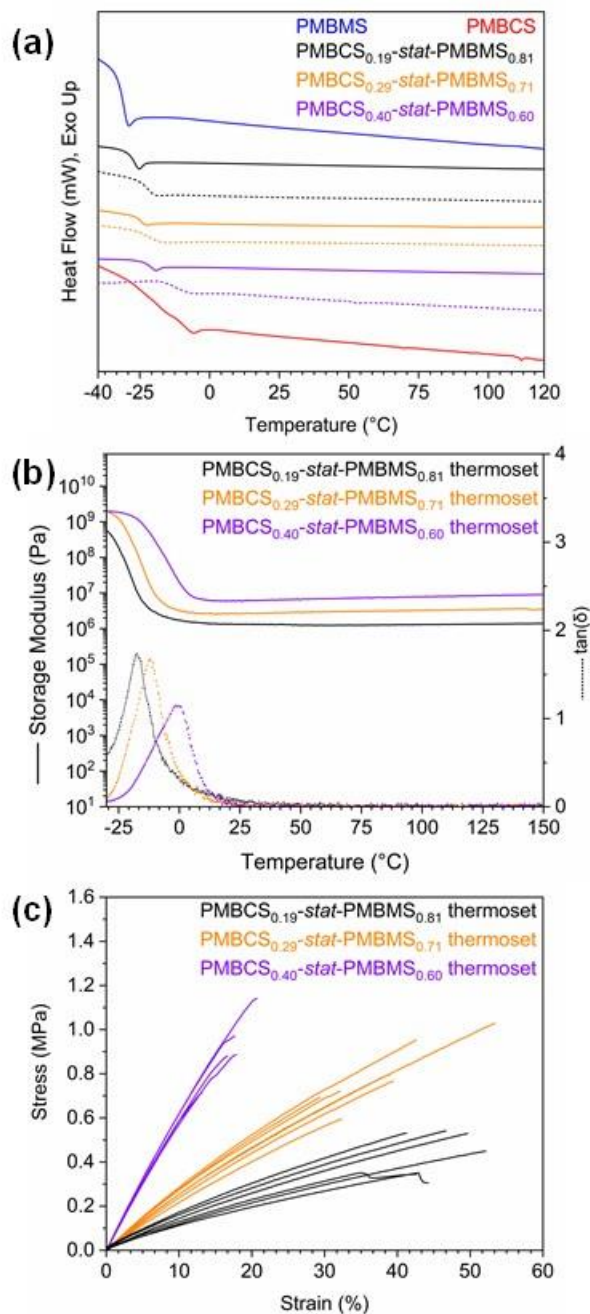


Figure 3.7. (a) Differential scanning calorimetry (DSC) heat flow vs temperature traces of various prepolymers (solid lines) or thermosets (dashed lines), exo up. (b) Dynamic mechanical thermal analysis (DMTA) storage modulus (left axis, solid lines) and $\tan(\delta)$ (right axis, dashed lines) vs temperature traces of thermosets. (c) Stress-strain curves of thermosets, where the end of each curve indicates a break point.

Chain extension with the potentially IA-derived MBL^{57,111} thus gave the previously unaccessed PMBL-PMBMS-PMBL triblock polymer (Figure 3.10). The

SEC trace exhibits a clear shift in elution volume to higher molar mass after chain extension and a decrease in dispersity from 2.30 to 1.80. The PMBL incorporation was determined to be 50 mol% PMBL (or 33 wt%) by ^1H NMR spectroscopy. Using the known M_n of 19.0 kg/mol (determined using light scattering) for the Br-PMBMS-Br macroinitiator, we then calculated the PMBL blocks to be 4.7 kg/mol, assuming all polymer chains initiated two PMBL blocks. This is in good agreement with an M_n of 3.8 kg/mol for the PMBL blocks determined by the differences in M_n of PMBL-PMBMS-PMBL and Br-PMBMS-Br from a refractive index detector calibrated against polystyrene standards on a DMF SEC. A small high molar mass tail was observed in Br-PMBMS-Br following HO-PMBMS-OH functionalization, likely due to chain-chain coupling (Figure S3.34), and this small impurity is also present in the triblock polymer sample, as is apparent by the peak in the SEC trace at ~22 min. This suggests that side reactions during the synthesis of Br-PMBMS-Br result in chains that do not participate in chain extension with MBL. Therefore, the molar mass of the PMBL blocks are likely an underestimate, as some of the assumed polymer chains may not participate in the chain extension reaction.

DSC analysis of the triblock shows two T_g s: one at $-33\text{ }^\circ\text{C}$ associated with the PMBMS block and one at $178\text{ }^\circ\text{C}$ associated with PMBL (Figure S3.28). This is slightly lower than the reported T_g of $187\text{ }^\circ\text{C}$ for a PMBL ($M_n = 12\text{ kg/mol}$) sample synthesized by RAFT polymerization (Figure 2.5).⁵⁷ To determine if this lowered T_g for the PMBL block was a result of phase-mixing, we synthesized two pure PMBL homopolymers following a known procedure.⁵⁷ The resulting PMBLs had M_n s of 2 and 6 kg/mol and T_g s of 140 and $160\text{ }^\circ\text{C}$, respectively (Figure S3.28). This demonstrates that lower molar

mass PMBL samples also have lower glass transition temperatures, with a critical molar mass above 12 kg/mol similar to poly(α -methylene- γ -valerolactone) (PMeMBL).¹¹² These data suggest that the lower T_g of 178 °C for the PMBL block relative to other PMBL homopolymer samples results mainly from the relatively low molar mass of the hard block rather than from phase mixing of both the hard and soft blocks.

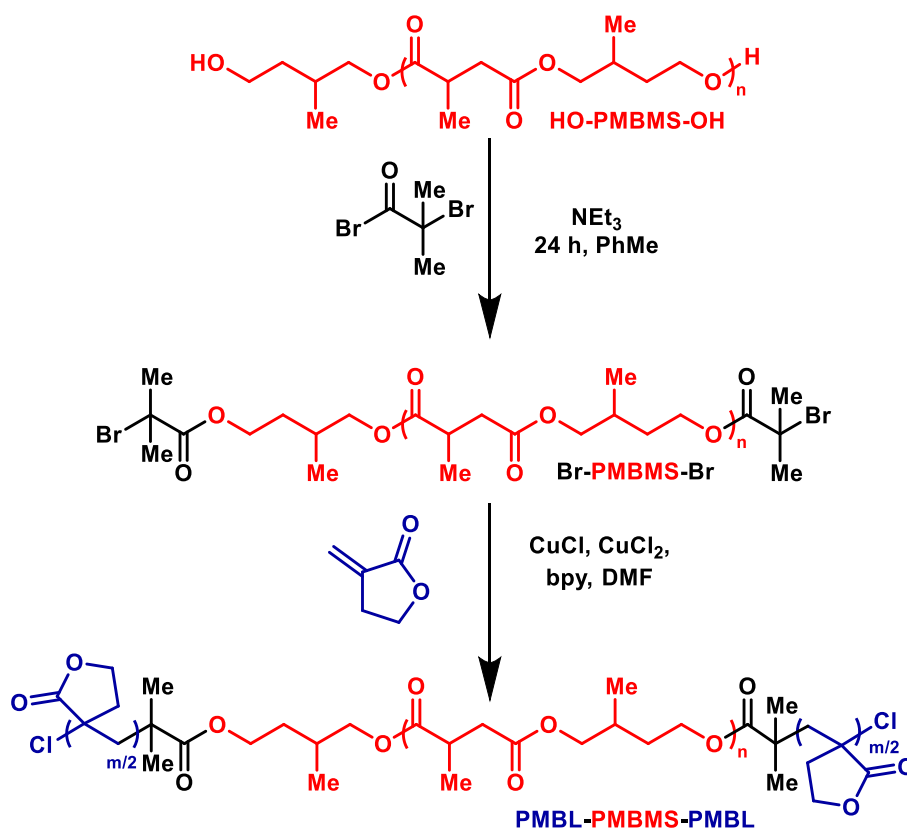


Figure 3.8. Chain extension of HO-PMBMS-OH to give PMBL-PMBMS-PMBL.

TGA of the triblock shows a decomposition temperature of 296 °C that is intermediate between that of PMBMS (246 °C) and PMBL (337 °C) (Figure S3.29).⁵⁷ Tensile testing of the 5-19-5 kg/mol triblock polymer establishes it as a thermoplastic

with $E = 185 \pm 26$ MPa, $\sigma_B = 7 \pm 2$ MPa, and $\epsilon_B = 226 \pm 80\%$, comparable to previously explored materials utilizing MBL as a hard block (Figure 3.11).^{113–115} The tensile properties of PMBL-PMBMS-PMBL demonstrate the ability to toughen PMBMS by chain extension with MBL. Additionally, from the modulus of the rubbery plateau apparent in shear dynamical mechanical analysis, we roughly estimated the entanglement molar mass (M_e) to be 10.5 kg/mol for PMBL (Figure S3.31) and 6.3 kg/mol for PMBMS (Figure S3.32). We anticipate that the mechanical properties of these thermoplastics could be improved by increasing the molar mass of both the PMBMS and PMBL blocks significantly above their M_e .

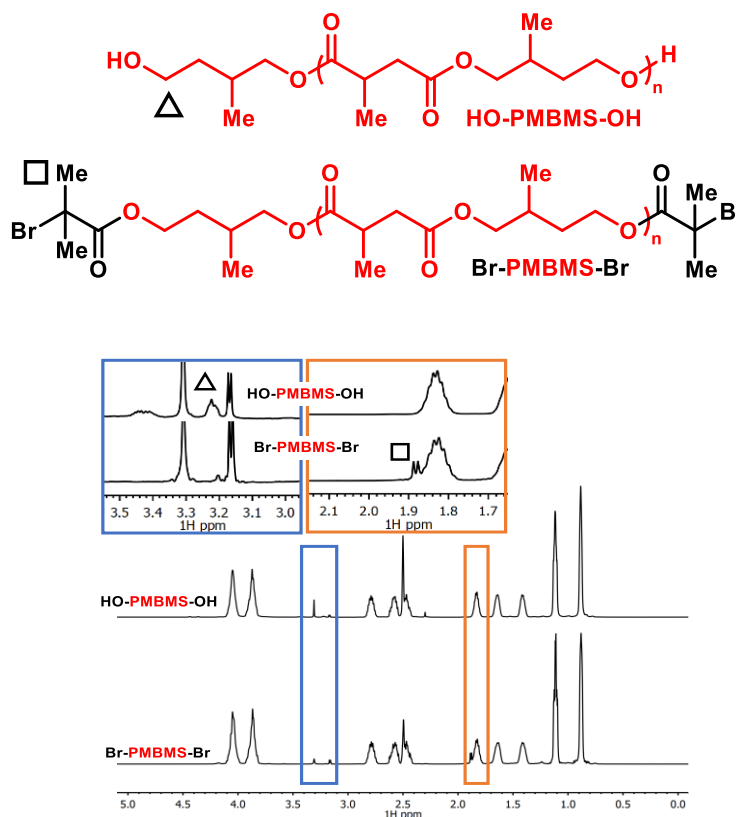


Figure 3.9. Synthesis and ^1H NMR spectra of end-group defined polymers.

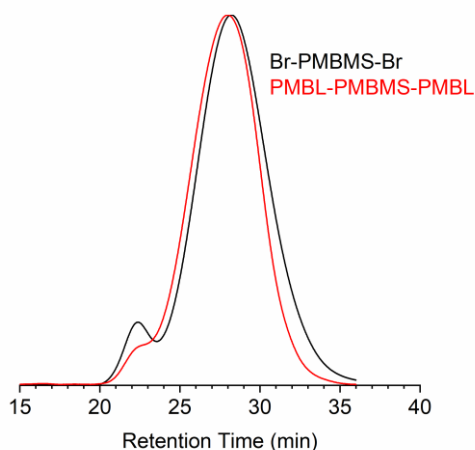


Figure 3.10. SEC traces of the chain extension of Br-PMBMS-Br (black) to PMBL-PMBMS-PMBL (red).

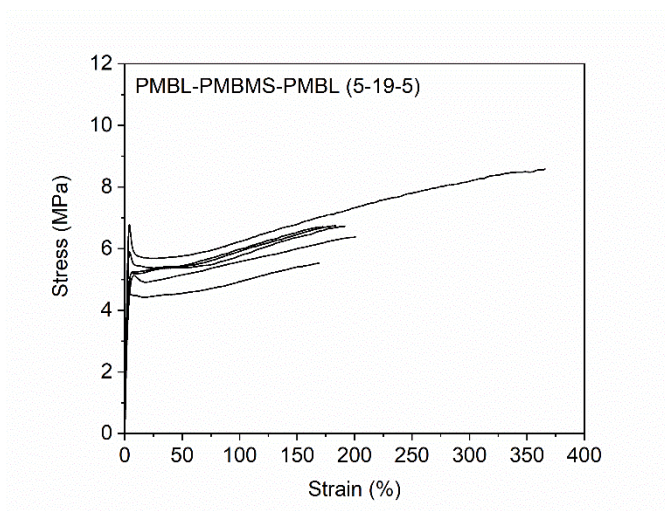


Figure 3.11. Stress-strain curves for PMBL-PMBMS-PMBL, where the end of the curve indicates a break point. $E = 185 \pm 26$ MPa, $\sigma_B = 7 \pm 2$ MPa, and $\epsilon_B = 226 \pm 80\%$.

Green Metrics. Green metrics¹¹⁶ of the small molecule transformations and polymerizations disclosed here were evaluated. In particular, isolated yields, atom economies (AEs),¹¹⁷ and process mass intensities (PMIs)¹¹⁸ are reported in Table 3.5. In general, isolated yields across all reactions are high, with the lowest yield (60%) for PMBCS likely the result of poor polymer recovery during purification by precipitation.

AE is the percent of the molar mass of the desired product compared to the molar mass of all starting reactants (Equation 3.10). The AE is 100% for addition reactions like the reduction of DMI to MS or the Diels-Alder cycloaddition of DMI and isoprene to give CS; for reactions with undesired byproducts, AE is lower. In the synthesis of MB, for example, 2 equiv of methanol are lost from the starting DMI, resulting in the lowest reported AE of 65%. The direct reduction of IA to MB, which we did not attempt, would increase AE from 65% to 79%. The step-growth polycondensation polymerizations have AE values ranging from 76 – 81%, which could be increased to 85 – 88% using the diacid forms of MS and CS, which we did not explore.

PMI is the ratio of the mass of all reagents used in the synthesis of the desired product (including mass of solvent and other materials such as silica used in purification) to the mass of the isolated product (Equation 3.11). Values closer to 1 indicate a smaller mass of material is required to synthesize 1 kg of product. PMI is low for most reactions reported here, reflecting little to no use of solvents or other reagents during the reaction, workup, or purification steps. The synthesis of MS, for example, does not employ any additional reagents other than the DMI, hydrogen gas, and Pd/C catalyst, resulting in a PMI of 1.1. PMI increases to 2.6 for the synthesis of MB, due to the lower yield and AE for this process. Reflecting the use of solvent during workup, the synthesis of CS has a PMI of 12. For polymers that are dissolved and then precipitated in solvent for purification, the PMI metric rises sharply (160 and 180 for PMBCS and PMBMS, respectively); without purification (such as the synthesis of PMBCS_{0.19-stat}-PMBMS_{0.81}, which was used directly for cross-linking) the PMI is

much lower at 1.7. There are many opportunities to improve PMI values, particularly by optimizing the purification steps and reducing solvent use.

Table 3.5. Green Metric Evaluation of Various Reactions Presented in this Work

Reaction	Isolated Yield (%)	AE (%) ^a	PMI (kg/kg) ^b
DMI to MB	82	65	2.6
DMI to MS	96	100	1.1
DMI to CS	67	100	12
MS + MB to PMBMS	77	76	180
CS + MB to PMBCS	60	81	160
MB + MS + CS to PMBCS _{0.19-stat} -PMBMS _{0.81}	92	77	1.7

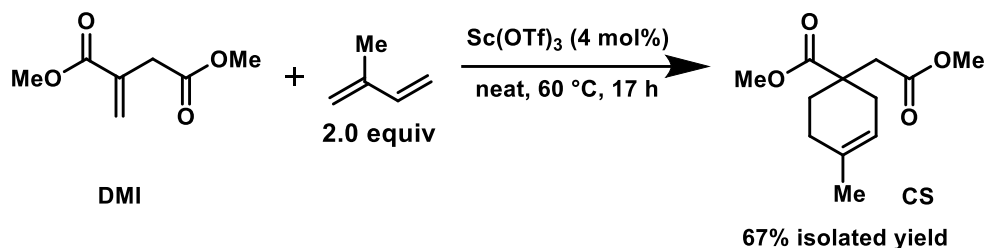
^aDefined by Equation 3.10 as the percent of the molar mass of the desired product compared to the molar mass of all starting reactants. ^bDefined by Equation 3.11 as mass (in kg) of the raw material input to mass (in kg) of isolated product.

CONCLUSIONS

In this work, we have shown the synthesis of diester and diol monomers (CS, MS, and MB) from DMI on large scale under neat and catalytic conditions. We report on a new method for the catalytic Diels-Alder reaction between IA-derived isoprene and DMI using the recyclable Sc(OTf)₃. All three monomers are easily purified through distillation and amenable to further scale-up. Subsequent binary or ternary step-growth polycondensation polymerizations produce high molar mass (> 10 kg/mol) polyesters that are either fully saturated (PMBMS), fully unsaturated (PMBCS), or partially saturated/unsaturated (PMBCS_{x-stat}-PMBCS_{1-x}). Both the small molecule

transformations and step-growth polymerizations typically have high isolated yields, while high atom economies and low process mass intensities for these reactions reflect green processes. We demonstrate that chain-end functionalization of PMBMS and subsequent chain-extension with MBL generates an almost completely IA-derived triblock polymer thermoplastic that exhibits ductile tensile properties. Thiol-ene functionalization of PMBCS proceeds in high conversion and thiol-ene cross-linking of $\text{PMBCS}_x\text{-stat-PMBCS}_{1-x}$ with a potentially renewable cross-linker generates IA-derived thermosets. The mechanical properties can be tuned by decreasing molar masses between cross-links with increasing F_{MBCS} . At room temperature these thermosets demonstrate hydrolytic degradation under basic conditions but are stable under neutral and acidic conditions. We believe that these new IA-derived materials demonstrate the ability to produce high value thermoplastics and thermosets from IA.

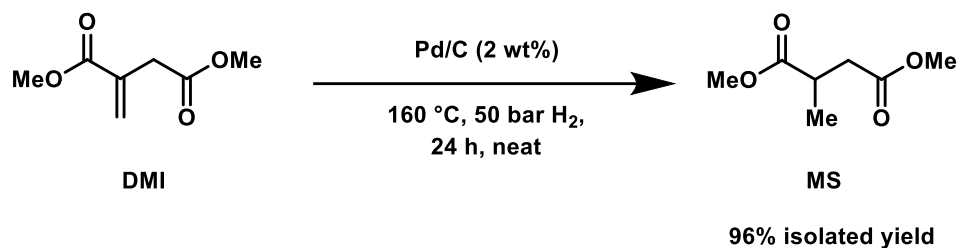
EXPERIMENTAL



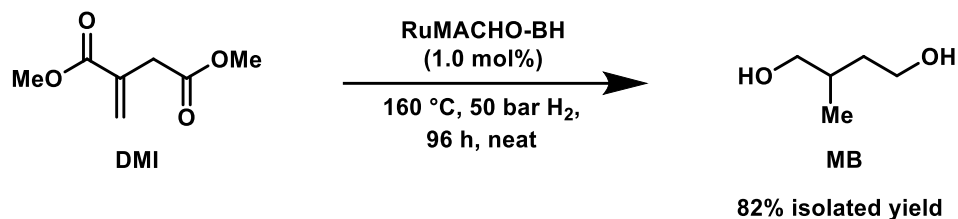
Synthesis of dimethyl 2-(4-methylcyclohex-3-ene)succinate (CS) using catalytic scandium(III) triflate. A 250 mL round bottom flask equipped with a stir bar, reflux condenser, and rubber septum was flame dried and then evacuated and backfilled with nitrogen three times. Following this, DMI (55.31 g, 0.3497 mol, 1.000 equiv) was added under positive pressure of nitrogen, followed by scandium triflate (6.56 g, 0.0133 mol, 3.80 mol%). The system was then again evacuated and backfilled three times with

nitrogen. Subsequently, isoprene (70.0 mL, 47.7 g, 0.700 mol, 2.00 equiv) was added by syringe. A nitrogen balloon was then added to the top of the reflux condenser and the system was heated to 60 °C and left to stir overnight. After 17 h, the reaction mixture was cooled to RT. The crude mixture was then diluted with ethyl acetate (ca. 20 mL) and washed three times with DI water (ca. 100 mL x 3), and once with brine (ca. 100 mL). The organic phase was then dried with magnesium sulfate (ca. 10 g), filtered, and concentrated down on a rotary evaporator. Distillation of the crude oil under vacuum (40 mTorr, 150 °C oil bath, 63 °C vapor temperature) gave a clear, colorless liquid with a ~3% DMI impurity; further heating of this mixture under vacuum (40 mTorr, 130 °C oil bath) distilled off the remaining DMI to give the pure product (52.92 g, 0.2339 mol) in 67% isolated yield. Characterization data matched those reported in the literature.⁷⁰ ¹H NMR (Figure S3.1, 500 MHz, CDCl₃, δ, ppm): 5.31 (s, 1H), 3.69 (s, 3H), 3.64 (s, 3H), 2.63 (q, *J* = 15.5 Hz, 4H), 2.51 (m, 1H), 2.05 – 1.93 (m, 4H) 1.79 (m, 1H), 1.64 (s, 3H).

Recovery of the Scandium Triflate in the synthesis of 2-(4-methylcyclohex-3-ene)succinate (CS). Following the standard procedure for the synthesis of CS, the aqueous phase obtained by washing the crude organic phase with DI water was concentrated down on a rotary evaporator. The off-white solid was then dried at 90 °C under vacuum (50 – 100 m Torr) for 19 h to afford 3.96 g of Sc(OTf)₃ (starting from 4.06 g of Sc(OTf)₃ used initial, 97% recovery).

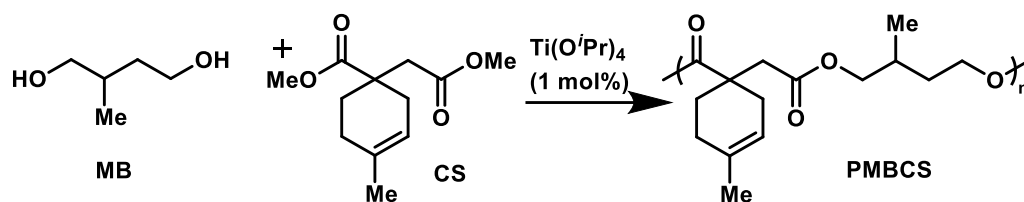


Synthesis of dimethyl 2-methylsuccinate (MS). *The reaction was run behind a blast shield with the hood sash closed in an isolated fume hood.* DMI (102.94 g, 0.6509 mol, 1.000 equiv) and 2.00 g Pd/C (10% Pd basis, 1.94 wt%) were added to a 300 mL Parr reactor. The reactor was then sealed with an open-ended wrench under atmosphere. The atmosphere was then replaced with hydrogen gas by pressurizing the reactor with hydrogen and venting it three times before being pressurized one last time with hydrogen (50 bar). The reaction was then stirred and heated in an oil bath at 160 °C, at which point the pressure read 60 bar. After 1 h, the pressure had dropped to 0 bar, and the Parr reactor was allowed to cool to RT. The reactor was then repressurized to 50 bar with hydrogen, and was heated back up to 160 °C where the pressure increased 60 bar. The reaction was then allowed to stir overnight for 14 h, by which point the pressure had not dropped from 60 bar. The Parr reactor was then allowed to cool to RT and was vented. The crude oil was distilled under reduced pressure (40 mTorr) to give a clear, colorless oil (100.33 g, 0.6265 mol) in 96% isolated yield. Characterization data matched those reported in the literature.⁵⁸ ¹H NMR (Figure S3.2, 400 MHz, CDCl₃, δ , ppm): 3.70 (s, 3H), 3.68 (s, 3H), 2.93 (m, 1H), 2.74 (dd, 1H, $J = 8.2$, Hz 16.7 Hz), 2.41 (dd, 1H, $J = 6.1$ Hz, 16.5 Hz, 1H), 1.22 (d, $J = 7.9$ Hz, 3H).



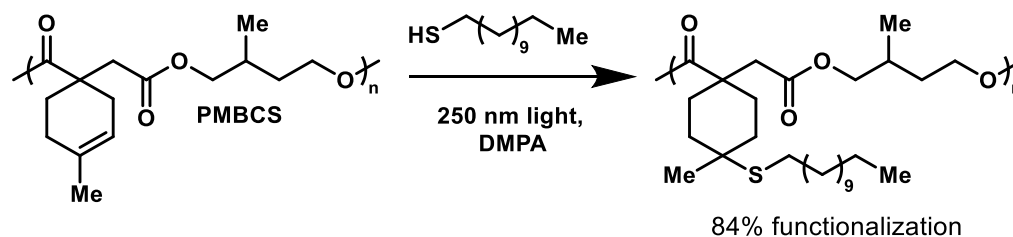
Synthesis of 2-methylbutane-1,4-diol (MB). *The reaction was run behind a blast shield with the hood sash closed in an isolated fume hood.* In a glovebox, a 300 mL Parr reactor was equipped with a stir bar. Dimethyl itaconate (61.76 g, 0.3905 mol, 1.000 equiv) was added to the reactor, followed by RuMACHO-BH (2.20 g, 0.00375 mol, 0.982 mol%). The Parr reactor was then sealed with an open-ended wrench inside the glovebox. The Parr reactor was then removed from the glovebox and the nitrogen atmosphere was replaced with hydrogen gas by pressurizing the reactor with hydrogen and venting it a total of three times. The reactor was then pressurized one last time with hydrogen (50 bar). The reaction was then stirred and heated in an oil bath to 160 °C, at which point the pressure read 60 bar. A few hours after the reaction started, the pressure had dropped to 0 bar, and the reaction was cooled to RT, repressurized to 50 bar, and heated back to 160 °C. This process was repeated a total of five times, whenever the hydrogen pressure at 160 °C decreased significantly below 60 bar. After 96 h the reaction was cooled to RT one final time and vented. After venting, the Parr reactor was then opened up, and the crude oil was distilled under reduced pressure (45 mTorr) to remove dimethyl 2-methylsuccinate (MS) (100 °C oil bath, 30 °C vapor temperature). After removal of the MS, the oil bath was heated further (45 mTorr, 130 °C oil bath, 70 °C vapor temperature) to give 2-methyl-1,4-butanediol (MB) as a clear, colorless, viscous liquid (33.23 g, 0.3195 mol) in 82% yield. Characterization data was consistent

with that previously reported in the literature.¹¹⁹ ¹H NMR (Figure S3.3, 500 MHz, CDCl₃, δ , ppm): 3.77 (m, 1H), 3.67 (m, 1H), 3.57 (m, 1H), 3.45 (m, 1H), 2.64 (m, 2H), 1.98 (m, 4H), 1.82 (m, 1H), 1.59 (m, 2H, OH), 0.93 (d, 3H, $J = 6.8$ Hz).



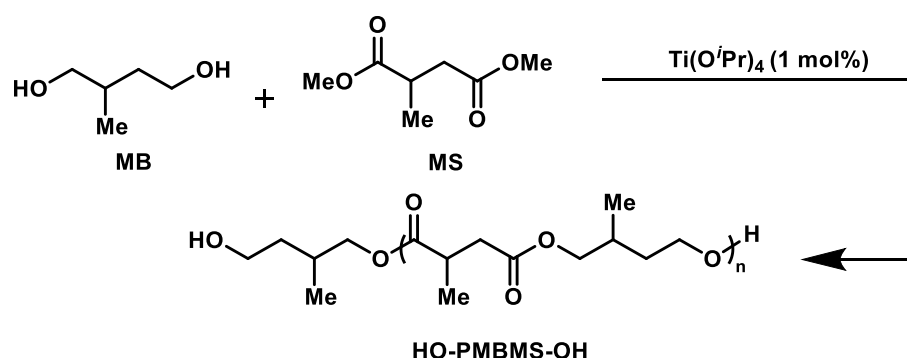
Synthesis of poly(MB-*alt*-CS) (PMBCS). The two-stage polycondensation polymerization method was adopted from a known procedure.⁷⁵ CS (1.55 g, 6.85 mmol, 1.00 equiv), MB (1.02 g, 9.79 mmol, 1.43 equiv), and 4-methoxyphenol (9.9 mg, 0.38 wt%) were added to a 50 mL round bottom flask equipped with a stir bar, reflux condenser, and rubber septum. Nitrogen gas was then purged through the system for 20 min while stirring to give a clear, colorless liquid. Ti(O^{*i*}Pr)₄ (0.030 mL, 0.10 mmol, 1.5 mol% relative to CS) was then injected and the reaction mixture turned a clear yellow color and was submerged into a 180 °C oil bath. The reaction was stirred for 3 h with nitrogen gas purging through the system to remove the methanol byproduct. The reflux condenser was then replaced with a short path distillation head, and the vacuum was applied to the system (400 Torr) while the temperature was increased to 200 °C. The pressure was then steadily lowered over 1 h to 0.05 Torr. After reaching 0.05 Torr, the short path distillation head was periodically heated to encourage distillation of the excess diol. After 5 h, the stirring of the mixture became more difficult at the stirring setting of 50 rpm, and the heat was increased briefly to 240 °C for 0.5 h. The reaction mixture was still stirring at 50 rpm and the reaction mixture was allowed to cool to RT

under vacuum. After cooling, the crude polymer solid was dissolved in dichloromethane (ca. 10 mL) and precipitated once from $-78\text{ }^{\circ}\text{C}$ methanol (ca. 200 mL). The solid was dried under vacuum to give the product (1.09 g) in 60% isolated yield. $M_n = 11.7\text{ kg/mol}$, $M_w = 25.7$, $D = 2.19$, and $dn/dc = 0.0867\text{ mL/g}$ were determined using a light scattering detector in THF solvent. ^1H NMR (Figure S3.4, 500 MHz, CDCl_3 , δ , ppm): 5.31 (s, 1H), 4.11 (m, 2H), 3.92 (m, 2H), 2.58 (m, 3H), 1.96 (m, 4H) 1.75 (m, 2H), 1.64 (s, 3H), 1.45 (m, 1H), 0.94 (m, 3H). ^{13}C NMR (Figure S3.5, 125 MHz, CDCl_3 , δ , ppm): 176.1, 171.5 – 171.4, 132.9, 118.5, 69.2 – 69.0, 62.7 – 62.4, 42.8 – 42.6, 40.3, 33.0, 32.2, 29.8, 27.1, 23.3, 16.7. IR (Figure S3.30, ATR, cm^{-1}): 2965, 2937, 2878, 1728, 1462, 1344, 1158, 1054, 989, 757.



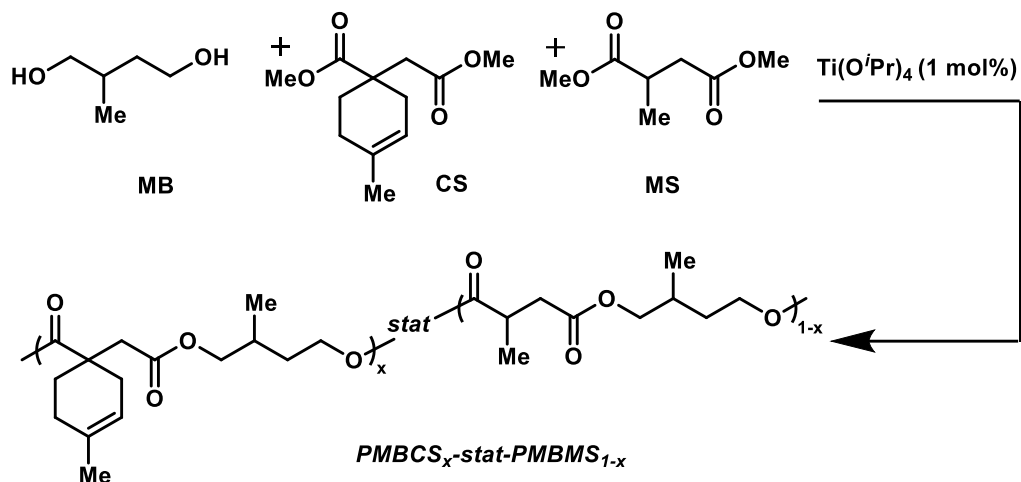
Functionalization of PMBCS with 1-dodecanethiol. PMBCS (100.2 mg, 0.3762 mmol, 1.000 equiv), DMPA (9.7 mg, 0.038 mmol, 0.10 equiv), and dodecanethiol (0.090 mL, 76.1 mg, 0.376 mmol, 1.00 equiv) were dissolved in DCM (1.00 mL, 0.100 g/mL) and solvent cast onto a mylar sheet. The mixture was allowed to dry in air to remove the DCM. The mixture was then covered with another mylar film and was irradiated with 250 nm light for 2 h. The mylar sheet / polymer mixture was then flipped over and irradiated further for 2 h. An aliquot by ^1H NMR showed 75% conversion. The mylar sheet / polymer mixture was then irradiated further for 18 h (22 h total). An aliquot

by ^1H NMR showed 84% conversion. The mylar sheet / polymer mixture was then stirred in chloroform to dissolve the polymer. The resulting solution was concentrated down to give a concentrated solution of polymer in chloroform (ca. 1 mL), and the polymer was then precipitated from $-78\text{ }^\circ\text{C}$ methanol (ca. 100 mL) and was dried under high vacuum to give predominantly dodecanethiol-functionalized PMBCS (74.1 mg, 0.1581 mmol) in 42% isolated yield (Figure S3.8).



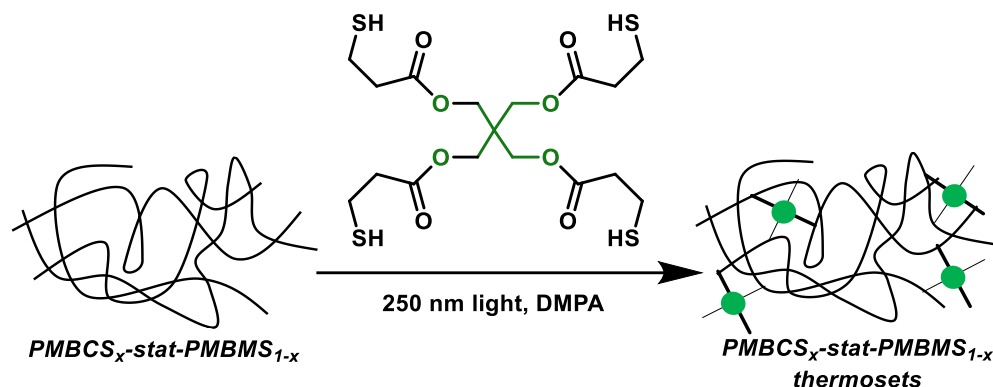
Synthesis of α,ω -hydroxy poly(MB-*alt*-MS) (HO-PMBMS-OH). MS (5.87 g, 36.7 mmol, 1.0 equiv), MB (7.60 g, 73.0 mmol, 1.99 equiv), and 4-methoxyphenol (57.6 mg, 0.43 wt%) were added to a 100 mL round bottom flask equipped with a stir bar, reflux condenser, and rubber septum. Nitrogen gas was then purged through the system for 20 min while stirring to give a clear, colorless liquid. $\text{Ti}(\text{O}^i\text{Pr})_4$ (0.140 mL, 0.473 mmol, 1.29 mol% relative to MS) was then injected and the reaction mixture turned a clear yellow color and was submerged into a $180\text{ }^\circ\text{C}$ oil bath. The reaction was stirred for 3 h with nitrogen gas purging through the system to remove the methanol byproduct. The reflux condenser was then replaced with a short path distillation head, and vacuum was applied to the system (400 Torr) while the temperature was increased to $200\text{ }^\circ\text{C}$. The pressure was then steadily lowered over 1 h to 0.05 Torr. After reaching 0.05 Torr, the

short path distillation head was periodically heated to encourage distillation of the excess diol. Within 0.5 h, the reaction mixture was barely stirring when the stirring was set to 50 rpm. After an additional 1.5 h (2.0 h total) the stir bar was stationary at 50 rpm, and the reaction mixture was allowed to cool to RT under vacuum. After cooling, the crude polymer solid was dissolved in dichloromethane (ca. 20 mL) and precipitated twice from $-78\text{ }^{\circ}\text{C}$ methanol (ca. 400 mL x 2) and then a final time from $-78\text{ }^{\circ}\text{C}$ hexanes (ca. 400 mL), dissolving the precipitated polymer back in dichloromethane (ca. 20 mL x 2) prior to each reprecipitation. The solid was dried under vacuum to give the product (5.62 g) in 76% isolated yield. $M_n = 15.7\text{ kg/mol}$, $M_w = 38.9\text{ kg/mol}$, $\bar{D} = 2.48$, and $dn/dc = 0.0660\text{ mL/g}$ were determined using a light scattering detector in THF solvent. $M_n = 15.9\text{ kg/mol}$, $M_w = 51.5\text{ kg/mol}$, and $\bar{D} = 3.24$ were determined using a refractive index detector in THF solvent calibrated against polystyrene standards. Characterization data was consistent with that previously reported in the literature.⁶³ ^1H NMR (Figure S3.6, 500 MHz, CDCl_3 , δ , ppm): 4.14 (m, 2H), 3.95 ppm (m, 2H), 3.49 (m, CH_2OH end groups), 2.91, (m, 1H), 2.74 (m, 1H), 2.41 (m, 1H), 1.93 (m, 1H), 1.75 (m, 1H), 1.49 (m, 1H), 1.22 (m, 3H), 0.97 (m, 3H). ^{13}C NMR (Figure S3.7, 125 MHz, CDCl_3 , δ , ppm): 175.3, 173.2, 172.0, 69.1, 62.7, 62.6, 37.6, 35.9 – 35.8, 32.2, 29.9 – 29.8, 17.2 – 17.1, 16.7 – 16.6. IR (Figure S3.30, ATR, cm^{-1}): 2965, 2937, 2878, 1728, 1462, 1344, 1158, 1054, 989, 757.



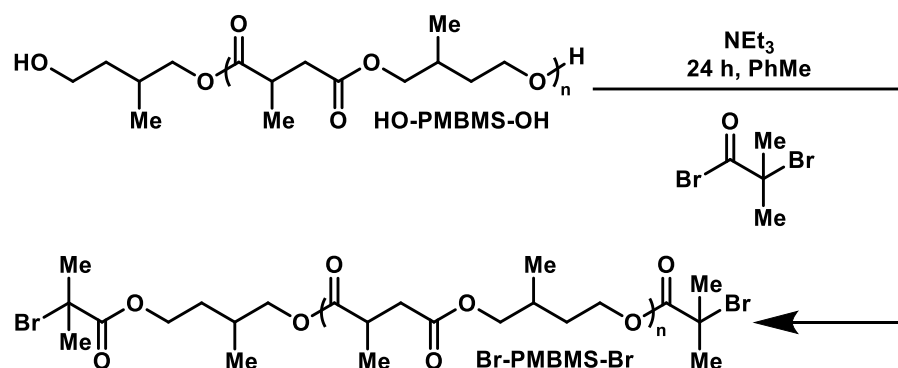
Synthesis of poly((MB-*alt*-CS)_x-*stat*-(MB-*alt*-MS)_{1-x}) (PMBCS_x-*stat*-PMBMS_{1-x}). In a typical reaction, the desired amount of CS and MS was weighed out (1.0 equiv of total diester consisting of a mixture of CS and MS) relative to MB (1.39 equiv). For $x = 0.19$: CS (1.36 g, 6.01 mmol, 0.21 equiv), MS (3.68 g, 22.98 mmol, 0.79 equiv), MB (4.20 g, 40.3 mmol, 1.39 equiv), and 4-methoxyphenol (53.2 mg, 0.57 wt%) were added to a 100 mL round bottom flask equipped with a stir bar, reflux condenser, and rubber septum. Nitrogen gas was then purged through the system for 20 min to give a clear, colorless liquid. Ti(O^{*i*}Pr)₄ (0.110 mL, 0.37 mmol, 1.3 mol% relative to 1.0 equiv total diester) was then injected and the reaction mixture turned yellow and was then submerged into a 180 °C in an oil bath. The reaction was stirred for 3 h with nitrogen gas purging through the system to remove the methanol byproduct. The reflux condenser was then replaced with a short path distillation head, and vacuum was applied to the system (400 Torr) while the temperature was increased to 200 °C. The pressure was then steadily lowered over 1 h to 0.05 Torr. After reaching 0.05 Torr, the short path distillation head was periodically heated to encourage distillation of the excess diol. The

polymerization was continued until the reaction mixture could no longer stir when the magnetic stirring was set 50 rpm (typically 1.0 h). The reaction mixture was then allowed to cool to RT under vacuum. An aliquot was taken of the crude sample for ^1H NMR, GPC, and DSC, and the mass was determined by the difference of the crude mixture with polymer and the tared round bottom flask and stir bar; polymer (5.67 g) was obtained in 92% isolated yield. For $x = 0.19$, $M_n = 21.5$ kg/mol, $M_w = 103$ kg/mol, $\bar{D} = 4.81$, and $dn/dc = 0.0700$ mL/g (calculated from the molar average using F_{MBCS} of the dn/dc values of PMBMS and PMBCS) were determined using a light scattering detector in THF solvent. M_n , M_w , and \bar{D} for $x = 0.29$ and 0.40 are reported in Table 3.3. The polymer was then dissolved in DCM and used without purification in the cross-linking experiments. ^1H NMR spectra contained all peaks associated with PMBMS and PMBCS. F_{MBCS} (0.19 for $x = 0.19$) was calculated from the ratio of PMBCS vinyl peak at ~ 5.3 ppm to PMBMS methyl peak at 1.22 ppm. For $x = 0.19$, ^1H NMR (Figure S3.9, 500 MHz, CDCl_3 , δ , ppm): 5.32 (s, 1H), 4.14 (m, 2x 2H), 3.95 ppm (m, 2x 2H), 2.91, (m, 1H), 2.74 (m, 1H), 2.58 (m, 3H), 2.40 (m, 1H), 1.95 (m, 1H and 4H), 1.75 (m, 1H and 2H), 1.64 (s, 3H), 1.50 (m, 1H and 3H), 1.22 (m, 3H), 0.97 (m, 2x 3H). ^{13}C NMR (Figure S3.10, 125 MHz, CDCl_3 , δ , ppm): 176.2, 175.3, 171.9, 171.5, 171.4, 132.9, 118.5, 69.2, 69.0, 62.7, 62.6, 62.5, 42.8, 42.7, 42.6, 40.4, 37.6, 35.9, 33.0, 32.2, 29.9, 27.1, 23.4, 17.2, 16.7. IR (Figure S3.30, ATR, cm^{-1}): 2965, 2937, 2878, 1728, 1462, 1344, 1158, 1054, 989, 757.



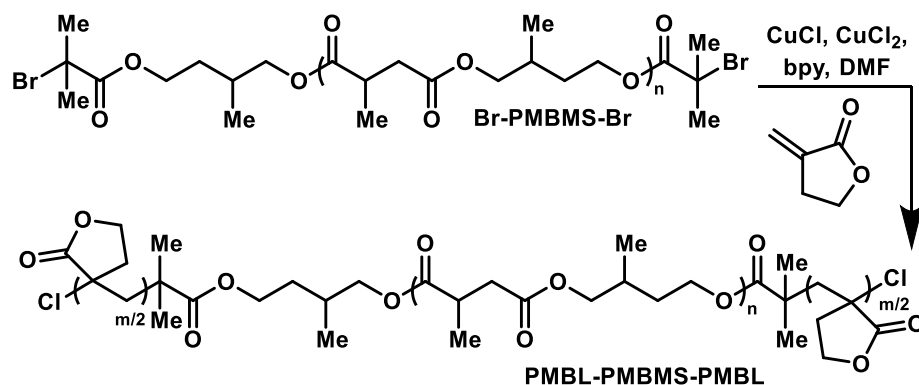
Cross-linking of poly((MB-*alt*-CS)_x-*stat*-(MB-*alt*-MS)_{1-x}) (PMBCS_x-*stat*-PMBMS_{1-x}). In a typical reaction, PMBCS_x-*stat*-PMBMS_{1-x} obtained directly from the crude reaction mixture described in the above section was dissolved in DCM. The desired amount of 2,2-dimethoxy-2-phenylacetophenone (DMPA, 0.10 equiv) initiator and pentaerythritol tetrakis(3-mercaptopropionate) (tetrathiol, 0.25 equiv) cross-linker was added to the polymer solution in DCM. For $x = 0.19$: PMBCS_{0.19}-*stat*-PMBMS_{0.81} (5.67 g, 5.14 mmol olefin) was dissolved in DCM (ca. 10 mL). Tetrathiol (0.45 mL, 1.18 mmol, 0.23 equiv) and DMPA (132.5 mg, 0.525 mmol, 0.102 equiv) was added to the solution. A mylar sheet was then clamped between a metal plate on the bottom and a 5.00" x 2.75" metal plate with a 3.50" x 1.25" rectangular mold cut-out on the top. Approximately one half of the DCM solution was then added to the mylar sheet in the metal plate cut-out until full and allowed to dry at room temperature (RT) overnight. After drying, a mylar sheet was carefully added to the top of the mold while avoiding trapping air between the mylar sheet and the neat mixture. The neat mixture was then irradiated with 250 nm hv, typically for 12 h. The thermoset and mylar films were then flipped over and irradiated further, typically for an additional 12 h. After irradiation, the mylar films were carefully removed from the cross-linked thermoset. The resulting

thermoset film was typically dried under high vacuum (0.05 Torr) for 48 h prior to analysis. A second film was also cast in the same manner with the remaining DCM solution, and the combined dried thermoset films (5.13 g) were obtained in 80% isolated yield based on mass recovery. For $x = 0.19$, IR (Figure S3.30, ATR, cm^{-1}): 2965, 2937, 2878, 1728, 1462, 1344, 1158, 1054, 989, 757.



Chain-end functionalization of α,ω -hydroxy-poly(MB-*alt*-MS) (HO-PMBMS-OH). The functionalization method was adapted from a known procedure.¹¹⁴ HO-PMBMS-OH (3.646 g, 18.21 mmol PMBMS repeat unit, $M_n = 15.7$ kg/mol, degree of polymerization = 78.4, 0.232 mmol HO-PMBMS-OH macroinitiator, 1.00 equiv) was dissolved in toluene (34.0 mL, 0.107 g/mL) in a 100 mL round bottom flask. Triethylamine (0.780 mL, 0.569 g, 5.63 mmol, 24.3 equiv) and α -bromoisobutyryl bromide (0.70 mL, 1.302 g, 5.66 mmol, 24.4 equiv) were added by syringe at RT. The reaction mixture was allowed to stir at RT for 26 h. The cloudy mixture was then filtered through a plug of magnesium sulfate in a fritted funnel and then the toluene was removed by concentrating under reduced pressure. The crude polymer was then dissolved in DCM (ca. 100 mL) and transferred to a separatory funnel, where the organic layer was washed three times with saturated bicarbonate in DI water (ca. 100 mL x 3),

five times with DI water (ca. 100 mL x 5), and three times with 3 M NaOH (ca. 100 mL x 3). The organic layer was then dried over anhydrous magnesium sulfate (ca. 50 g), filtered, and concentrated down. The polymer was then dissolved in DCM (ca. 20 mL) and precipitated twice from $-78\text{ }^{\circ}\text{C}$ methanol (ca. 400 mL x 2) and finally once from $-78\text{ }^{\circ}\text{C}$ hexanes (ca. 400 mL). The precipitated polymer was dissolved back in dichloromethane (ca. 20 mL x 2) prior to each reprecipitation. The polymer was then dried under vacuum to afford Br-PMBMS-Br (1.144 g) in 31% isolated yield (based on 100% conversion of chain ends and mass recovery). $M_n = 19.0\text{ kg/mol}$, $M_w = 159$, $\bar{D} = 7.42$, and $dn/dc = 0.0650\text{ mL/g}$ were determined using a light scattering detector in THF solvent. $M_n = 21.3\text{ kg/mol}$, $M_w = 141\text{ kg/mol}$, and $\bar{D} = 7.44$ were determined using a refractive index detector in THF solvent calibrated against polystyrene standards. $M_n = 25.7\text{ kg/mol}$, $M_w = 59.1$, and $\bar{D} = 2.30$ were determined using a refractive index detector in DMF solvent calibrated against polystyrene standards. ^1H NMR (Figure S3.25, 500 MHz, DMSO- d_6 , δ , ppm): 4.05 (m, 2H), 3.87 ppm (m, 2H), 2.80, (m, 1H), 2.58 (m, 1H), 2.47 (m, 1H), 1.89 (s, CH_3 end group), 1.88 (s, CH_3 end group), 1.83 (m, 1H), 1.64 (m, 1H), 1.42 (m, 3H), 1.12 (m, 3H), 0.89 (m, 3H).



Chain extension of α,ω -bromo-poly(MB-*alt*-MS) (Br-PMBMS-Br). The chain extension of Br-PMBMS-Br was adapted from a known procedure.¹²⁰ Br-PMBMS-Br (0.9063 g, 4.527 mmol repeat unit, $M_n = 19.0$ kg/mol, degree of polymerization = 94.9, 0.0131 mmol Br-PMBMS-Br macroinitiator, 1.00 equiv) was dissolved in DMF (1.80 mL, 0.504 g/mL) in a Schlenk bomb. 2,2'-bipyridine (27.4 mg, 0.180 mmol, 0.0493 equiv), CuCl (33.9 mg, 0.342 mmol, 0.0937 equiv), CuCl₂ (9.7 mg, 0.072 mmol, 0.0197 equiv), and MBL (0.320 mL, 0.358 g, 3.65 mmol, 1.00 equiv) were then added to the bomb. The reaction mixture was degassed by three freeze-pump-thaw cycles and then placed in a 60 °C oil bath and stirred for 16 h. Aliquot analysis by ¹H NMR showed >99% conversion of MBL. The DMF solution was then precipitated from – 78 °C cold methanol (ca. 100 mL). The polymer was isolated and dissolved in DCM (ca. 10 mL) and then passed through a plug of basic Al₂O₃ on a fritted funnel to remove the copper catalyst. The filtrate was then precipitated three times from – 78 °C methanol (ca. 100 mL x 3) and finally once from – 78 °C hexanes (ca. 100 mL). The precipitated polymer was dissolved back in dichloromethane (ca. 20 mL x 4) prior to each reprecipitation. The purified polymer was then dried under vacuum to afford PMBL-PMBMS-PMBL (0.8774 g) in 69% isolated yield (based on 100% conversion of MBL and mass recovery). $M_n = 33.3$ kg/mol, $M_w = 60.0$, and $D = 1.80$ were determined using a refractive index detector in DMF solvent calibrated against polystyrene standards. ¹H NMR (Figure S3.26, 500 MHz, DMSO-d₆, δ , ppm): 4.36 (m, 2H), 4.05 (m, 2H), 3.87 (m, 2H), 2.79, (m, 1H), 2.58 (m, 1H), 2.48 (m, 1H), 2.07, (m, 4H), 1.84 (m, 1H), 1.65 (m, 1H), 1.41 (m, 1H), 1.12 (m, 3H), 0.89 (m, 3H). ¹³C NMR (Figure S3.27, 125 MHz,

DMSO-d₆, δ , ppm): 180.2 – 180.0, 174.4, 171.2, 68.2, 65.1, 62.0, 61.9, 44.5 – 44.0, 36.8, 35.3 – 35.2, 31.5, 29.3 – 29.2, 16.7 – 16.6, 16.7 – 16.3.

2D NMR Spectroscopy of PMBCS and PMBMS for regioregularity determination and end-group analysis for PMBMS. The regioregularity of the polymer was determined after assigning individual ¹H and ¹³C peaks for both PMBMS and PMBCS through COSY, HSQC, and HMBC 2D experiments. During this process, multiple peaks integrating to a single carbon from quantitative ¹³C spectra were observed, corresponding to the same carbon along the polymer repeat unit position in different chemical environments as a result of local polymer regiochemistry. For both PMBMS and PMBCS, line fitting analysis using MestReNova was used to determine the ratio of the α -carbonyl carbon (a quaternary carbon for PMBCS at ~43 ppm or a tertiary carbon for PMBMS at ~36 ppm) interacting with either the head or tail end of the MB comonomer in the polymer repeat unit. The individual peaks associated with a head or tail interaction with MB were not assigned; a 1.0:1.0 ratio was measured, indicating that interaction of MS with the head or tail end of MB occurred in equal amounts. PMBCS sample analyzed by 2D NMR was synthesized using the general procedure described above (Figure S3.11 – Figure S3.15). PMBMS analyzed by 2D NMR was synthesized according to the general procedure above, in a 1.0:1.2 MS:MB ratio (Figure S3.16 – Figure S3.20).

Conversion vs time for the polymerization of MB and MS to PMBMS. The PMBMS polymerization was followed through both stages of the polycondensation method following the general procedure using SEC to determine M_n and \bar{D} and ¹H NMR analysis to determine conversion (Figure S3.21, Figure S3.22, and Table S3.1).

Swell tests for gel fraction determination. Swell tests of cross-linked poly((MB-*alt*-CS)_x-*stat*-(MB-*alt*-MS)_{1-x}) (PMBCS_x-PMBMS_{1-x}). Typically, small pieces of the thermosets were weighed (ca. 10 – 50 mg) and placed in 20 mL scintillation vials. 10.0 mL of DCM was then added to the vial, which was capped. The sample was equilibrated for 48 h. After 48 h, the samples were removed, patted down with a Kimwipe®, and quickly weighed while swollen. Then the samples were dried under reduced pressure (0.05 Torr) for 48 h and weighed again. Swell tests were performed in triplicate and the results were averaged. Gel fractions were calculated with the following equations:

$$Sol\ fraction = \left[\frac{W_o - W_i}{W_o} \right] \quad \text{Equation 3.2}$$

$$Gel\ fraction = 1 - Sol\ fraction \quad \text{Equation 3.3}$$

Where W_o is the initial weight of the dried thermoset and W_i is the mass of the dried thermoset following the DCM extraction during the swell test.⁹² Time points taken during a test swelling experiment indicated constant values of mass for the swollen thermoset were obtained between 24 and 114 h, demonstrating that equilibrium for these systems is achieved rapidly and within 48 h.

Estimation of Cross-linking Density Using the Flory-Rehner Equation. Molar mass between cross-links (M_x) were estimated using the Flory-Rehner equation⁹² shown below

$$M_x = - \frac{d_p V_s \left(V_f^{\frac{1}{3}} - \frac{V_f}{2} \right)}{\ln(1 - V_f) + V_f + \chi V_f^2} \quad \text{Equation 3.4}$$

where d_p is the experimentally determined density of the thermosets (1.16 g/mL for all thermosets), V_s is the molar volume of the swelling solvent (64 mL/mol for DCM), V_f

is the volume fraction of the polymer, and χ is the solvent interaction parameter. V_f is further defined as

$$V_f = \left[1 + \frac{d_p}{d_s} \left(\frac{M_a}{M_b} - 1 \right) \right]^{-1} \quad \text{Equation 3.5}$$

where d_s is the swelling solvent density (1.327 g/cm³ for DCM), M_a is the mass of the swollen thermoset and M_b is the mass of the dried thermoset prior to swelling, with both M_a and M_b obtained during the swell tests described above and a V_f value calculated for each swell test run. Furthermore, χ can be estimated by the equation below¹²¹

$$\chi = 0.34 + \frac{V_s}{RT} (\delta_1 - \delta_2)^2 \quad \text{Equation 3.6}$$

where R is the ideal gas constant in units of J/(mol·K), T is temperature in K, V_s is the molar volume of the solvent as defined previously, and δ_1 and δ_2 , the solubility parameter of the thermoset and solvent, respectively, both with units of (J/cm³)^{1/2}. Solubility parameters of common solvents such as DCM ((20.2 J/cm³)^{1/2}) have been tabulated,¹²² while the solubility parameter for both PMBMS and PMBCS were calculated using the Small's cohesive energies equation^{123,124}

$$\delta = d_p \frac{\sum F_1}{M_0} \quad \text{Equation 3.7}$$

where $\sum F_1$ is the sum of the group molar attraction constants and M_0 is the molar mass of the repeat unit. δ_{PMBMS} and δ_{PMBCS} were calculated to be 19.4 (J/cm³)^{1/2} and 18.2 (J/cm³)^{1/2}, respectively, and were similar to that calculated for the structurally similar poly(butylene succinate).¹²⁵ Solvent parameters for each thermoset were then calculated as a weighted average of the PMBMS and PMBCS solvent parameters, with

$$\delta_1 = \delta_{thermoset} = (1 - F_{MBCS})\delta_{PMBMS} + F_{MBCS}\delta_{PMBCS} \quad \text{Equation 3.8}$$

The values of M_a , M_b , V_f , δ_1 , χ , and M_x are tabulated in Table S3.2.

M_x values determined using the Flory-Rehner equation (Equation 3.4) are approximately half the values of M_x determined by DMTA results. Despite these differences, $M_{x,\text{swell}}$ values decrease with increasing F_{MBCS} , as observed for $M_{x,\text{DMTA}}$ values (Table S3.3). Disparities in M_x values determined from swelling and DMTA experiments have been previously reported and are likely due to the limitations of the Flory-Rehner equation for this system resulting from the lower limit for M_x of just a few hundred grams per mole.^{93–95}

Degradation experiments of cross-linked poly((MB-co-CS)_x-stat-(MB-co-MS)_{1-x}) (PMBCS_x-stat-PMBMS_{1-x}). The stability of PMBCS_x-stat-PMBMS_{1-x} thermosets suspended in 3 M solutions of HCl or NaOH in DI water, as well as in DI water were determined under ambient conditions. Three square specimens were cut out of a previously set sheet of cross-linked material. For $F_{\text{MBCS}} = 0.19$, specimen samples were typically 6 x 6 x 1 mm in dimensions and typically weighed ~40 mg. Each specimen sample (performed in triplicate for each pH solution) was immersed in the above three solutions (typically 10 mL) in 20 mL scintillation vials. The samples were capped and left to sit undisturbed. At each time point the samples were removed from their respective media, washed in DI water, and dried under reduced pressure (40 mTorr) at room temperature for 24 h. The samples were weighed and immersed back in their original vial with the aqueous solution. This process was repeated at each time point. Results are compiled in Table S3.4 and shown graphically in Figure S3.23.

Dynamic mechanical analysis for the determination of M_e . Dynamic analysis of PMBMS and PMBL were performed at various temperatures within the linear

viscoelastic regime. For this analysis, an oscillatory stress is applied to the material and the sinusoidal stress response is measured; this affords a complex modulus that is decoupled into the in-phase (G') and out-of-phase (G'') components. The loss tangent ($\tan(\delta)$), or the ratio of the viscous modulus G'' to the elastic modulus G' , was also calculated. For PMBL, data were collected at 250 and 260 °C (Figure S3.31) – above this temperature, PMBL began to degrade on the rheometer. For PMBMS, horizontal shift factors (a_T) were determined by aligning the loss tangent curves and subsequently applied to each frequency sweep to generate a master curve via time-temperature superposition. Using data from the master curve, the entanglement molar mass (M_e) was estimated using the following equation¹²¹

$$M_e = \frac{\rho RT}{G_N} \quad \text{Equation 3.9}$$

where ρ is the density, R is the universal gas constant, T is the temperature, and G_N is the plateau modulus. The plateau modulus was defined as the point during the rubbery plateau where the loss tangent ($\tan(\delta)$) is at a minimum, as this corresponds to the point at which the elastic modulus is most dominant.

Using a temperature of 20 °C, densities of 1.12 g/mL for PMBMS or 1.38 g/mL for PMBL, and G_N of 358820 Pa for PMBMS or 435430 Pa for PMBL, the entanglement molar masses were roughly estimated as 6.3 kg/mol for PMBMS and 10.6 kg/mol for PMBL.

Green Metrics. Green metrics¹¹⁶ were evaluated for various small molecule transformations and polymerizations reported in the main text (see Table 3.5). Isolated yields were calculated in the usual way, as the ratio of the moles of product isolated

from the moles of the limiting reagent starting material multiplied by one hundred. Atom economies (AEs)¹¹⁷ were calculated with the equation below.

$$AE (\%) = \frac{\text{molecular weight of the desired product}}{\text{molecular weight of all the reactants}} \times 100 \quad \text{Equation 3.10}$$

Additionally, process mass intensities (PMIs)¹¹⁸ were estimated with the equation below.

$$PMI = \frac{\text{total mass of materials used in a process (kg)}}{\text{mass of isolated product (kg)}} \quad \text{Equation 3.11}$$

APPENDIX

General Reagent Information. Ethyl acetate (99.5%, Fisher), hexanes (98.5%, Fisher), methanol (99.8%, Fisher), chloroform (99.8%, J.T. Baker), Celite[®] 545 (Sigma-Aldrich), diethyl ether (Laboratory grade, Fisher), dimethyl sulfoxide (99.9%, Fisher), benzene (99.0%, EMD Millipore), ethanol (200 proof, Decon Labs Inc.), chloroform-D (99.8%, Cambridge Isotope Laboratories, Inc.), dimethyl sulfoxide-d₆ (DMSO-d₆, 99.9%, Cambridge Isotope Laboratories, Inc.), anhydrous magnesium sulfate (98.0%, EMD Millipore), dimethyl itaconate (DMI, >98.0%, TCI or 99%, Aldrich), isoprene (99.0%, Aldrich), aluminum(III) chloride (≥99.0%, Honeywell), ytterbium(III) trifluoromethanesulfonate (Y(OTf)₃, 98%, Sigma), lutetium(III) trifluoromethanesulfonate (Fluka Chemical Corporation), lanthanum(III) trifluoromethanesulfonate (Fluka Chemical Corporation), scandium(III) trifluoromethanesulfonate (Sc(OTf)₃, 99%, Sigma or >98.0%, TCI), carbonylhydrido(tetrahydroborato)[bis(2-diphenylphosphinoethyl)amino]ruthenium(II) (RuMACHO-BH, min. 98%, Strem), palladium on carbon (Pd/C, 10% Pd basis, Aldrich), pentaerythritol tetrakis(3-

mercaptopropionate) (>95%, Aldrich), titanium(IV) isopropoxide (97+%, Alfa Aesar), 4-methoxyphenol (MEHQ, 99%, Aldrich), 2,2-dimethoxy-2-phenylacetophenone (DMPA, 99%, Aldrich), 1-dodecanethiol ($\geq 98\%$, Aldrich), α -bromoisobutyryl bromide (98%, Aldrich), triethylamine (NEt_3 , 100.0%, J.T. Baker), copper(II) chloride (min. 98%, Strem), 2,2'-bipyridine (98%, Alfa Aesar), 2-cyano-2-propyl benzodithioate (97%, Sigma-Aldrich), basic aluminum oxide (alumina, activated, Brockmann Grade I, 58 angstroms, Alfa Aesar), hydrogen (Ultra high purity 5.0 grade, Airgas), and argon (High purity grade 4.8, Airgas) were used as received. Deionized (DI) water was obtained by reverse osmosis. Tetrahydrofuran (THF, 99%, Macron) was degassed by sparging with argon for 30 min and then purified by passing through two packed columns of neutral alumina on the JC Meyer solvent system. Toluene (PhMe, 99.9%, Fisher) was degassed by sparging with argon for 30 min and then purified by passing through a packed column of neutral alumina followed by a packed column of Q5 reactant, a copper(II) oxide oxygen scavenger on a JC Meyer solvent system. *N,N*-dimethylformamide (DMF, Macron) was degassed by sparging with argon for 30 min and then purified by passing through two packed columns of activated molecular sieves followed by a packed column of isocyanide on the JC Meyer solvent system. Azobisisobutyronitrile (AIBN, Sigma, 98.0%) was recrystallized from methanol before use. Hydrochloric acid (HCl, Macron) was used as received and diluted with DI water to make a 3.0 M or 0.5 M solution. Copper(I) chloride (97%, Sigma) was purified by dissolving it in hydrochloric acid and then precipitating it by adding it to DI water.¹²⁶ The solid was then filtered and washed with ethanol, diethyl ether, dried under reduced pressure (0.05 TorrTorr) for 24 h, and stored under nitrogen in a desiccator. Mylar sheets

(10'' x 10'' x 0.04'') were obtained from Carver, Inc. Quartz tubes were obtained from the Cornell Chemistry Glass Shop (Cornell University, Department of Chemistry and Chemical Biology, S. T. Olin Chemistry Research Wing, Room B66). α -methylene- γ -butyrolactone (MBL, >95.0%, TCI) was passed through a plug of basic alumina to remove radical inhibitor prior to use. 3 M sodium hydroxide was prepared by dissolving sodium hydroxide (NaOH, Macron) in DI water.

General Analytical Information. Polymers samples were analyzed using size exclusion chromatography (SEC) instruments operating with a THF or DMF eluent. For the SEC with THF eluent, a Tosoh EcoSec HLC 8320GPC system with two SuperHM-M columns in series at a flow rate of 0.350 mL/min at 40 °C was used. Number-average molar masses (M_n), weight-average molar masses (M_w), and dispersities (\bar{D}) for polymer samples were determined by light scattering using a Wyatt mini Dawn Treos multi-angle light scattering detector at 25 °C. The dn/dc values of the polymer samples were estimated using size exclusion chromatography with samples of known concentrations in THF. This indirect ("in-line") method uses the total area of the RI signal and the assumption that 100% of the sample mass is recovered to calculate the polymer dn/dc values. M_n , M_w , and \bar{D} values were also determined from the refractive index chromatogram against polystyrene (TSKgel) standards. For the SEC with DMF eluent, polymer samples were analyzed using a GPC system composed of a Waters 1515 Isocratic HPLC pump and three PSS GRAM columns (100–1000–3000) in series at a flow rate of 1.0 mL/min at 35 °C. A 0.05 % LiBr solution in DMF was used as the eluent and M_n s, M_w s, and \bar{D} s were determined from refractive index chromatograms against polystyrene standards (Polymer Standards Service USA, Inc., Amherst, MA) using a

Waters 2414 differential refractive index detector. Nuclear magnetic resonance (NMR) spectra were recorded on a Mercury 300 MHz, a Varian 400 MHz, a Bruker 500 MHz, or a Varian 600 MHz instrument. Mass spectra were obtained on an Exactive Plus Orbitrap Mass Spectrometer with a DART SVP ion source from Ion Sense. The Fourier transform infrared (FTIR) spectra were obtained on a Bruker Alpha Platinum or a Thermo Scientific Smart Orbit Nicolet Avatar 370 DTGS spectrometer equipped with a diamond crystal in attenuated total reflection (ATR) mode at a resolution of 4/cm with 32 scans obtained for each spectrum. Differential scanning calorimetry (DSC) was performed using a TA Instruments Q1000. Samples were prepared in aluminum pans and were analyzed using the following heating program: $-50\text{ }^{\circ}\text{C}$ to $150\text{ }^{\circ}\text{C}$ at $30\text{ }^{\circ}\text{C}/\text{min}$, $150\text{ }^{\circ}\text{C}$ to $-50\text{ }^{\circ}\text{C}$ at $10\text{ }^{\circ}\text{C}/\text{min}$, and $-50\text{ }^{\circ}\text{C}$ to $150\text{ }^{\circ}\text{C}$ at $30\text{ }^{\circ}\text{C}/\text{min}$. The data were processed using Universal Analysis 2000 for Windows software. All reported T_g s were observed on the second heating cycle. Thermogravimetric analysis (TGA) was performed on a TA Instruments Q500 Thermogravimetric Analyzer. Typically, samples were heated at $10\text{ }^{\circ}\text{C}/\text{min}$ to $550\text{ }^{\circ}\text{C}$ under nitrogen. Data were processed using Universal Analysis 2000 for Windows software. To melt process the thermoplastics, PMBL-PMBMS-PMBL was placed between two Teflon sheets and melt pressed in a rectangular mold at 2500 lbs and $190\text{ }^{\circ}\text{C}$ and then quenched by cooling to RT using water cooling at a rate of $35\text{ }^{\circ}\text{C}/\text{min}$ to yield a 0.5 mm thick film. PMBL was placed between two Teflon sheets and melt pressed in a rectangular mold at 2500 lbs and $235\text{ }^{\circ}\text{C}$ and then quenched by cooling to RT using water cooling at a rate of $35\text{ }^{\circ}\text{C}/\text{min}$. Using 8 mm parallel plates, TA Instruments Rheometric Series ARES instrument was used for dynamic mechanical analysis. Heating was controlled under nitrogen

atmosphere, and the samples were equilibrated at the designated temperature for 10 minutes before testing. Thermoset materials were solvent cast into a 0.8 mm thick film and cured under 250 nm light (Sylvania G8T5 germicidal 12” bulbs for utilized as the 254 nm source). Dog-bone-shaped tensile bars for both the thermosets and thermoplastics were punched out resulting in samples with approximately 3 mm gauge width and 16 mm gauge length. Samples were tested to the point of break using Shimadzu Autograph AGS-X Tensile Tester and an extension rate of 5 mm/min. Extensional dynamic mechanical thermal analysis was performed on a TA Instruments RSA-G2 in tension mode on rectangular polymer films with 0.5 mm thickness and 3 mm gauge width. DMTA experiments were conducted at a heating rate of 5 °C/min with an oscillating strain of 0.05% and angular frequency of 1 Hz. High-pressure hydrogenations were performed using a 300 mL Parr reactor obtained from Parr Instrument Company (Moline, Illinois). Thermoset and PMBL densities were determined to be 1.16 g/cm³ and 1.38 g/cm³, respectively, using a Mettler-Toledo XPE205 DeltaRange equipped with a Mettler-Toledo MS-DNY-54 density kit. The density of PMBMS was estimated to be 1.12 g/cm³ using sink-or-float tests. Vacuum pressures between 100 and 760 Torr were obtained using a vacuum regulator (item # YX-00910-10) obtained from Davis Instruments.

Supplementary Figures and Tables

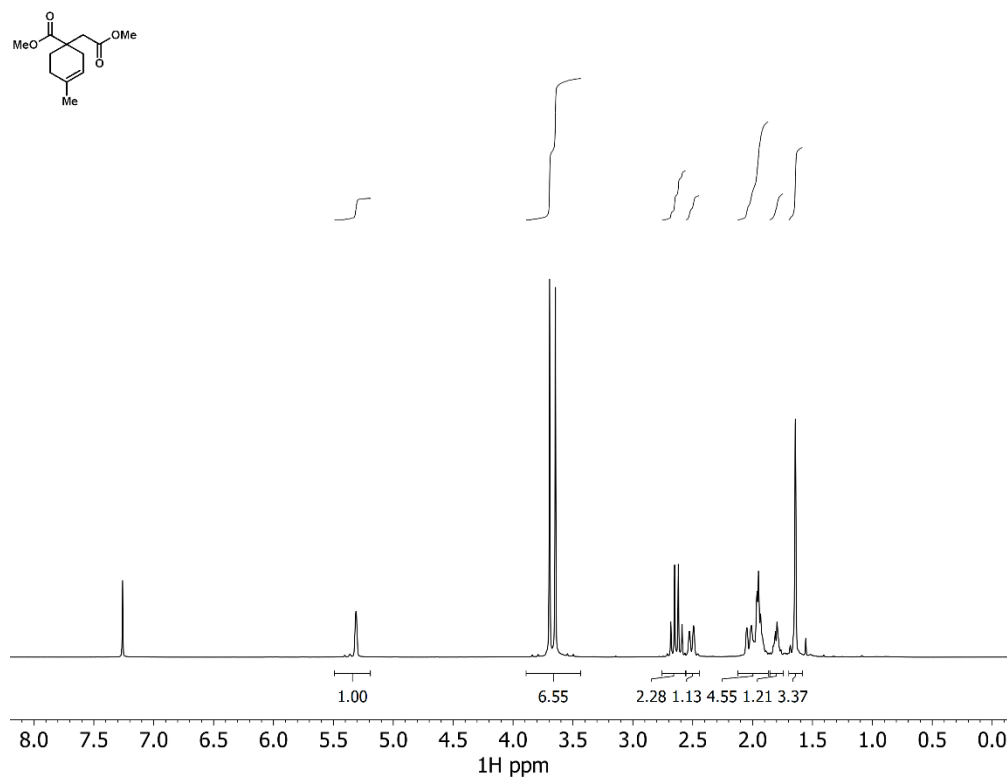


Figure S3.1. ¹H NMR spectra of 2-(4-methylcyclohex-3-ene)succinate (CS) in CDCl₃.

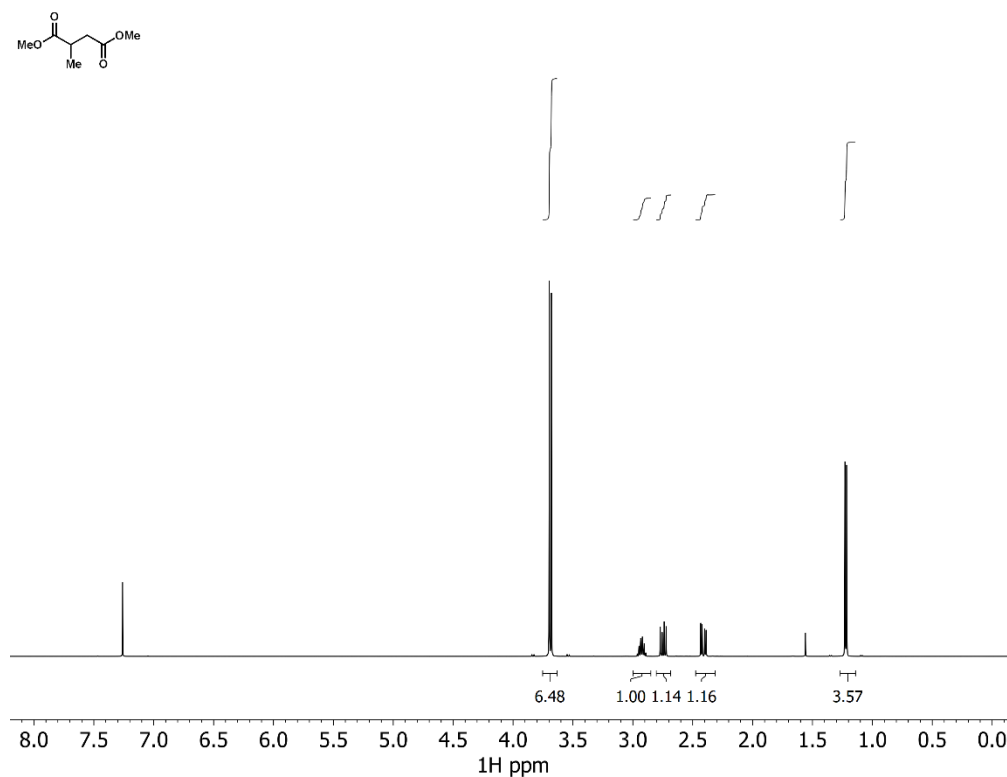


Figure S3.2. ¹H NMR spectra of dimethyl 2-methylsuccinate (MS) in CDCl₃.

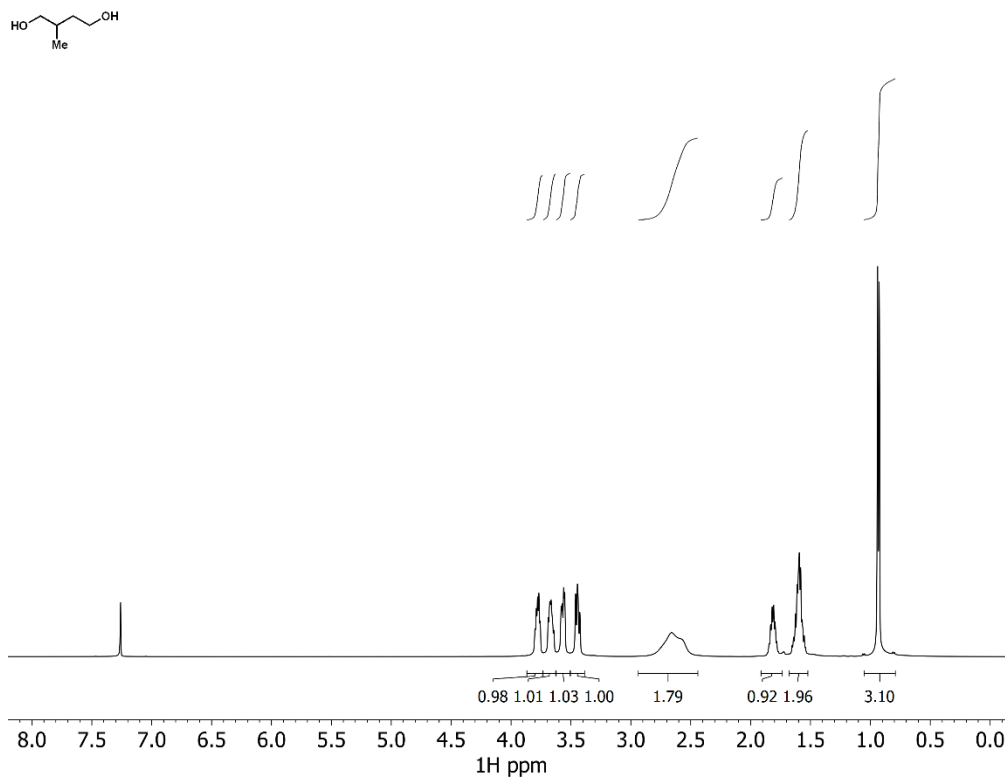


Figure S3.3. ¹H NMR of 2-methyl-1,4-butanediol (MB) in CDCl₃.

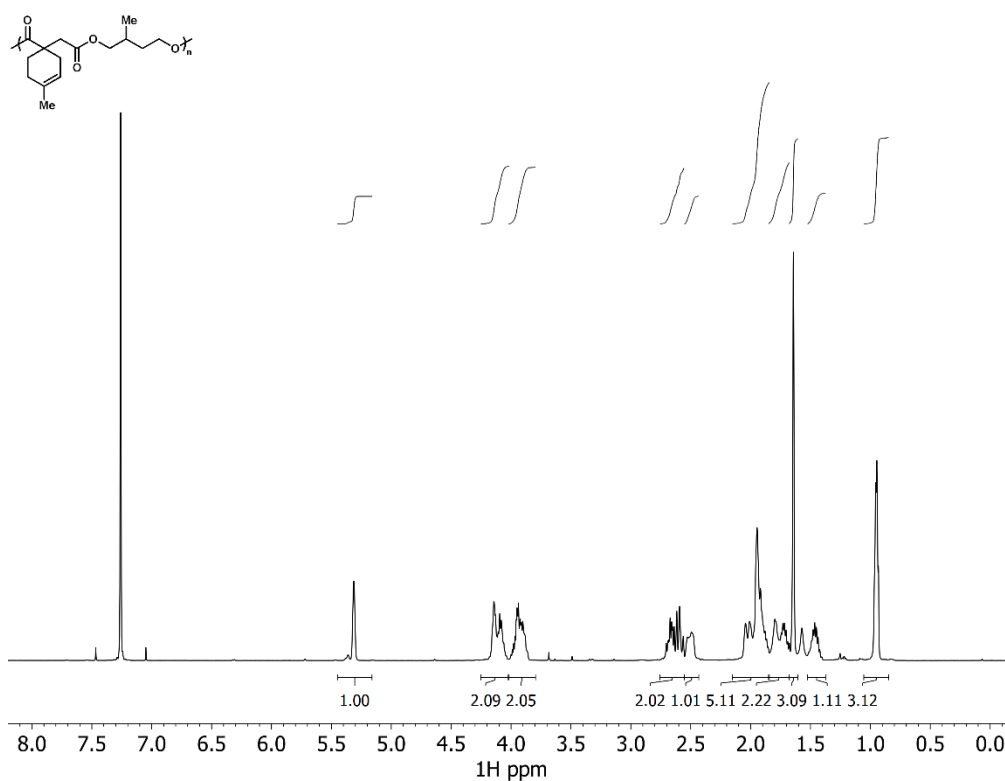
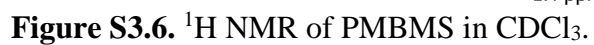


Figure S3.4. ¹H NMR of PMBCS in CDCl₃.



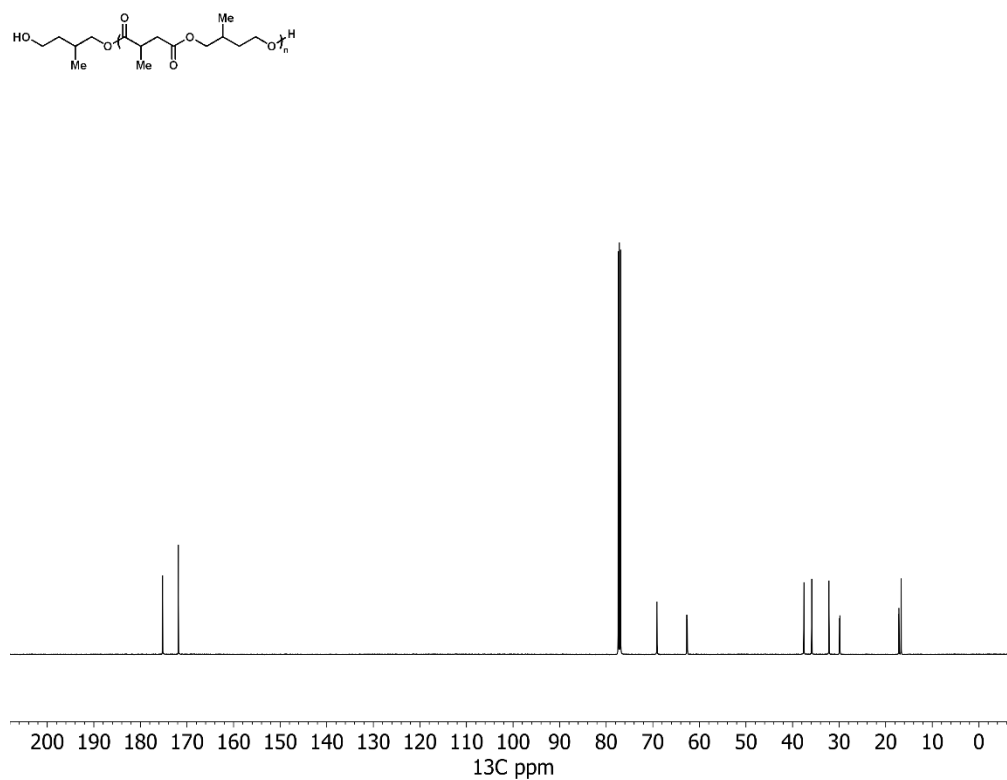


Figure S3.7. ^{13}C NMR of PMBMS in CDCl_3 .

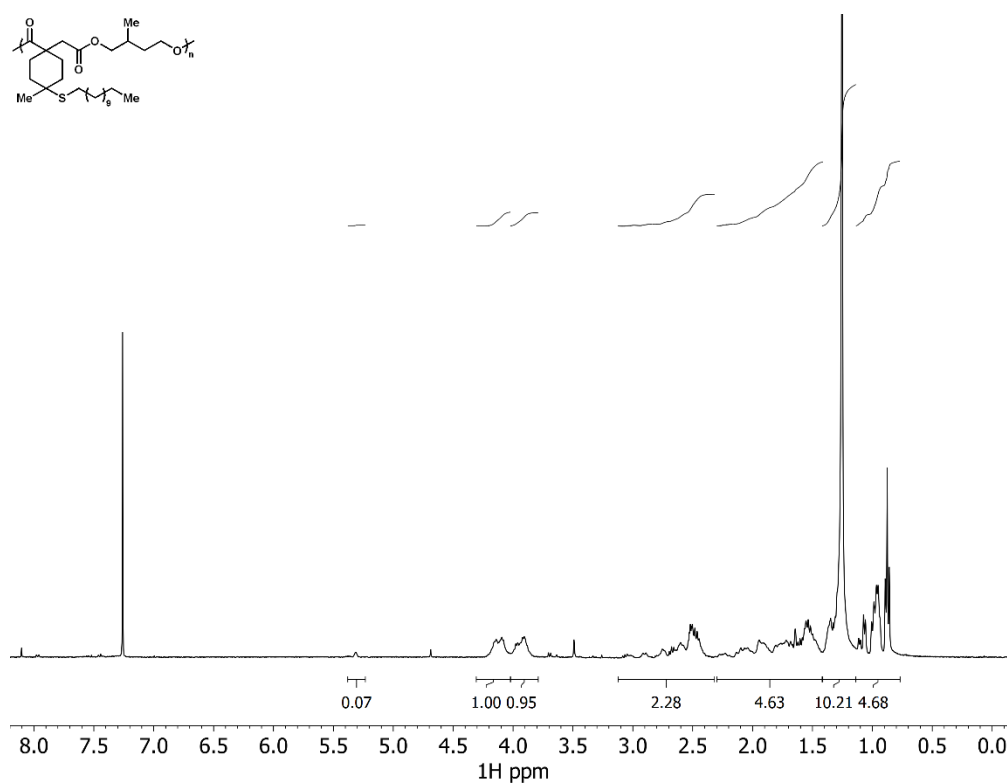


Figure S3.8. ^1H NMR spectra of dodecanethiol-functionalized PMBCS in CDCl_3 .

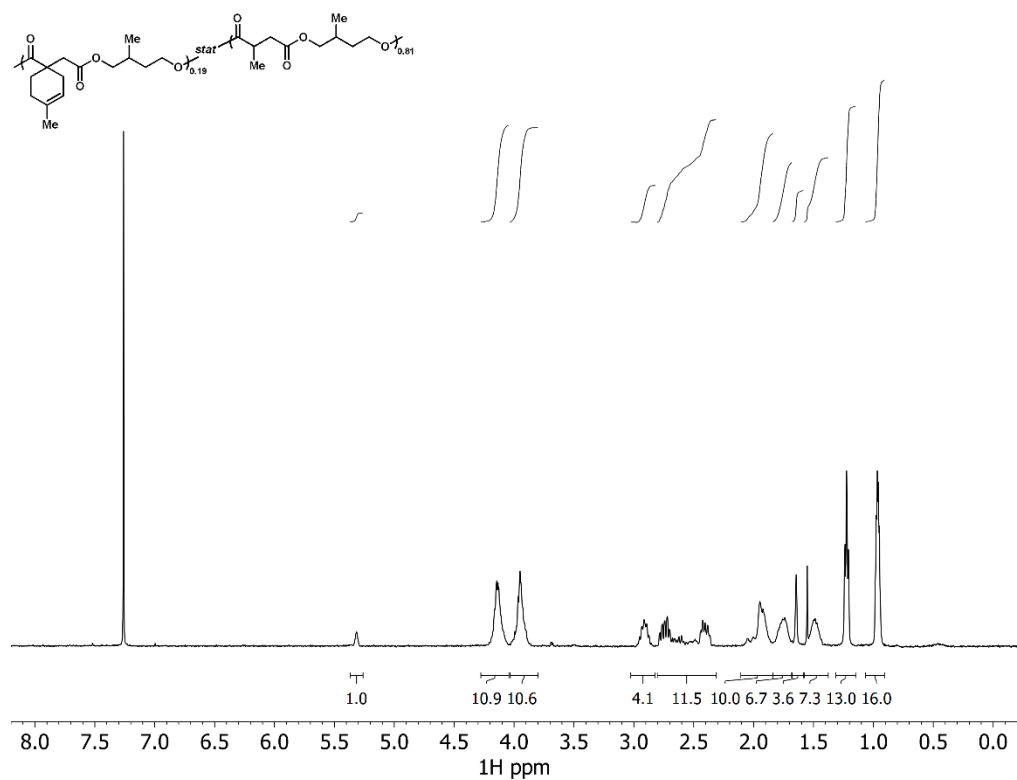


Figure S3.9. ¹H NMR of PMBCS_x-stat-PMBMS_{1-x} (x = 0.19) in CDCl₃.

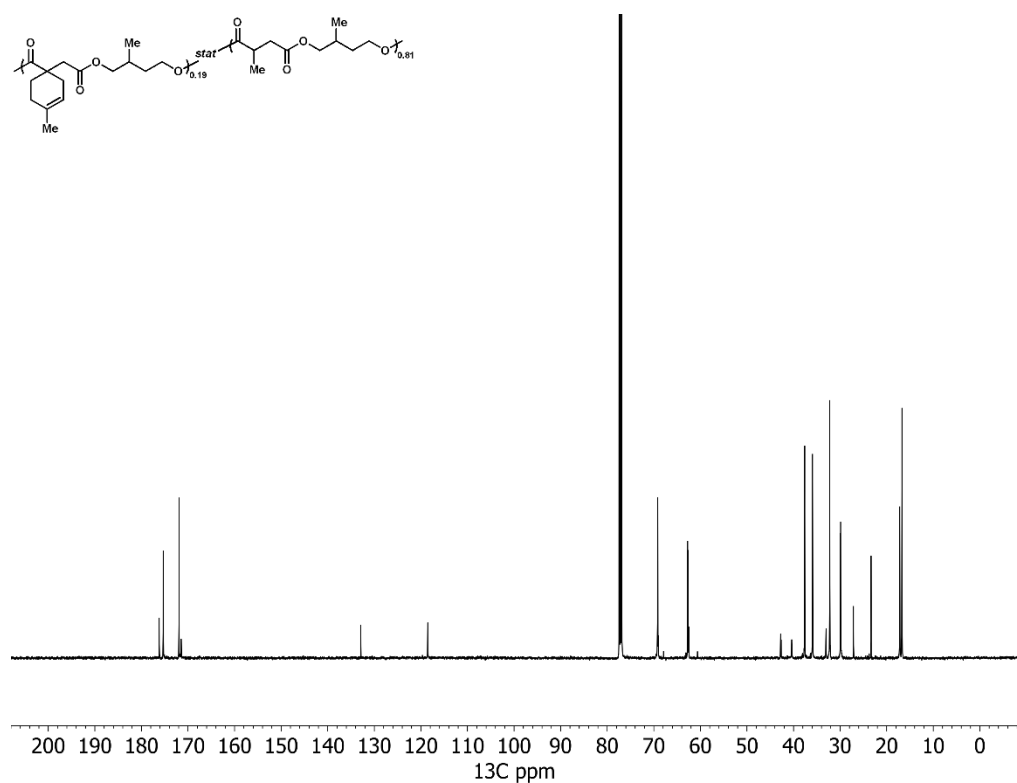


Figure S3.10. ¹³C NMR of PMBCS_x-stat-PMBMS_{1-x} (x = 0.19) in CDCl₃.

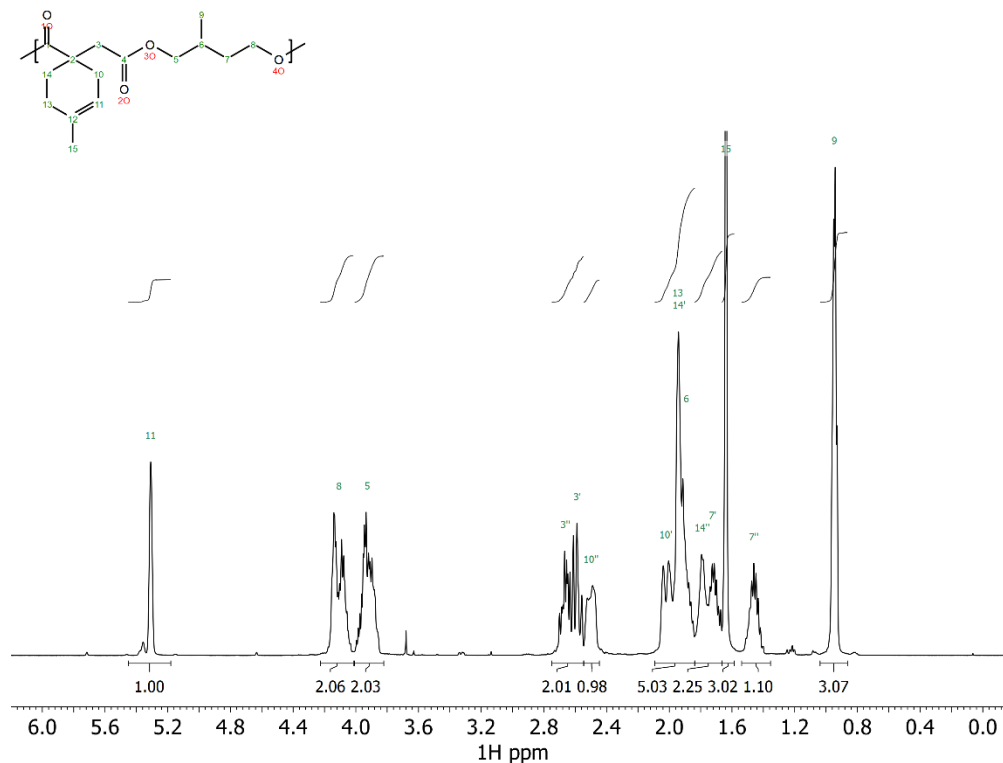


Figure S3.11. Quantitative ¹H NMR spectrum of PMBCS in CDCl₃ with assignments.

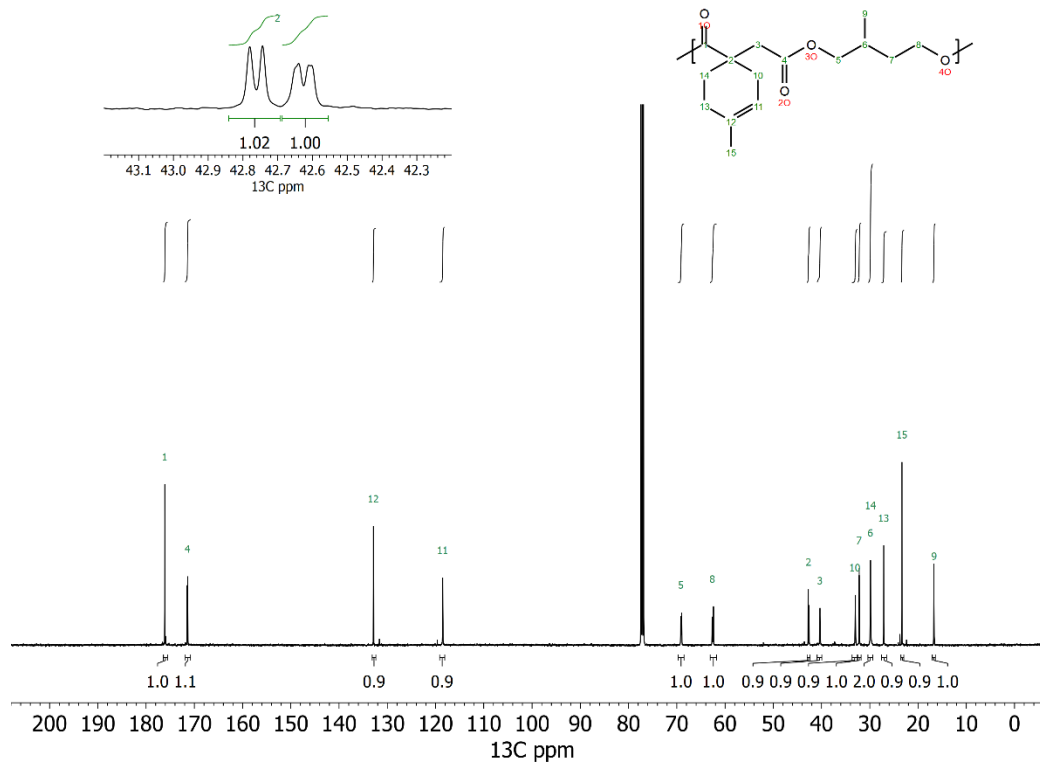


Figure S3.12. Quantitative ¹³C NMR spectrum of PMBCS in CDCl₃ with assignments. Insert in top-left depicts the peaks associated with the quaternary carbon (carbon 1).

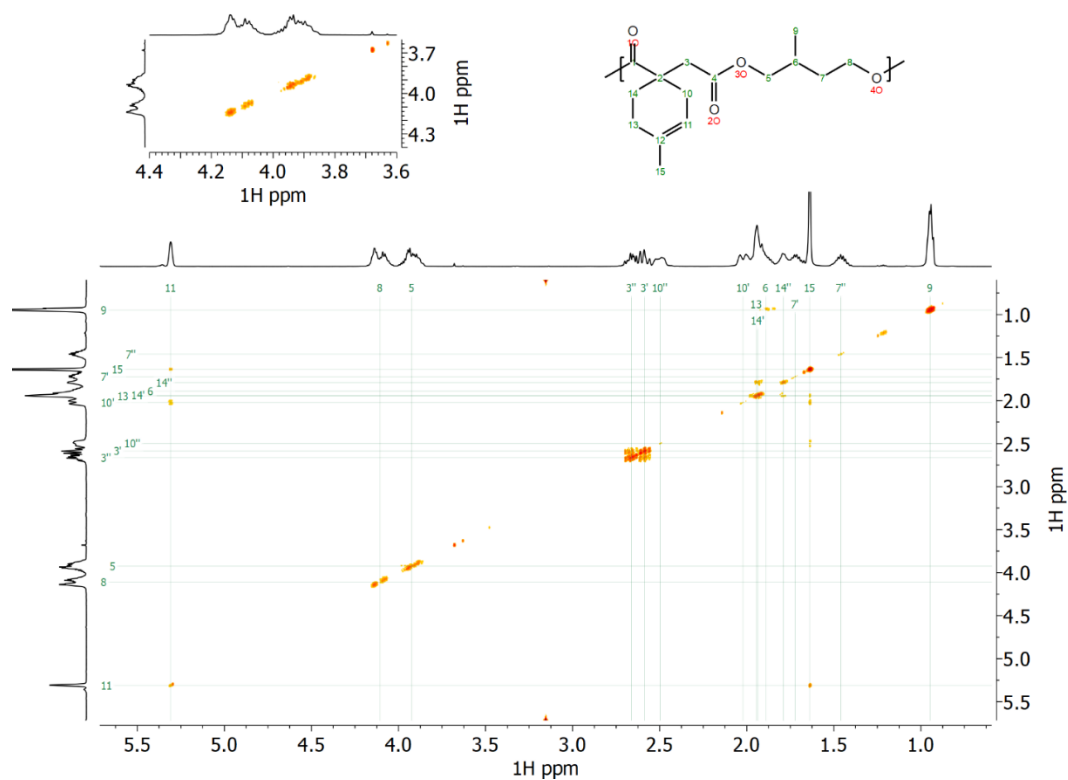


Figure S3.13. COSY spectrum of PMBCS in CDCl₃ with assignments. Insert in top-left depicts the cross-peaks associated with the methylene protons adjacent to the alcohols (carbons 5 and 8).

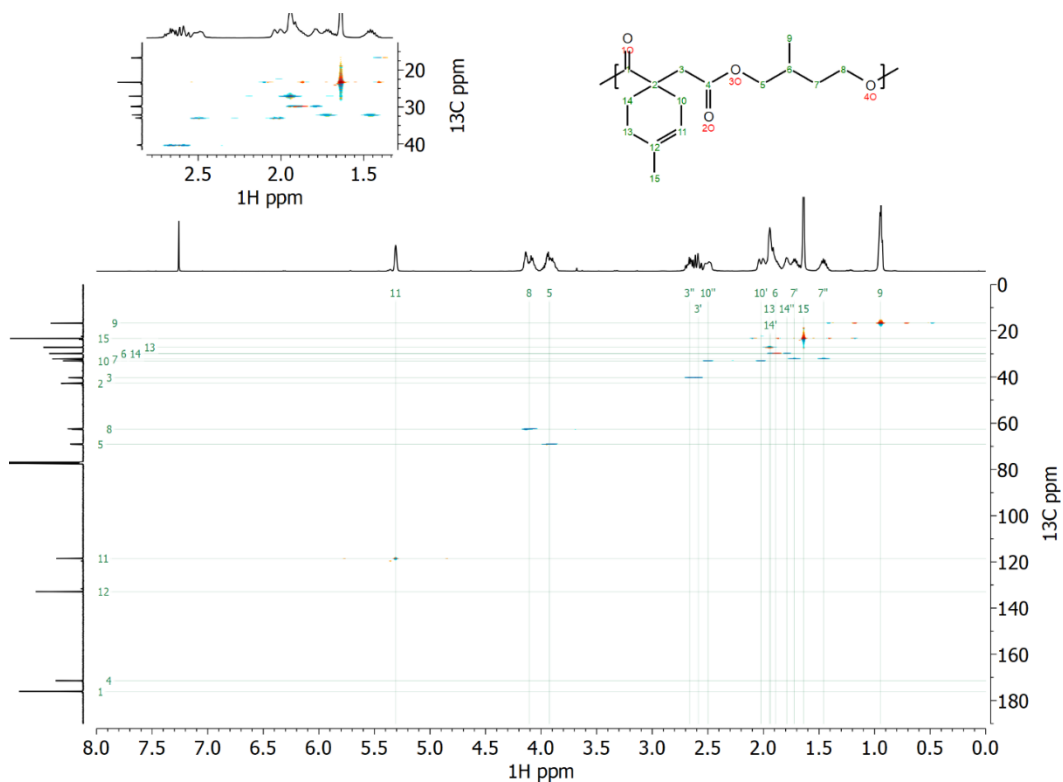


Figure S3.14. HSQC spectrum of PMBCS in CDCl₃ with assignments. Insert in top-left depicts the cross-peaks associated with the aliphatic protons not adjacent to the alcohols.

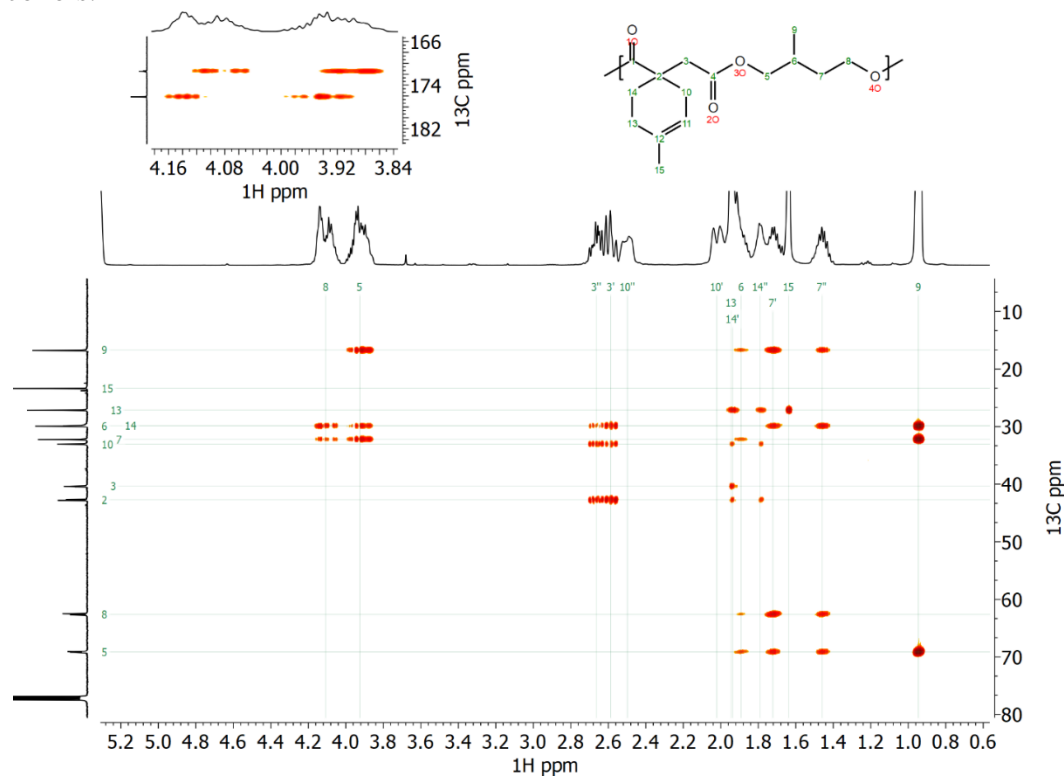


Figure S3.15. HMBC spectrum of PMBCS in CDCl₃ with assignments. Insert in top-left depicts the cross-peaks associated with the methylene protons adjacent to the alcohols (carbons 5 and 8).

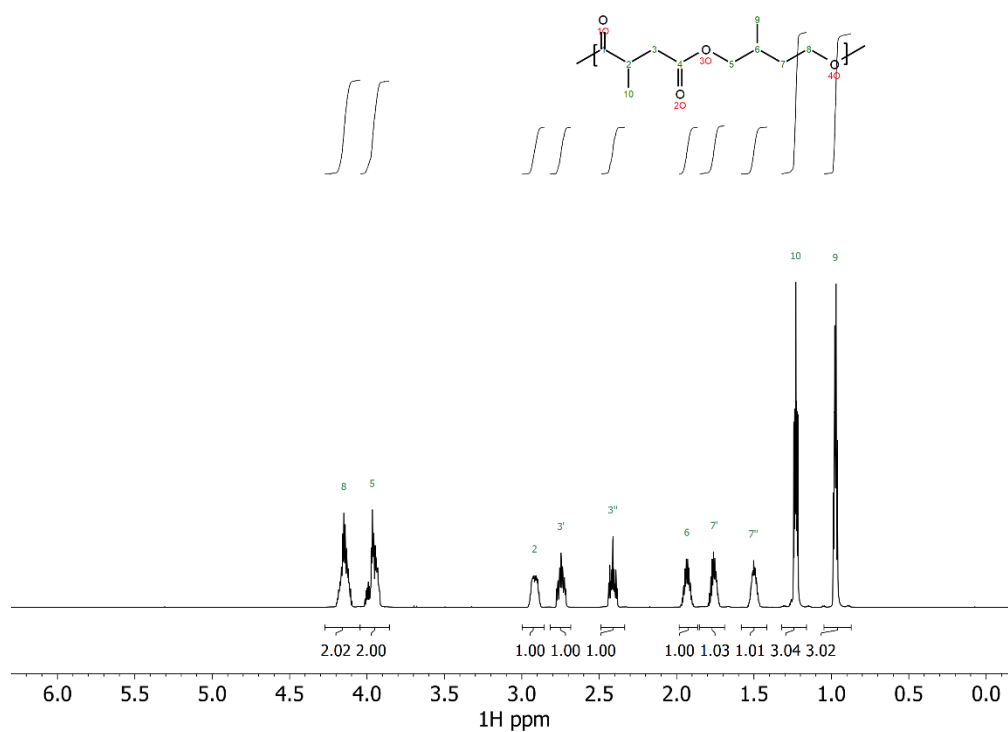


Figure S3.16. Quantitative ^1H NMR spectrum of PMBMS in CDCl_3 with assignments.

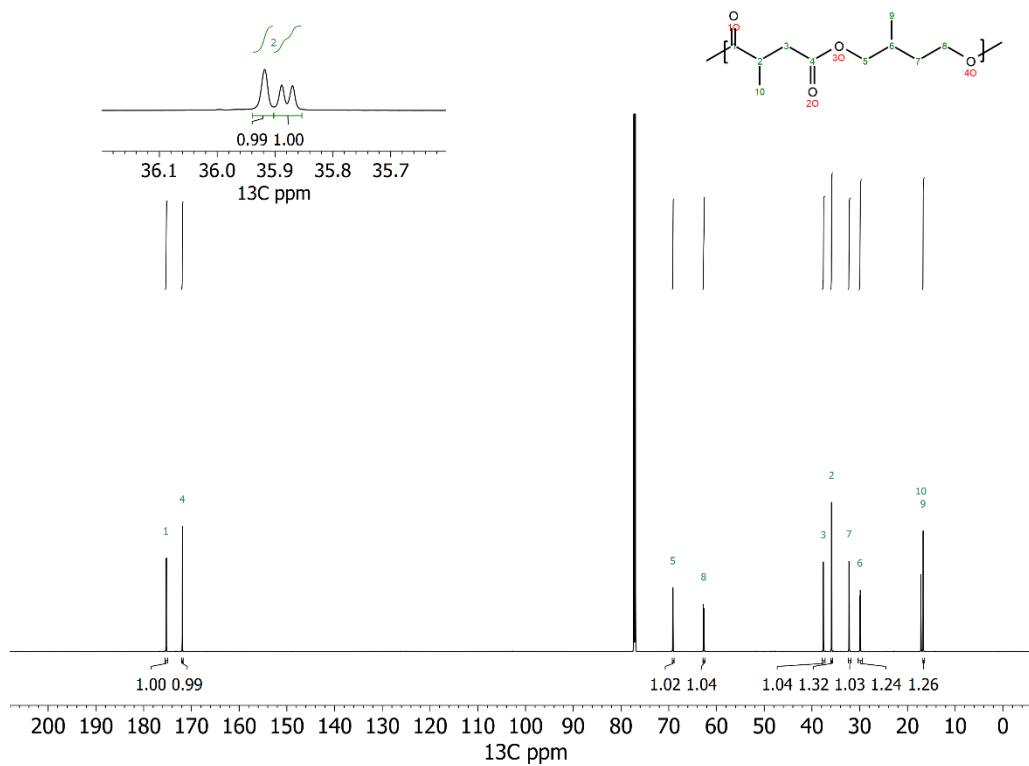


Figure S3.17. Quantitative ^{13}C NMR spectrum of PMBMS in CDCl_3 with assignments.

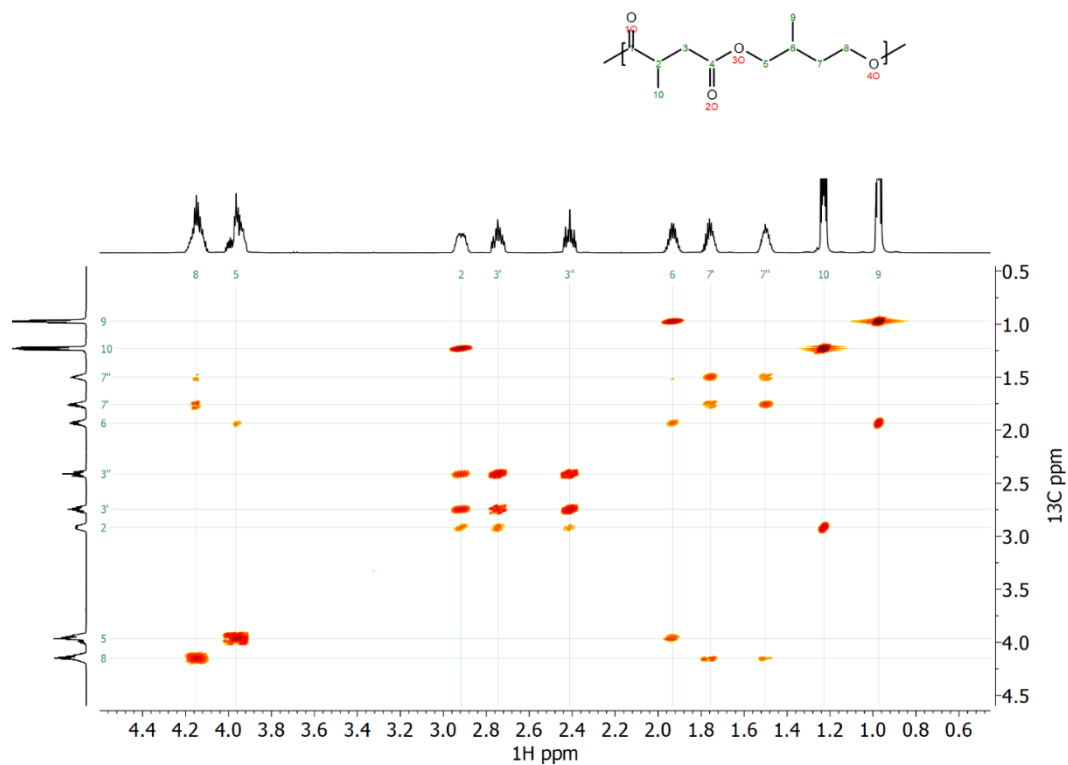


Figure S3.18. COSY spectrum of PMBMS in CDCl_3 with assignments.

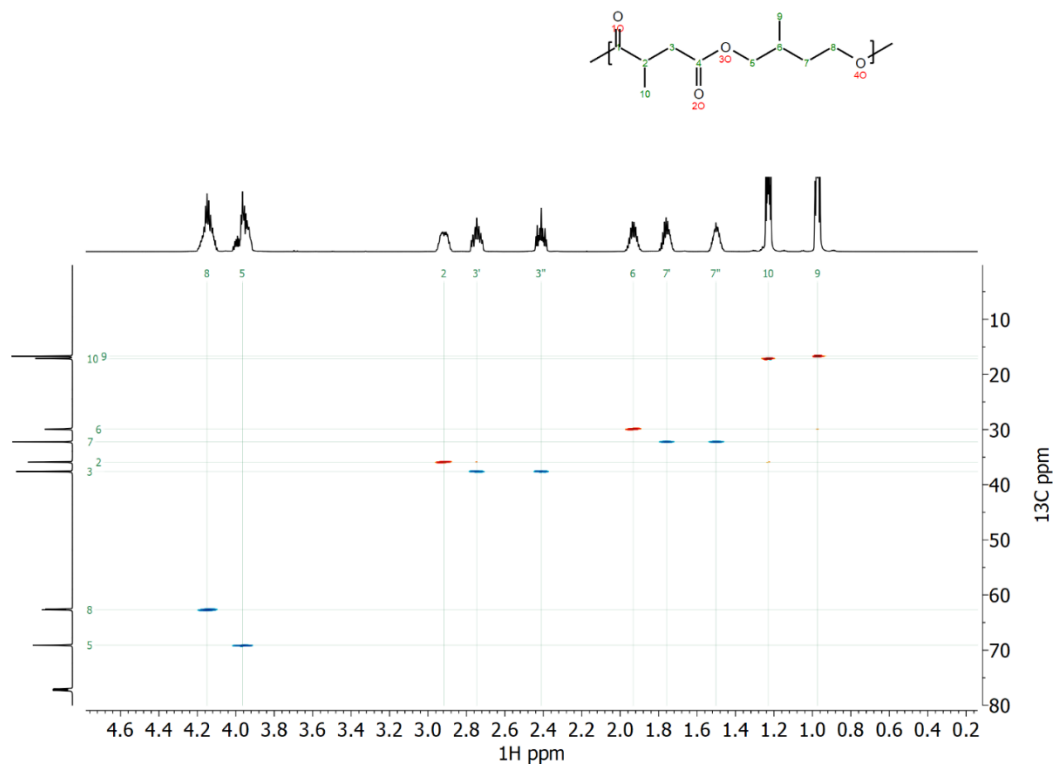


Figure S3.19. HSQC spectrum of PMBMS in CDCl_3 with assignments.

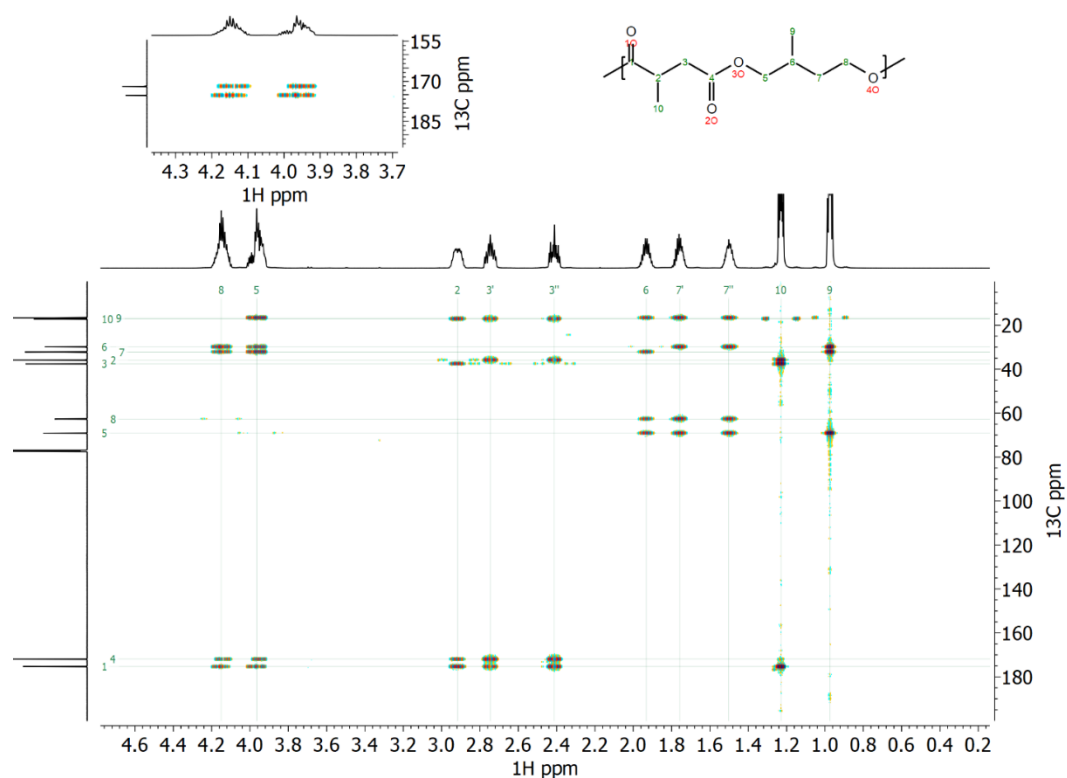


Figure S3.20. HMBC spectrum of PMBCS in CDCl₃. Insert in top-left depicts the cross-peaks associated with the methylene protons adjacent to the alcohols (carbons 5 and 8).

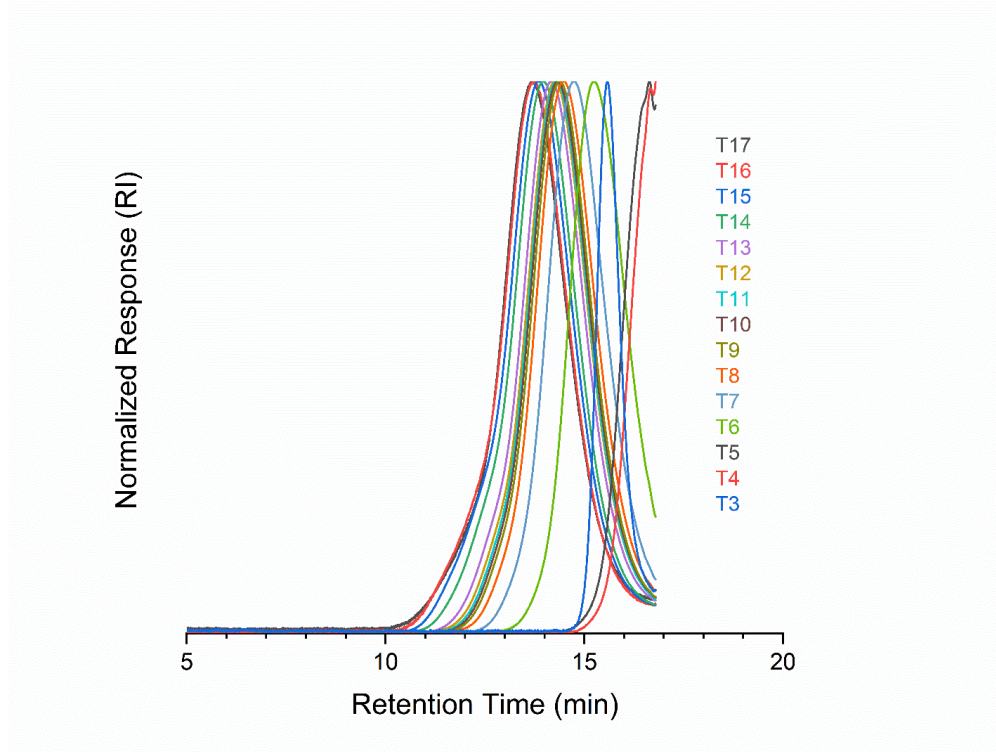


Figure S3.21. SEC results monitoring the polymerization of MB and MS as detected by RI (Table S3.1).

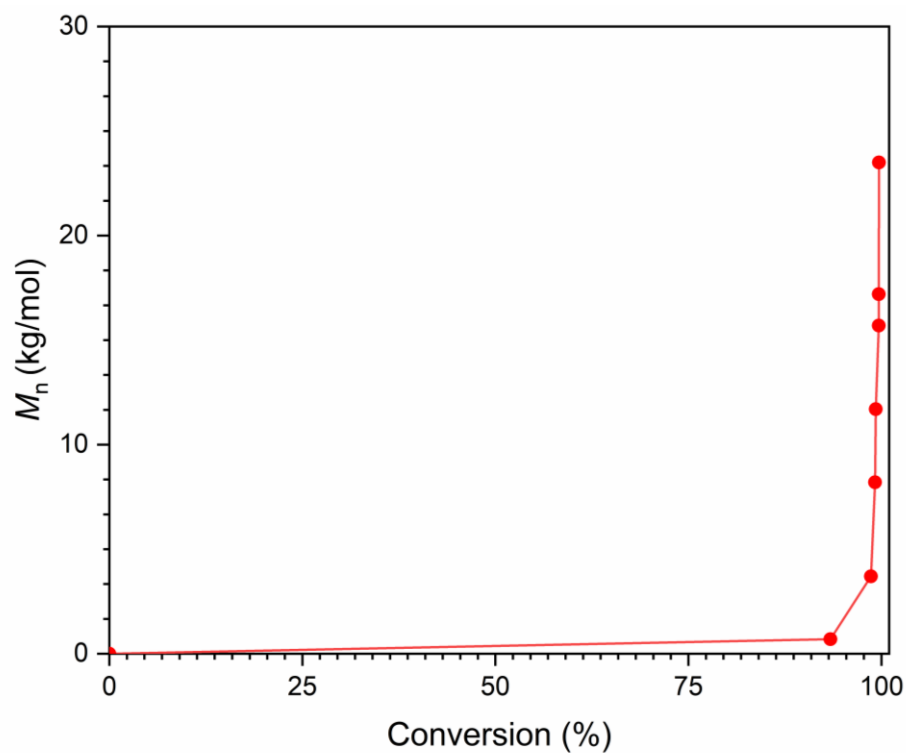


Figure S3.22. Plot of M_n vs conversion for the synthesis of PMBMS.

Table S3.1. Conversion (p), Degree of Polymerization ($1/(1-p)$), M_n , and \bar{D} as a Function of Time for PMBMS Synthesis

Condition	Timepoint t	Time (min)	p	RI		LS	
				M_n (kg/mol)	\bar{D}	M_n (kg/mol)	\bar{D}
T = 180 °C, P = 760 Torr	T0	0	2.5	0	-	0	-
	T1	30	33.9	0	-	0	-
	T2	60	59.1	0	-	0	-
	T3	90	72.2	1.3	1.16	0	-
	T4	150	80.2	2.6	1.30	0	-
	T5	215	84.2	1.5	1.28	0	-
T = 200 °C, P = 0.05 Torr	T6	231	96.5	3.8	1.81	0	-
	T7	241	97.9	6.2	2.09	5.4	2.02

T8	248	98.4	7.7	2.28	7.3	2.06
T9	253	98.6	8.6	2.38	8.8	2.09
T10	258	98.6	9.0	2.43	8.7	2.25
T11	264	98.7	9.3	2.48	9.2	2.24
T12	269	98.8	9.5	2.61	9.4	2.35
T13	279	98.9	10.3	2.68	10.9	2.39
T14	293	99.1	12.5	3.01	13.6	2.75
T15	309	99.2	14.4	3.22	16.0	2.98
T16	337	99.3	15.8	3.43	13.3	4.01
T17	362	99.3	15.3	3.72	14.8	3.29

Table S3.2. Tabulated Values for the Flory-Rehner Equation Estimation of Molar Mass Between Cross-Links (M_x)

F_{MBCS}	M_a (mg)	M_b (mg)	V_f	δ_1 (J/cm ³) ^{1/2}	χ	M_x (kg/mol)	Average M_x (kg/mol)
0.40 (1)	71.9	17.5	0.269			1.0	
0.40 (2)	38.8	11.9	0.336	18.9	0.385	0.6	0.8 ± 0.2 ($\pm 20\%$)
0.40 (3)	49.7	14.0	0.310			0.7	
0.29 (1)	170.6	34.1	0.222			1.42	
0.29 (2)	202.3	38.9	0.214	19.0	0.377	1.53	1.48 ± 0.05 ($\pm 3\%$)
0.29 (3)	195.1	38.1	0.217			1.49	
0.19 (1)	323.1	42.9	0.149			3.1	
0.19 (2)	321.4	42.3	0.148	19.1	0.370	3.2	3.0 ± 0.1 ($\pm 5\%$)
0.19 (3)	359.0	49.9	0.156			2.9	

Table S3.3. Gel Fractions and M_x Values Determined for the Thermosets from DMTA and Swell Test Results

Entry	F_{MBCS}	Gel Fraction	$M_{x,\text{DMTA}}$ (kg /mol)	$M_{x,\text{swell}}$ (kg /mol)
1	0.40	0.95 ± 0.07	1.4	0.8 ± 0.2
2	0.29	0.92 ± 0.01	3.2	1.5 ± 0.1
3	0.19	0.89 ± 0.01	6.3	3.0 ± 0.1

Table S3.4. Degradation (as Percentages of Initial Mass) Data for Thermoset ($F_{\text{MBCS}} = 0.19$) Degradation Experiments

Day	3 M HCl (% mass)	DI water (% mass)	3 M NaOH (% mass)
0	100	100	100
7	98.5 ± 0.2	100.0 ± 0.2	93 ± 5
14	98.2 ± 0.2	100.1 ± 0.6	90 ± 5
20	96.9 ± 0.9	99.7 ± 0.9	88 ± 5
29	97.3 ± 0.2	98.9 ± 0.7	82 ± 4

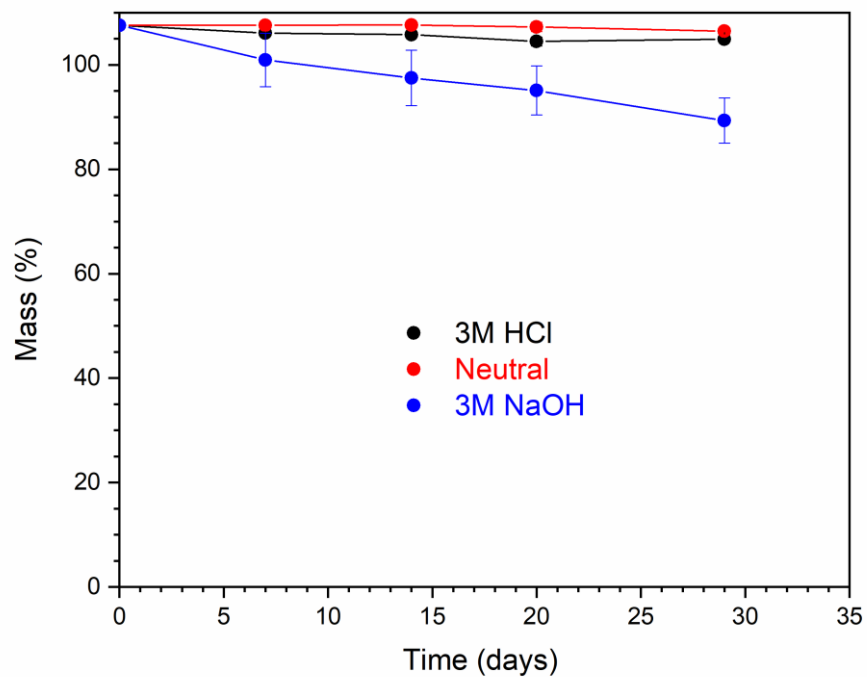


Figure S3.23. Graphical representation of data in Table S3.4.

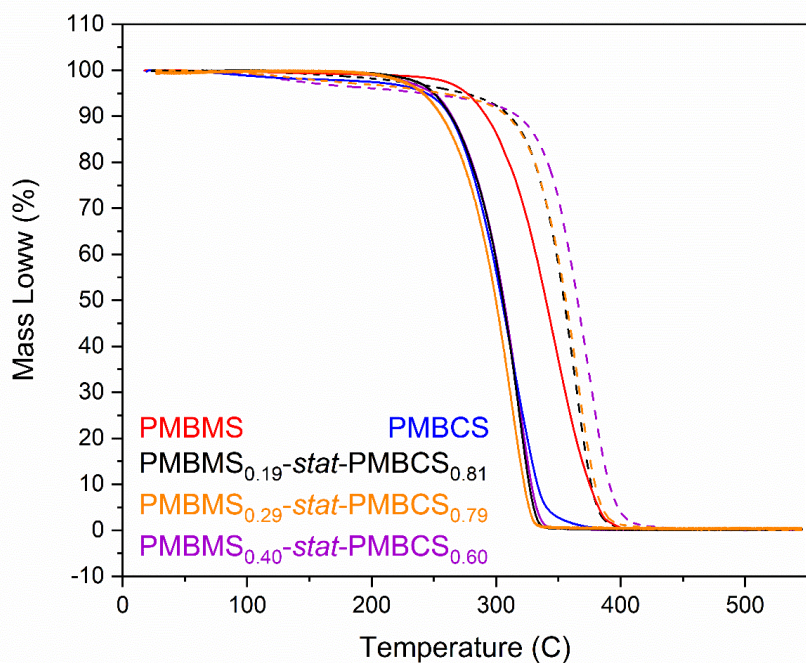


Figure S3.24. (a) Thermal gravimetric analysis mass loss (%) vs temperature (10 °C/min) traces of various prepolymers (solid lines) or cross-linked thermosets (dashed lines).

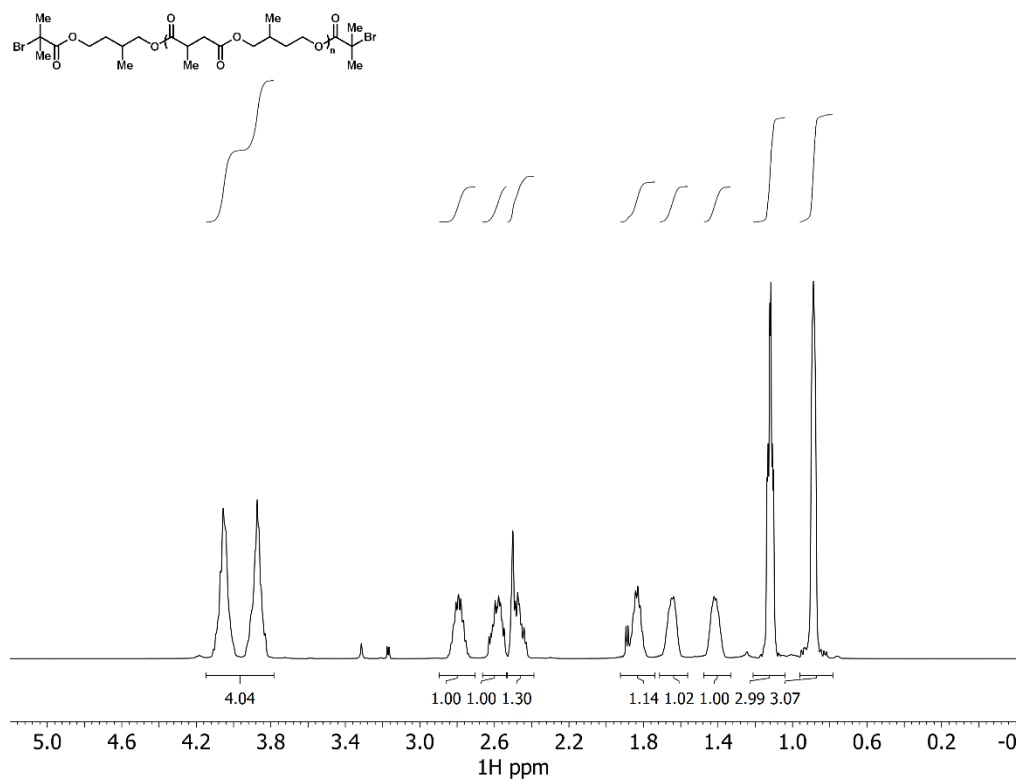


Figure S3.25. ¹H NMR spectra of Br-PMBMS-Br in DMSO-d₆.

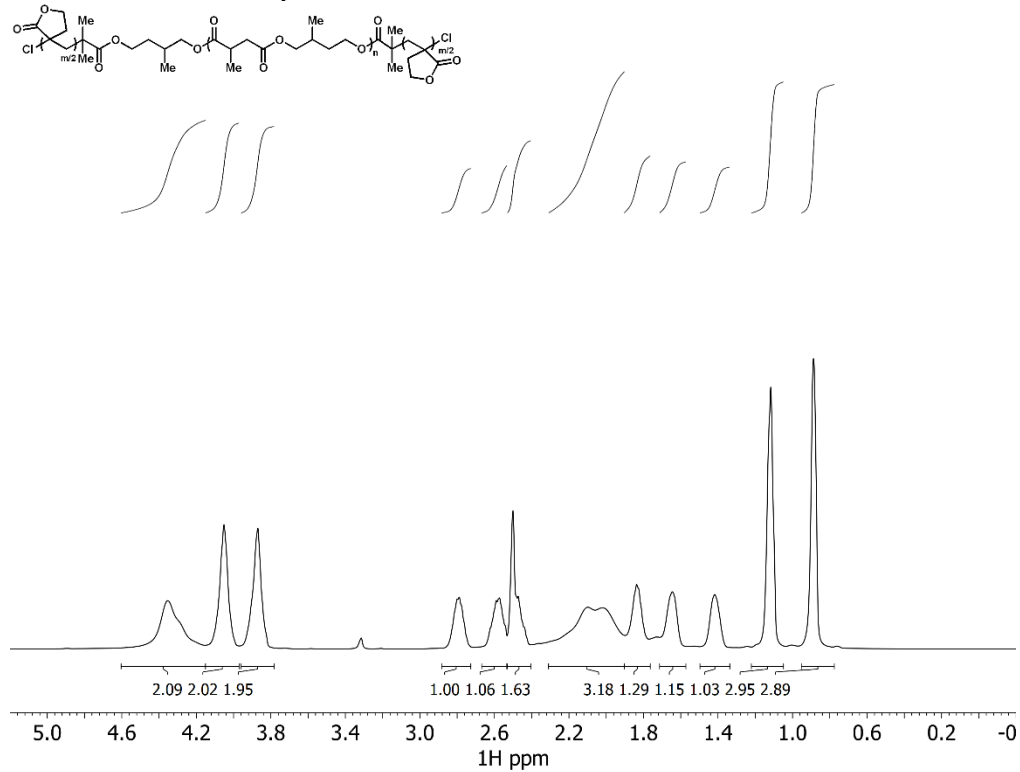


Figure S3.26. ¹H NMR spectra of PMBL-PMBMS-PMBL in DMSO-d₆.

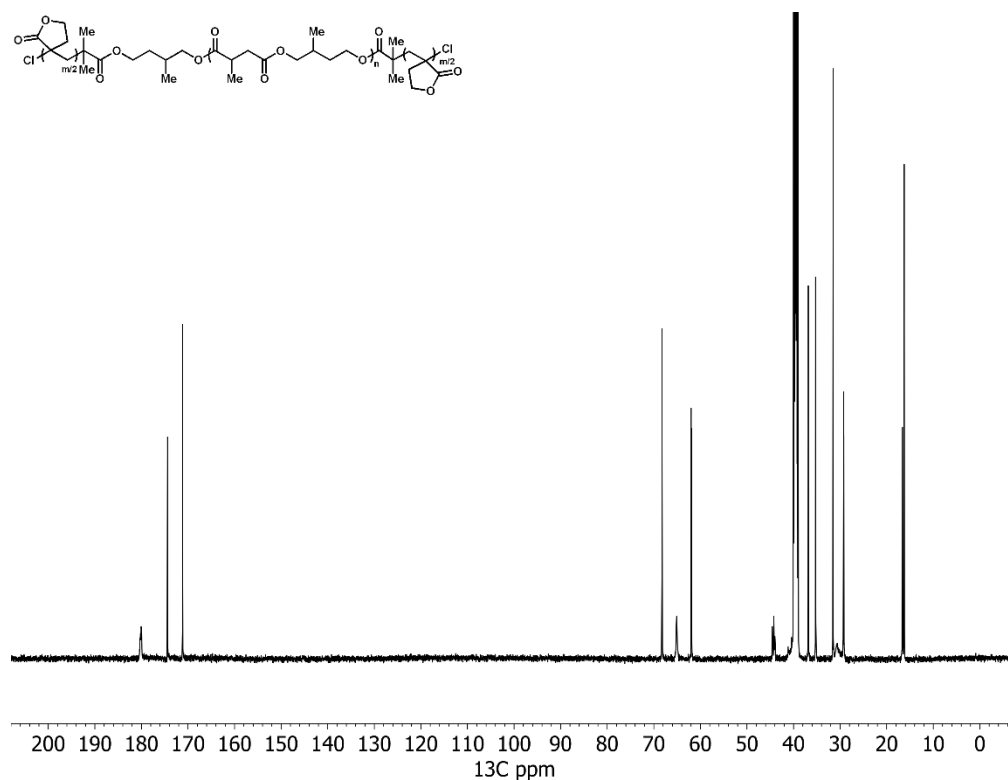


Figure S3.27. ^{13}C NMR spectra of PMBL-PMBMS-PMBL in DMSO-d_6 .

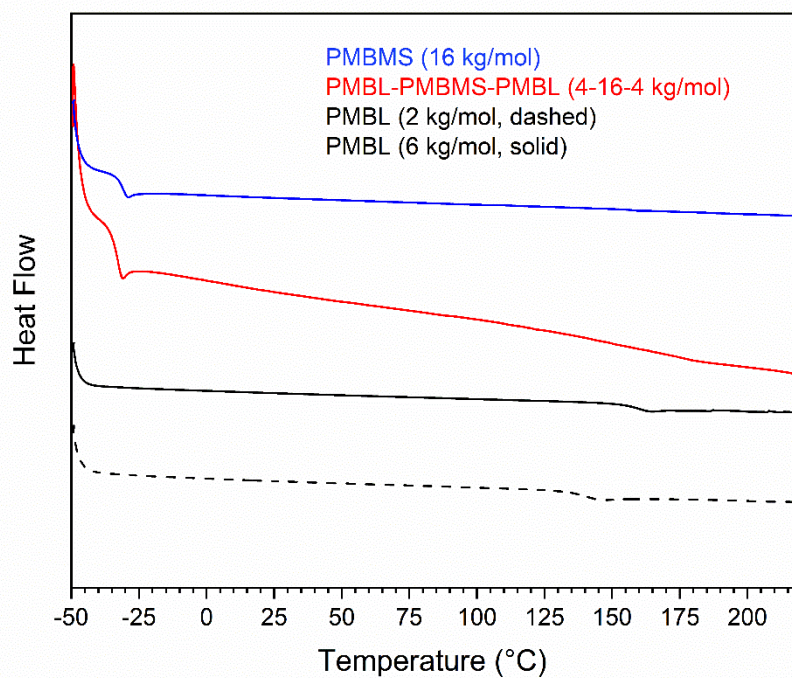


Figure S3.28. Differential scanning calorimetry heat flow vs temperature (30 $^{\circ}\text{C}/\text{min}$, second heat) traces of homo- or triblock polymers of PMBMS and PMBL, exo up.

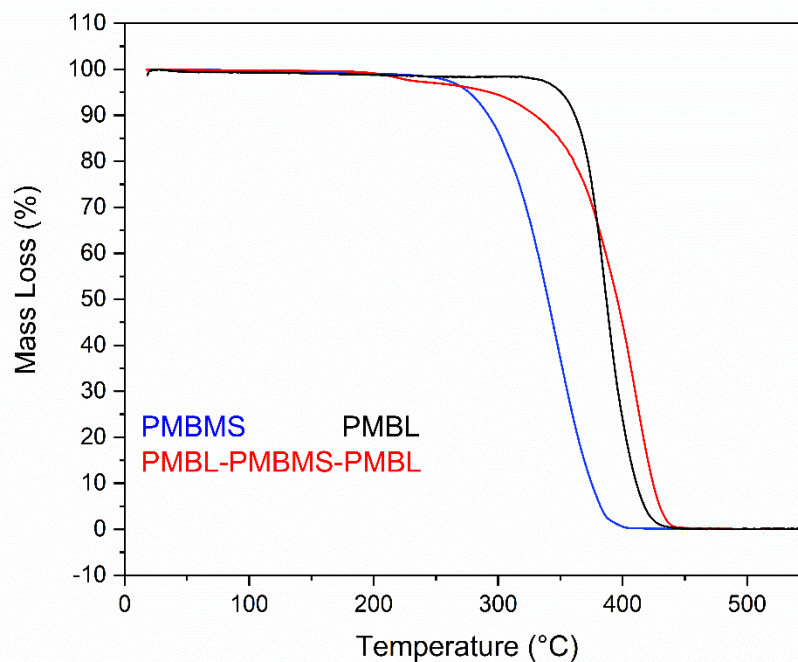


Figure S3.29. Thermal gravimetric analysis mass loss (%) vs temperature (10 °C/min for PMBMS, 30 °C/min for PMBL-PMBMS-PMBL or PMBL) traces of homo- or triblock polymers of PMBMS and PMBL.

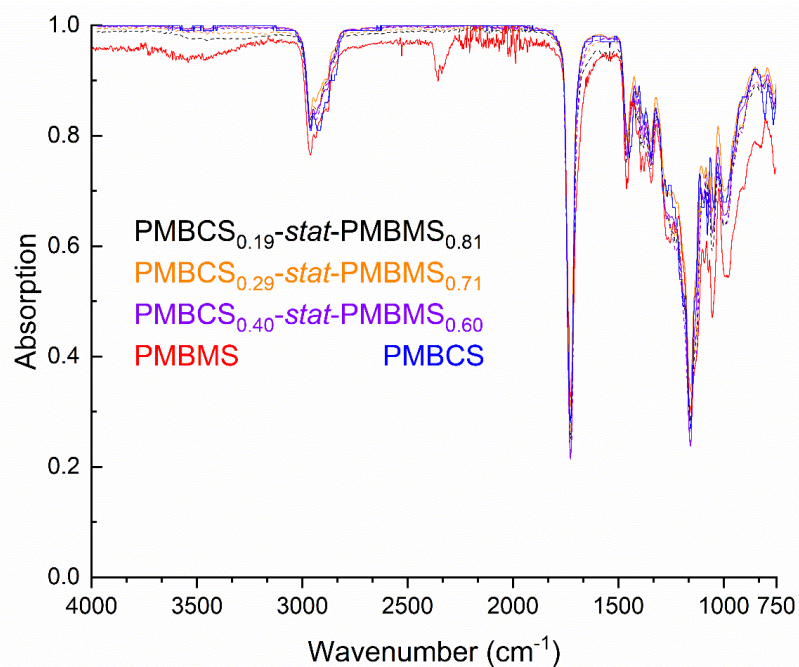


Figure S3.30. Superimposed infrared (IR) spectra of the PMBMS, PMBCS, and prepolymers (solid lines) or cross-linked thermosets (dashed lines).

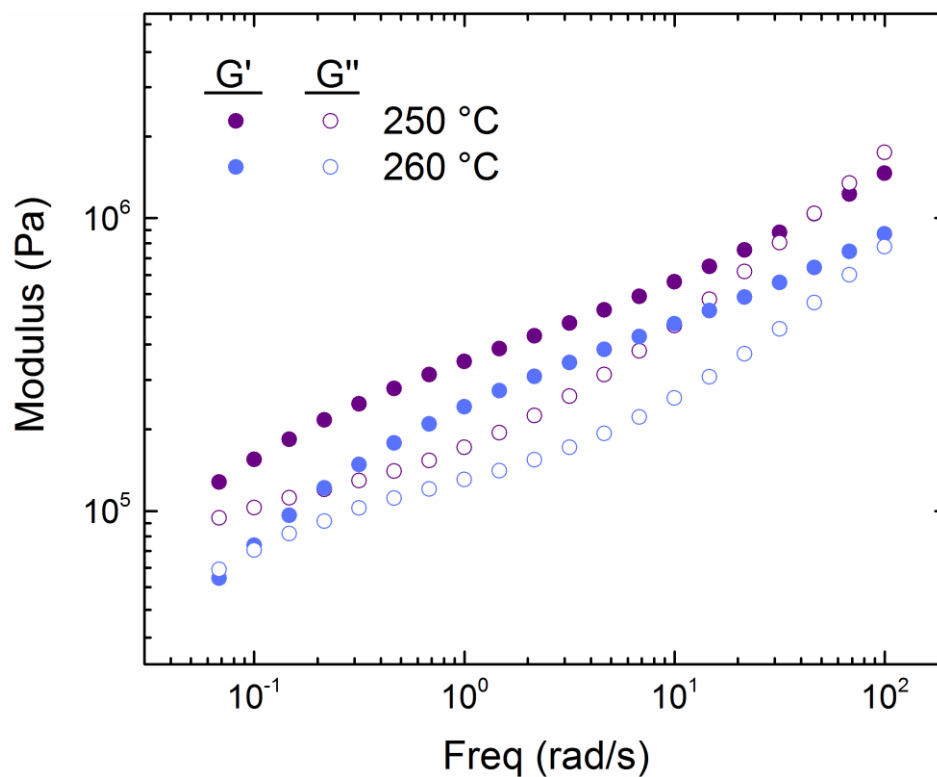


Figure S3.31. Dynamic frequency sweeps of PMBL, measuring the modulus as a function of frequency at 250 and 260 °C. PMBL degraded on the rheometer above 260 °C, and moduli vs frequency data was not acquired at higher temperatures. The plateau modulus, G_N , was roughly estimated to be 358820 Pa at the minimum $\tan(\delta)$ value ($M_e = 10.5$ kg/mol). The strain used in these experiments was 0.05%.

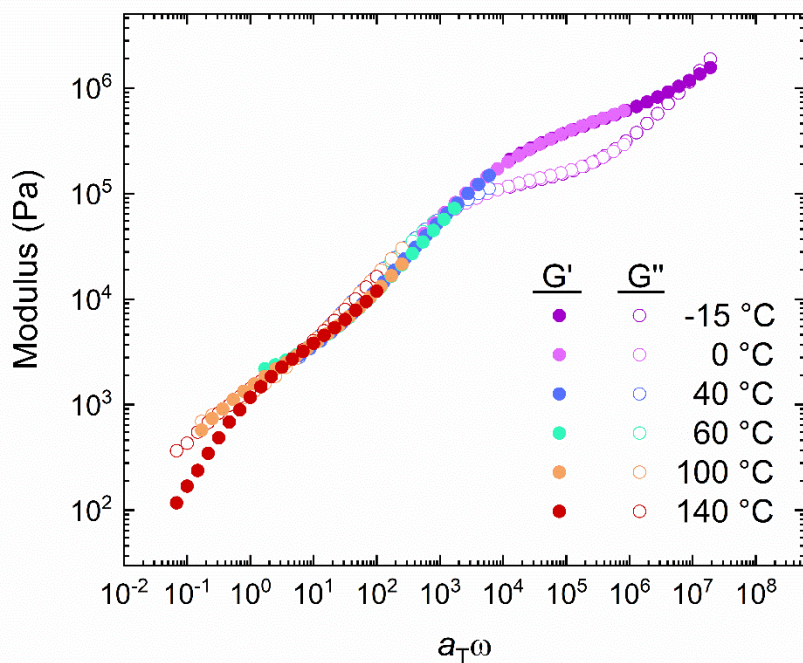


Figure S3.32. A master curve of PMBMS generated from applying shift factors (a_T) to dynamic frequency sweep data obtained at various temperatures. The plateau modulus, G_N , was roughly estimated to be 435000 Pa at the minimum $\tan(\delta)$ value ($M_e = 6.3$ kg/mol). The strain used in these experiments was 0.05%.

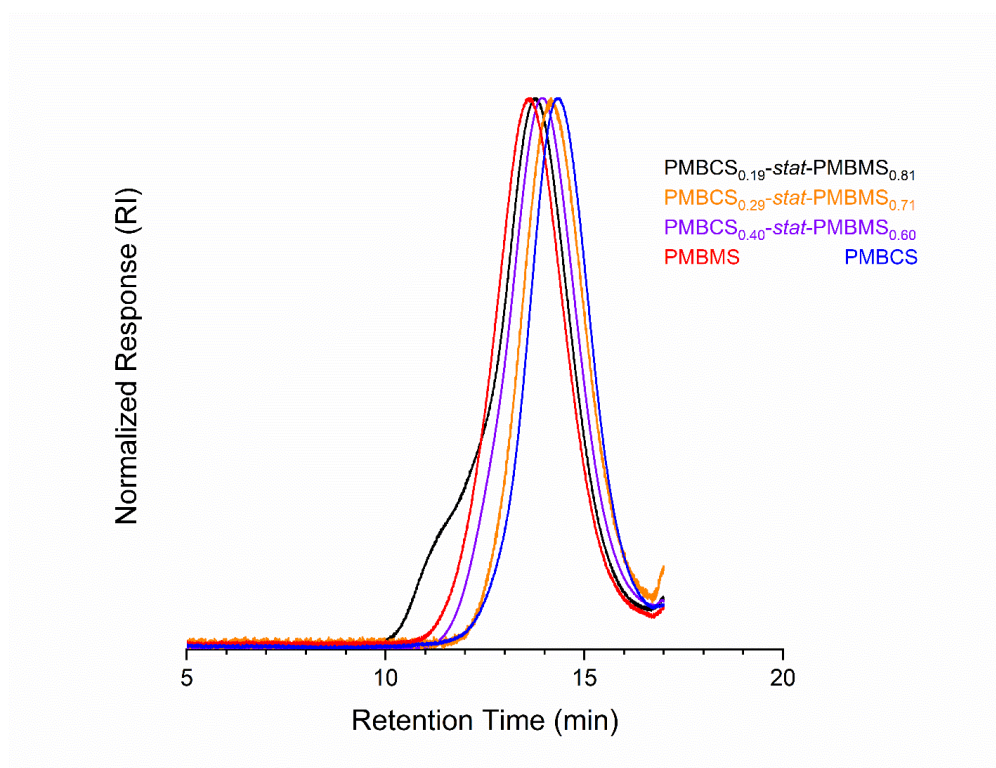


Figure S3.33. Size exclusion chromatography (SEC) traces for PMBMS, PMBCS, and PMBCS_x-stat-PMBMS_{1-x} statistical terpolymers that served as thermoset prepolymers.

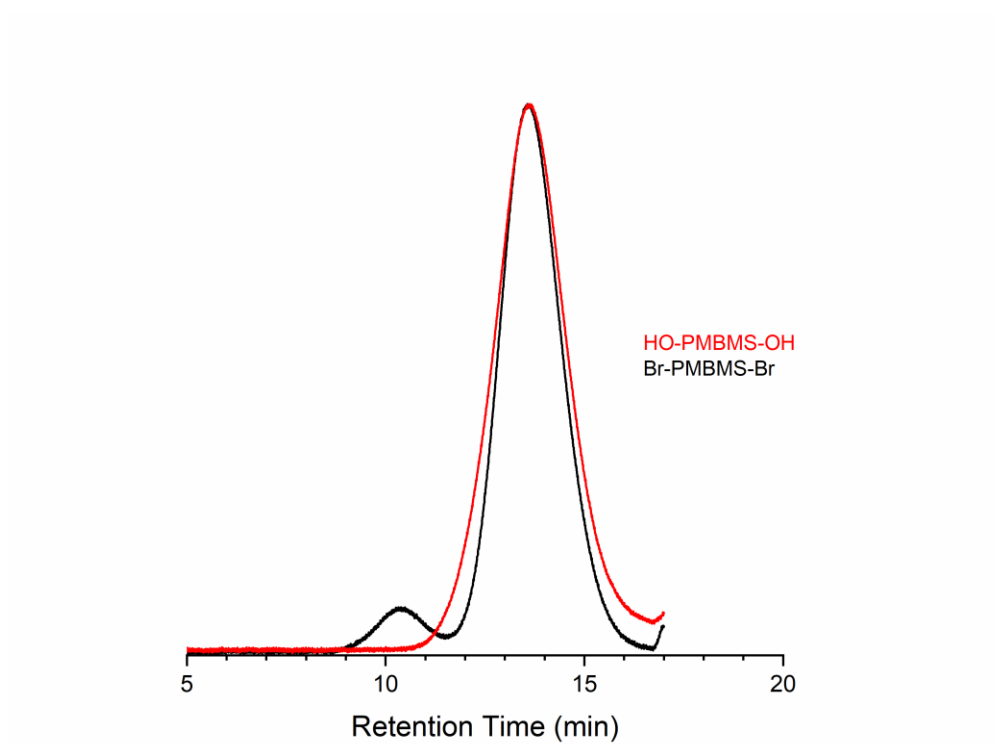


Figure S3.34. Size exclusion chromatography (SEC) for HO-PMBMS-OH (red) and Br-PMBMS-Br (black), indicating a high molar mass tail in Br-PMBMS-Br after HO-PMBMS-OH functionalization.

REFERENCES

- (1) Trotta, J.; Watts, A.; Wong, A.; LaPointe, A. M.; Hillmyer, M. A.; Fors, B. P. Renewable Thermosets and Thermoplastics from Itaconic Acid. *ACS Sustainable Chem. Eng.* **2018**, 7, 2691–2701.
- (2) Schneiderman, D. K.; Hillmyer, M. A. 50th Anniversary Perspective: There Is a Great Future in Sustainable Polymers. *Macromolecules* **2017**, 50, 3733–3749.
- (3) Garcia, J. M.; Robertson, M. L. The Future of Plastics Recycling. *Science* **2017**, 358, 870–872.
- (4) Hillmyer, M. A. The Promise of Plastics from Plants. *Science* **2017**, 358, 868–870.
- (5) Farmer, T. J.; Comerford, J. W.; Pellis, A.; Robert, T. Post-Polymerisation Modification of Bio-Based Polymers: Maximising the High Functionality of Polymers Derived from Biomass. *Polym. Int.* **2018**, 67, 775–789.
- (6) Auvergne, R.; Caillol, S.; David, G.; Boutevin, B.; Pascault, J.-P. Biobased Thermosetting Epoxy: Present and Future. *Chem. Rev.* **2014**, 114, 1082–1115.
- (7) Raquez, J. M.; Deléglise, M.; Lacrampe, M. F.; Krawczak, P. Thermosetting (Bio)Materials Derived from Renewable Resources: A Critical Review. *Prog. Polym. Sci.* **2010**, 35, 487–509.
- (8) De Hoe, G. X.; Zumstein, M. T.; Tiegs, B. J.; Brutman, J. P.; McNeill, K.;

- Sander, M.; Coates, G. W.; Hillmyer, M. A. Sustainable Polyester Elastomers from Lactones: Synthesis, Properties, and Enzymatic Hydrolyzability. *J. Am. Chem. Soc.* **2018**, *140*, 963–973.
- (9) Hillmyer, M. A.; Tolman, W. B. Aliphatic Polyester Block Polymers: Renewable, Degradable, and Sustainable. *Acc. Chem. Res.* **2014**, *47*, 2390–2396.
- (10) Shin, J.; Kim, Y. W.; Kim, G. J. Sustainable Block Copolymer-Based Thermoplastic Elastomers. *Appl. Chem. Eng.* **2014**, *25*, 121–133.
- (11) Watts, A.; Kurokawa, N.; Hillmyer, M. A. Strong, Resilient, and Sustainable Aliphatic Polyester Thermoplastic Elastomers. *Biomacromolecules* **2017**, *18*, 1845–1854.
- (12) Brutman, J. P.; Delgado, P. A.; Hillmyer, M. A. Polylactide Vitrimers. *ACS Macro Lett.* **2014**, *3*, 607–610.
- (13) Snyder, R. L.; Fortman, D. J.; De Hoe, G. X.; Hillmyer, M. A.; Dichtel, W. R. Reprocessable Acid-Degradable Polycarbonate Vitrimers. *Macromolecules* **2018**, *51*, 389–397.
- (14) Fortman, D. J.; Brutman, J. P.; Cramer, C. J.; Hillmyer, M. A.; Dichtel, W. R. Mechanically Activated, Catalyst-Free Polyhydroxyurethane Vitrimers. *J. Am. Chem. Soc.* **2015**, *137*, 14019–14022.
- (15) Ishibashi, J. S. A.; Kalow, J. A. Vitrimeric Silicone Elastomers Enabled by Dynamic Meldrum’s Acid-Derived Cross-Links. *ACS Macro Lett.* **2018**, *7*,

482–486.

- (16) Okabe, M.; Lies, D.; Kanamasa, S.; Park, E. Y. Biotechnological Production of Itaconic Acid and Its Biosynthesis in *Aspergillus Terreus*. *Appl. Microbiol. Biotechnol.* **2009**, *84*, 597–606.
- (17) Baup, S. Ueber Eine Neue Pyrogen-Citronensäure, Und Über Benennung Der Pyrogen-Säuren Überhaupt. *Ann. Pharm.* **1836**, *19*, 29–38.
- (18) Werpy, T.; Petersen, G.; Aden, A.; Bozell, J.; Holladay, J.; White, J.; Manheim, A. *Top Value Added Chemicals from Biomass Volume I — Results of Screening for Potential Candidates from Sugars and Synthesis Gas*; 2004.
- (19) Willke, T.; Vorlop, K.-D. Biotechnological Production of Itaconic Acid. *Appl. Microbiol. Biotechnol.* **2001**, *56*, 289–295.
- (20) Klement, T.; Büchs, J. Itaconic Acid - A Biotechnological Process in Change. *Bioresource Technol.* **2013**, *135*, 422–431.
- (21) ITACONIX, L. *Development of Integrated Production of Polyitaconic Acid from Northeast Hardwood Biomass*; 2009.
- (22) Marvel, C. S.; Shepherd, T. H. Polymerization Reactions of Itaconic Acid and Some of Its Derivatives. *J. Org. Chem.* **1959**, *24*, 599–605.
- (23) Fernández-García, M.; Fernández-Sanz, M.; De La Fuente, J. L.; Madruga, E. L. Atom-Transfer Radical Polymerization of Dimethyl Itaconate. *Macromol. Chem. Phys.* **2001**, *202*, 1213–1218.
- (24) Nagai, S.; Yoshida, K. Studies on Polymerization and Polymers of Itaconic

Acid Derivatives. IV. Polymerization of Itaconic Acid in Aqueous Solution.

Kobunshi Kagaku **1960**, *17*, 748–752.

- (25) Braun, V. D.; El Sayed, I. A. A. Über Die Struktur Der Polymeren Aus Itaconsäure. *Die Makromol. Chem.* **1966**, *96*, 100–121.
- (26) Tate, B. E. The Decarboxylation of Itaconic Acid Polymers. *Die Makromol. Chem.* **1967**, *209*, 176–193.
- (27) Askarov, M. A.; Semenova, L. N.; Babadzhanova, E. N. Properties of Some Synthetic Water-Soluble Polymers Based on Itaconic Acid. *Uzb. Khim. Zh.* **1968**, *12*, 38–40.
- (28) Nakamoto, H.; Ogo, Y.; Imoto, T. Polymerization of Itaconic Acid under High Pressure. *Die Makromol. Chem.* **1968**, *111*, 104–114.
- (29) Yokota, K.; Hirabayashi, T.; Takashima, T. The Preparation of Poly(Itaconic Acid). *Die Makromol. Chem.* **1975**, *176*, 1197–1205.
- (30) Grespos, E.; Hill, D. J. T.; Donnelly, J. H. O.; Sullivan, P. W. O.; Young, T. L.; East, G. C.; Zvin, K. J. Polymerization of Itaconic Acid in Aqueous Solution: Structure of the Polymer and Polymerization Kinetics at 25 °C, Studied by ¹³C NMR. *Makromol. Chem., Rapid Commun.* **1984**, *5*, 489–494.
- (31) Veličković, J.; Filipović, J.; Djakov, D. P. The Synthesis and Characterization of Poly(Itaconic) Acid. *Polym. Bull.* **1994**, *32*, 169–172.
- (32) Mao, Z.; Yang, C. Q. Polymeric Multifunctional Carboxylic Acids as Crosslinking Agents for Cotton Cellulose: Poly(Itaconic Acid) and In Situ

- Polymerization of Itaconic Acid. *J. Appl. Polym. Sci.* **2001**, 79, 319–326.
- (33) Lárez, C.; Canelón, F.; Millán, E.; Perdomo, G.; Katime, I. New Results on the Polymerisation of the Itaconic Acid in Aqueous Medium. *Polym. Bull.* **2002**, 49, 119–126.
- (34) Stawski, D.; Połowiński, S. Polymerization of Itaconic Acid. *Polimery* **2005**, 50, 118–122.
- (35) Połowiński, S. Study of Poly(Itaconic Acid) in Aqueous Solutions. *Polimery* **2006**, 51, 270–275.
- (36) Bednarz, S.; Błaszczuk, A.; Błazejewska, D.; Bogdał, D. Free-Radical Polymerization of Itaconic Acid in the Presence of Choline Salts: Mechanism of Persulfate Decomposition. *Catal. Today* **2015**, 257, 297–304.
- (37) Hirano, T.; Takeyoshi, R.; Seno, M.; Sato, T. Chain-Transfer Reaction in the Radical Polymerization of Di-n-Butyl Itaconate at High Temperatures. *J. Polym. Sci., Part A: Polym. Chem.* **2002**, 40, 2415–2426.
- (38) Szablan, Z.; Toy, A. A.; Davis, T. P.; Hao, X.; Stenzel, M. H.; Barner-Kowollik, C. Reversible Addition Fragmentation Chain Transfer Polymerization of Sterically Hindered Monomers: Toward Well-Defined Rod/Coil Architectures. *J. Polym. Sci., Part A: Polym. Chem.* **2004**, 42, 2432–2443.
- (39) Szablan, Z.; Toy, A. A.; Terrenoire, A.; Davis, T. P.; Stenzel, M. H.; Müller, A. H. E.; Barner-Kowollik, C. Living Free-Radical Polymerization of Sterically

Hindered Monomers: Improving the Understanding of 1,1-Disubstituted Monomer Systems. *J. Polym. Sci., Part A: Polym. Chem.* **2006**, *44*, 3692–3710.

- (40) Satoh, K.; Lee, D. H.; Nagai, K.; Kamigaito, M. Precision Synthesis of Bio-Based Acrylic Thermoplastic Elastomer by RAFT Polymerization of Itaconic Acid Derivatives. *Macromol. Rapid Commun.* **2014**, *35*, 161–167.
- (41) Kumar, S.; Krishnan, S.; Samal, S. K.; Mohanty, S.; Nayak, S. K. Itaconic Acid Used as a Versatile Building Block for the Synthesis of Renewable Resource-Based Resins and Polyesters for Future Prospective: A Review. *Polym. Int.* **2017**, *66*, 1349–1363.
- (42) Robert, T.; Friebe, S. Itaconic Acid – a Versatile Building Block for Renewable Polyesters with Enhanced Functionality. *Green Chem.* **2016**, *18*, 2922–2934.
- (43) Barrett, D. G.; Merkel, T. J.; Luft, J. C.; Yousaf, M. N. One-Step Syntheses of Photocurable Polyesters Based on a Renewable Resource. *Macromolecules* **2010**, *43*, 9660–9667.
- (44) Dai, J.; Ma, S.; Wu, Y.; Han, L.; Zhang, L.; Zhu, J.; Liu, X. Polyesters Derived from Itaconic Acid for the Properties and Bio-Based Content Enhancement of Soybean Oil-Based Thermosets. *Green Chem.* **2015**, *17*, 2383–2392.
- (45) Wei, T.; Lei, L.; Kang, H.; Qiao, B.; Wang, Z.; Zhang, L.; Coates, P.; Hua, K. C.; Kulig, J. Tough Bio-Based Elastomer Nanocomposites with High Performance for Engineering Applications. *Adv. Eng. Mater.* **2012**, *14*, 112–118.

- (46) Lei, W.; Qiao, H.; Zhou, X.; Wang, W.; Zhang, L.; Wang, R.; Hua, K. C. Synthesis and Evaluation of Bio-Based Elastomer Based on Diethyl Itaconate for Oil-Resistance Applications. *Sci. China: Chem.* **2016**, *59*, 1376–1383.
- (47) Lei, W.; Russell, T. P.; Hu, L.; Zhou, X.; Qiao, H.; Wang, W.; Wang, R.; Zhang, L. Pendant Chain Effect on the Synthesis, Characterization, and Structure-Property Relations of Poly(Di-n-Alkyl Itaconate-Co-Isoprene) Biobased Elastomers. *ACS Sustainable Chem. Eng.* **2017**, *5*, 5214–5223.
- (48) Qiao, H.; Wang, R.; Yao, H.; Zhou, X.; Lei, W.; Hu, X.; Zhang, L. Preparation of Graphene Oxide/Bio-Based Elastomer Nanocomposites through Polymer Design and Interface Tailoring. *Polym. Chem.* **2015**, *6*, 6140–6151.
- (49) Zhou, X.; Zhang, Q.; Wang, R.; Guo, B.; Lvov, Y.; Hu, G. H.; Zhang, L. Preparation and Performance of Bio-Based Carboxylic Elastomer/Halloysite Nanotubes Nanocomposites with Strong Interfacial Interaction. *Compos. Part A* **2017**, *102*, 253–262.
- (50) Qiao, H.; Xu, W.; Chao, M.; Liu, J.; Lei, W.; Zhou, X.; Wang, R.; Zhang, L. Preparation and Performance of Silica/Epoxy Group-Functionalized Biobased Elastomer Nanocomposite. *Ind. Eng. Chem. Res.* **2017**, *56*, 881–889.
- (51) Dai, J.; Ma, S.; Teng, N.; Dai, X.; Shen, X.; Wang, S.; Liu, X.; Zhu, J. 2,5-Furandicarboxylic Acid- and Itaconic Acid-Derived Fully Biobased Unsaturated Polyesters and Their Cross-Linked Networks. *Ind. Eng. Chem. Res.* **2017**, *56*, 2650–2657.
- (52) Lv, A.; Li, Z.-L.; Du, F.-S.; Li, Z.-C. Synthesis, Functionalization, and

- Controlled Degradation of High Molecular Weight Polyester from Itaconic Acid via ADMET Polymerization. *Macromolecules* **2014**, *47*, 7707–7716.
- (53) Winkler, M.; Lacerda, T. M.; Mack, F.; Meier, M. A. R. Renewable Polymers from Itaconic Acid by Polycondensation and Ring-Opening-Metathesis Polymerization. *Macromolecules* **2015**, *48*, 1398–1403.
- (54) Agarwal, S.; Jin, Q.; Maji, S. Biobased Polymers from Plant-Derived Tulipalin A. *ACS Symp. Ser.* **2012**, *1105*, 197–212.
- (55) Ali, M. A.; Tateyama, S.; Oka, Y.; Kaneko, D.; Okajima, M. K.; Kaneko, T. Syntheses of High-Performance Biopolyamides Derived from Itaconic Acid and Their Environmental Corrosion. *Macromolecules* **2013**, *46*, 3719–3725.
- (56) Wang, Y.; Xu, S.; Hoye, T. R. Poly(α -Methyleneglutarimide)s from Radical Polymerization of α -Methyleneglutarimides. *J. Polym. Sci. Part A Polym. Chem.* **2018**, *56*, 1020–1026.
- (57) Trotta, J. T.; Jin, M.; Stawiasz, K. J.; Michaudel, Q.; Chen, W.-L.; Fors, B. P. Synthesis of Methylene Butyrolactone Polymers from Itaconic Acid. *J. Polym. Sci., Part A: Polym. Chem.* **2017**, *55*, 2730–2737.
- (58) Hargrave, J. D.; Herbert, J.; Bish, G.; Frost, C. G. Rhodium-Catalysed Addition of Organotrialkoxysilanes to Alpha-Substituted Acrylic Esters. *Org. Biomol. Chem.* **2006**, *4*, 3235–3241.
- (59) Wu, L.; Mascal, M.; Farmer, T. J.; Arnaud, S. P.; Wong Chang, M. A. Electrochemical Coupling of Biomass-Derived Acids: New C8 Platforms for

Renewable Polymers and Fuels. *ChemSusChem* **2017**, *10*, 166–170.

- (60) Achiwa, K. The Mechanism of Asymmetric Hydrogenation Catalysed by Rhodium Complexes of Chiral Pyrrolidinobiphosphines. *J. Organomet. Chem.* **1981**, *218*, 249–260.
- (61) vom Stein, T.; Meuresch, M.; Limper, D.; Schmitz, M.; Hölscher, M.; Coetzee, J.; Cole-Hamilton, D. J.; Klankermayer, J.; Leitner, W. Highly Versatile Catalytic Hydrogenation of Carboxylic and Carbonic Acid Derivatives Using a Ru-Triphos Complex: Molecular Control over Selectivity and Substrate Scope. *J. Am. Chem. Soc.* **2014**, *136*, 13217–13225.
- (62) Liu, X.; Wang, X.; Liu, Q.; Xu, G.; Li, X.; Mu, X. A Sustainable Process for the Production of 2-Methyl-1,4-Butanediol by Hydrogenation of Biomass-Derived Itaconic Acid. *Catal. Today* **2016**, *274*, 88–93.
- (63) Spanjers, C. S.; Schneiderman, D. K.; Wang, J. Z.; Wang, J.; Hillmyer, M. A.; Zhang, K.; Dauenhauer, P. J. Branched Diol Monomers from the Sequential Hydrogenation of Renewable Carboxylic Acids. *ChemCatChem* **2016**, *8*, 3031–3035.
- (64) Petty, J. D.; Huckins, J. N.; David, A. Novel Ruthenium Carbonyl Complex Having Tridentate Ligand, Its Production Method and Use. U. S. Patent 0,237,814, 2011.
- (65) Fairweather, N. T.; Gibson, M. S.; Guan, H. Homogeneous Hydrogenation of Fatty Acid Methyl Esters and Natural Oils under Neat Conditions. *Organometallics* **2015**, *34*, 335–339.

- (66) Retuert, J.; Yazdani-Pedram, M.; Martinez, F.; Jeria, M. Soluble Itaconic Acid-Ethylene Glycol Polyesters. *Bull. Chem. Soc. Jpn.* **1993**, *66*, 1707–1708.
- (67) Shiraishi, S.; Sato, R. Preparation of Aliphatic Tetracarboxylic Acid and Its Anhydrides. J.P. 07,069,971, 1995.
- (68) Kacan, M.; Karabulut, H. R. F. Diels-Alder Reactions Using 5 M LiClO₄-Diethyl Ether. *Turk. J. Chem.* **2002**, *26*, 251–254.
- (69) Abdelrahman, O. A.; Park, D. S.; Vinter, K. P.; Spanjers, C. S.; Ren, L.; Cho, H. J.; Zhang, K.; Fan, W.; Tsapatsis, M.; Dauenhauer, P. J. Renewable Isoprene by Sequential Hydrogenation of Itaconic Acid and Dehydro-Decyclization of 3-Methyl-Tetrahydrofuran. *ACS Catal.* **2017**, *7*, 1428–1431.
- (70) Kato, J.; Seo, A.; Kiso, K.; Kudo, K.; Shiraishi, S. Synthesis of 2,8-Dioxaspiro[4.5]Decane-1,3,7,9-Tetrone and the Reactions with Amines. *Bull. Chem. Soc. Jpn.* **1999**, *72*, 1075–1081.
- (71) Westwell, A. D.; Williams, J. M. J. Auxiliary Accelerated Reactions: Transition-Metal Promoted Diels-Alder Cycloadditions. *J. Chem. Soc., Chem. Commun.* **1994**, 2501–2502.
- (72) Shiramizu, M.; Toste, F. D. On the Diels-Alder Approach to Solely Biomass-Derived Polyethylene Terephthalate (PET): Conversion of 2,5-Dimethylfuran and Scrolein into p-Xylene. *Chem. - A Eur. J.* **2011**, *17*, 12452–12457.
- (73) Inai, Y.; Hirabayashi, T. Synthesis of Aliphatic Polyesters by Direct Polyesterification of Dicarboxylic Acids with Diols under Mild Conditions

- Catalyzed by Reusable Rare-Earth Triflate. *Macromolecules* **2003**, *36*, 1772–1774.
- (74) Thiele, U. K. The Current Status of Catalysis and Catalyst Development for the Industrial Process of Poly(Ethylene Terephthalate) Polycondensation. *Int. J. Polym. Mater.* **2001**, *50*, 387–394.
- (75) Thiagarajan, S.; Vogelzang, W.; J. I. Knoop, R.; Frissen, A. E.; van Haveren, J.; van Es, D. S. Biobased Furandicarboxylic Acids (FDCAs): Effects of Isomeric Substitution on Polyester Synthesis and Properties. *Green Chem.* **2014**, *16*, 1957–1966.
- (76) Bikiaris, D. N.; Achilias, D. S. Synthesis of Poly(Alkylene Succinate) Biodegradable Polyesters, Part II: Mathematical Modelling of the Polycondensation Reaction. *Polymer* **2008**, *49*, 3677–3685.
- (77) Odian, G. *Principles of Polymerization*; Wiley: New York, 2004.
- (78) Lavilla, C.; Alla, A.; de Ilarduya, A. M.; Muñoz-Guerra, S. High Tg Bio-Based Aliphatic Polyesters from Bicyclic D-Mannitol. *Biomacromolecules* **2013**, *14*, 781–793.
- (79) Lowe, A. B. Thiol-Ene “Click” Reactions and Recent Applications in Polymer and Materials Synthesis: A First Update. *Polym. Chem.* **2010**, *1*, 17–36.
- (80) Hoyle, C. E.; Bowman, C. N. Thiol-Ene Click Chemistry. *Angew. Chem. Int. Ed.* **2010**, *49*, 1540–1573.
- (81) Tang, X.; Hong, M.; Falivene, L.; Caporaso, L.; Cavallo, L.; Chen, E. Y.-X.

The Quest for Converting Biorenewable Bifunctional α -Methylene- γ -Butyrolactone into Degradable and Recyclable Polyester: Controlling Vinyl-Addition/Ring-Opening/Cross-Linking Pathways. *J. Am. Chem. Soc.* **2016**, *138*, 14326–14337.

- (82) Fleischmann, C.; Gopez, J.; Lundberg, P.; Ritter, H.; Killops, K. L.; Hawker, C. J.; Klinger, D. A Robust Platform for Functional Microgels via Thiol-Ene Achemistry with Reactive Polyether-Based Nanoparticles. *Polym. Chem.* **2015**, *6*, 2029–2037.
- (83) VoxtarTM Pure advantage https://www.perstorp.com/products/voxtar_m100.
- (84) Song, J.; Chen, L.; Wang, Y.; Chen, W.; Wang, R. Kinetics of UV Curable Alkyl 3-Mercaptopropionate-Vinyl Silizane. *Front. Chem. Eng. China* **2008**, *2*, 390–395.
- (85) Woodbury, R. P.; Wood, D. Preparation of 3-Mercaptopropionitrile and 3-Mercaptopropionic Acid. U.S. Patent 5,391,820, 1995.
- (86) Li, J.; Yan, W. Production Method of 3-Mercaptopropionic Acid. C.N. Patent 105,218,421, 2016.
- (87) Karp, E. M.; Eaton, T. R.; Sànchez i Nogué, V.; Vorotnikov, V.; Biddy, M. J.; Tan, E. C. D.; Brandner, D. G.; Cywar, R. M.; Liu, R.; Manker, L. P.; et al. Renewable Acrylonitrile Production. *Science* **2017**, *358*, 1307–1310.
- (88) Griebel, J. J.; Glass, R. S.; Char, K.; Pyun, J. Polymerizations with Elemental Sulfur: A Novel Route to High Sulfur Content Polymers for Sustainability,

Energy and Defense. *Prog. Polym. Sci.* **2016**, *58*, 90–125.

- (89) Parker, D. J.; Jones, H. A.; Petcher, S.; Cervini, L.; Griffin, J. M.; Akhtar, R.; Hasell, T. Low Cost and Renewable Sulfur-Polymers by Inverse Vulcanisation, and Their Potential for Mercury Capture. *J. Mater. Chem. A* **2017**, *5*, 11682–11692.
- (90) Araki, T.; Furuya, M.; Hayashi, H. Method for Producing 3-Mercaptopropionic Acid or Salt Thereof. U.S. Patent 0,040,418, 2012.
- (91) Guzmán, D.; Mateu, B.; Fernández-Francos, X.; Ramis, X.; Serra, A. Novel Thermal Curing of Cycloaliphatic Resins by Thiol-Epoxy Click Process with Several Multifunctional Thiols. *Polym. Int.* **2017**, *66*, 1697–1707.
- (92) Majid, S.; Bukhari, H.; Khan, S.; Rehanullah, M.; Ranjha, N. M. Synthesis and Characterization of Chemically Cross-Linked Acrylic Acid/Gelatin Hydrogels: Effect of PH and Composition on Swelling and Drug Release. *Int. J. Polmyer Sci.* **2015**, 1–15.
- (93) Chen, J.-S.; Ober, C. K.; Poliks, M. D.; Zhang, Y.; Wiesner, U.; Cohen, C. Controlled Degradation of Epoxy Networks: Analysis of Crosslink Density and Glass Transition Temperature Changes in Thermally Reworkable Thermosets. *Polymer* **2004**, *45*, 1939–1950.
- (94) Bell, J. P. Structure of a Typical Amine-Cured Epoxy Resin. *J. Polym. Sci., Part A-2: Polym. Phys.* **1970**, *8*, 417–436.
- (95) Murayama, T.; Bell, J. P. Relation between the Network Structure and Dynamic

- Mechanical Properties of a Typical Amine-Cured Epoxy Polymer. *J. Polym. Sci., Part A-2: Polym. Phys.* **2018**, 8, 437–445.
- (96) Lee, C. W.; Na, C.; Kimura, Y.; Masutani, K. ABCBA Pentablock Copolymers Consisting of Poly(l-Lactide) (PLLA: A), Poly(d-Lactide) (PDLA: B), and Poly(Butylene Succinate) (PBS: C): Effects of Semicrystalline PBS Segments on the Stereo-Crystallinity and Properties. *Macromol. Mater. Eng.* **2016**, 301, 1121–1132.
- (97) Shen, D.; Shi, Y.; Fu, Z.; Yang, W.; Cai, X.; Lin, R.; Zhang, D. Synthesis of Polystyrene-Block-Polycarbonate-Block-Polystyrene and Polycarbonate-Graft-Polystyrene Using Tandem Condensation Polymerization and Atom Transfer Radical Polymerization. *Polym. Bull.* **2003**, 49, 321–328.
- (98) Feng, C.; Zhu, C.; Yao, W.; Lu, G.; Li, Y.; Lv, X.; Jia, M.; Huang, X. Constructing Semi-Fluorinated PDEAEMA-b-PBTFVBP-b-PDEAEMA Amphiphilic Triblock Copolymer via Successive Thermal Step-Growth Cycloaddition Polymerization and ATRP. *Polym. Chem.* **2015**, 6, 7881–7892.
- (99) Sandeau, A.; Mazières, S.; Vergelati, C.; Corriol, C.; Destarac, M. Dixanthate-Terminated Poly(Butylene Terephthalate). A Novel RAFT/MADIX Agent for the Synthesis of Well-Defined Triblock Copolymers Resulting from Consecutive Step- and Chain-Growth Polymerization Processes. *Polym. Chem.* **2011**, 2, 2490–2499.
- (100) Dan, K.; Ghosh, S. Stimuli Responsive Triblock Copolymers by Chain-Growth Polymerization from Telechelic Macroinitiators Prepared via a Step-Growth

Polymerization. *Polym. Chem.* **2014**, *5*, 3901–3909.

- (101) Huang, X.; Lu, G.; Peng, D.; Zhang, S.; Qing, F. L. Synthesis and Characterization of a Novel Perfluorocyclobutyl Aromatic Ether-Based ABA Triblock Copolymer. *Macromolecules* **2005**, *38*, 7299–7305.
- (102) Mennicken, M.; Nagelsdiek, R.; Keul, H.; Höcker, H. A Novel Macroinitiator for the Synthesis of Triblock Copolymers via Atom Transfer Radical Polymerization: Polystyrene-Block-Poly(Bisphenol A Carbonate)-Block-Polystyrene and Poly(Methyl Methacrylate)-Block-Poly(Bisphenol A Carbonate)-Block-Poly(Methyl Met. *Macromol. Chem. Phys.* **2004**, *205*, 143–153.
- (103) Zhang, Y.; Im, S. C.; Huang, J.; Matyjaszewski, K.; Pakula, T. Structure and Properties of Poly(Butyl Acrylate-Block-Sulfone-Block-Butyl Acrylate) Triblock Copolymers Prepared by ATRP. *Macromol. Chem. Phys.* **2005**, *206*, 33–42.
- (104) Li, D.; Sha, K.; Li, Y.; Liu, X.; Wang, W.; Wang, S.; Xu, Y.; Ai, P.; Wu, M.; Wang, J. Synthesis of Diblock Copolymer Poly(10-Hydroxydecanoic Acid)/Polystyrene by Combining Enzymatic Condensation Polymerization and ATRP. *Polym. Bull.* **2006**, *56*, 111–117.
- (105) Sha, K.; Li, D.; Li, Y.; Ai, P.; Liu, X.; Wang, W.; Xu, Y.; Wang, S.; Wu, M.; Zhang, B.; et al. Chemoenzymatic Synthesis of an AB-Type Diblock Copolymer Combining Enzymatic Self-Condensation Polymerization and Atom Transfer Radical Polymerization. *J. Polym. Sci., Part A: Polym. Chem.* **2006**,

44, 3393–3399.

- (106) Verma, H.; Tharanikkarasu, K. Synthesis and Characterization of Novel Polystyrene-Block-Polyurethane-Block-Polystyrene Tri-Block Copolymers through Atom Transfer Radical Polymerization. *Polym. Int.* **2008**, *57*, 226–232.
- (107) Tharanikkarasu, K.; Verma, H.; Jang, W.; Lee, S. K.; Seo, J.; Baek, S.; Han, H. Novel Poly(Methyl Methacrylate)-Block-Polyurethane-Block-Poly(Methyl Methacrylate) Tri-Block Copolymers through Atom Transfer Radical Polymerization. *J. Appl. Polym. Sci.* **2008**, *108*, 1538–1544.
- (108) Gaynor, S. G.; Matyjaszewski, K. Step-Growth Polymers as Macroinitiators for “Living” Radical Polymerization: Synthesis of ABA Block Copolymers. *Macromolecules* **1997**, *30*, 4241–4243.
- (109) Kricheldorf, H. R.; Behnken, G.; Schwarz, G. Telechelic Polyesters of Ethane Diol and Adipic or Sebacic Acid by Means of Bismuth Carboxylates as Non-Toxic Catalysts. *Polymer* **2005**, *46*, 11219–11224.
- (110) Jihoon, S.; Chang, A. Y.; Brownell, L. V.; Racoma, I. O.; Ozawa, C. H.; Chung, H.-Y.; Peng, S.; Bae, C. Hydrophilic Graft Modification of a Commercial Crystalline Polyolefin. *J. Polym. Sci., Part A: Polym. Chem.* **2008**, *46*, 3533–3545.
- (111) Yokota, K.; Hirabayashi, T. Manufacture of α -Methylene- γ -Butyrolactone. JP Patent 04,049,288, 1992.
- (112) Miyake, G. M.; Zhang, Y.; Chen, E. Y.-X. Living Polymerization of Naturally

Renewable Butyrolactone-Based Vinylidene Monomers by Ambiphilic Silicon Propagators. *Macromolecules* **2010**, *43*, 4902–4908.

- (113) Mosnáček, J.; Yoon, J. A.; Juhari, A.; Koynov, K.; Matyjaszewski, K. Synthesis, Morphology and Mechanical Properties of Linear Triblock Copolymers Based on Poly(α -Methylene- γ -Butyrolactone). *Polymer* **2009**, *50*, 2087–2094.
- (114) Shin, J.; Lee, Y.; Tolman, W. B.; Hillmyer, M. A. Thermoplastic Elastomers Derived from Menthide and Tulipalin A. *Biomacromolecules* **2012**, *13*, 3833–3840.
- (115) Ding, K.; John, A.; Shin, J.; Lee, Y.; Quinn, T.; Tolman, W. B.; Hillmyer, M. A. High-Performance Pressure-Sensitive Adhesives from Renewable Triblock Copolymers. *Biomacromolecules* **2015**, *16*, 2537–2539.
- (116) Tobiszewski, M.; Marć, M.; Gałuszka, A.; Namieśnik, J. Green Chemistry Metrics with Special Reference to Green Analytical Chemistry. *Molecules* **2015**, *20*, 10928–10946.
- (117) Jiménez-González, C.; Constable, D. J. C.; Ponder, C. S. Evaluating the “Greenness” of Chemical Processes and Products in the Pharmaceutical Industry - A Green Metrics Primer. *Chem. Soc. Rev.* **2012**, *41*, 1485–1498.
- (118) Jimenez-Gonzalez, C.; Ponder, C. S.; Broxterman, Q. B.; Manley, J. B. Using the Right Green Yardstick: Why Process Mass Intensity Is Used in the Pharmaceutical Industry to Drive More Sustainable Processes. *Org. Process Res. Dev.* **2011**, *15*, 912–917.

- (119) Nishiyama, H.; Kitajima, T.; Matsumoto, M.; Itoh, K. Silylmethyl Radical Cyclization: New Stereoselective Method for 1,3-Diol Synthesis from Allylic Alcohols. *J. Org. Chem.* **1984**, *49*, 2298–2300.
- (120) Mosnáček, J.; Matyjaszewski, K. Atom Transfer Radical Polymerization of Tulipalin A: A Naturally Renewable Monomer. *Macromolecules* **2008**, *41*, 5509–5511.
- (121) Hiemenz, P. C.; Lodge, T. P. *Polymer Chemistry*, Second.; CRC Press, Taylor & Francis Group: Boca Raton, FL, 2007.
- (122) Hansen, C. M. *Hansen Solubility Parameters*, Second.; Hansen, C., Ed.; CRC Press, Taylor & Francis Group: Boca Raton, FL, 2007.
- (123) Small, P. A. Some Factors Affecting the Solubility of Polymers. *J. Appl. Chem.* **1953**, *3*, 71–80.
- (124) Fedors, R. F. A Method for Estimating Both the Solubility Parameters and Molar Volumes of Liquids. *Polym. Eng. Sci.* **1974**, *14*, 147–154.
- (125) Fortunati, E.; Puglia, D.; Iannoni, A.; Terenzi, A.; Kenny, J. M.; Torre, L. Processing Conditions, Thermal and Mechanical Responses of Stretchable Poly(Lactic Acid)/Poly(Butylene Succinate) Films. *Materials (Basel)*. **2017**, *10*, 1–16.
- (126) Armarego, W. L. F.; Chai, C. L. L. *Purification of Laboratory Chemicals*; 2009.

Chapter 4 POLYETHERS FROM ITACONIC ACID

ABSTRACT

Herein, we report the synthesis and characterization of a new biorenewable polyether based on the itaconic acid-derived α -methylene- γ -butyrolactone. This new polyether (PMBLO) is an amorphous material with high glass transition (106 °C) and decomposition (348 °C) temperatures. Comparison with other common polyethers highlight the potential utility of this new material, and the polymerization of similar renewable epoxide monomers are explored.

INTRODUCTION

Polyethers are a class of polymers that serve as important precursors to polyurethane-based materials¹ and electrolytic components of batteries.² The synthesis of polyethers through the ring opening polymerization (ROP) of epoxides has been extensively studied.^{3,4} In particular, controlled polymerizations catalyzed by chromium or cobalt,^{5–13} aluminum,^{14–18} and uranium¹⁹ have been reported. Additionally, more traditional anionic methods for the synthesis of polyethers from epoxides have been explored,^{20–22} including systems initiated by metal alkoxides.^{23,24} One major limitation in the production of polyethers is their derivation from petroleum sources, often from the oxidation of olefins such as ethylene, propylene, or isobutylene.³ While some routes to these olefins and their epoxides from biomass have been explored,²⁵ the synthesis of biorenewable epoxides and polyethers is still an emerging area of research.

MBL is a renewable methyl methacrylate surrogate that can be accessed from the reduction β -monomethyl itaconate, and IA derivative.^{26,27} MBL and related exo-olefin derivatives and their polymerization (Figure 4.1a) have been extensively explored

using various polymerization strategies, with the resulting polymers exhibiting high T_g s, T_{ds} , good solvent resistance, and excellent optical properties.^{28,29} Despite these promising physiochemical properties, the polyether analogue of poly(MBL) that could be accessed from the ROP of MBL oxide (MBLO, Figure 4.1b) has not been reported. The resulting poly(MBLO) (PMBLO) could exhibit high T_g s, T_{ds} , good solvent resistance, and excellent optical properties, like PMBL, but also find uses in polyether-based applications. Additionally, we anticipated that MBL derivatives including MeMBL, Me₂MBL, as well as a variety of itaconimides, could be oxidized and polymerized to give a number of high-value IA-based polyethers. To access PMBLO, we first sought an efficient method for the oxidation of MBL to MBLO, and then we turned our attention to the polymerization of MBLO to PMBLO and the characterization of this polymer's physiochemical properties.

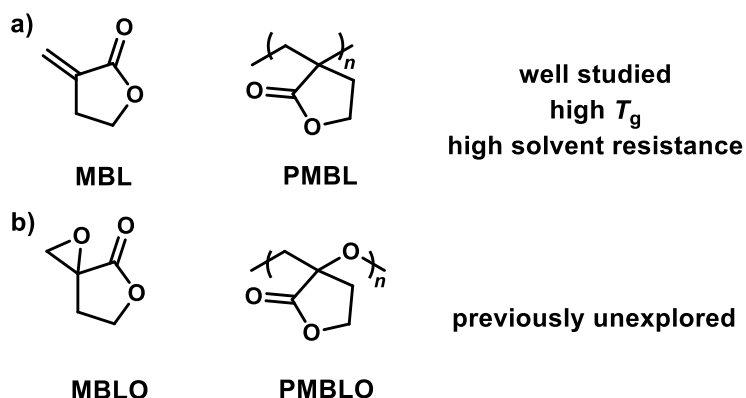


Figure 4.1. a) MBL and its polymer, PMBL, are well studied. PMBL possesses a high T_g and high solvent resistance. b) MBLO and its polymer, PMBLO, are previously unexplored.

RESULTS AND DISCUSSION

Synthesis of MBLO from MBL. The synthesis of MBLO from MBL was first reported in 1985 by Murray and Reid through oxidation using *m*CPBA (22% yield, Figure 4.2a),³⁰ and then again in 2003 by Otto and Liebscher through oxidation with dimethyl

dioxirane (DMDO) (72% yield, Figure 4.2b).³¹ While these methods provide access to MBLO, we were interested in optimizing to give higher yields or pursuing alternative synthetic routes entirely. The reported oxidation of MBL with *m*CPBA, for example, is low yielding, while the preparation of DMDO requires large amounts of solvent and careful storage under extremely dilute conditions, making the use of large quantities of DMDO challenging.^{32–34} The oxidation of itaconic anhydride, a related derivative, has also been reported using HOF·MeCN, though this synthetic strategy was not explored for the oxidation of MBL since it requires the use of fluorine,³⁵ an extremely corrosive and toxic gas. For these reasons, we began our search for alternative routes for the transformation of MBL to MBLO (Figure 4.2).

Our first attempt to form MBLO was through the nucleophilic oxidation of MBL with hydrogen peroxide and sodium hydroxide as a base (Figure 4.2c). In the presence of small amounts of inhibitor (2,6-*tert*-butylphenol) at 50 °C in MeOH, only unreacted starting material was observed. At higher temperatures (80 or 100 °C) in a variety of solvents, a combination of unreacted starting material, degradation products, and oligomers were observed, consistent with a previous report.³⁰ In all cases, no transformation of MBL to MBLO was detected.

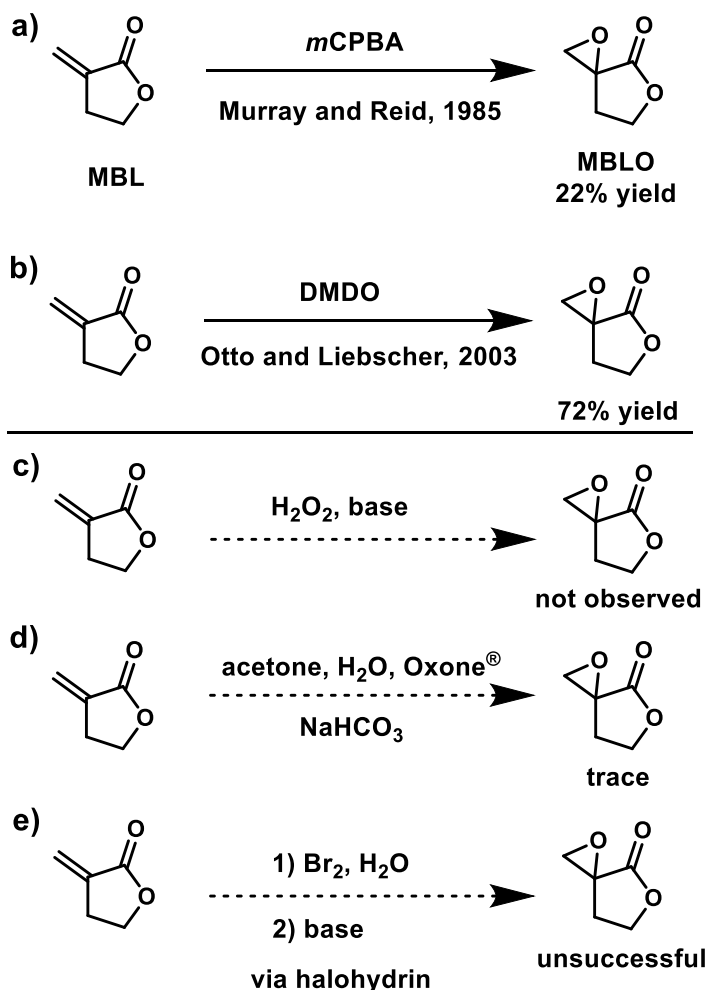


Figure 4.2. a-b) Previous methods known for the oxidation of MBL to MBLO; c-d) synthetic strategies for accessing MBLO from MBL, including c) nucleophilic oxidation, d) *in situ* formation of DMDO for oxidation and e) ring-closing epoxidation of a halohydrin intermediate

With the nucleophilic oxidation of MBL unsuccessful, we turned our attention to use of DMDO. Despite the limitations previously mentioned, oxidation of MBL with DMDO led to the formation of MBLO in 78% yield from MBL, in agreement with the original report for this process.³¹ To avoid preparing large amounts of dilute DMDO solution, we sought to perform the MBL oxidation through the formation of DMDO *in situ* (Figure 4.2d) using mixtures of MBL with acetone, water, sodium bicarbonate, and Oxone[®]. At RT or 50 °C, unreacted starting material with only trace formation of

MBLO was observed.³⁶ While no other major products were determined by ¹H NMR, mass balances less than 100% may be indicative of water-soluble degradation products that do not go into the organic phase used for analysis. Attempts to perform this oxidation using phase transfer catalysts such as tetrabutyl ammonium bromide or 18-crown-6 with various solvent mixtures and buffers also gave similar results, and so we did not pursue this oxidation method further.

We also attempted to generate MBLO from MBL through the formation of a bromohydrin intermediate, followed by base-initiated ring-closing to form the epoxide (Figure 4.2e). Surprisingly, we observed mainly the formation of a dibromide when elemental bromide (1.2 equiv) was added to MBL (1 mmol) in organic solvents such as THF, acetonitrile, or acetone with varying amounts of water.³⁷ From here, we hypothesized that we could encourage bromohydrin, rather than dibromide, formation through the use of a hydroxide base, which should be a stronger nucleophile for the ring-opening of the presumed bromonium ion intermediate. Unfortunately, attempts to favor bromohydrin formation by performing the bromine addition under basic, aqueous conditions still resulted in dibromide formation, as well as degradation of the starting material, with no formation of the desired bromohydrin observed. While some bromohydrin formation was observed when the halogenation was performed in the presence of stoichiometric silver nitrate, we did not pursue this method due to the impracticality of using a stoichiometric silver reagent.

With initial attempts to elucidate alternative methods towards the formation of MBLO from MBL unsuccessful, we returned to the original oxidation method using *m*CPBA.³⁰ Using this method, we obtained the product in 16% isolated yield. We

noticed by ^1H NMR that MBLO degraded upon aqueous work-up, which was likely the cause of the low yields. After some minor optimization, we found that 3 equiv of *m*CPBA with 0.1 equiv inhibitor (2,6-di-*tert*-butylphenol) in the absence of aqueous work-up resulted in improved yields; by purifying the crude reaction mixture directly with column chromatography we isolated 5 g of MBLO in 53% yield (Figure 4.3).

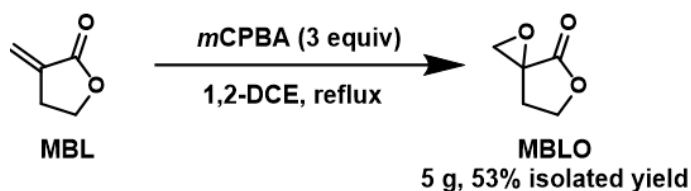


Figure 4.3. Scaled-up and optimized formation of MBLO from MBL.

Homopolymerization of PMBLO from MBLO. We first sought to polymerize MBLO based on a report that explored the ring-opening epoxide polymerization of styrene oxide using 18-crown-6 as an activator for potassium *tert*-butoxide initiator ($t\text{BuOK}$).²⁴ To our knowledge, no one has previously reported the polymerization of MBLO. When mixed with $t\text{BuOK}$ and 18-crown-6 in THF, MBLO was polymerized with high conversion after 24 h at 50 °C (Table 4.1, entry 1) to give a polymer with an M_n of 7.4 kg/mol and a dispersity of 1.16. The theoretical M_n value ($M_{n,\text{theo}}$) was larger than the experimentally determined value (12.3 kg/mol compared with 7.4 kg/mol), indicating that some polymer chains were being initiated by species other than the initiator. This could potentially be due to chain-transfer to monomer resulting from deprotonation of the γ -proton in MBLO, or from insolubility of PMBLO in the polymerization media.

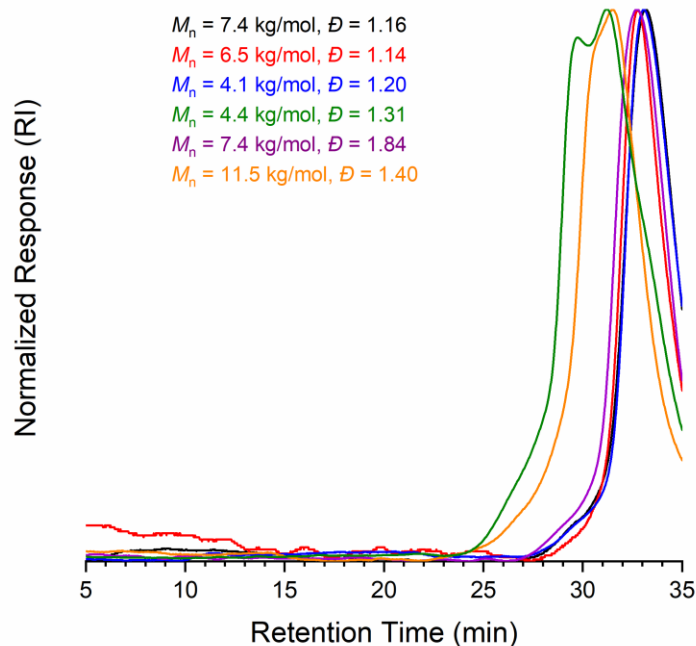


Figure 4.4. SEC curves for PMBLO samples synthesized by the ROP of MBLO.

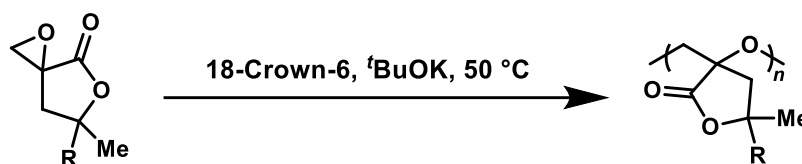
Attempts to affect higher molar masses through varying the MBLO:^tBuOK ratio resulted in similar experimental M_n s in all cases (entries 2 to 5 and Figure 4.5) that were significantly lower than $M_{n,theo}$. As MBLO:^tBuOK increased, dispersity values of the resulting PMBLO also increased, indicating a higher number of termination events. Additionally, the polymerization requires the presence of 18-crown-6 to activate the ^tBuOK initiator; in the absence of 18-crown-6, the polymerization did not proceed (entry 6). Since PMBLO could be precipitating out of THF in the reaction mixture, we ran the polymerization under neat conditions to access higher molar mass polymers (entry 7). Under these conditions we observed only a slightly higher molar mass polymer with an M_n of 11.5 kg/mol and a dispersity of 1.40. Other polymerization solvents such as diglyme or 1,4-dioxane were also tested but did not result in polymerization. Upon scale-up (with ~ 600 mg of MBLO) PMBLO was obtained in 72% isolated yield after

precipitating from methanol, and SEC analysis using a light scattering detector in DMF with an estimated dn/dc value of 0.0652 mL/g determined that the polymer had an M_n of 16.4 kg/mol and a dispersity of 2.10 before precipitation and an M_n of 17.7 kg/mol and a dispersity of 2.22 after precipitation (entry 8 and Figure S4.1). This polymer sample was used to characterize the physiochemical properties of the material.

Table 4.1. Polymerization Conditions for MBLO

<div style="text-align: center;"> </div>						
Entry	MBLO:I ^a	THF (mL)	Conversion (%) ^b	M_n (kg/mol) ^c	\bar{D}	$M_{n,theo}$ (kg/mol) ^d
1	100:1	0.02	100	7.4	1.16	12.3
2	200:1	0.02	92	6.5	1.14	21.7
3 ^e	300:1	0.02	100	4.1	1.20	33.7
4 ^e	500:1	0.02	96	4.4	1.31	48.5
5	900:1	0.02	77	7.4	1.84	78.9
6 ^f	1100:1	0.07	0	-	-	-
7 ^e	500:1	Neat	85	11.5	1.40	46.7
8 ^{e,g}	600:1	Neat	87	16.4 ^h	2.10 ^h	60.6

Reactions with 0.001 mmol ^tBuOK and 0.001 mmol 18-crown-6 for 24 h at 50 °C unless otherwise specified; ^aMonomer (MBLO) to initiator (^tBuOK) ratio ^bDetermined from ¹H NMR; ^c M_n and \bar{D} determined on a DMF SEC against PS standards; ^dDetermined using the MBLO:^tBuOK ratio and % conversion; ^e48 h; ^fRun without 18-crown-6; ^gRan with 0.01 mmol ^tBuOK ^h M_n and \bar{D} were determined on a DMF SEC using a light-scattering detector

Table 4.2. Polymerization Conditions for MeMBLO and Me₂MBLO

Entry	R	M:I ^a	THF (mL)	t (h)	Conversion (%) ^b	<i>M_n</i> (kg/mol) ^c	<i>M_{n,theo}</i> (kg/mol) ^d
1	H	700:1	0.07	9	23	< 1	20.2
2	H	600:1	0.02	9	29	< 1	23.8
3	H	600:1	Neat	24	25	< 1	20.8
4	H	500:1	Neat	120	79	< 1	49.8
5 ^e	Me	700:1	0.07	72	6	< 1	6.3
6 ^e	Me	700:1	0.02	72	8	< 1	7.8

Reactions run with 0.001 mmol *t*BuOK and 0.001 mmol 18-crown-6 for 24 h at 50 °C unless otherwise specified; ^aMonomer (R₂MBLO) to initiator (*t*BuOK) ratio; ^bDetermined from ¹H NMR; ^c*M_n* and *D* determined by a light scattering on a DMF SEC against PS standards; ^e70 °C.

Polymerization of other MBLO epoxide derivatives with methyl substitution at the γ position of the ring was also attempted (Table 4.2). Both MeMBL and Me₂MBL were effectively oxidized with *m*CPBA (see experimental) to afford the corresponding epoxides MeMBLO or Me₂MBLO. We attempted to polymerize both of these monomers using the 18-crown-6 and *t*BuOK system, which would afford methyl substituted PMBLO derivatives with potentially higher *T_g*s and improved solubility.²⁷ Starting with MeMBLO, we observed only low conversion to oligomers (*M_n* < 1 kg/mol) after 9 h at 50 °C (Table 4.2, entry 1). By increasing the concentration of MeMBLO in THF (entry 2), we saw a modest increase in conversion to 29%, though still only oligomers were formed (entry 2). Running the reaction neat and for longer did not improve the degree of polymerization: while conversion of monomer increased from

25% to 79% between 24 and 120 h (entries 3 and 4), only oligomers were formed. Knowing that MeMBLO undergoes slower conversion relative to MBLO, and that the more highly substituted Me₂MBL undergoes slower conversion in RAFT polymerization relative to the less substituted MBL,²⁷ we next attempted the polymerization of the more substituted Me₂MBLO at higher temperatures (70 °C). Under these conditions we saw very low conversion to oligomers (entries 5 and 6). Further optimization of the polymerization conditions to achieve faster conversions to higher molar mass polymers was not attempted.

Physical Properties of PMBLO. PMBLO showed a T_d of 348 °C (Figure 4.5) and a T_g of 106 °C (Figure 4.6). The sharp drop below baseline in the T_g of PMBL is due to an endothermic hysteresis peak super-imposed on the high-temperature side of the glass transition.³⁸ Like PMBL, PMBLO shows insolubility in common organic solvents such as THF and solubility in polar aprotic solvents such as DMF or DMSO.

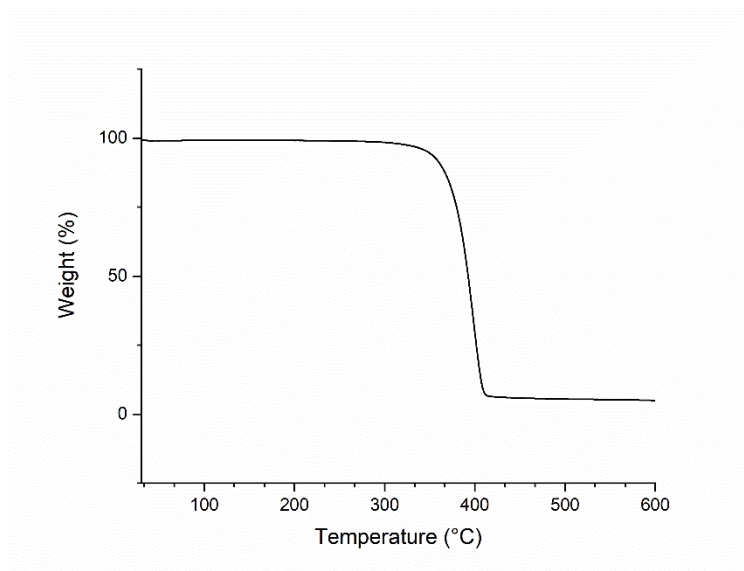


Figure 4.5. Thermal gravimetric analysis (TGA) trace of PMBLO.

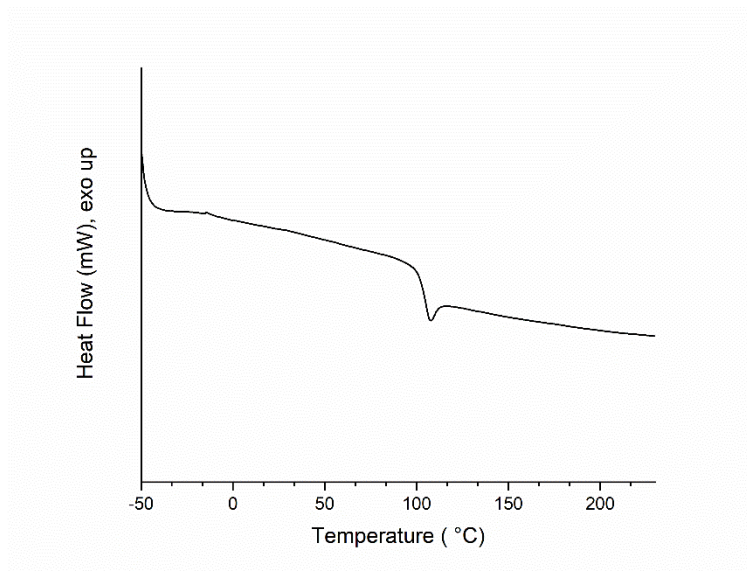


Figure 4.6. Differential scanning calorimetry (DSC) heat flow vs. temperature (30 °C/min, second heat) traces of PMBLP, exo up.

Representative values or ranges for T_g s, T_d s, solubilities, T_m s, and molar masses between entanglements (M_e) are reported for common polyethers in Table 4.3. Poly(ethylene oxide) (PEO) and poly(propylene oxide) (PPO) are well known polyethers used in a wide-variety of applications that exhibit low glass transition temperatures (< -60 °C), crystallinity ($T_m \sim 65$ °C), low M_e s, and good solubilities in a wide variety of organic solvents and water (though the solubility in water of PEO and PPO is dependent on the molar mass of the polymer). Poly(isobutylene oxide) (PIBO), a less studied analogue of PEO and PPO, exhibits higher T_g (-30 °C) and T_m ($110 - 180$ °C) values and shows similar solubility in organic solvents (though we found no reports of this material to be water-soluble).³⁹ To our knowledge, rheological measurements of PIBO have not been reported. Both PEO and PPO have T_d s around 350 °C, while the decomposition temperature of PIBO is slightly lower at ~ 300 °C. In contrast to these materials, poly(2,6-dimethyl-1,4-phenylene oxide) (PPhO), a well-known aromatic polyether, exhibits both a high T_g ($210 - 220$ °C) and T_d (425 °C) and

is often used for high-temperature applications. Unlike PEO, PPO, and PIBO, PPhO does not exhibit high levels of crystallinity, though melting temperatures between 220 and 250 °C have been reported. Additionally, PPhO is soluble in common organic solvents and has a low M_e of ~ 2 kg/mol.

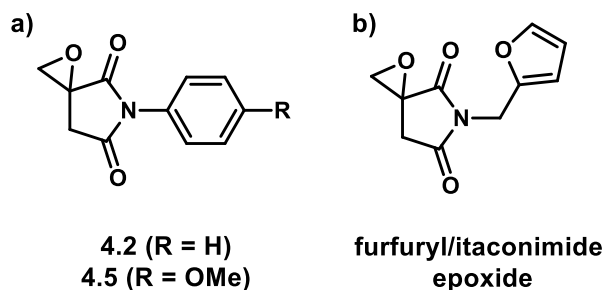
PMBLO, like its related analogue PMBL, is an amorphous and shows poor solubility in common organic solvents, instead requiring highly polar aprotic solvents such as DMF or DMSO for dissolution, though PMBLO does show partial solubility in DCM. The T_g of PMBLO is quite high for a polyether (~ 100 °C), and the ~ 100 °C differences in T_g s between PMBL and PMBLO can be attributed to the slightly longer and more flexible backbone repeat unit of PMBLO relative to PMBL.

Synthesis and Polymerization of Other Itaconate Based Epoxides. While MBLO and its corresponding polymer proved to have interesting physiochemical properties, we were also interested in the synthesis and polymerization of related epoxides based on itaconimides (Figure 4.7a). The synthesis of itaconimides is well known,⁴⁰ and their transformation into the corresponding epoxides has been reported before using hydrogen peroxide and trifluoroacetic anhydride.⁴¹ These materials contain phenyl groups that originate from aniline, which is petroleum derived. As a sustainable alternative, we were interested in the use of furfuryl amine in place of aniline to generate a furfuryl/itaconimide-based epoxide (Figure 4.7b). This epoxide would have almost 100% of its atoms sourced from biomass. Unfortunately, while the precursor *N*-furfuryl itaconimide was successfully synthesized, this material spontaneously gelled upon storage and further epoxidations were not attempted (4.7, see experimental).

Table 4.3. Physiochemical Properties of Various Polyethers

Polymer	T_g (°C)	T_d (°C)	Solubility	T_m (°C) ^a	M_e (kg/mol)
PMBLO	106	348	DMF, DMSO, DCM (partially)	-	-
PEO ^{2,3,42-48}	- 65	380	Water, various organic solvents including CHCl ₃ , THF, toluene, DCM, MeOH, acetone	65	1.6 – 2.2
PPO ^{3,6,44,47,49}	- 70	360	Water, various organic solvents including THF, CHCl ₃ , toluene, MeCN	57 – 67	3.9 – 4.0
PIBO ^{39,50}	- 29	290	Various organic solvents including DCM, toluene, o- dichlorobenzene	108 – 175	Unknown
PPhO ^{47,51-54}	205 – 219	425	Toluene, THF, CHCl ₃	219 – 254	1.7
PMBL ^{27,55}	187	337	DMF, DMSO	-	10.5

^aCrystallinity varies by sample, and poly(phenylene oxide) generally exhibits low levels of crystallinity

**Figure 4.7.** Itaconimide based monomers explored in this work.

Using the *m*CPBA as an oxidant, N-phenyl itaconimide (**4.1**, synthesized following a known procedure⁴⁰) was transformed to give the corresponding epoxide (**4.2**) in 29% isolated yield (Figure 4.8). **4.2** was then subjected to with ^tBuOK and 18-crown-6. Under these conditions oligomers were formed (based on ¹H NMR and SEC analysis), with allyl alcohol **4.3** generated as as a major side product in ~30% yield (Figure 4.9).

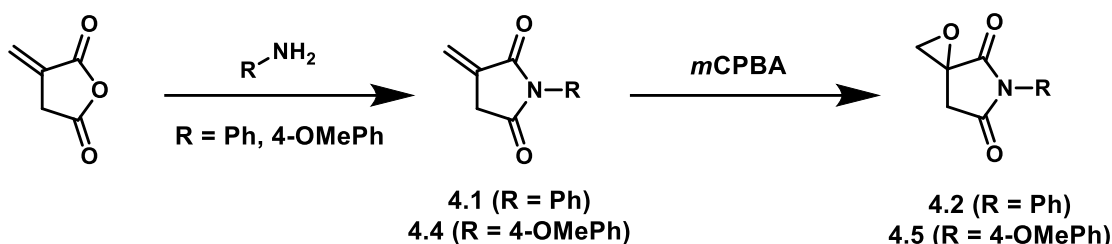


Figure 4.8. Synthesis of itaconimide-based epoxides from ItAnh.

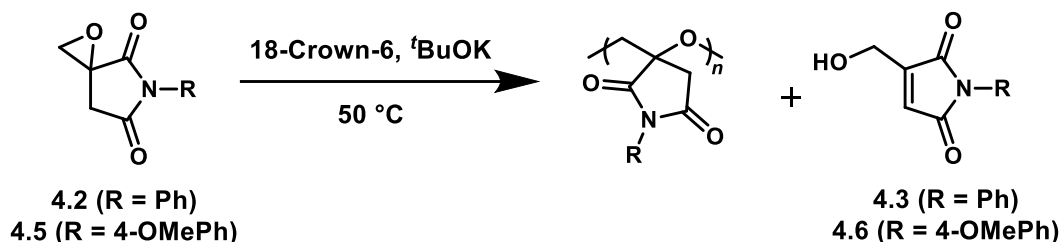


Figure 4.9. ROP of itaconimide epoxides leads to oligomers and an allyl alcohol.

Since deprotonation of the aliphatic proton in **4.2** appears to be responsible for the formation of **4.3**, we sought ways to mitigate that pathway. We hypothesized that by increasing the electron density of the itaconimide π system through the addition of electron donating groups to the phenyl ring, we could decrease the acidity of the aliphatic proton in the lactone ring and avoid the generation of the allyl alcohol. For this reason, we used our standard protocol to synthesize **4.5** from **4.4**, which contains an electron donating methoxy group in the phenyl ring. Unfortunately, when subjected to

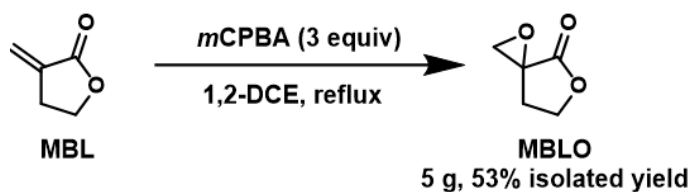
the polymerization conditions used with epoxide **4.2**, **4.5** also formed the corresponding allyl alcohol **4.6** (~30% yield), in addition to oligomers.

Future work will optimize the reaction conditions in the monomer synthesis for higher overall yields from the starting IA source and will explore greener methods for this epoxidation. Other polymerization systems will also be studied to access these high value, renewable polyethers.

CONCLUSIONS

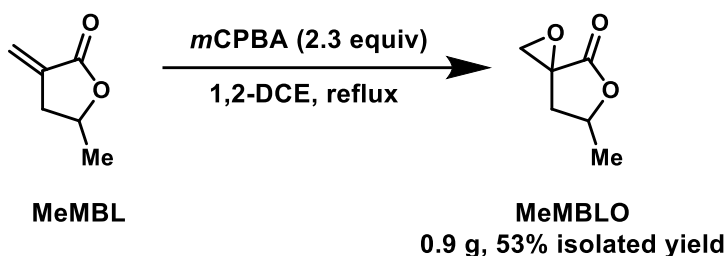
In this work, we have shown that relatively high molar mass PMBLO ($M_n \sim 18$ kg/mol) can be effectively synthesized in an uncontrolled fashion from IA-derived MBLO. This material shows a remarkably high T_g (~ 100 °C) relative to other common polyethers such as PEO and PPO, and as a result PMBLO could find applications in various high-temperature applications. Polymerizations of other IA-based epoxides were also explored but only generated oligomers. We anticipate that improvements in the polymerization procedures could result in a wide variety of renewable polyethers with tunable physiochemical properties.

EXPERIMENTAL



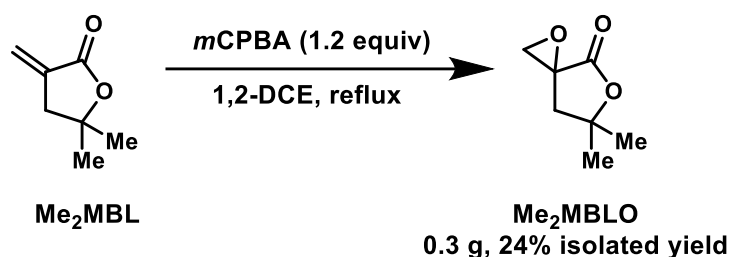
Synthesis of α -methylene- γ -butyrolactone oxide (MBLO). A 500 mL round bottom flask was equipped with a stir bar and a reflux condenser. MBL (7.83 g, 79.8 mmol, 1.00 equiv), 2,6-di-*tert*-butylphenol (1.65 g, 8.00 mmol, 0.100 equiv) and *m*CPBA (55.12 g, 75 wt% pure, 239.6 mmol, 3.00 equiv) were then added, followed by 1,2-DCE

(240 mL). The system was refluxed at 100 °C for 3 h. The reaction mixture was then cooled to 0 °C in an ice/water bath where a large amount of solids precipitated. The solids were filtered off through a fritted funnel and washed with DCM. The filtrate was concentrated under reduced pressure and the crude reaction mixture was purified directly without any further work-up. Purification by chromatography (SiO₂, 20% ethyl acetate, 80% hexanes) gave MBLO (4.82 g, 53% isolated yield). Care was taken to treat the organic waste with Na₂S₂O₃ prior to disposal to destroy any remaining peroxide. Characterization data matched those reported in the literature.³⁰ ¹H NMR (Figure S4.2, 400 MHz, CDCl₃, δ, ppm): 4.59 (td, 1H, *J* = 4.8 Hz, *J* = 9.4 Hz), 4.48 (dt, 1H, *J* = 9.3 Hz, *K* = 7.9 Hz), 3.24 (d, 1H, *J* = 5.9 Hz), 3.12 (d, 1H, *J* = 6.1 Hz), 2.56 (m, 2H).



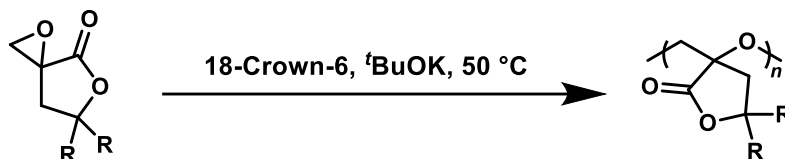
Synthesis of γ -methyl- α -methylene- γ -butyrolactone oxide (MeMBLO). A 250 mL round bottom flask was equipped with a stir bar and a reflux condenser. MeMBL (1.54 g, 13.7 mmol, 1.00 equiv), 2,6-di-*tert*-butylphenol (0.296 g, 1.43 mmol, 0.104 equiv) and *m*CPBA (7.16 g, 75 wt% pure, 31.1 mmol, 2.27 equiv) were then added, followed by 1,2-DCE (40 mL). The system was refluxed at 100 °C for 3 h. The reaction mixture was then cooled to 0 °C in an ice/water bath where a large amount of solids precipitated. The solids were filtered off through a fritted funnel and washed with DCM. The filtrate was concentrated under reduced pressure and the crude reaction mixture was purified directly without any further work-up. Purification by chromatography (SiO₂, 25% ethyl

acetate, 75% hexanes) gave MeMBLO (0.937 g, 53% isolated yield) as a mixture of diastereomers, observed in a 3:2 ratio by ^1H NMR. Care was taken to treat the organic waste with $\text{Na}_2\text{S}_2\text{O}_3$ prior to disposal to destroy any remaining peroxide. ^1H NMR (Figure S4.3, 500 MHz, CDCl_3 , δ , ppm): Major diastereomer: 4.59 (m, 1H), 3.29 (d, 1H, $J = 6.0$ Hz), 3.07 (d, 1H, $J = 6.0$ Hz), 2.59 (m, 1H), 2.20 (m, 1H), 1.51 (d, 3H, $J = 6.7$ Hz). Minor diastereomer: 4.76 (m, 1H), 3.23 (d, 1H, $J = 6.2$ Hz), 3.09 (d, 1H, $J = 6.1$ Hz), 2.59 (m, 1H), 2.20 (m, 1H), 1.55 (d, 3H, $J = 6.2$ Hz).

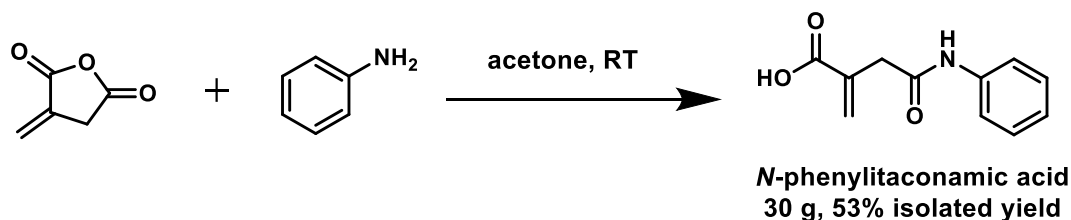


Synthesis of γ,γ -dimethyl- α -methylene- γ -butyrolactone oxide (Me₂MBLO). A 100 mL round bottom flask was equipped with a stir bar and a reflux condenser. Me₂MBL (1.00 g, 7.93 mmol, 1.00 equiv), 2,6-di-*tert*-butylphenol (0.07 g, 0.3 mmol, 0.04 equiv) and *m*CPBA (2.21 g, 75 wt% pure, 9.60 mmol, 1.21 equiv) were then added, followed by 1,2-DCE (24 mL). The system was refluxed at 100 °C for 4 h. The crude reaction mixture was then cooled to RT and diluted with DCM, saturated $\text{Na}_2\text{S}_2\text{O}_3$, water, saturated bicarbonate, and brine. The resulting mixture formed an emulsion that was broken by passing the mixture through a plug of Celite[®]. The organic layer was then isolated, dried with MgSO_4 , filtered, then concentrated under reduced pressure. Purification by chromatography (SiO_2 , 25% ethyl acetate, 75% hexanes) gave Me₂MBLO (0.27 g, 24% isolated yield). ^1H NMR (Figure S4.4, 400 MHz, CDCl_3 , δ , ppm): 3.24 (d, 1H, $J = 6.0$ Hz), 3.05 (d, 1H, $J = 6.2$ Hz), 2.34 (d, 2H, $J = 2.7$ Hz), 1.57

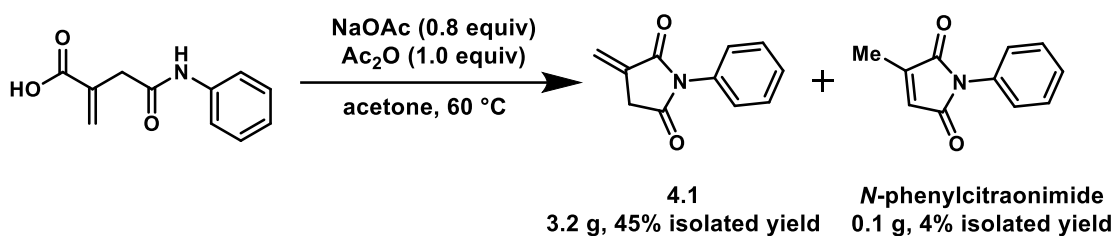
(s, 3H), 1.51 (s, 3H). ^{13}C NMR (Figure S4.5, 100 MHz, CDCl_3 , δ , ppm): 168.4, 82.3, 56.8, 39.2, 29.1 – 28.7,



Ring-opening epoxide polymerization of R_2MBLO . In a glovebox, a 2-dram vial was equipped with a stir bar and a cap and septum. MBLO ($\text{R} = \text{H}$, 102 mg, 0.892 mmol, 900 equiv) was dissolved in THF (0.05 mL), and then 0.01 mL of a $t\text{BuOK}$ stock solution (11 mg/mL, 0.1 mg, 0.001 mmol, 1 equiv) and 0.01 mL of an 18-crown-6 stock solution (34 mg/mL, 0.3 mg, 0.001 mmol, 1 equiv) was added to the solution of MBLO. The reaction mixture was then heated at 50 °C outside of the glovebox for 24 h. An aliquot was taken for ^1H NMR (DMSO-d_6) to determine conversion (77%) and SEC (DMF) to determine molar mass (7.4 kg/mol M_n , 7.4 kg/mol M_w , 1.84 D). The crude mixture was dissolved in DMSO-d_6 , precipitated from cold MeOH (– 20 °C), and filtered / rinsed with MeOH. The solid was then dried under vacuum (40.6 mg, 40% isolated yield). ^1H NMR (Figure S4.6, 500 MHz, DMSO-d_6 , δ , ppm): 4.27 (m, 2H), 3.80 (m, 1H), 3.62 (m, 1H), 2.41 (m, 1H). ^{13}C NMR (Figure S4.7, 125 MHz, DMSO-d_6 , δ , ppm): 174.0 – 173.7, 79.4, 79.3, 79.0, 78.9, 65.7, 65.6, 65.4 – 65.2, 64.9, 64.6, 29.6, 28.9. Oligomers from the polymerization of MeMBLO and Me_2MBLO monomers were not isolated.

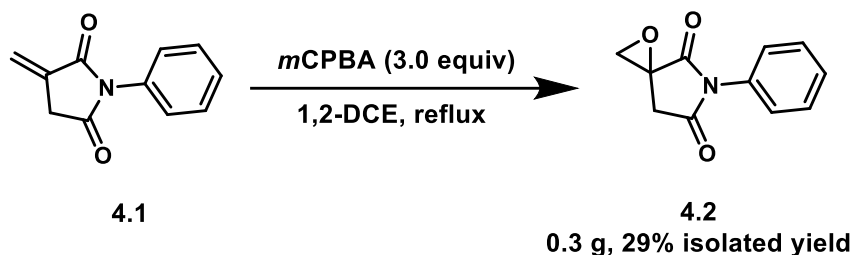


Synthesis of N-phenylitaconamic acid. N-phenylitaconamic acid was synthesized following a known procedure.⁴⁰ A 250 mL round bottom flask was equipped with a stir bar. Itaconic anhydride (ItAnh, 30.32 g, 0.2705 mol, 1.00 equiv) was added, followed by acetone (100 mL). Aniline (25.0 mL, 25.74 g, 0.2764 mol, 1.02 equiv) was then added dropwise to the stirring reaction mixture, which turned cloudy and produced heat over the course of the addition. The reaction mixture was then allowed to stir at RT for 1 h, at which point the solids were isolated by filtration and washed with water. The crude solid (53 g) was dissolved in a mixture of EtOAc:MeOH (~200 mL, 10:1 v/v) with heat and then placed at – 20 °C to crystallize. The recrystallized product was then collected by filtration and dried under vacuum to give the pure N-phenylitaconamic acid (29.63 g, 53% isolated yield). ¹H NMR (Figure S4.8, 500 MHz, DMSO-d₆, δ, ppm): 12.52 (s, 1H), 9.98 (s, 1H), 7.57 (m, 2H), 7.28 (m, 2H), 7.02 (m, 1H), 7.17 (s, 1H), 5.74 (s, 1H), 3.34 (s, 2H). ¹³C NMR (Figure S4.9, 125 MHz, DMSO-d₆, δ, ppm): 168.5, 167.6, 139.3, 135.8, 128.7, 127.5, 123.0, 118.9.



Synthesis of N-phenylitaconimide (4.1). N-phenylitaconimide acid was synthesized following a known procedure.⁴⁰ A 100 mL round bottom flask was equipped with a stir bar and a reflux condenser. N-phenylitaconamic acid (7.73 g, 37.67 mmol, 1.00 equiv) was added, followed by NaOAc (2.61 g, 31.82 mmol, 0.845 equiv) and acetone (27 mL). Acetic anhydride (3.6 mL, 3.89 g, 38.08 mmol, 1.01 equiv) was then added dropwise and the reaction mixture was submerged in an oil bath pre-heated to 60 °C. The reaction

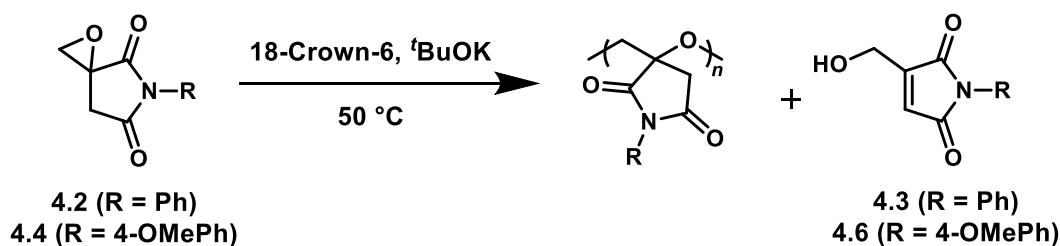
was allowed to stir at this temperature for 16 h and then was cooled to RT. The reaction mixture was then washed three times with water and once with brine before being dried with MgSO₄, filtered, and concentrated under reduced pressure. The crude product was then purified by chromatography (SiO₂, gradient from 5% ethyl acetate, 95% hexanes to 20% ethyl acetate, 80% hexanes gradient) to give the pure **4.1** (3.192 g, 45% isolated yield for this step, 24% overall isolated yield from itaconic anhydride). Characterization data is consistent with those reported in the literature.⁴⁰ ¹H NMR (Figure S4.25, 400 MHz, CDCl₃, δ , ppm): 7.49 (m, 2H), 7.40 (m, 1H), 7.33 (m, 2H), 6.48 (m, 1H), 5.75 (m, 1H), 3.52 (m, 2H). N-phenylcitraconimide was also collected from the chromatographic purification (0.076 g, 4%). ¹H NMR (Figure S4.10, 400 MHz, CDCl₃, δ , ppm): 7.46 (m, 2H), 7.35 (m, 2H), 6.48 (m, 1H), 2.18 (m, 2H).



Synthesis of 5-phenyl-1-oxa-5-azaspiro[2.4]heptane-4,6-dione (4.2). A 50 mL round bottom flask was equipped with a stir bar and a reflux condenser. **4.1** (1.02 g, 5.45 mmol, 1.00 equiv), 2,6-di-*tert*-butylphenol (0.12 g, 0.58 mmol, 0.11 equiv) and *m*CPBA (3.71 g, 75 wt% pure, 16.12 mmol, 2.96 equiv) were then added, followed by 1,2-DCE (16 mL). The system was refluxed at 100 °C and was stirred for 2 h. The reaction mixture was then cooled to 0 °C in an ice/water bath where a large amount of solids precipitated. The solids were filtered off through a fritted funnel and washed with DCM. The filtrate was concentrated under reduced pressure and the crude reaction mixture was purified

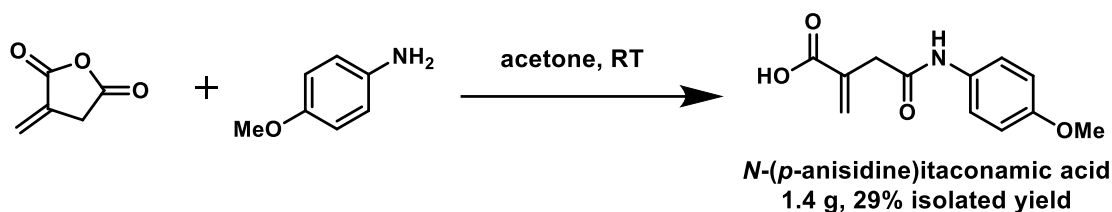
directly without any further work-up. Purification by chromatography (SiO₂, 40% ethyl acetate, 80% hexanes) gave **4.2** (0.32 g, 29% isolated yield from this step, 7% overall yield from itaconic anhydride). Care was taken to treat the organic waste with Na₂S₂O₃ prior to disposal to destroy any remaining peroxide. Characterization data was consistent with those reported in the literature, though taken in different solvents.⁴¹

¹H NMR (**Error! Reference source not found.**, 500 MHz, CDCl₃, δ , ppm): 7.50 (m, 2 H), 7.43 (m, 1H), 7.33 (m, 2H), 3.53 (d, 1H, J = 6.0 Hz), 3.23 (d, 1H, J = 6.1 Hz), 3.22 (d, 1H, J = 18.9 Hz), 3.13 (d, 1H, J = 19.2 Hz). ¹³C NMR (Figure S4.13, 125 MHz, CDCl₃, δ , ppm): 173.1, 172.0, 131.5, 129.5, 129.2, 126.4, 55.0, 51.9, 33.3.

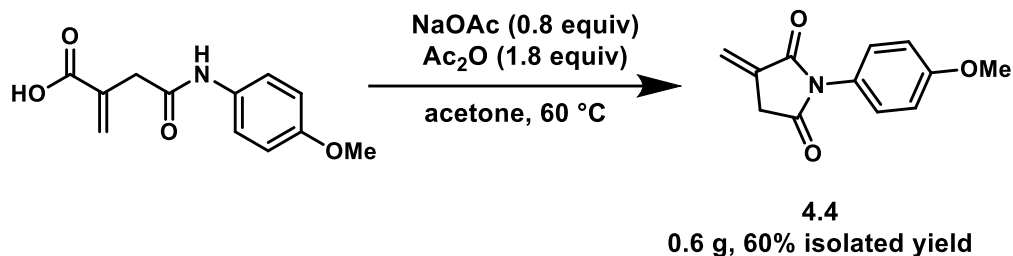


Ring-opening epoxide polymerization attempt of 4.2. In a glovebox, a 2-dram vial was equipped with a stir bar and a cap and septum. *N*-phenylitaconimide (**4.1**, 44 mg, 0.22 mmol, 220 equiv) was added to the vial, and then 0.01 mL of a ^tBuOK stock solution (10 mg/mL, 0.1 mg, 0.001 mmol, 1 equiv) and 0.01 mL of an 18-crown-6 stock solution (30 mg/mL, 0.3 mg, 0.001 mmol, 1 equiv) were added. The reaction mixture was then heated at 50 °C outside of the glovebox for 21 h. An aliquot was taken for ¹H NMR (DMSO-d₆) which showed 27% yield of allyl alcohol **4.3** using THF as an internal standard. Only oligomers were detected by SEC analysis. The crude mixture was purified by chromatography (SiO₂, 20% ethyl acetate, 80% hexanes to 60% ethyl acetate, 40% hexanes gradient) to isolate the allyl alcohol byproduct **4.3**. ¹H NMR

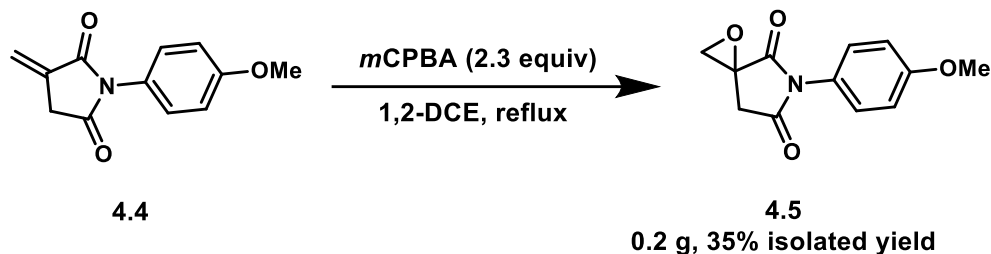
(Figure S4.14, 500 MHz, CDCl₃, δ , ppm): 7.47 (m, 2H), 7.36 (m, 3H), 6.69 (s, 1H), 4.70 (s, 2H). ¹³C NMR (Figure S4.15, 125 MHz, CDCl₃, δ , ppm): 169.7, 169.3, 148.4, 131.4, 129.4, 128.2, 127.0, 126.2, 57.6.



Synthesis of *N*-(*p*-anisidine)itaconamic acid. A 50 mL round bottom flask was equipped with a stir bar. Itaconic anhydride (2.28 g, 20.34 mmol, 1.00 equiv) was added, followed by acetone (5 mL). *p*-Anisidine (2.56 g, 20.79 mmol, 1.03 equiv) was then added portion-wise to the stirring reaction mixture, which warmed slightly and gelled upon addition. Additional acetone (10 mL) was added to break up the gel, and the reaction mixture was allowed to stir for 1 h. The solids were then collected by filtration and rinsed with acetone. The filtrate was concentrated down under reduced pressure to give additional solid powder. The combined solids were then recrystallized from EtOAc:MeOH (~80 mL, 1:1) with heat and then placed at – 20 °C to crystallize. The recrystallized product was then filtered and rinsed with acetone, before being recrystallized a second time in the same manner. The crystals were again filtered and rinsed with acetone before being dried under vacuum to give the pure *N*-(*p*-anisidine)itaconamic acid (1.41 g, 29% isolated yield). ¹H NMR (Figure S4.21, 500 MHz, CDCl₃, δ , ppm): 12.50 (s, 1H), 9.83 (s, 1H), 7.47 (m, 2H), 6.86 (m, 2H), 6.15 (s, 1H), 5.72 (s, 1H), 3.71 (s, 3H), 3.30 (s, 2H). ¹³C NMR (Figure S4.22, 125 MHz, CDCl₃, δ , ppm): 167.9, 167.6, 155.0, 135.9, 132.5, 127.4, 120.4, 113.8, 55.1.

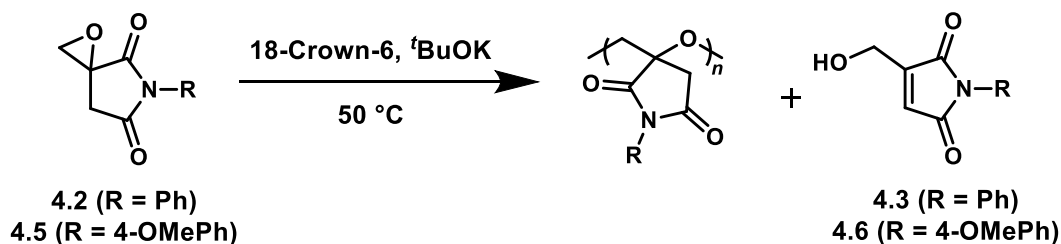


Synthesis of N-(*p*-anisidine)itaconimide 4.4. A 25 mL round bottom flask was equipped with a stir bar and a reflux condenser. N-(*p*-anisidine)itaconamic acid (1.013 g, 4.306 mmol, 1.00 equiv) was added, followed by NaOAc (0.291 g, 3.55 mmol, 0.825 equiv) and acetone (4.3 mL). Acetic anhydride (0.73 mL, 0.79 g, 7.72 mmol, 1.79 equiv) was then added dropwise and the reaction mixture was submerged in an oil bath pre-heated to 60 °C. The reaction mixture was then diluted with water and extracted three times with DCM. The combined organics were dried with MgSO₄, filtered, and concentrated under reduced pressure. The crude product was then purified by chromatography (SiO₂, gradient from 10% ethyl acetate, 90% hexanes) to give pure **4.4** (0.565 g, 60% isolated yield for this step, 17% overall yield from itaconic anhydride). Characterization data matched those previously reported in the literature.⁵⁶ ¹H NMR (Figure S4.18, 600 MHz, CDCl₃, δ, ppm): 7.25 (m, 2H), 7.00 (m, 2H), 6.47 (m, 1H), 5.73 (m, 1H), 3.84 (s, 3H), 3.50 (m, 2H). ¹H NMR (Figure S4.19, 500 MHz, DMSO-d₆, δ, ppm): 7.22 (m, 2H), 7.04 (m, 2H), 6.19 (m, 1H), 5.73 (m, 1H), 3.79 (s, 3H), 3.50 (m, 2H). ¹³C NMR (Figure S4.20, 125 MHz, DMSO-d₆, δ, ppm): 173.5, 168.8, 158.9, 134.5, 128.3, 125.0, 119.7, 114.1, 55.4, 33.8.

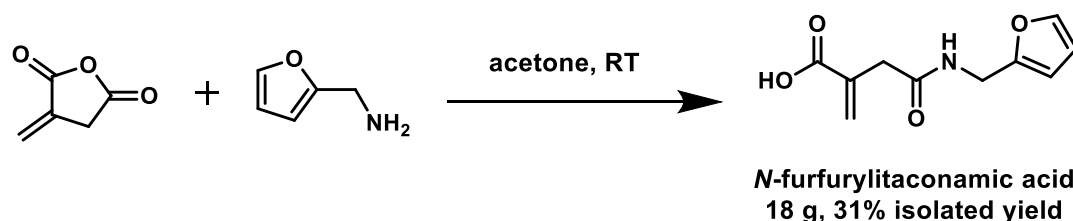


Synthesis of 5-(4-methoxyphenyl)-1-oxa-5-azaspiro[2.4]heptane-4,6-dione (5.5). A

25 mL round bottom flask was equipped with a stir bar and a reflux condenser. **4.4** (0.404 g, 1.86 mmol, 1.00 equiv), 2,6-di-*tert*-butylphenol (0.040 g, 0.19 mmol, 0.10 equiv) and *m*CPBA (0.999 g, 75 wt% pure, 4.34 mmol, 2.33 equiv) were then added, followed by 1,2-DCE (6 mL). The system was at 100 °C and was stirred for 2.5 h. The reaction mixture was then cooled to 0 °C in an ice/water bath where a large amount of solids precipitated. The solids were filtered off through a fritted funnel and washed with DCM. The filtrate was concentrated under reduced pressure and the crude reaction mixture was purified directly without any further work-up. Care was taken to treat the organic waste with Na₂S₂O₃ prior to disposal to destroy any remaining peroxide. Purification by chromatography (SiO₂, 25% ethyl acetate, 75% hexanes) gave **4.5** (0.154 g, 35% isolated yield for this step; 6% overall isolated yield from itaconic anhydride). ¹H NMR (Figure S4.21, 500 MHz, CDCl₃, δ, ppm): 7.46 (m, 2H), 7.699 (m, 2H), 3.83 (s, 3H), 3.52 (d, 1H, J = 6.0 Hz), 3.22 (d, 1H, J = 5.8 Hz), 3.20 (d, 1H, J = 19.0 Hz), 3.11 (d, 1H, J = 18.9 Hz). ¹³C NMR (Figure S4.22, 125 MHz, CDCl₃, δ, ppm): 173.3, 172.3, 159.9, 127.6, 124.1, 114.8, 55.7, 55.0, 51.9, 33.3.

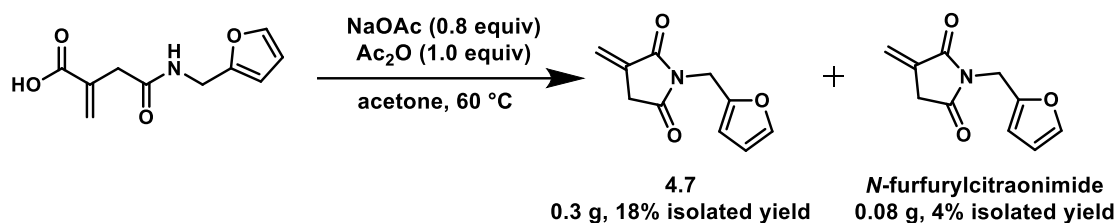


Ring-opening epoxide polymerization attempt of 4.5. In a glovebox, a 2-dram vial was equipped with a stir bar and a cap and septum. **4.5** (21 mg, 0.09 mmol, 90 equiv) was added to the vial, and then 0.01 mL of a ^tBuOK stock solution (10 mg/mL, 0.1 mg, 0.001 mmol, 1 equiv) and 0.01 mL of an 18-crown-6 stock solution (30 mg/mL, 0.3 mg, 0.001 mmol, 1 equiv) were added. The reaction mixture was then heated at 50 °C outside of the glovebox for 22 h. An aliquot was taken for ¹H NMR (DMSO-d₆) which showed 33% yield of allyl alcohol **4.6** using THF as an internal standard. Only oligomers were detected by SEC analysis. ¹H NMR (crude reaction mixture, Figure S4.23, 500 MHz, CDCl₃, δ, ppm): 7.47 (t, 2H, J = 7.7 Hz), 7.36 (m, 3H), 6.69 (s, 1H), 4.70 (s, 2H).



Synthesis of N-furfurylitaconamic acid. A 250 mL round bottom flask was equipped with a stir bar. Itaconic anhydride (30.29 g, 0.2703 mol, 1.00 equiv) was added, followed by acetone (100 mL). Furfurylamine (24.0 mL, 26.38 g, 0.2716 mol, 1.01 equiv) was then added dropwise to the stirring reaction mixture. The resulting solution was then cooled to 0 °C in an ice/water bath and stirred for 1h. The solution was then placed at – 20 °C and left to crystallize overnight. The solids were then isolated by filtration and washed with EtOAc. The crude solid (8 g) was dissolved in a mixture of EtOAc:hexanes:MeOH (~ 80 mL, 10:10:1 v/v/v) with heat and then placed at – 20 °C to crystallize. The recrystallized product was then collected by filtration, washed with Et₂O, and dried under vacuum. The filtrate was left to sit at – 20 °C at which point more crystals formed. These crystals were collected by filtration, washed with Et₂O, and dried

under vacuum. The combined recrystallized product was then isolated to give the pure N-furfurylitaconamic acid (17.55 g, 31% isolated yield). ^1H NMR (Figure S4.24, 400 MHz, DMSO- d_6 , δ , ppm): 12.48 (s, 1H), 8.33 (m, 1H), 7.56 (s, 1H), 6.38 (m, 1H), 6.22 (m, 1H), 6.10 (s, 1H), 5.66 (s, 1H), 4.24 (d, 1H, $J = 5.6$ Hz), 3.12 (s, 1H).



Synthesis of N-furfurylcitraonimide 4.7. A 50 mL round bottom flask was equipped with a stir bar and a reflux condenser. N-furfurylitaconamic acid (2.014 g, 9.63 mmol, 1.00 equiv) was added, followed by NaOAc (0.677 g, 8.25 mmol, 0.857 equiv) and acetone (10 mL). Acetic anhydride (0.93 mL, 1.00 g, 9.83 mmol, 1.02 equiv) was then added dropwise and the reaction mixture was submerged in an oil bath pre-heated to 60 $^\circ\text{C}$. The reaction was allowed to stir at this temperature for 15 h and then was cooled to RT. The reaction mixture was then washed three times with water and once with brine before being dried with MgSO_4 , filtered, and concentrated under reduced pressure. The crude product was then purified by chromatography (SiO_2 , gradient from 5% ethyl acetate, 95% hexanes to 20% ethyl acetate, 80% hexanes gradient) to give pure **4.7** (0.330 g, 18% isolated yield for this step, 6% overall yield from itaconic anhydride). ^1H NMR (Figure S4.25, 400 MHz, CDCl_3 , δ , ppm): 7.33 (s, 1H), 6.38 (m, 1H), 6.35 (m, 1H), 5.64 (m, 1H), 4.76 (m, 2H), 3.35 (m, 2H). N-furfurylcitraonimide was also collected from the chromatographic purification (0.076 g, 4% isolated yield). ^1H NMR (Figure S4.26, 400 MHz, CDCl_3 , δ , ppm): 7.32 (s, 1H), 6.34 (m, 1H), 6.29 (s, 2H), 4.66 (s, 2H), 2.08 (m, 3H).

APPENDIX

General Reagent Information. Dimethyl sulfoxide-d₆ (DMSO-d₆, 99.9%, Cambridge Isotope Laboratories, Inc.), chloroform-D (99.8%, Cambridge Isotope Laboratories, Inc.), methanol (MeOH, 99.8%, Fisher), acetone (\geq 99.5%, Fisher), aniline (99%, Sigma-Aldrich), 2,6-di-*t*-butylphenol (98%, Alfa Aesar), *meta*-Chloroperoxybenzoic acid (*m*CPBA, 75%, Oakwood Chemical), itaconic anhydride (97%, Alfa Aesar), furfuryl amine (\geq 99%, Aldrich), sodium hydroxide (Macron), sodium thiosulfate (Na₂S₂O₃, 100%, Chem-Impex Int'l. Inc.), *p*-anisidine (\geq 99% Aldrich), ethyl acetate (EtOAc, 99.5%, Fisher), acetic anhydride (Ac₂O, 99%, EMD), anhydrous magnesium sulfate (98.0%, EMD Millipore), Celite[®] 545 (Sigma-Aldrich), α -methylene- γ -butyrolactone (MBL, $>95.0\%$, TCI), α -methylene- γ -methyl- γ -butyrolactone (MeMBL, $>96.0\%$, TCI), sodium acetate (NaOAc, anhydrous, 99%, Alfa Aesar), silver nitrate (ACS grade, Mallinckrodt), potassium *tert*-butoxide (99.16%, Chem-Impex Int'l. Inc.), sodium bicarbonate (ACS grade, Macron), sodium chloride (ACS grade, VWR), Oxone[®] (Monopersulfate, 2KHSO₅·KHSO₄·K₂SO₄, Alfa Aesar), bromine (99.5%, Alfa Aesar), diethyl ether (Et₂O, Laboratory grade, Fisher), and argon (High purity grade 4.8, Airgas) were used as received. Me₂MBL was synthesized following a known procedure.²⁷ Dimethyl dioxirane (DMDO) was synthesized following a known procedure,³³ stored in a freezer ($-20\text{ }^{\circ}\text{C}$) and titrated to determine its concentration immediately prior to its use.³⁴ 18-crown-6 was recrystallized three times from MeCN and dried under vacuum (50 mTorr) prior to use.⁵⁷ Deionized (DI) water was obtained by reverse osmosis. Brine solution was made by saturating water with salt. Saturated bicarbonate solution was made by saturating water with sodium bicarbonate. Saturated

sodium thiosulfate solution was made by saturating water with sodium thiosulfate. Acetonitrile (MeCN, $\geq 99.9\%$, VWR) and tetrahydrofuran (THF, 99%, Macron) were degassed by sparging with argon for 30 min and then purified by passing through two packed columns of neutral alumina on the JC Meyer solvent system. *N,N*-dimethylformamide (DMF, Macron) was degassed by sparging with argon for 30 min and then purified by passing through two packed columns of activated molecular sieves followed by a packed column of isocyanide on the JC Meyer solvent system. Mylar sheets (10" x 10" x 0.04") were obtained from Carver, Inc.

General Analytical Information. Polymers samples were analyzed using size exclusion chromatography (SEC) instruments operating with a THF or DMF eluent. For the SEC with THF eluent, a Tosoh EcoSec HLC 8320GPC system with two SuperHM-M columns in series at a flow rate of 0.350 mL/min at 40 °C was used. Number-average molar masses (M_n), weight-average molar masses (M_w), and dispersities (\bar{D}) for polymer samples were determined by light scattering using a Wyatt mini Dawn Treos multi-angle light scattering detector at 25 °C. M_n , M_w , and \bar{D} values were also determined from the refractive index chromatogram against polystyrene (TSKgel) standards. For the SEC with DMF eluent, polymer samples were analyzed using a GPC system composed of a Waters 1515 Isocratic HPLC pump and three PSS GRAM columns (100–1000–3000) in series at a flow rate of 1.0 mL/min at 35 °C. A 0.05% LiBr solution in DMF was used as the eluent and M_{ns} , M_{ws} , and \bar{D}_s were determined from refractive index chromatograms against polystyrene standards (Polymer Standards Service USA, Inc., Amherst, MA) using a Waters 2414 differential refractive index detector. A second DMF SEC equipped with a light scattering detector was also used to analyze a PMBLO

sample. This sample was analyzed using a GPC system composed of a Agilent 1200 pump and autosampler, a Viscotek (Model I-MBMMW-3078) pump (Exclusion Limit MW for PS of 200 kg/mol, max more size of 10,000 Å) with a flow rate of 1 mL/min operating at 50 °C. A 0.05 M LiBr solution in DMF was used as the eluent and M_n s, M_w s, and \bar{D} s were determined for polymer samples were determined by light scattering using a Wyatt DAWN HELEOS-II multi-angle light scattering (MALS) detector equipped with a 658 nm wavelength laser operating 25 °C. The dn/dc values of PMBLO was estimated to be 0.0652 mL/g using size exclusion chromatography with samples of known concentrations in DMF. This indirect ("in-line") method uses the total area of the RI signal and the assumption that 100% of the sample mass is recovered to calculate the polymer dn/dc values. Nuclear magnetic resonance (NMR) spectra were recorded on a Mercury 300 MHz, a Varian 400 MHz, a Bruker 500 MHz, or a Varian 600 MHz instrument. Differential scanning calorimetry (DSC) was performed using a TA Instruments Q1000. Samples were prepared in aluminum pans and were analyzed using the following heating program: -50 °C to 150 °C at 30 °C/min, 150 °C to -50 °C at 10 °C/min, and -50 °C to 150 °C at 30 °C/min. The data were processed using Universal Analysis 2000 for Windows software. All reported T_g s were observed on the second heating cycle. Thermogravimetric analysis (TGA) was performed on a TA Instruments Q500 Thermogravimetric Analyzer or an Instruments Q500 Analyzer. Typically, samples were heated at 10 °C/min to 550 °C under nitrogen. Data were processed using Universal Analysis 2000 for Windows software. To melt process PMBLO, the solid powder obtained after polymerization of MBLO and subsequent precipitation was placed between two Mylar sheets and melt pressed in a rectangular mold at 2000 lbs

and 150 °C and then quenched by cooling to RT under ambient conditions to yield a brittle solid. Using 8 mm parallel plates, TA Instruments DHR3 Rheometer was used for dynamic mechanical analysis. Heating was controlled under nitrogen atmosphere, and the samples were equilibrated at the designated temperature for 5 minutes before testing.

Supplementary Figures

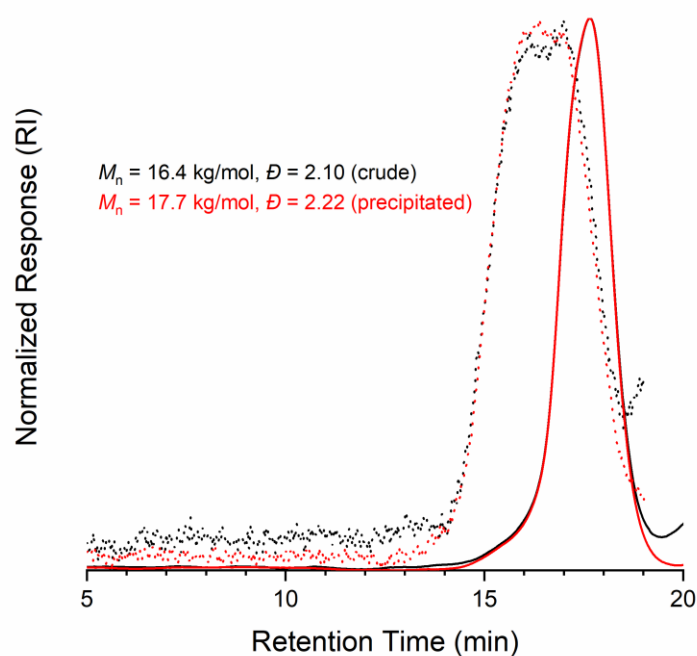


Figure S4.1. SEC traces (solid line = refractive index trace, dotted line = light scattering trace) for crude (black) and precipitated (red) PMBLO sample (Table 4.1, entry 8).

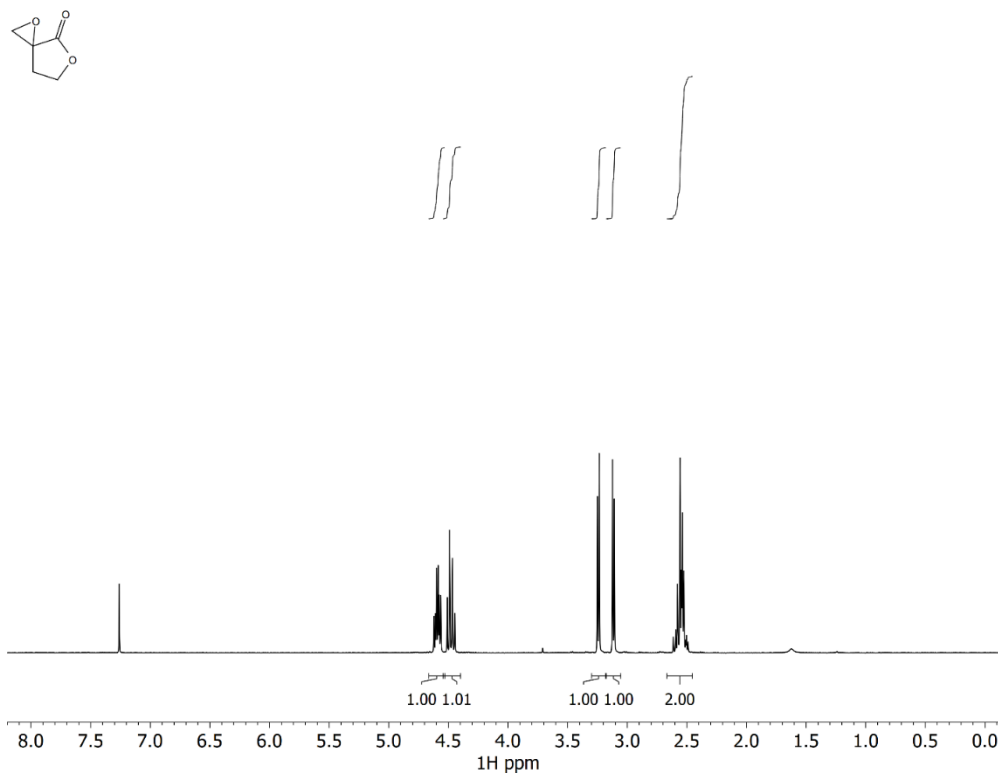


Figure S4.2. ^1H NMR spectra of α -methylene- γ -butyrolactone oxide (MBLO) in CDCl₃.

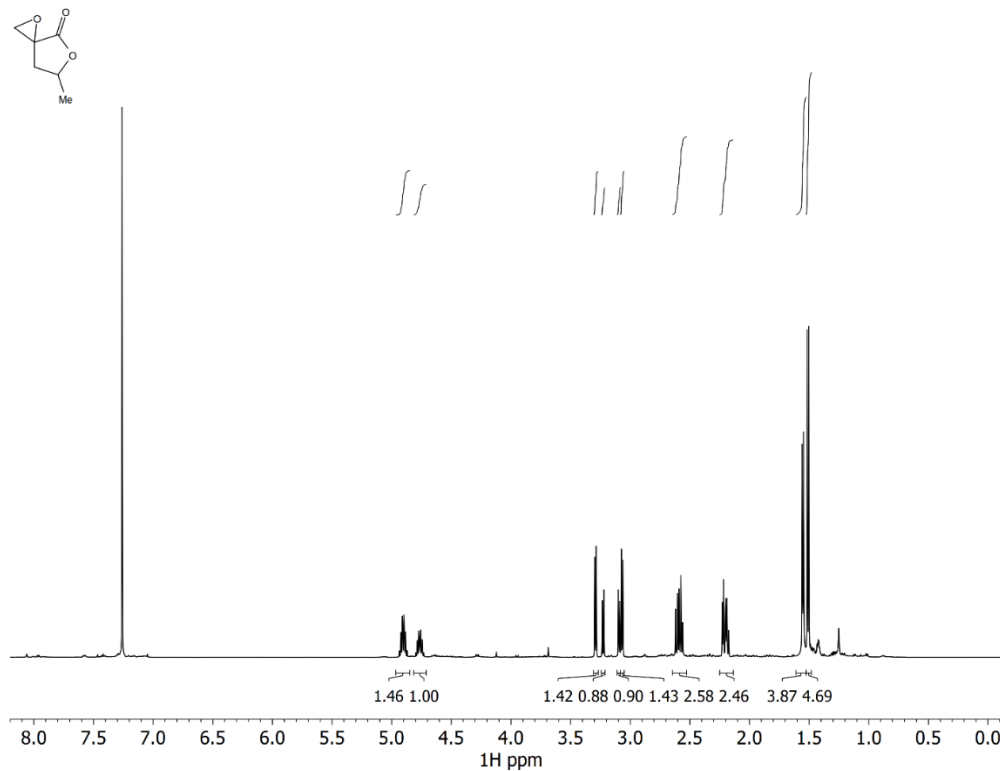


Figure S4.3. ^1H NMR spectra of γ -methyl- α -methylene- γ -butyrolactone oxide (MeMBLO) in CDCl₃.

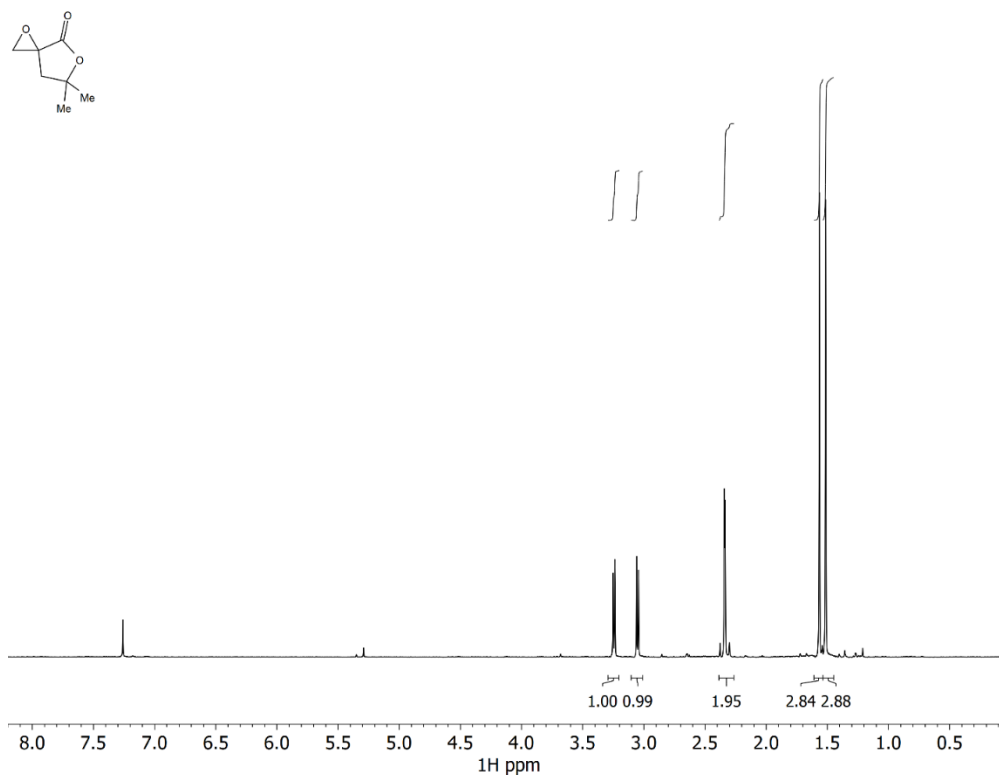


Figure S4.4. ¹H NMR spectra of γ,γ -dimethyl- α -methylene- γ -butyrolactone oxide (Me₂MBLO) in CDCl₃.

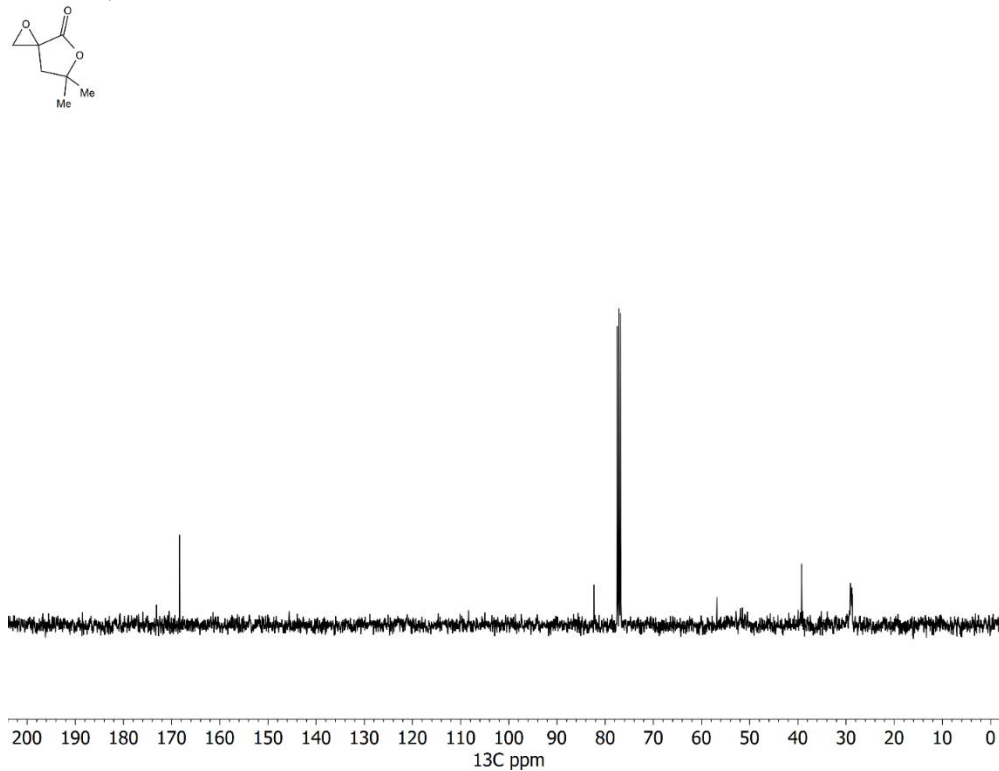


Figure S4.5. ¹³C NMR spectra of γ,γ -dimethyl- α -methylene- γ -butyrolactone oxide (Me₂MBLO) in CDCl₃.

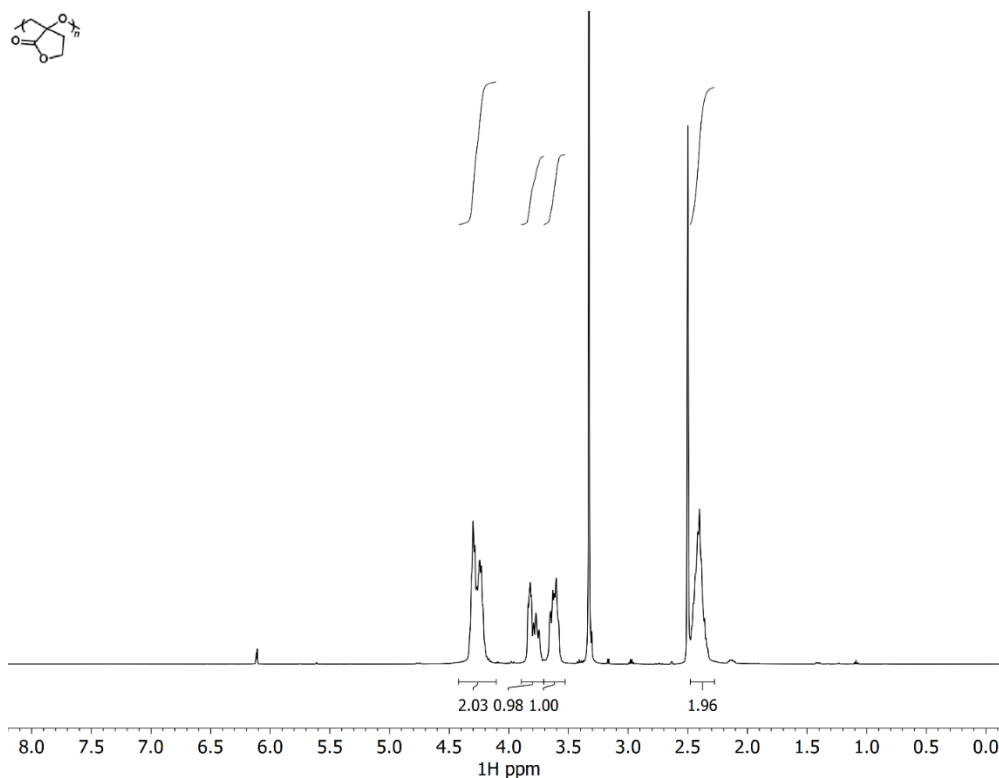


Figure S4.6. ^1H NMR spectra of poly(α -methylene- γ -butyrolactone oxide) (PMBLO) in DMSO- d_6 .

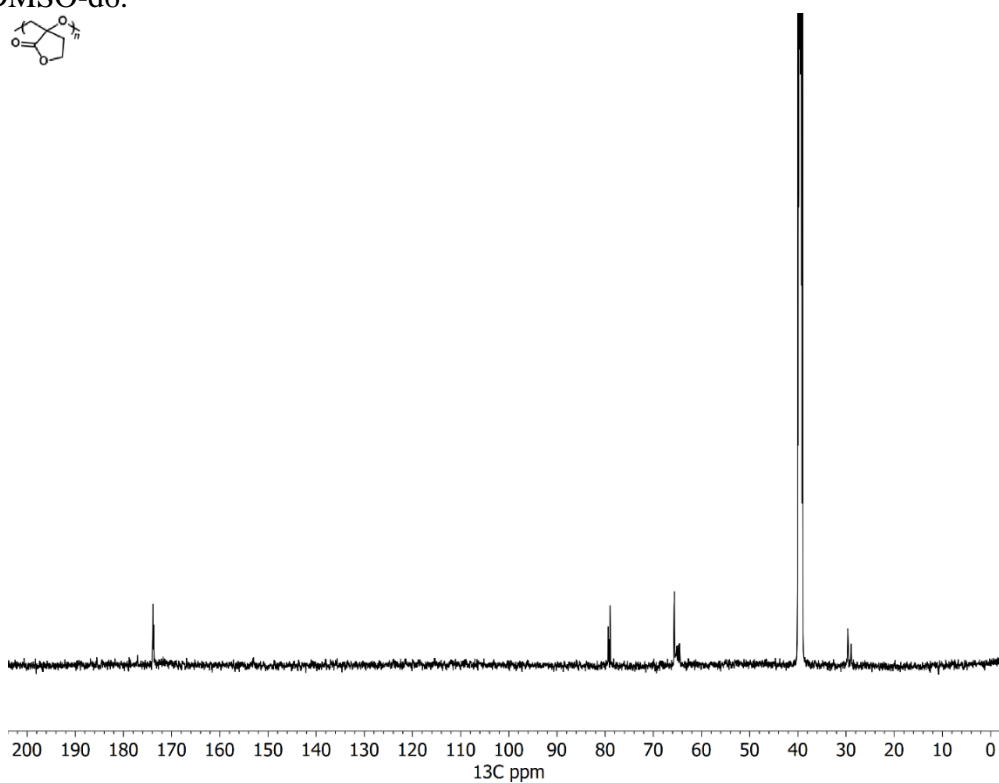


Figure S4.7. ^{13}C NMR spectra of poly(α -methylene- γ -butyrolactone oxide) (PMBLO) in DMSO- d_6 .

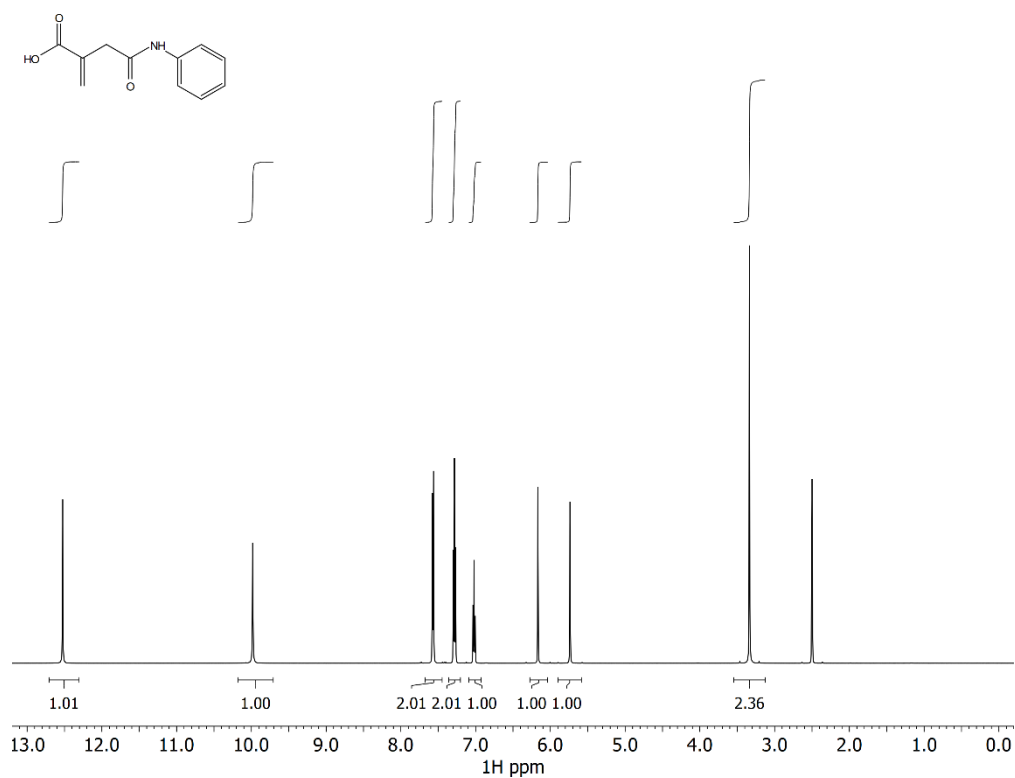


Figure S4.8. ¹H NMR spectra of N-phenylitaconamic acid in DMSO-d₆.

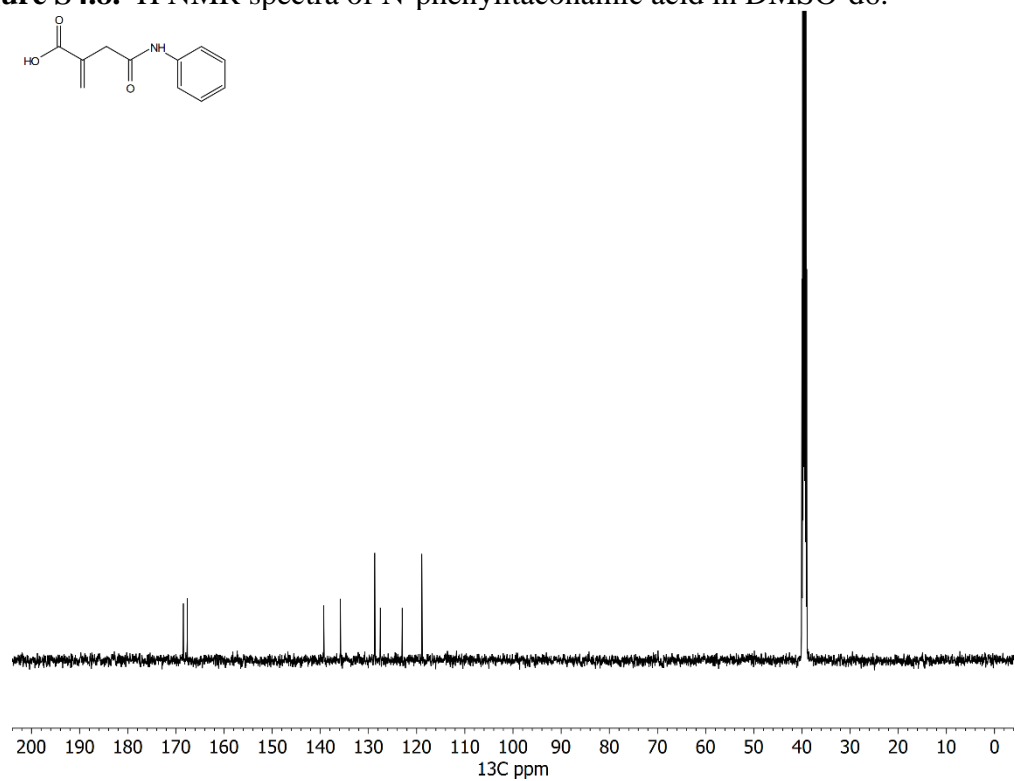


Figure S4.9. ¹³C NMR spectra of N-phenylitaconamic acid in DMSO-d₆.

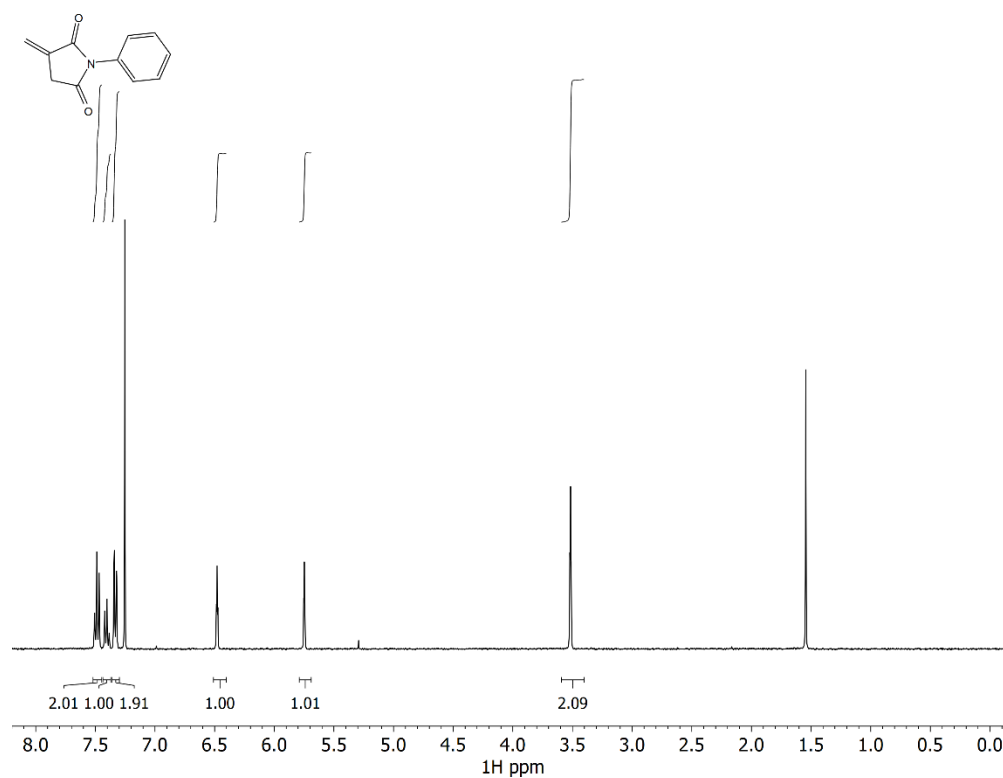


Figure S4.10. ¹H NMR spectra N-phenylitaconimide (**4.1**) in CDCl₃.

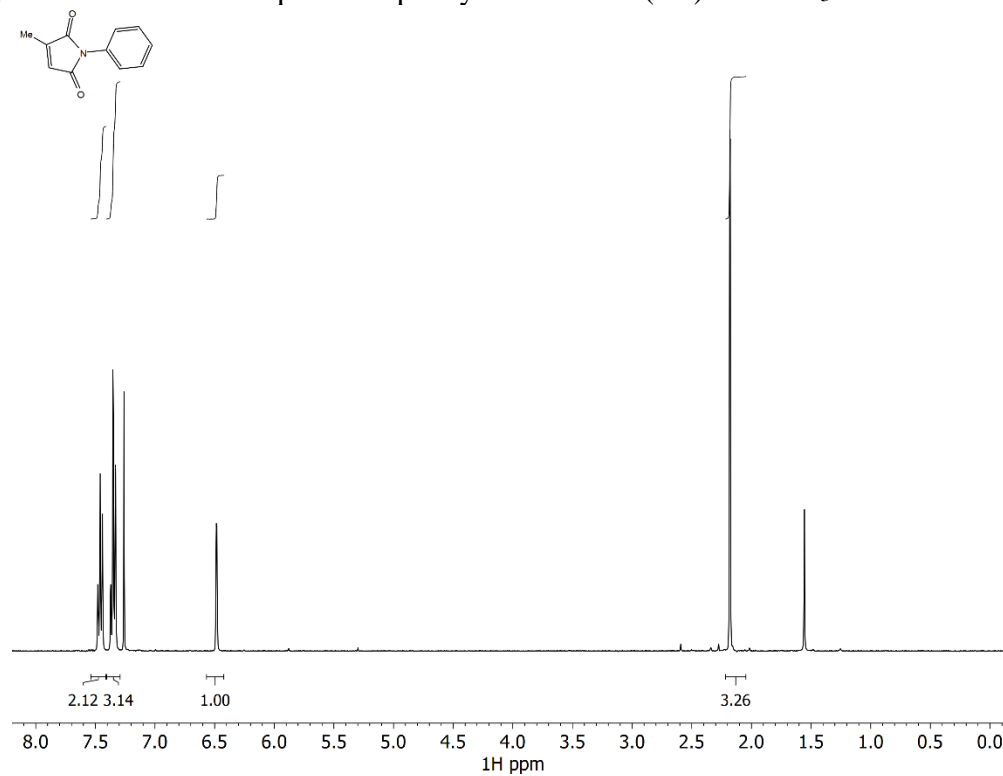


Figure S4.11. ¹H NMR spectra of N-phenylcitraconimide in CDCl₃.

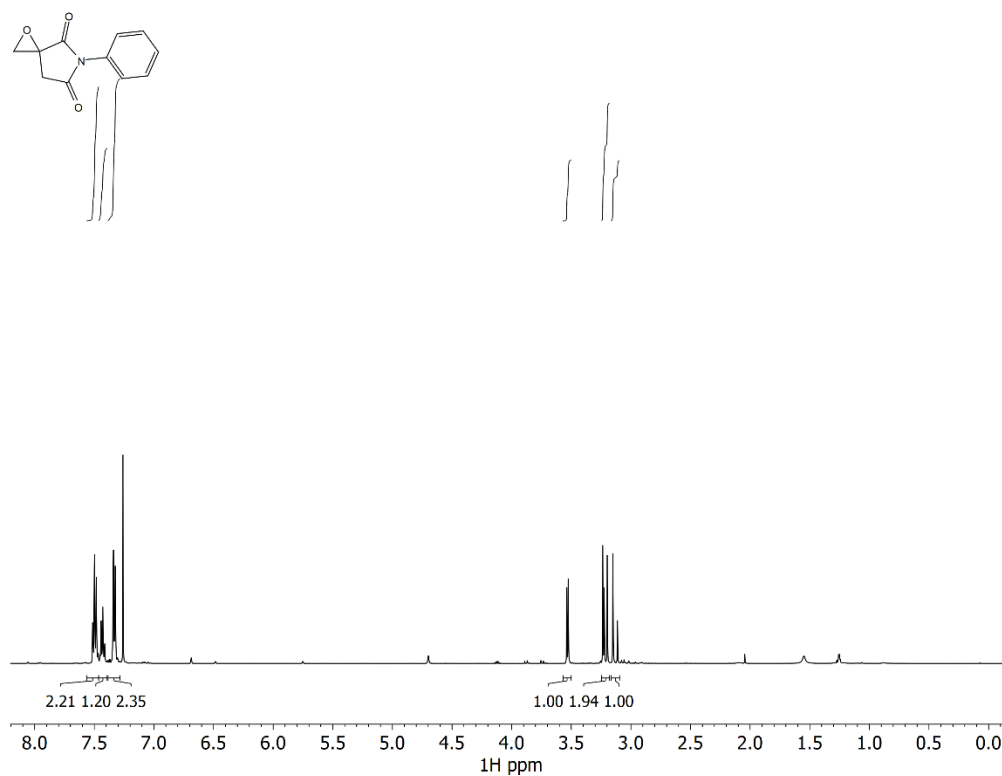


Figure S4.12. ¹H NMR spectra of 5-phenyl-1-oxa-5-azaspiro[2.4]heptane-4,6-dione (4.2) in CDCl₃.

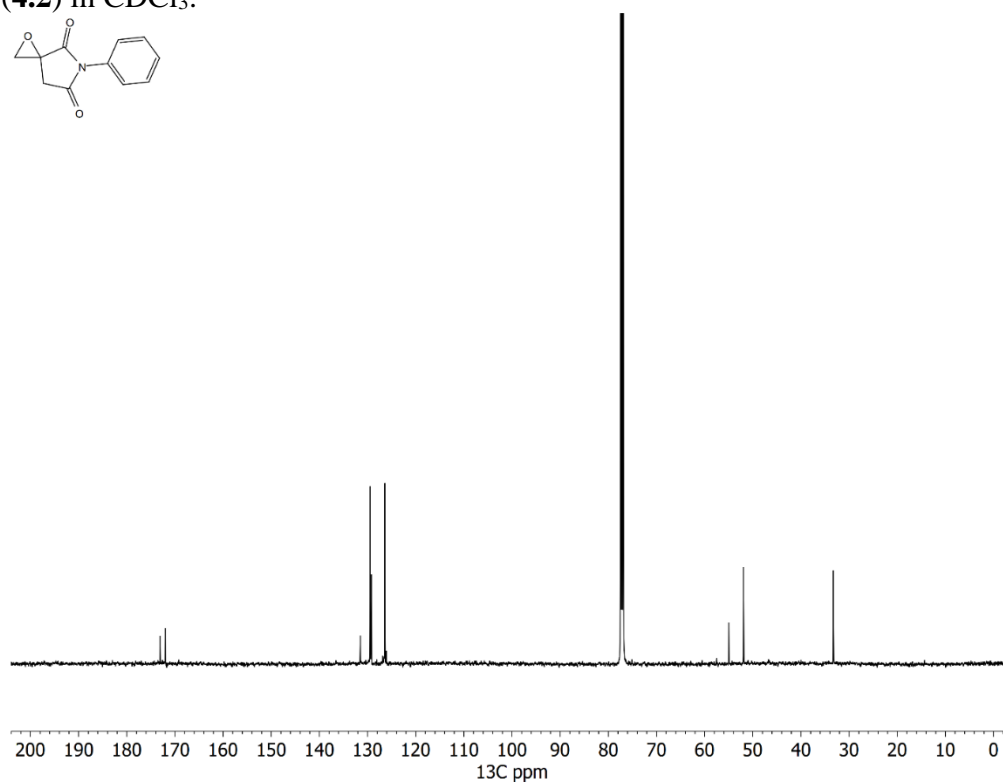


Figure S4.13. ¹³C NMR spectra of 5-phenyl-1-oxa-5-azaspiro[2.4]heptane-4,6-dione (4.2) in CDCl₃.

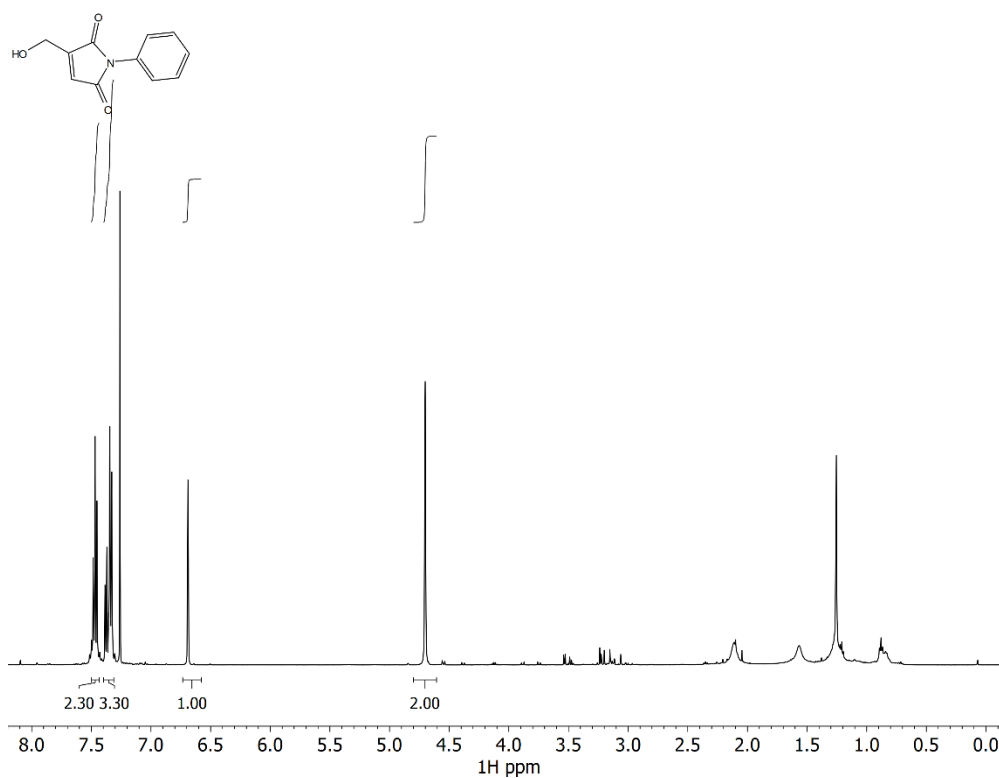


Figure S4.14. ¹H NMR spectra of 3-(hydroxymethyl)-1-phenyl-1H-pyrrole-2,5-dione (4.3) in CDCl₃.

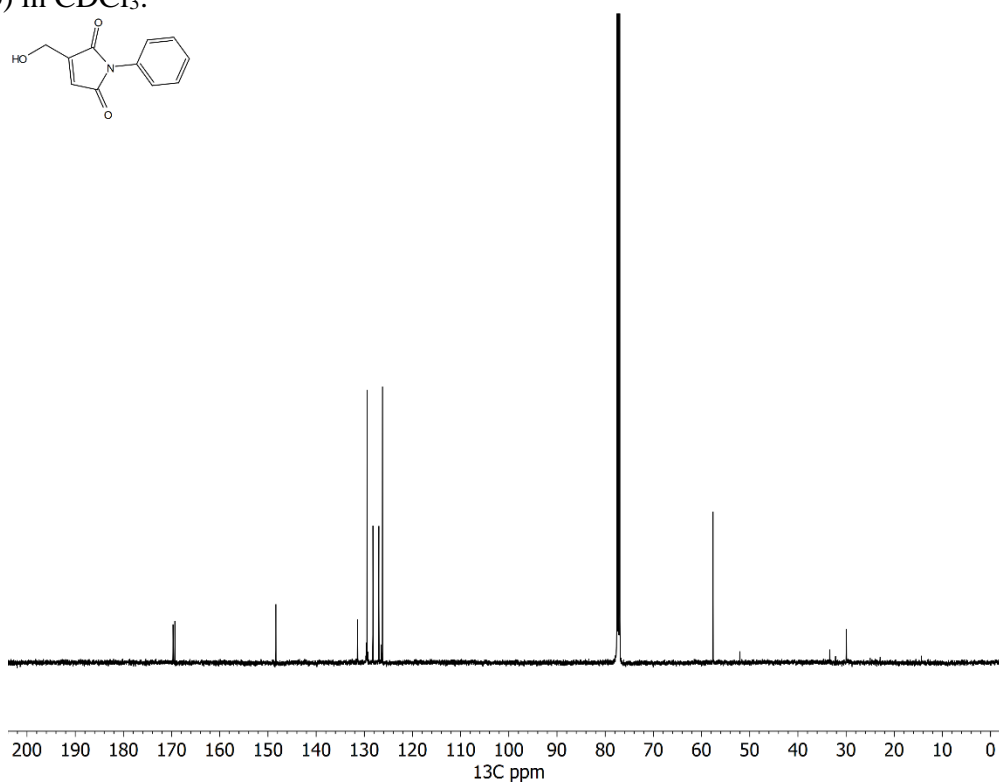


Figure S4.15. ¹³C NMR spectra of 3-(hydroxymethyl)-1-phenyl-1H-pyrrole-2,5-dione (4.3) in CDCl₃.

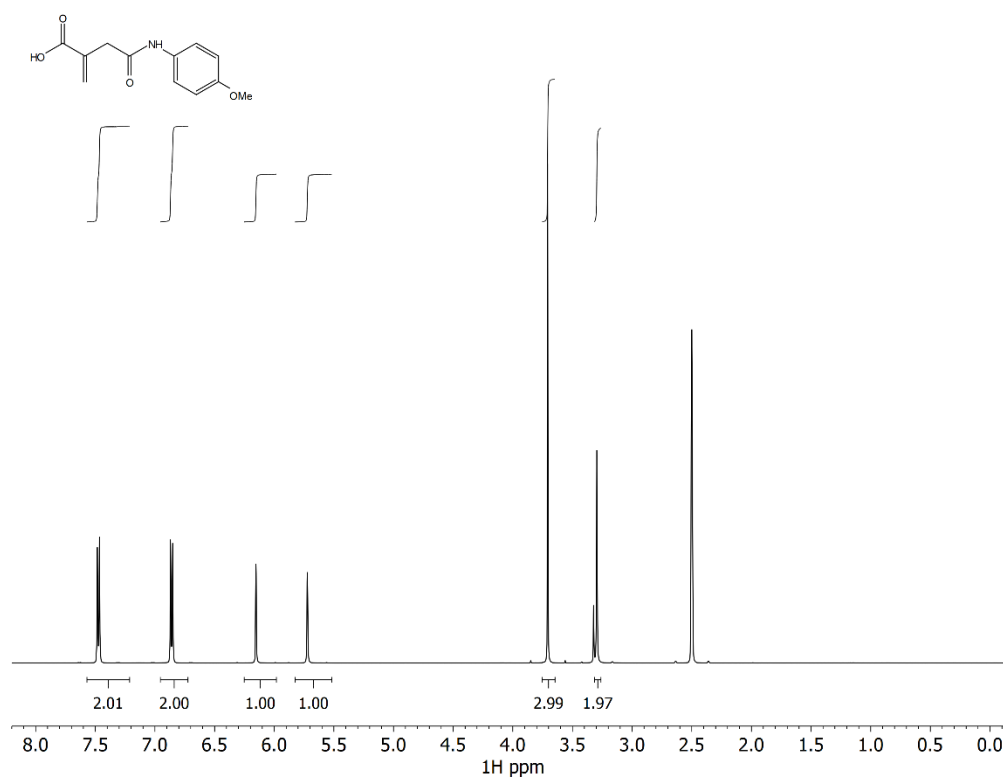


Figure S4.16. ¹H NMR spectra of N-(*p*-anisidine)itaconamic acid in DMSO-d₆.

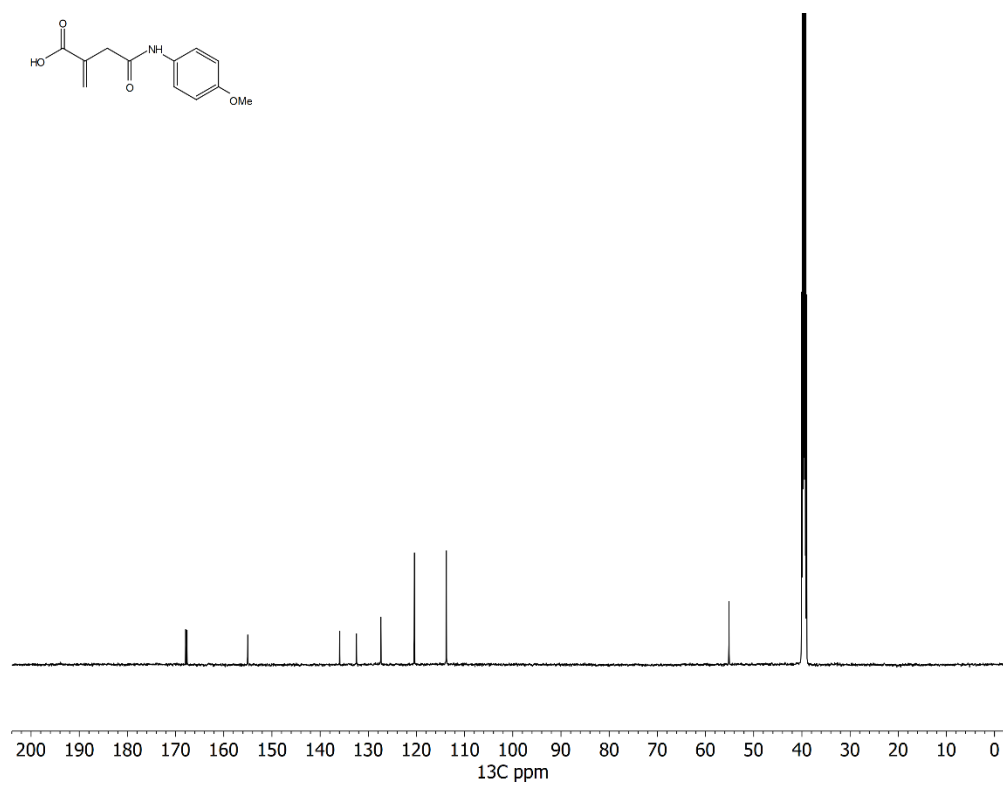


Figure S4.17. ¹³C NMR spectra of N-(*p*-anisidine)itaconamic acid in DMSO-d₆.

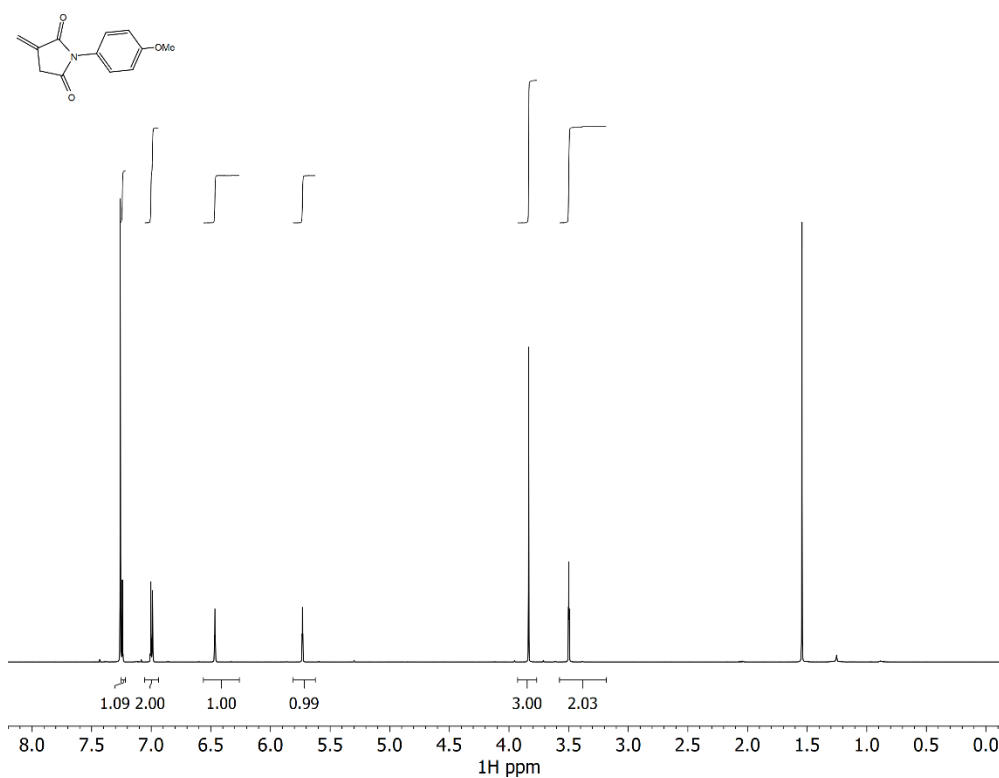


Figure S4.18. ¹H NMR spectra of N-(*p*-anisidine)itaconimide (**4.4**) in CDCl₃.

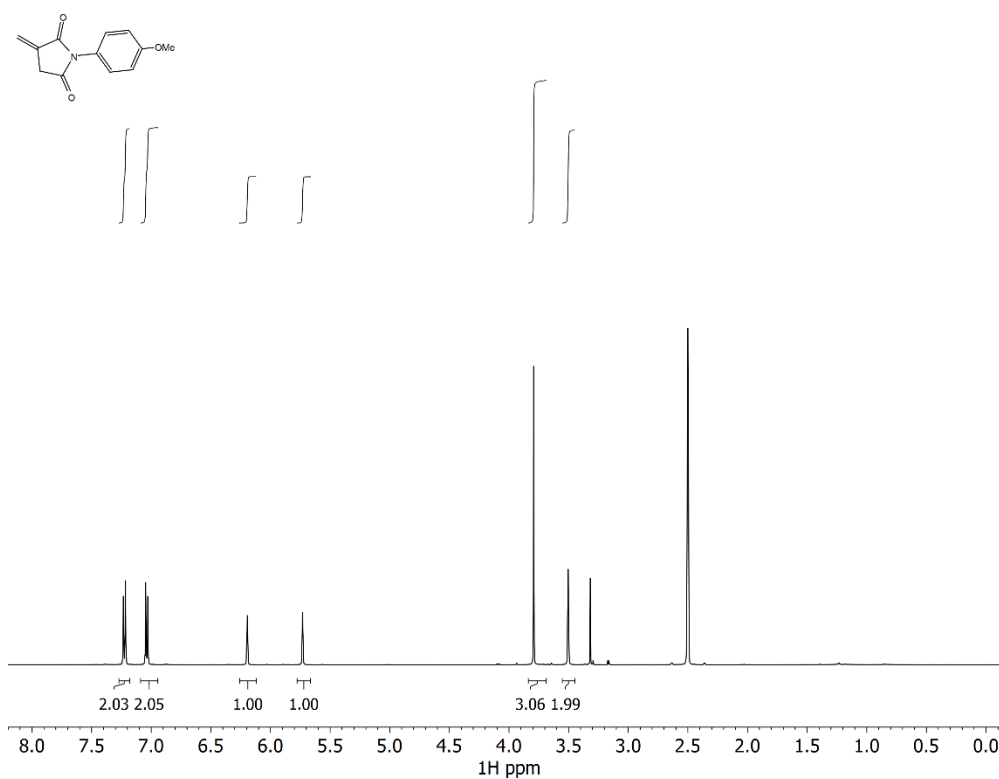


Figure S4.19. ¹H NMR spectra of N-(*p*-anisidine)itaconimide (**4.4**) in DMSO-d₆.

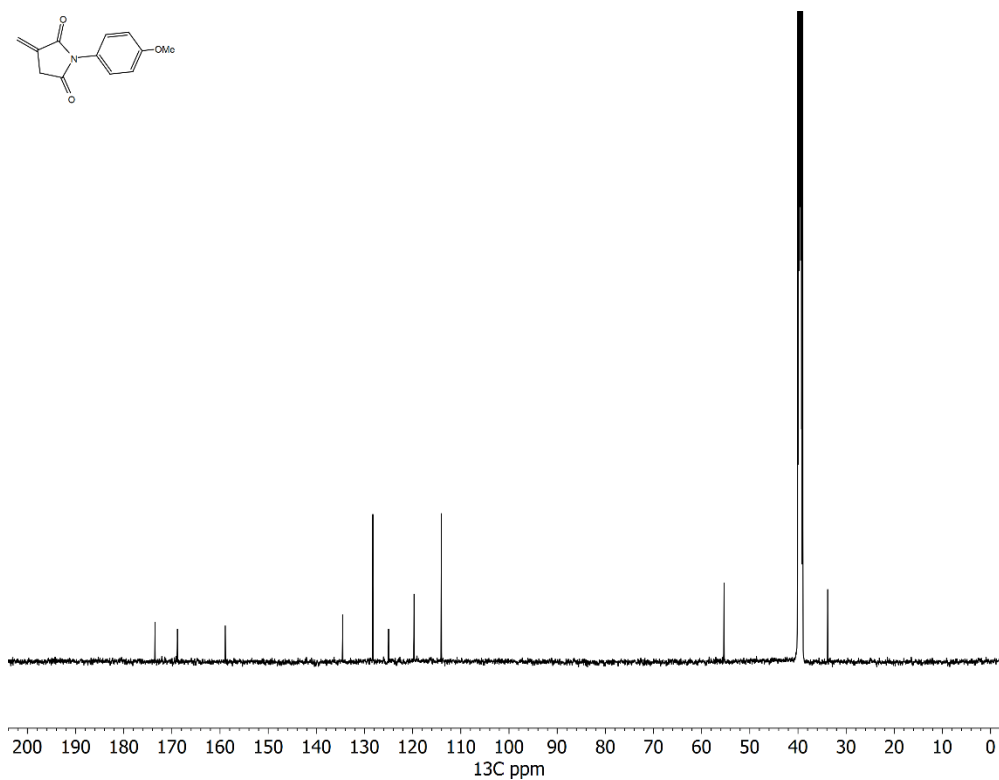


Figure S4.20. ¹³C NMR spectra of N-(*p*-anisidine)itaconimide (**4.4**) in DMSO-d₆.

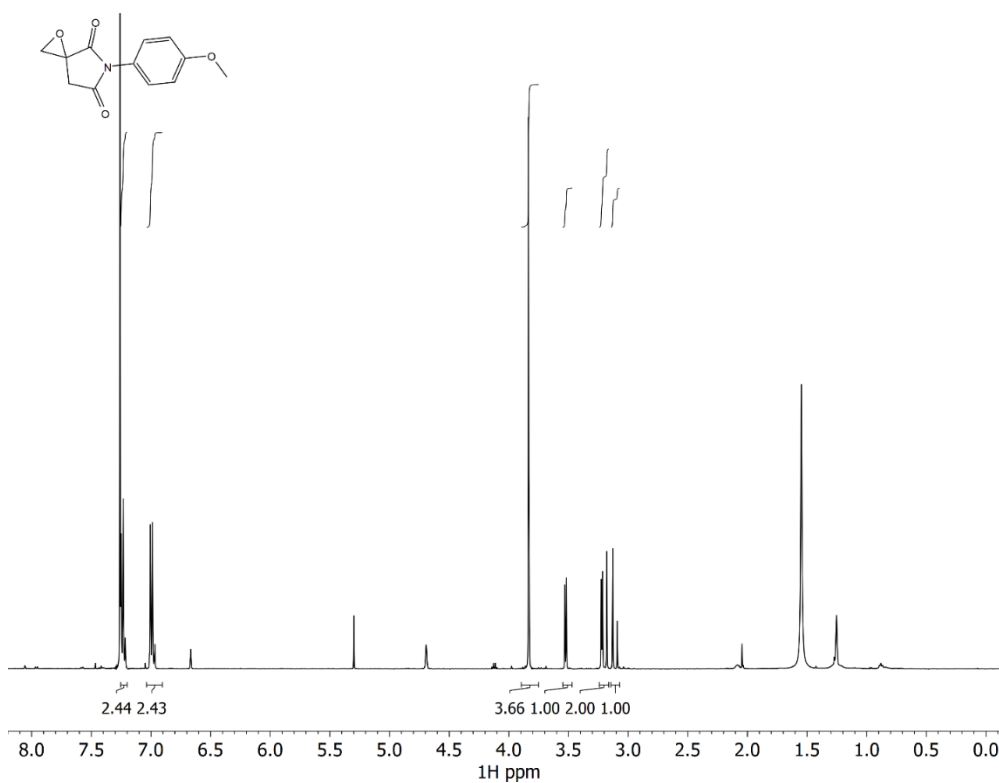


Figure S4.21. ¹H NMR spectra of 5-(4-methoxyphenyl)-1-oxa-5-azaspiro[2.4]heptane-4,6-dione (**4.5**) in CDCl₃.

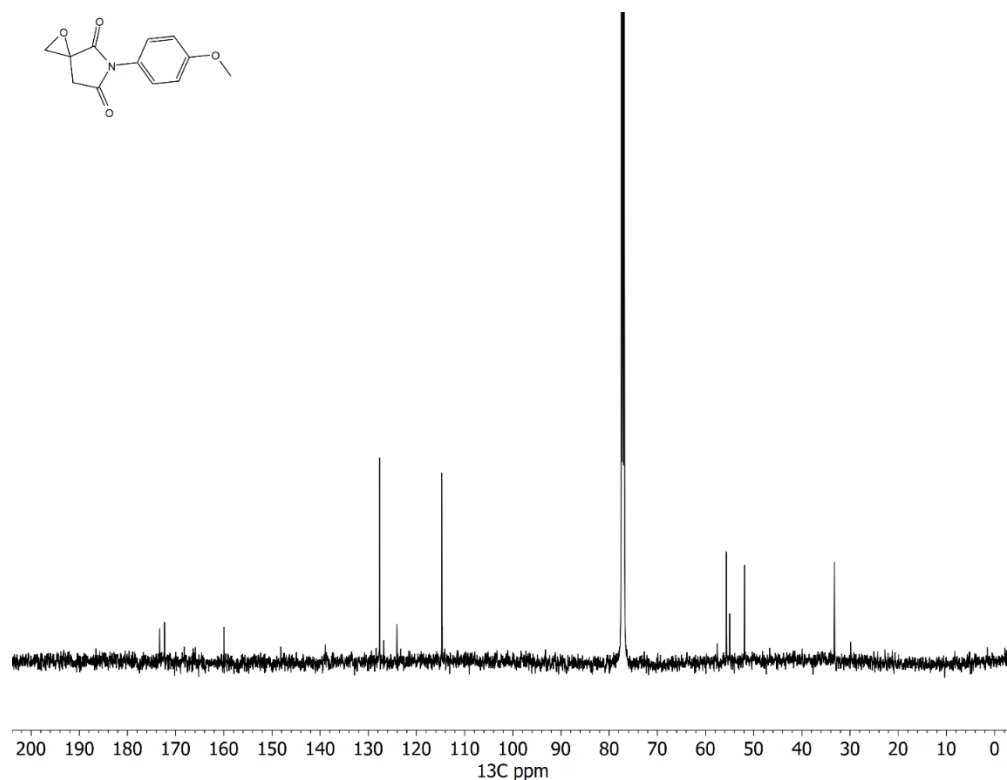


Figure S4.22. ^{13}C NMR spectra of 5-(4-methoxyphenyl)-1-oxa-5-azaspiro[2.4]heptane-4,6-dione (**4.5**) in CDCl_3 .

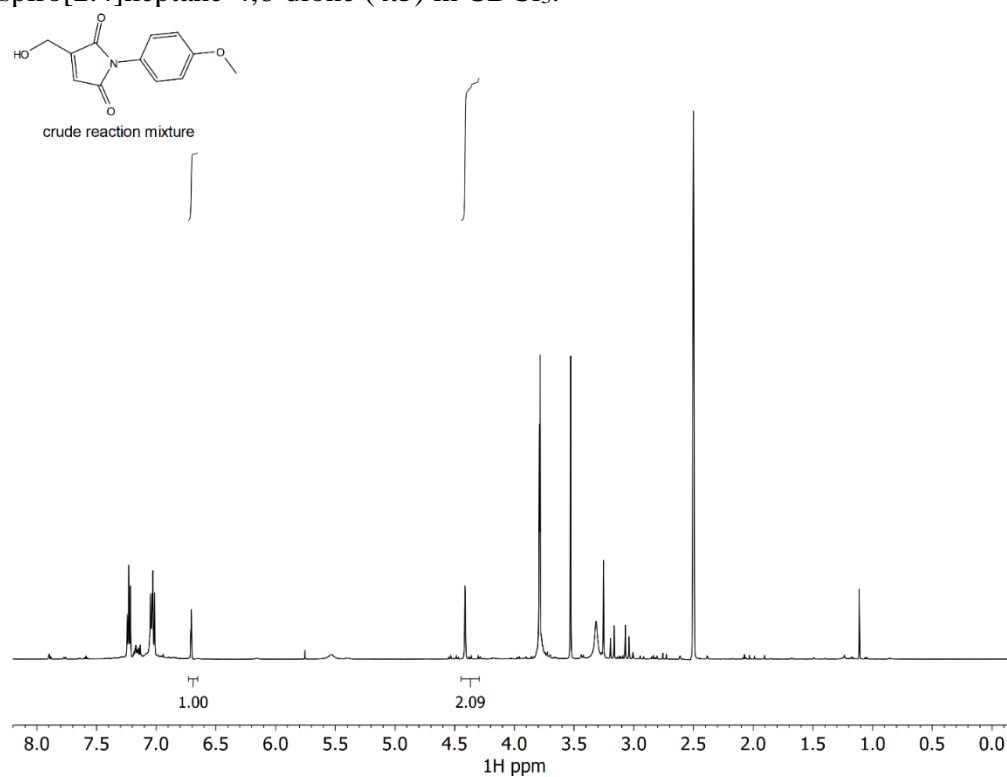


Figure S4.23. ^1H NMR spectra of 3-(hydroxymethyl)-1-(4-methoxyphenyl)-1H-pyrrole-2,5-dione (**4.6**), as part of a crude reaction mixture) CDCl_3 .

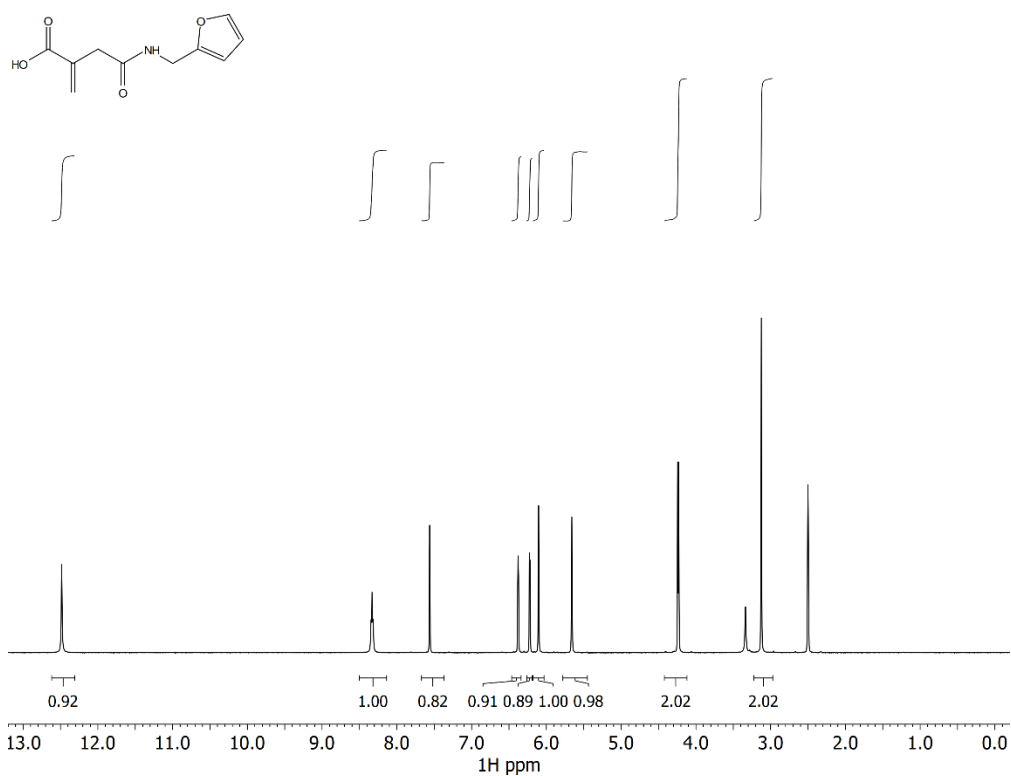


Figure S4.24. ¹H NMR spectra N-furfurylitaconamic acid in DMSO-d₆.

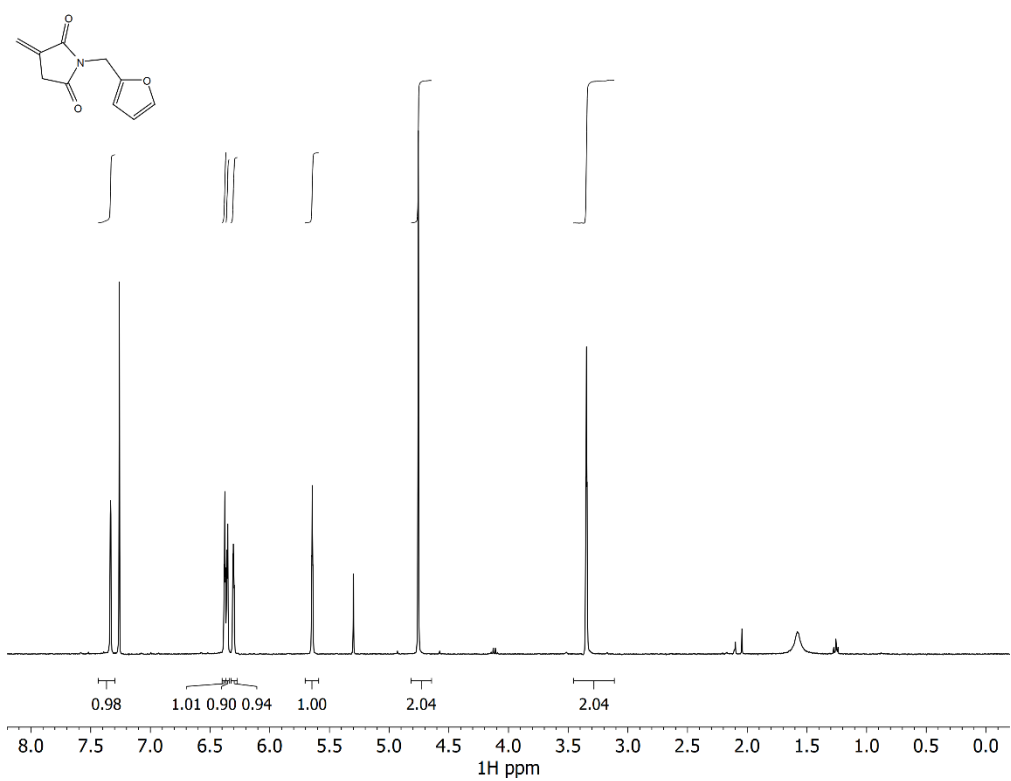


Figure S4.25. ¹H NMR spectra N-furfurylitaconimide (**4.7**) in CDCl₃.

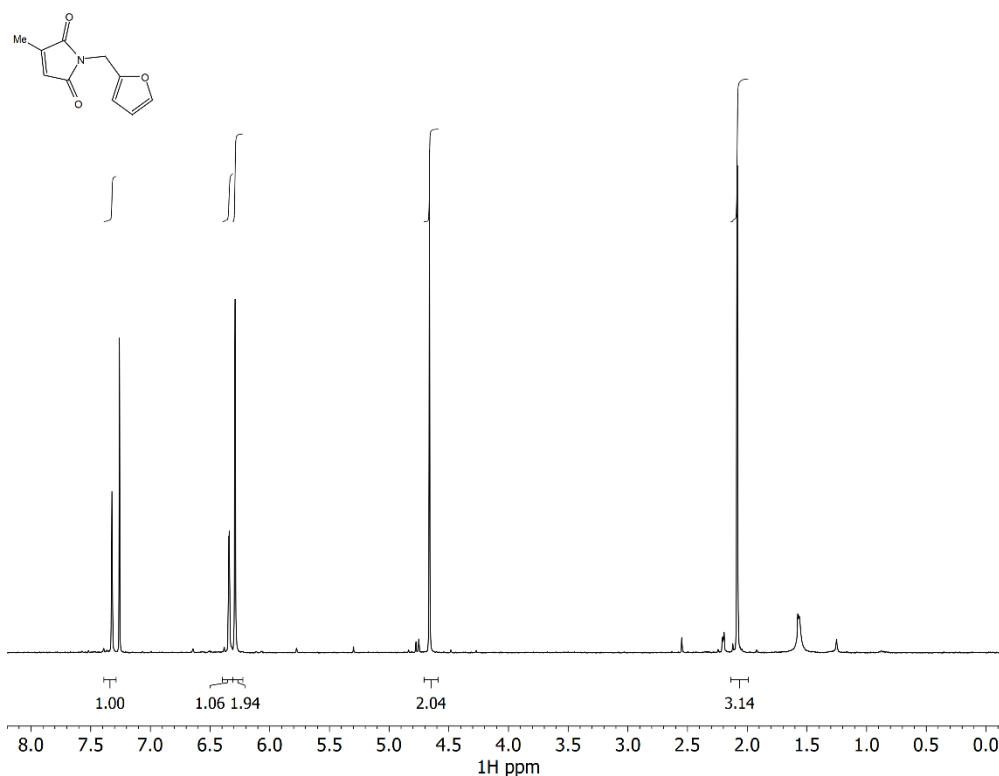


Figure S4.26. ¹H NMR spectra N-furfuryleitraconimide in CDCl₃.

REFERENCES

- (1) Engels, H.-W.; Pirkel, H.-G.; Albers, R.; Albach, R. W.; Krause, J.; Hoffmann, A.; Casselmann, H.; Dormish, J. Polyurethanes: Versatile Materials and Sustainable Problem Solvers for Today's Challenges *Angewandte Chemie Int. Ed.* **2013**, 52, 9422–9441.
- (2) Xue, Z.; He, D.; Xie, X. Poly(Ethylene Oxide)-Based Electrolytes for Lithium-Ion Batteries. *J. Mater. Chem. A* **2015**, 3, 19218–19253.
- (3) Herzberger, J.; Niederer, K.; Pohlitz, H.; Seiwert, J.; Worm, M.; Wurm, F. R.; Frey, H. Polymerization of Ethylene Oxide, Propylene Oxide, and Other Alkylene Oxides: Synthesis, Novel Polymer Architectures, and Bioconjugation. *Chem. Rev.* **2016**, 116, 2170–2243.

- (4) Childers, M. I.; Longo, J. M.; Van Zee, N. J.; Lapointe, A. M.; Coates, G. W. Stereoselective Epoxide Polymerization and Copolymerization. *Chem. Rev.* **2014**, *114*, 8129–8152.
- (5) Peretti, K. L.; Ajiro, H.; Cohen, C. T.; Lobkovsky, E. B.; Coates, G. W. A Highly Active, Isospecific Cobalt Catalyst for Propylene Oxide Polymerization. *J. Am. Chem. Soc.* **2005**, *127*, 11566–11567.
- (6) Childers, M. I.; Vitek, A. K.; Morris, L. S.; Widger, P. C. B.; Ahmed, S. M.; Zimmerman, P. M.; Coates, G. W. Isospecific, Chain Shuttling Polymerization of Propylene Oxide Using a Bimetallic Chromium Catalyst: A New Route to Semicrystalline Polyols. *J. Am. Chem. Soc.* **2017**, *139*, 11048–11054.
- (7) Widger, P. C. B.; Ahmed, S. M.; Coates, G. W. Exploration of Cocatalyst Effects on a Bimetallic Cobalt Catalyst System: Enhanced Activity and Enantioselectivity in Epoxide Polymerization. *Macromolecules* **2011**, *44*, 5666–5670.
- (8) Widger, P. C. B.; Ahmed, S. M.; Hirahata, W.; Thomas, R. M.; Lobkovsky, E. B.; Coates, G. W. Isospecific Polymerization of Racemic Epoxides: A Catalyst System for the Synthesis of Highly Isotactic Polyethers. *Chem. Commun.* **2010**, *46*, 2935–2937.
- (9) Thomas, R. M.; Widger, P. C. B.; Ahmed, S. M.; Jeske, R. C.; Hirahata, W.; Lobkovsky, E. B.; Coates, G. W. Enantioselective Epoxide Polymerization Using a Bimetallic Cobalt Catalyst. *J. Am. Chem. Soc.* **2010**, *132*, 16520–16525.
- (10) Ajiro, H.; Peretti, K. L.; Lobkovsky, E. B.; Coates, G. W. On the Mechanism of

Isospecific Epoxide Polymerization by Salen Cobalt(III) Complexes: Evidence for Solid-State Catalysis. *Dalton Trans.* **2009**, No. 41, 8803–8810.

- (11) Hirahata, W.; Thomas, R. M.; Lobkovsky, E. B.; Coates, G. W.
Enantioselective Polymerization of Epoxides: A Highly Active and Selective Catalyst for the Preparation of Stereoregular Polyethers and Enantiopure Epoxides Design of a Bimetallic, Enantioselective Epoxide Polymerization Catalyst. *J. Am. Chem. Soc.* **2008**, *130*, 17658–17659.
- (12) Morris, L. S.; Childers, M. I.; Coates, G. W. Bimetallic Chromium Catalysts with Chain Transfer Agents: A Route to Isotactic Poly(Propylene Oxide)s with Narrow Dispersities. *Angew. Chem.* **2018**, *130*, 5833–5836.
- (13) Ahmed, S. M.; Poater, A.; Childers, M. I.; Widger, P. C. B.; Lapointe, A. M.; Lobkovsky, E. B.; Coates, G. W.; Cavallo, L. Enantioselective Polymerization of Epoxides Using Biaryl-Linked Bimetallic Cobalt Catalysts: A Mechanistic Study. *J. Am. Chem. Soc.* **2013**, *135*, 18901–18911.
- (14) Lundberg, P.; Lee, B. F.; van der Berg, S. A.; Pressly, E. D.; Lee, A.; Hawker, C. J.; Lynd, N. A. Poly[(Ethylene Oxide)-Co-(Methylene Ethylene Oxide)]: A Hydrolytically Degradable Poly(Ethylene Oxide) Platform. *ACS Macro Lett.* **2012**, *1*, 1240–1243.
- (15) Rodriguez, C. G.; Ferrier, R. C.; Helenic, A.; Lynd, N. A. Ring-Opening Polymerization of Epoxides: Facile Pathway to Functional Polyethers via a Versatile Organoaluminum Initiator. *Macromolecules* **2017**, *50*, 3121–3130.
- (16) Ferrier, R. C.; Imbrogno, J.; Rodriguez, C. G.; Chwatko, M.; Meyer, P. W.; Lynd, N. A. Four-Fold Increase in Epoxide Polymerization Rate with Change

- of Alkyl-Substitution on Mono- μ -Oxo-Dialuminum Initiators. *Polym. Chem.* **2017**, *8*, 4503–4511.
- (17) Ferrier, R. C.; Pakhira, S.; Palmon, S. E.; Rodriguez, C. G.; Goldfeld, D. J.; Iyiola, O. O.; Chwatko, M.; Mendoza-Cortes, J. L.; Lynd, N. A. Demystifying the Mechanism of Regio- and Iselective Epoxide Polymerization Using the Vandenberg Catalyst. *Macromolecules* **2018**, *51*, 1777–1786.
- (18) Imbrogno, J.; Ferrier, R. C.; Wheatle, B. K.; Rose, M. J.; Lynd, N. A. Decoupling Catalysis and Chain-Growth Functions of Mono(μ -Alkoxo)Bis(Alkylaluminums) in Epoxide Polymerization: Emergence of the N-Al Adduct Catalyst. *ACS Catal.* **2018**, *8*, 8796–8803.
- (19) Baker, R. J.; Walshe, A. New Reactivity of the Uranyl Ion: Ring Opening Polymerisation of Epoxides. *Chem. Commun.* **2012**, *48*, 985–987.
- (20) Touris, A.; Lee, S.; Hillmyer, M. A.; Bates, F. S. Synthesis of Tri- and Multiblock Polymers with Asymmetric Poly(Ethylene Oxide) End Blocks. *ACS Macro Lett.* **2012**, *1*, 768–771.
- (21) Ghosh, S.; Lund, H.; Jiao, H.; Mejía, E. Rediscovering the Isospecific Ring-Opening Polymerization of Racemic Propylene Oxide with Dibutylmagnesium. *Macromolecules* **2017**, *50*, 1245–1250.
- (22) Lee, B. F.; Wolffs, M.; Delaney, K. T.; Sprafke, J. K.; Leibfarth, F. A.; Hawker, C. J.; Lynd, N. A. Reactivity Ratios and Mechanistic Insight for Anionic Ring-Opening Copolymerization of Epoxides. *Macromolecules* **2012**, *45*, 3722–3731.
- (23) Lee, B. F.; Kade, M. J.; Chute, J. A.; Gupta, N.; Campos, L. M.; Fredrickson,

- G. H.; Kramer, E. J.; Lynd, N. A.; Hawker, C. J. Poly(Allyl Glycidyl Ether)-A Versatile and Functional Polyether Platform. *J. Polym. Sci., Part A: Polym. Chem.* **2011**, *49*, 227–235.
- (24) Grobelny, Z.; Matlengiewicz, M.; Jurek-Suliga, J.; Golba, S.; Skrzeczyna, K.; Kwapulińska, D. Ring Opening Polymerization of Styrene Oxide Initiated with Potassium Alkoxides and Hydroxyalkoxides Activated by 18-Crown-6: Determination of Mechanism and Preparation of New Polyether-Polyols. *Polym. Bull.* **2017**, *74*, 4763–4780.
- (25) Zhang, D.; del Rio-Chanona, E. A.; Shah, N. Screening Synthesis Pathways for Biomass-Derived Sustainable Polymer Production. *ACS Sustainable Chem. Eng.* **2017**, *5*, 4388–4398.
- (26) Yokota, K.; Hirabayashi, T. Manufacture of α -Methylene- γ -Butyrolactone. JP Patent 04,049,288, 1992.
- (27) Trotta, J. T.; Jin, M.; Stawiasz, K. J.; Michaudel, Q.; Chen, W.-L.; Fors, B. P. Synthesis of Methylene Butyrolactone Polymers from Itaconic Acid. *J. Polym. Sci., Part A: Polym. Chem.* **2017**, *55*, 2730–2737.
- (28) Gowda, R. R.; Chen, E. Y.-X. Sustainable Polymers from Biomass-Derived α -Methylene- γ -Butyrolactone. *Encycl. Polym. Sci. Technol.* **2013**.
- (29) Agarwal, S.; Jin, Q.; Maji, S. Biobased Polymers from Plant-Derived Tulipalin A. *ACS Symp. Ser.* **2012**, *1105*, 197–212.
- (30) Murray, A. W.; Reid, R. G. Convenient Synthesis of α -Epoxy lactones (4-Oxo-1,5-Dioxaspiro[2.4]Heptanes and-[2.5]Octanes). *Synthesis* **1985**, 35–38.
- (31) Otto, A.; Liebscher, J. Synthesis of Hydroxyalkyl Heterocycles by Ring

- Transformation of Spiroepoxy Lactones with Binucleophiles. *Synthesis* **2003**, No. 8, 1209–1214.
- (32) Murray, R. W.; Singh, M. Synthesis of Epoxides Using Dimethyldioxirane: Trans-Stilbene Oxide. *Org. Synth.* **1997**, 74, 91–96.
- (33) Adam, W.; Bialas, J.; Hadjiarapoglou, L. A Convenient Preparation of Acetone Solutions of Dimethyldioxirane. *Chem. Ber.* **1991**, 124, 2377.
- (34) Mikula, H.; Svatunek, D.; Lumpi, D.; Glöcklhofer, F.; Hametner, C.; Fröhlich, J. Practical and Efficient Large-Scale Preparation of Dimethyldioxirane. *Org. Process Res. Dev.* **2013**, 17, 313–316.
- (35) Golan, E.; Hagooly, A.; Rozen, S. An Easy Way for Constructing Hard-to-Make Epoxides Employing HOF·CH₃CN. *Tetrahedron Lett.* **2004**, 45, 3397–3399.
- (36) Charbonneau, L.; Foster, X.; Zhao, D.; Kaliaguine, S. Catalyst-Free Epoxidation of Limonene to Limonene Dioxide. *ACS Sustainable Chem. Eng.* **2018**, 6, 5115–5121.
- (37) Fuchs, M.; Schober, M.; Orthaber, A.; Faber, K. Asymmetric Synthesis of β -Substituted α -Methylenebutyrolactones via TRIP-Catalyzed Allylation: Mechanistic Studies and Application to the Synthesis of (S)-(-)-Hydroxymatairesinol. *Adv. Synth. Catal.* **2013**, 355, 2499–2505.
- (38) Menczel, J. D.; Prime, R. B. *Thermal Analysis of Polymers*; 2009; Vol. 91.
- (39) Boor, J.; Bauer, R. S. Preparation and Characterization of Poly(Isobutylene Oxide). *J. Appl. Polym. Sci.* **1974**, 18, 3699–3721.
- (40) Chetana, D.; Baby, C.; Nadkarni, V. S.; Behera, R. N.; Chauhan, R. Synthesis,

Characterization, and Computational Study of Potential Itaconimide-Based Initiators for Atom Transfer Radical Polymerization. *RSC Adv.* **2014**, *4*, 48163–48176.

- (41) Světlík, J.; Veverka, M. A Convenient Preparative Route to 1-Oxa-5-Azaspiro[2.4]Heptane Systems. *Liebigs Ann. der Chemie* **1990**, 111–112.
- (42) Silva, E. F.; Pereira, R. P.; Rocco, A. M. Ternary Blends of Poly(Ethylene Oxide) and Acrylate-Based Copolymers: Crystallinity, Miscibility, Interactions and Proton Conductivity. *Eur. Polym. J.* **2009**, *45*, 3127–3137.
- (43) Chen, J.; Spear, S. K.; Huddleston, J. G.; Rogers, R. D. Polyethylene Glycol and Solutions of Polyethylene Glycol as Green Reaction Media. *Green Chem.* **2005**, *7*, 64–82.
- (44) Fetters, L. J.; Lohse, D. J.; Richter, D.; Witten, T. A.; Zirkel, A. Connection between Polymer Molecular Weight, Density, Chain Dimensions, and Melt Viscoelastic Properties. *Macromolecules* **1994**, *27*, 4639–4647.
- (45) Anilkumar, K. M.; Jinisha, B.; Manoj, M.; Jayalekshmi, S. Poly(Ethylene Oxide) (PEO) – Poly(Vinyl Pyrrolidone) (PVP) Blend Polymer Based Solid Electrolyte Membranes for Developing Solid State Magnesium Ion Cells. *Eur. Polym. J.* **2017**, *89*, 249–262.
- (46) Ratna, D.; Abraham, T.; Karger-Kocsis, J. Thermomechanical and Rheological Properties of High-Molecular-Weight Poly(Ethylene Oxide)/Novolac Blends. *Macromol. Chem. Phys.* **2008**, *209*, 723–733.
- (47) Aharoni, S. M. Correlations between Chain Parameters and the Plateau Modulus of Polymers. *Macromolecules* **1986**, *19*, 426–434.

- (48) Hawker, C. J.; Chu, F.; Pomery, P. J.; Hill, D. J. T. Hyperbranched Poly(Ethylene Glycol)s: A New Class of Ion-Conducting Materials. *Macromolecules* **1996**, *29*, 3831–3838.
- (49) Costa, L.; Camino, G.; Luda, M. P.; Cameron, G. G.; Qureshi, M. Y. The Thermal Degradation of Poly(Propylene Oxide) and Its Complexes with LiBr and LiI. *Polym. Degrad. Stab.* **1995**, *48*, 325–331.
- (50) Kanazawa, A.; Kanaoka, S.; Aoshima, S. Concurrent Cationic Vinyl-Addition and Ring-Opening Copolymerization Using B(C₆F₅)₃ as a Catalyst: Copolymerization of Vinyl Ethers and Isobutylene Oxide via Crossover Propagation Reactions. *J. Am. Chem. Soc.* **2013**, *135*, 9330–9333.
- (51) Boiko, Y. M. New Simple Method of Measuring the Surface Glass Transition Temperature of Polymers. *J. Polym. Sci. Part B Polym. Phys.* **2010**, *48*, 2012–2021.
- (52) Shuai, W.; Li, B.; Zhang, Y. Compatibilization of Poly(2,6-Dimethyl-1,4-Phenylene Oxide)/Polyamide 6 Blends with Styrene-Maleic Anhydride Copolymers: Mechanical Properties, Morphology, Crystallization, and Melting Behavior. *J. Appl. Polym. Sci.* **2010**, *118*, 3545–3551.
- (53) Zhuang, G. L.; Wey, M. Y.; Tseng, H. H. The Density and Crystallinity Properties of PPO-Silica Mixed-Matrix Membranes Produced via the in Situ Sol-Gel Method for H₂/CO₂ Separation. II: Effect of Thermal Annealing Treatment. *Chem. Eng. Res. Des.* **2015**, *104*, 319–332.
- (54) Kwei, T. K.; Frisch, H. L. Interaction Parameter in Polymer Mixtures. *Macromolecules* **1978**, *11*, 1267–1271.

- (55) Trotta, J.; Watts, A.; Wong, A.; LaPointe, A. M.; Hillmyer, M. A.; Fors, B. P. Renewable Thermosets and Thermoplastics from Itaconic Acid. *ACS Sustainable Chem. Eng.* **2019**, 7, 2691–2701.
- (56) Chauhan, R.; Choudhary, V. Copolymerization of Methyl Methacrylate with N-(Methoxyphenyl) Itaconimides. *J. Polym. Sci.* **2008**, 109, 987.
- (57) Armarego, W. L. F.; Chai, C. L. L. *Purification of Laboratory Chemicals*; 2009.